The stratigraphic record of submarine channel-lobe transition zones

Menno Hofstra

Submitted in accordance with the requirements for the degree of Doctor of Philosophy

The University of Leeds
School of Earth and Environment

August, 2016

The candidate confirms that the work submitted is his own, except where work which has formed part of jointly-authored publications has been included. The contribution of the candidate and the other authors to this work has been explicitly indicated below. The candidate confirms that appropriate credit has been given within the thesis where reference has been made to the work of others.

(1) Hofstra, M., Hodgson, D.M., Peakall, J., Flint, S.S. (2015) Giant scour-fills in ancient channel-lobe transition zones: architecture, facies and formative processes. Sedimentary Geology, V329, 98-114.

Related to Chapter 4: Main author was principal investigator and wrote the manuscript. Fieldwork assistance was provided by Hodgson and manuscript review by Hodgson, Peakall and Flint.

(2) Hofstra, M., Pontén, A.S.M., Peakall, J., Flint, S.S., Nair, K.N., Hodgson, D.M. (2016) The impact of fine-scale reservoir geometries on streamline flow patterns in submarine lobe deposits using outcrop analogues from the Karoo Basin. Petroleum Geoscience.

Related to Chapter 7: Main author was principal investigator and wrote the manuscript. Assistance in modeling was provided by Pontén and Nair. Fieldwork assistance by Hodgson. Manuscript review by Hodgson, Peakall, Pontén and Flint.

Acknowledgements

First of all, I would like to thank Dave Hodgson, Jeff Peakall and Steve Flint for giving me the opportunity to write this thesis and their continuous support, guidance and encouragement during the whole four years of my PhD. I am especially grateful to Dave for introducing me to the rocks of the Karoo, making a proper 'Karoo-dog' out of me and providing me with the many opportunities during the project.

As this work was funded by the LOBE2 consortium research project, I am grateful for the financial support from: Anadarko, Bayerngas Norge, BG Group, BHP Billiton, BP, Chevron, Dong Energy, E.ON, ENGIE, Maersk Oil, Marathon Oil, Shell, Statoil, Total, VNG Norge, and Woodside.

Anna Pontén is very much thanked for providing me with the opportunity to perform the reservoir modelling work at the Statoil Research Centre and her continuous support during the LOBE2 project. I am also grateful to Krishna, Ingunn and others for all their help and making my stay in Trondheim more than enjoyable.

I would also like to acknowledge the Karoo farmers for their hospitality and permission to conduct the fieldwork, DeVille Wickens for his support in the field and during the coring process and Graham Botha for his excellent service and hospitality during the many 'dark' core logging sessions in Blackheath.

In the span of four years, many espresso's were drunk, beers were shared and braais lit. Thanks to all my colleagues and friends in Leeds, Manchester and Utrecht of which there are way too many to name them all, for making my time so much more fun. Thanks to Chris Stevenson, Matthieu Cartigny and others for the many fruitful discussions that helped to shape this thesis. Ricci for being such an awesome flatmate and for the many late hours spent in Leeds. Yvonne for the many great times in SA and for being so much more organised, when I was not.

Renée, Nienke, Marisa and Marcello are very much thanked for the many long and sweaty logging days in the field. I could not have done it without you. I am further grateful to Lewis and Ben for their help on the LOBE2-report and the digitising work.

And finally, I would like to thank my family and friends for their continuous support and especially Renée de Bruijn for her inexhaustible patience, encouragement and love throughout the last four years.

Abstract

Channel-lobe transition zones (CLTZs) represent critical areas between the submarine slope and basin floor systems, where sediment gravity flows transition from confined to unconfined. In modern systems, this area is characterised by a distinctive assemblage of erosional and depositional features. However, the transfer of the CLTZ into the stratigraphic record is not well constrained.

By the detailed study of various well-constrained exhumed base-of-slope systems within the Tanqua and Laingsburg depocentres of the Karoo Basin, South Africa, the sedimentary and stratigraphic record of CLTZs is investigated. The first detailed study of key depositional and erosional bedforms that characterise ancient CLTZs, including sediment waves and giant scour-fills, are presented. Their process record suggests complicated flow-bedform interactions, where both the preservation and sedimentary characteristics are dependent on the evolution of the feeder channel and the lateral position to the channel-mouth. Within the base-of-slope environments, juxtaposition of lobes and channel-fills is common. The lobes in these proximal fan environments are sandstone-prone and differ in facies and architectural characteristics to lobes downdip on the basin floor.

The sand-rich nature and juxtaposition of elements in ancient CLTZs means that they are considered attractive hydrocarbon reservoir targets in the subsurface. However, fine-scale reservoir modelling and streamline simulations suggests that the relatively limited sand-volume of channel-fills in comparison to lobe deposits in these environments can have a negative impact on reservoir performance due to its effect on reservoir connectivity.

Overall, the stratigraphic record of CLTZs shows high diversity in architecture, facies characteristics and volume, which can be related to three primary controls: a) spatial variability, b) flow efficiency and c) channel evolution. These three controls infer that CTLZs are highly dynamic, migrating and changing in dimensions over time; this needs to be considered when assessing how CLTZs are recorded in the rock record.

Table of Contents

List of Tables

List of Figures

Chapter 1:
Thesis Rationale

1.1 Thesis background

A major physiographic transition zone on the Earth's surface is the passage from submarine channels, which are conduits for confined sediment gravity flows, to submarine lobe systems, deposited by largely unconfined flows. Commonly, these channel-lobe transition zones (CLTZs) are found on the continental rise of passive margins, or at the base-of-slope on basin margins (Wynn et al., 2002a; Van der Merwe et al., 2014; Stevenson et al., 2015). The majority of clastic sediment is deposited on basin-floor settings (e.g. Covault et al., 2011), however these sediment sinks are the least understood of all clastic systems in particular due to their deepwater setting. CLTZs have been imaged in multiple modern systems (e.g. Palanques et al., 1995; Nelson et al., 2000; Wynn et al., 2002a; Bonnel et al., 2005), and are characterized by a range of erosional (e.g. scours) and depositional (e.g. sediment waves) bedforms. The CLTZ acts as an area of sediment bypass (Wynn et al., 2002a; Stevenson et al., 2015) and is highly dynamic with complicated interactions between erosional and depositional processes. However, the transfer of this geographically defined zone into the stratigraphic record is not well understood. There remain significant inconsistencies between the interpretation of the stratigraphic record of CLTZs (e.g. Mutti and Normark, 1987; Gardner et al., 2003; Ito et al., 2014; Van der Merwe et al., 2014) and the recognition criteria from modern systems (Wynn et al., 2002a). The widespread extent (> 10 km^2) of these areas of sediment bypass (e.g. Palanques et al., 1995; Wynn et al., 2002a) as recognised in modern systems suggests, however, that significant evidence should prevail within the stratigraphic record. The expression of CLTZs as surfaces or sedimentary packages is key to comparing the ancient and the modern. To establish criteria for the identification of the stratigraphic record of CLTZs, and to

understand process interactions in this key area of submarine fan systems, requires exhumed systems with exceptional outcrop control.

The sedimentary infill of the Karoo Basin (South Africa) was identified in the early 90's (Bouma and Wickens, 1991; 1994; Wickens, 1994) as a world-unique site for the study of sand-prone submarine fan systems, in particular due to the extensive nature of the exposure in combination with the accessibility of the outcrop. After more than 25 years, new discoveries are still being made, and in recent years the studies on these Permian age fan systems have significantly increased our understanding of the depositional architecture of basin-floor lobe deposits (Prélat et al., 2009; Prélat and Hodgson, 2013). These studies have focused on the most distal parts of the fan system in order to avoid erosional features such as scours and channels. The knowledge gained from analysis of lobe deposits in basin-floor settings can be utilised to compare with the depositional architecture of lobes in more proximal base-of-slope settings, where erosional processes and variety in architectural elements complicate the stratigraphic record.

The unpredictable nature of areas of rapid decrease in flow confinement, typical of CLTZ settings, makes it an important area for geohazard prediction. Turbidity currents are known to disrupt telecommunication infrastructure and pipelines (e.g. Urlaub et al., 2013). Furthermore, the seabed morphology associated with CLTZ environments can facilitate niche deep-water habitats (e.g. Crimes et al. 1992; Green et al., 1999; Callow and Mcllroy, 2011), supporting specific opportunistic species within an otherwise low-relief seafloor landscape.

Improved understanding of the stratigraphic record of the CLTZ environment and base-of-slope settings is of great importance for the hydrocarbon industry for a number of reasons. Firstly, the detachment of submarine lobe deposits from their feeder channels (e.g. Mutti and Normark, 1987; Gardner et al., 2003; Van der Merwe et al., 2014) can act as a stratigraphic trapping mechanism, and therefore understanding the conditions behind lobe

detachment will help to improve stratigraphic trap appraisal. Recognition of stratigraphic traps is becoming increasingly important as in many exploration areas structural traps have been largely exploited (e.g.Walker, 1978; Jennette et al., 2003; Prather, 2003; Stoker et al., 2006). Furthermore, as the CLTZ acts as a zone of bypass (Wynn et al., 2002a; Stevenson et al., 2015), improved constraints on the facies characteristics and stratigraphic record of flow bypass can aid in the understanding of down dip deepwater exploration targets. In many exploration areas only a limited amount of borehole data is available, so the accurate recognition of bypass surfaces could lead to predictions of large volumes of sediment and therefore potential reservoirs down system. Finally the effect of channel-and-lobe juxtaposition is not well understood, as most of the focus on fine-scale heterogeneities has been on slope channel systems (e.g. Alpak et al., 2013; Labourdette et al., 2013; Eschard et al., 2014). Due to the large volumes of sediment and sand-prone nature, lobe deposits have significant reservoir potential (e.g. Pirmez et al., 2000; Prélat et al., 2010) and may therefore represent more dominant reservoir components compared to channels. Outcrop study of CLTZ and base-of-slope environments can most efficiently aid in overcoming these problems, due to the importance of both 2D and 3D constraints and the understanding of sub-seismic scale architecture.

This thesis examines the variety of depositional and erosional components of CLTZs and their representation within the stratigraphic record. It examines the implications of fine-scale architecture on reservoir behaviour and attempts to unravel part of the complicated process record that is preserved in these areas by studying the deposits in detail.

1.2 Key research questions

The aims of this study can be divided in two main topics of which the first will carry the most significance, where it is attempted to document the variety of elements associated with ancient preserved CLTZ environments in the Karoo Basin (South Africa). This first topic is therefore subdivided into a set of problems.

1. Stratigraphic record of Channel-lobe transition zones

    - What are the key representative facies, architectural elements, and stacking patterns that characterize CLTZs in the rock record?

Rationale: There are very limited criteria to differentiate CLTZ environments from lobe and channel-levee environments.

    - How is the assemblage of depositional and erosional elements that characterize channel-lobe-transition zones transferred into the stratigraphic record of base-of-slope settings?

Rationale: The depositional process record of the different elements within the CLTZ is not well understood.

2. Reservoir implications of fine-scale architectures in lobe and CLTZ reservoirs

    - What is the impact of channel-lobe juxtaposition and lobe amalgamation on base-of-slope reservoirs?

Rationale: The impact of CLTZ-related fine-scale architectures on reservoir connectivity within sand-prone base-of-slope settings is not well understood.

1.3 Research objectives

To answer the research questions stated in Section 1.2, the principal objectives of this thesis are:

- To find key criteria for the recognition for scour-fills and sediment waves within the stratigraphic record;
- To better understand the process record of erosional and depositional bedforms within channel-lobe transition zone settings;
- To better define the variability in character of channel-lobe transition zones;

- To define the main factors controlling reservoir connectivity within base-of-slope environments.

These objectives will be fulfilled within all following chapters of this thesis, by extensive studies on the ancient fan systems of the Karoo Basin (South-Africa). A summary of all generic insights will be discussed in Chapter 9.

1.4 Lobe 2 JIP background

The Lobe Phase 2 Joint Industry Project started in May 2012 and builds upon the results and experience of the earlier Lobe Phase 1 project. It was supported by a consortium of 16 different companies and had its major focus on the Karoo Basin (South Africa), but also extended its scope to the Neuquén Basin (Argentina). Seven new research boreholes, totalling 2 km of core, were drilled as part of this research programme: three in the Tanqua area and four in the Laingsburg area. The scientific rationale for collecting these research boreholes was to provide direct calibration with outcrop datasets and constraining the depositional architecture of the system. Lobe Phase 2 has compiled the largest outcrop-based dataset ever collected in terms of logged sections from lobe dominated successions and is one of only a small number of such projects that have been complemented by research wells.

1.5 Field & core methodology

An integrated dataset was collected from outcrop and research boreholes (See Appendices A and B). For this thesis, a large amount of sedimentary logs (127 in thesis, >200 collected) (See Appendix B.3) were collected from two fan systems in the Tanqua depocentre (Fan 3 & Unit 5) and two fan systems from the Laingsburg depocentre (Unit A5 & Unit B), with a cumulative thickness exceeding 4 km. Many of these sedimentary logs (> 1 km cumulative thickness) have been logged at centimetre scale. Correlation panels were created by following out key surfaces and using handheld GPS for accurate positioning. Well over a

thousand palaeocurrents (1083 in thesis, ~1500 collected ; See Appendix B.2) were measured from rippled bed tops, flute and groove marks. Correlations and the corrections on correlation panels and photo-panel interpretations were performed in the field. A GigaPan system was used for creating ultra-detailed photo-panels of large outcrop sections. For this thesis, a total of ~500 m of core has been logged at cm-scale detail from both the Tanqua and the Laingsburg areas (See Appendix A). During core logging a hand lens and a USB Dino-Lite were used for studying sub-centimetre features.

1.6 Thesis outline

- *Chapter 2: Current understanding of channel-lobe transition zones and their stratigraphic record:* Provides a literature background on channel-lobe transition zones (CLTZs) and highlights the inconsistencies between our understanding of CLTZ from recent systems and the stratigraphic record.
- *Chapter 3: Tectonostratigraphy of the SW Karoo Basin and deep-water architectural and facies framework:* Introduces the stratigraphic framework and background information on the Karoo Basin, its dominant deep-water facies, architectural elements and methodology used for outcrop and core data collection.
- *Chapter 4: Giant scour-fills in ancient channel-lobe transition zones: architecture, facies and formative processes:* Presents the first detailed record of giant scour-fills (> 15m deep; <1 km long) from ancient CLTZ environments. Two case studies from the Karoo Basin (Tanqua and Laingsburg depocentre) have been recorded in detail. Their process sedimentology and formation are discussed and explanations are given for the diversity in infill characteristics. Published as: Hofstra, M., Hodgson, D.M., Peakall, J., Flint, S.S., 2015. Giant scour-fills in ancient channel-lobe transition zones: architecture, facies and formative processes. *Sedimentary Geology,* 329, 98-114.

- *Chapter 5: Architecture and morphodynamics of sediment waves in an ancient channel-lobe transition zone:* Presents the architecture and facies characteristics of sand-prone sediment waves from ancient CLTZ environments. Different datasets from a base-of-slope system in the Laingsburg depocentre show pinch-and-swell bedforms (>1 m high; >20 m wavelength) with significant spatial facies variability on sub-metre scale. Their process record, the significance of scale and the importance of channel-mouth position are discussed in detail.
- *Chapter 6: The stratigraphic record of submarine lobe deposits at base-of-slope settings:* Presents the stratigraphic record of submarine lobe deposits at base-of-slope settings. Two base-of-slope systems from the Tanqua depocentre show High Amalgamation Zones and sandstone-prone tabular packages, which indicate the presence of lobes with alternative facies, architecture and stacking patterns compared to lobes at basin-floor settings downdip. Differences in lobe characteristics are linked to flow efficiency and sediment grain size segregation.
- *Chapter 7: The impact of fine-scale reservoir geometries on streamline flow patterns in submarine lobe deposits using outcrop analogues from the Karoo Basin:* Presents a full 3D reservoir modelling workflow to test the impact of fine-scale heterogeneities within basin-floor lobe complexes and CLTZ environments on reservoir connectivity. Synthetic reservoirs were created based on various outcrop datasets from the Karoo Basin. With the help of single-phase streamline flow simulations the impact of sedimentary concepts and fine-scale architectures on reservoir connectivity and performance is tested. Submitted as: Hofstra, M., Pontén, A.S.M., Hodgson, D.M., Peakall, J., Flint, S.S., Nair, K.N., (*in review*). The impact of fine-scale reservoir geometries on streamline flow patterns in submarine lobe deposits using outcrop analogues from the Karoo Basin. In: *Petroleum Geoscience.*

- *Chapter 8: Controls on the stratigraphic record of the channel-lobe transition zone:* Integrates the findings of previous chapters (2-5) and covers additional observations on CLTZs from the Karoo Basin, summarising generic insights. Preservation potential and the variability within the stratigraphic record is discussed, which is linked to position, efficiency and system evolution.
- *Chapter 9: Conclusions:* Provides short summary answers for the key research questions that have been posed in Section 1.2 to give better insight how the main aims for this thesis (Section 1.3) have been covered.

Chapter 2:
Current understanding of channel-lobe transition zones and their stratigraphic record

Channel-to-Lobe Transition Zones (CLTZ), or Channel-lobe transitions, have been identified as important regions among submarine fan system (Mutti and Normark, 1987; 1991; Kenyon et al., 1995; Wynn et al., 2002a; Gardner et al., 2003; Van der Merwe et al., 2014; Pemberton et al., 2016). Submarine fan systems are the largest detrital accumulations on Earth (e.g. Shanmugam and Moiola, 1985; Mutti and Normark, 1987; Bouma, 2000), which are mainly fed by turbidity currents (e.g. Lowe 1982; Meiburg and Kneller, 2010): subaqueous turbulence-dominated sediment-laden gravity flows. Until two decades ago, Channel-lobe transition zones were largely overlooked within studies on turbidite systems. However, the arrival of high resolution data (Fig. 2.1) from modern systems (e.g. Piper and Sayoye., 1993; Palanques et al., 1995; Morris et al., 1998; Wynn et al., 2002a; Habgood et al., 2003; Bonnel et al., 2005), as an important information source for constraining the character of channel (elongated conduits for fully or partially confined flows) (e.g. McHargue et al. 2011) to lobe (unconfined lobate-shaped deposits) (e.g. Prélat et al., 2009) transitions has significantly reshaped our understanding.

However, progress in reconstructing CLTZ palaeogeography from outcrop studies has remained challenging due to the large surface area of submarine fan systems.

The CLTZ was initially defined by Mutti and Normark (1987) as the area that shows the spatial transition from well-defined channels and channel-fills to well-defined lobes or lobe facies (Mutti and Normark, 1987; 1991; Wynn et al. 2002a). Among narrow and confined basins (e.g. Agadir Basin) with respect to flow size, clear lobe morphologies may be lacking, and CLTZ may show a downdip transition into what is described as basin-floor 'sheet sands' (Wynn et al., 2002a). The CLTZ is expressed as an area dominated by sediment bypass (Wynn et al., 2002a; Van der Merwe et al., 2014; Stevenson et al., 2015) and the location

of a CLTZ is largely dependent on the seabed gradient and flow conditions, occuring at any position along the profile of a turbidite system (Wynn et al., 2002a; Gardner et al., 2003; Stevenson et al., 2015). However, CLTZs are commonly associated with base-of-slope environments (e.g. Brunt et al., 2013a; Van der Merwe et al., 2014), related to an abrupt gradient change and lack of gravitational energy resulting in flow expansion and depletive conditions (Kneller et al., 1995; Mulder and Alexander, 2001). Canyon-mouth settings have also been classified as channel-lobe transition zone areas (Wynn et al., 2002a; Ito et al., 2014), due to their similarity with channel-mouth settings. Some rare sediment bypass zones separating channels from lobes have also been constrained in the outcrop record (Van der Merwe et al. 2014). The mechanisms influencing the occurrence of detached or attached lobe deposits are however not well understood (Mutti and Normark, 1987; Van der Merwe et al., 2014). Furthermore, the mechanisms for the transfer of the spatially defined CLTZ into the stratigraphic record remains a rarely discussed issue.

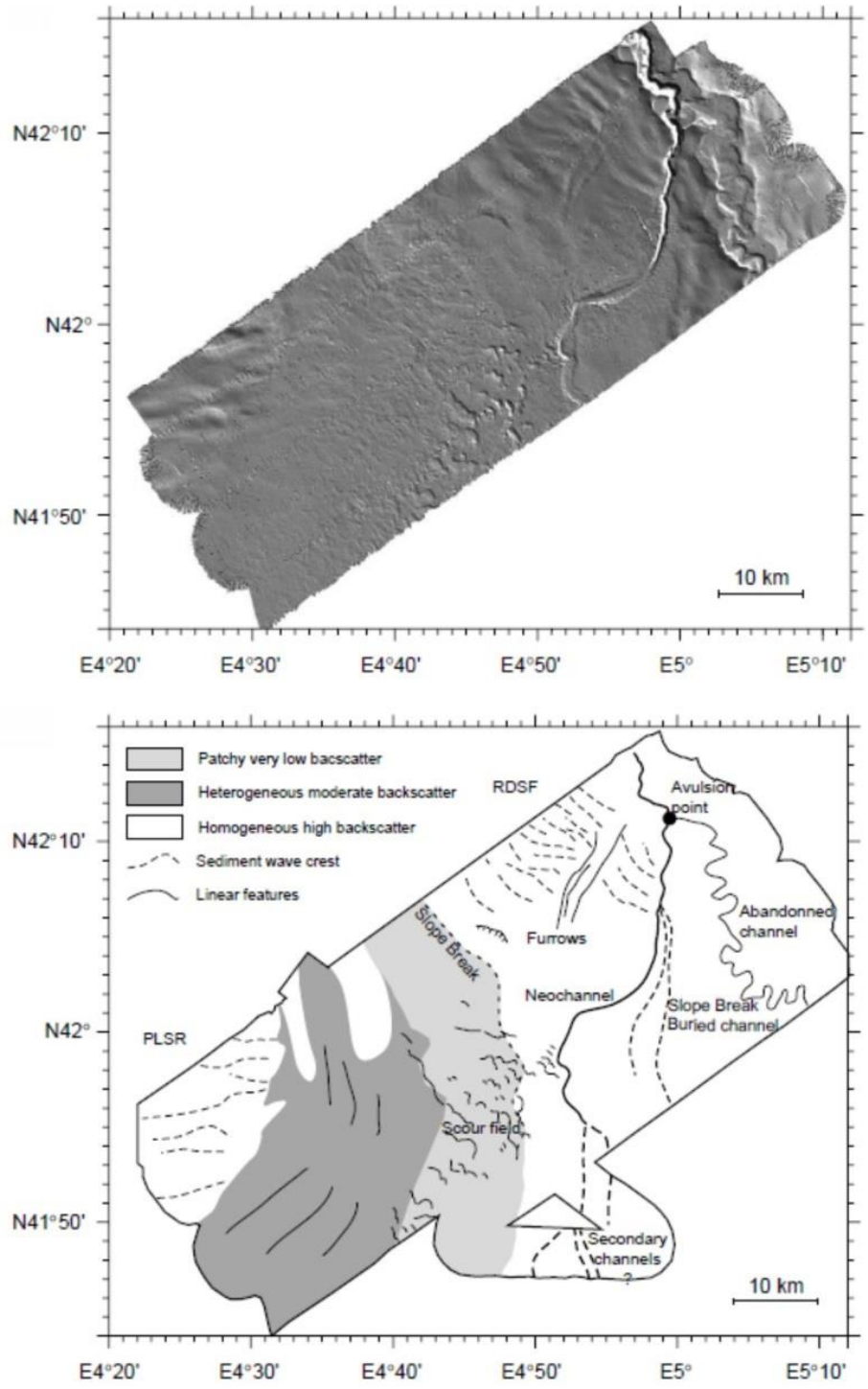

Figure 2.1 *(top) Shaded swath bathymetry of the Rhone Deep Sea Neo-fan. (bottum) Morpho-acoustic interpretation of the same dataset showing the independent nature of the Neo-channel mouth and a large scour field developed downdip of a slope break. (from Bonnel et al., 2005).*

2.1 CLTZ bathymetric record

The primary model for CLTZs as a bypass zone (Fig. 2.2), presented by Wynn et al. (2002a), is based on their bathymetric and acoustic backscatter expression in recent systems (e.g. Fig. 2.1). This model shows a spatial distribution of a characteristic assemblage of erosional and depositional bedforms (Fig. 2.1). The largest erosional features (amalgamated scours) focus close to the channel mouth, whereas depositional elements are primarily focused closer to the lobe downstream. As the CLTZ is a region of sediment bypass, where the majority of the sediment reaching the CLTZ is deposited further into the basin, the deposits that tend to be in this area are relatively coarse-grained, patchily distributed and extensively reworked (Wynn et al., 2002a).

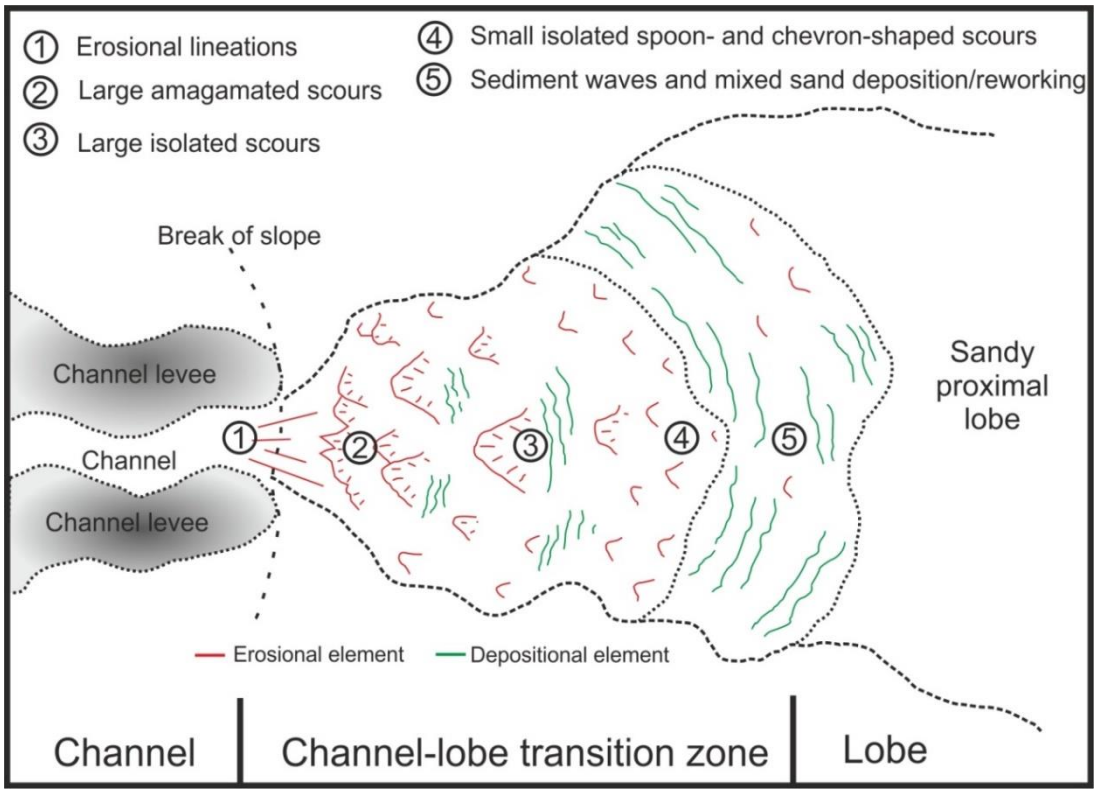

Figure 2.2 *Planform bathymetric CLTZ model showing the spatial distribution of erosional and depositional features. Erosional elements are more prone close to the channel-mouth and depositional elements dominate the areas proximal to lobe deposition. Redrawn from Wynn et al. (2002a).*

2.1.1 Erosional bedforms

Extensive seafloor erosion is expected in the region where turbidity currents exit channel confinement, due to significant flow expansion and increased turbulence (e.g. Palanques et al., 1995; Morris et al., 1998; Wynn et al., 2002a; Bonnel et al., 2005; Ercilla et al., 2008). In a well-defined modern expression of a CLTZ, this results in variety of erosional features (Fig. 2.2). The presence of these features changes with distance from the channel or canyon mouth.

- Erosional lineation parallel to flow direction directly at break of slope

These longitudinal streaks are up to 15 km long and typically space 0.5-2 km apart (Wynn et al., 2002a). Even though direct evidence is lacking, due to their proximity within channel-mouth settings they are believed to be of an erosional origin.

- Large amalgamated scours

Amalgamated scours have a rather chaotic appearance due to interference of multiple individual scours. They tend to form very proximal to the channel-mouth as a complex zone of erosional relief. Dimensions vary significantly, but typical depths are several metres, up to tens of metres, with maximum widths of 9 km and lengths of 6 km (Wynn et al., 2002a). More recently Macdonald et al. (2011a) have revealed the remarkable longevity (> 0.2 Myr) of some modern scours as well as the complicated cut-and-fill histories of composite (amalgamated) scour features. Pre-existing irregularities in the substrate have been linked to the inception of larger scour features (Shaw et al., 2013).

- Large isolated scours and small isolated chevron/spoon shaped scours

Isolated spoon-shaped scours are mostly aligned parallel to the main flow direction (Fig. 2.2). Typical dimensions are 20 m deep, 2 km wide, and 2.5 km long (Wynn et al., 2002a; Macdonald et al., 2011a). Due to resolution limitations of seabed imaging, the lower dimension limits are unknown. In a longitudinal cross-section the spoon-shaped scours are asymmetrical, with a steeper upslope face than its downslope face (Malinverno et al., 1988; Morris et al., 1998; Wynn et al., 2002a; Macdonald et al., 2011a; Shaw et al., 2013) .

In a transverse cross-section they show a similar typical U-shaped morphology as most submarine channels (Wynn et al., 2002a). Chevron shaped scours (Morris et al., 1998) are commonly found in slightly more distal settings, away from the proximal and axial settings. Typical dimension are <10 m deep, 200-800 m wide and 400-100 m long (Wynn et al., 2002a; Macdonald et al., 2011a).

2.1.2 Depositional bedforms

The following depositional bedforms have been associated with the bathymetric an acoustic backscatter record of CLTZs (Normark and Piper, 1991; Wynn et al., 2002a; 2002b; Ercilla et al., 2008):

- Sediment waves

Sediment waves are aligned orthogonal to the main flow direction, and have wavelengths of 1-2 km, wave heights of 4 m and crest lengths of maximum 4 km (Normark and Piper, 1991; Wynn and Stow, 2002; Wynn et al., 2002b; Klaucke et al., 2004; Ercilla et al., 2008). Sediment waves are most abundant in the central and distal parts of the CLTZ and can show 'high backscatter' flow parallel streaks among modern datasets , which have been interpreted as reworking and erosion by subsequent flows (Wynn et al., 2002a; 2002b). The few direct observations of sediment waves suggest a sand-gravel composition (Piper et al., 1985; Kidd et al., 1998; Migeon et al., 2001; Wynn et al., 2002b).

- Sediment mounds

Composed of gravel and pebbly sand and mostly located immediately downslope of large isolated erosional scours, suggesting a link between scour and sediment mound formation. Dimensions are typically up to 40 m long and 1.5 m high (Wynn et al, 2002a).

- Patches of thin reworked sands

Typically found in the more distal settings of CLTZs, showing very variable dimensions (metre to kilometre scale) (Wynn et al., 2002a). These reworked sands are recognised as

irregularly shaped patches, by sonar imaging and seem to be streaked out in a down current direction.

2.2 CLTZ stratigraphic record

A variety of sedimentary characteristics and bedforms have been ascribed to the CLTZ based on outcrop datasets (Mutti, 1977; Mutti and Normark, 1987; 1991; Wynn et al., 2002a; Ito et al., 2014; Pemberton et al. 2016) Mutti and Normark (1987) were the first to characterise the CLTZ as an area of bed roughness and irregularity resulting from various depositional and erosional features (Fig. 2.3). Similarly, Ito et al. (2014) looked at a canyon-mouth setting of the Boso Peninsula (Japan) and summarised a variety of elements and sedimentary characteristics associated with the outcrop expression of CLTZ settings. Erosional features are represented by scour-fills, which show a variety of morphologies and dimensions (Mutti and Normark, 1987; Ito et al., 2014), commonly around 1-5 m in depth and up to 50 m wide with exceptions of 10 m deep and 140 m wide. Mud-drapes are commonly observed in scour-fills associated with CLTZs (Mutti and Normark, 1987; Morris and Normark, 2000; Wynn et al., 2002a; Macdonald et al. ,2011a; Ito et al., 2014). In coarse-grained systems, such as the Boso Peninsula (Ito et al., 2014), these drapes (up to 60 cm thick) have been reported to be primarily composed of sandy and coarse siltstones. The drapes are dominantly structureless, but can locally contain sandy laminations in the basal part and show sharp contacts with underlying and overlying deposits (Ito et al., 2014). Scour-fills which do not show mud-draping are primarily represented by the exact same facies as surrounding deposits (Morris and Normark, 2000; Wynn et al., 2002a; Ito et al., 2014). Upstream-inclined backset bedding in scour-fills have also been reported (Ito et al., 2014), in association with subangular mudstone clasts and upstream-inclined basal erosional surfaces.

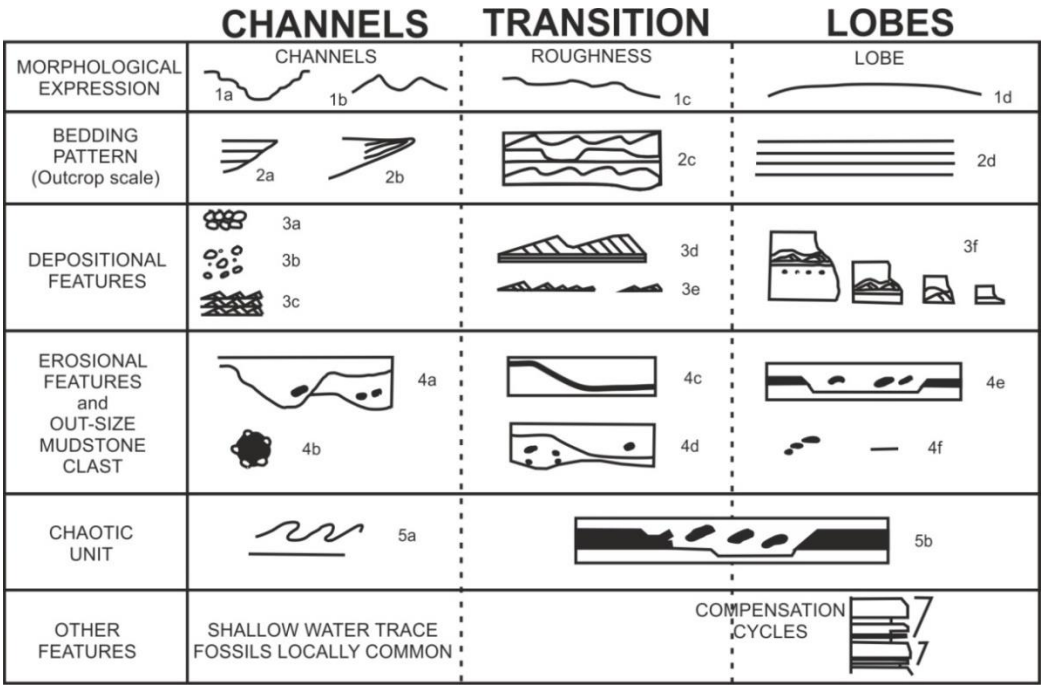

Figure 2.3 *Main characteristics of submarine channels, channel-lobe transitions and lobe deposits as originally described by Mutti and Normark (1987). With: 1a = erosional channel; 1b = depositional channel; 1c ='zone of roughness'; 1d = lobate relief; 2a = beds truncating against channel margin; 2b = beds converging against channel edge; 2c = bedding irregularity resulting from scours and large-scale bedforms; 2d = even-parallel bedding; 3a = clast-supported conglomerates; 3b = mud-supported conglomerates; 3c = thin-bedded overbank deposits; 3d+e = coarse-grained, internally stratified sandstone facies; 3f = complete and base-missing Bouma sequences; 4a = deep and relative narrow scours locally associated with stone clasts; 4b = armoured mudstone clasts; 4c = mud-draped scours; 4d = broad scours, locally associated with mudstone clasts; 4e = tabular scours invariably associated with mudstone rip-up clasts from underlying substratum; 4f = nests of mudstone clasts commonly showing inverse grading and 'take-off' attitude of individual clasts; 5a = slump units; 5b = impact features (redrawn from Mutti and Normark, 1987)*

The outcrop expression of depositional features within CLTZs is less well defined. They have generally been described as coarse-grained and internally stratified by Mutti and Normark (1987). In the Albian Black Flysch of NE Spain (Vicente Bravo and Robles, 1995) described some large scale hummock- and wave-like bedforms associated with CLTZs (Wynn et al., 2002a). The hummock-like bedforms show sinusoidal patterns in transverse and longitudinal sections with wavelengths ranging between 5 to 40 m and heights from a few decimetres up to 1.5 m, inferred to be genetically related to scours (Vicente Bravo and Robles, 1995). The wave-like bedforms varied in wavelengths ranging between 5 and 30 m

and amplitudes up to 0.7 m, showing symmetric to slightly asymmetric gravel-rich geometries. Similar wave-form bedding or tractional structures were also described by Ito et al. (2014) for the Boso Peninsula in pebbly medium to coarse-grained sandstones, with wavelengths (Type I in Ito et al., 2014) up to 40 m and heights up to 2 m. These tractional structures show lateral transitions towards plane parallel stratification (Type II), with typical upward transitions to graded or massive bedding. Isolated coarse-grained (pebbly sandstones to conglomerates) dunes (Type III) were also described, forming lenticular geometries (< 5 m long, <0.4 m height), intercalated or encased in sandy siltstones and showing foreset bedding inclined in the downcurrent direction. Pemberton et al. (2016) described cross-stratified depositional bedforms (1-4.5 m thick, 55- 135 m across) within a CLTZ setting of the Magallanes Basin of southern Chile, which were interpreted to have migrated upslope.

Alongside bedforms, more general sedimentary characteristics have been attributed to the CLTZ. Ito et al. (2014) showed that the average bed thickness increases away from the CLTZ in the downcurrent direction. Furthermore, amalgamation of sandstones (cut-and-fill) is common and the ratio of siltstones relative to interbedded sandstones is gradually increasing in the downslope direction.

2.2.1 Channel-lobe juxtaposition

For characterising the CLTZ in the rock record, it is vital to look at lateral and longitudinal migration of features and deposits associated with this zone. The expression of the migration can be inferred from the juxtaposition (Fig. 2.4) of lobes and channel-fills (Gardner et al., 2003; Macdonald et al., 2011b; Morris et al., 2014a; Grundvåg et al., 2014; Pyles et al., 2015). Lobes in lobe complexes may show variable stacking behaviour (Fig. 2.4), however longitudinal compensation of lobes has been previously largely overlooked (Pyles et al., 2015). Depositional cycles have been suggested by Gardner et al. (2003) based on the Brushy Canyon (US), with downdip extension due to channel propagation through

lobes and retreat due to filling and spilling of these same channel-elements. Among these studies (Gardner et al., 2003, Macdonald et al., 2011b; Morris et al., 2014a; Grundvåg et al., 2014; Pyles et al., 2015), the CLTZ is mostly defined by a surface or very limited deposits, instead of a rock volume with well-developed bedform features. Other studies have showed clear transitions from isolated and amalgamated scours to low aspect-ratio channels (Pemberton et al., 2016), indicating more significant CLTZ stratigraphy development.

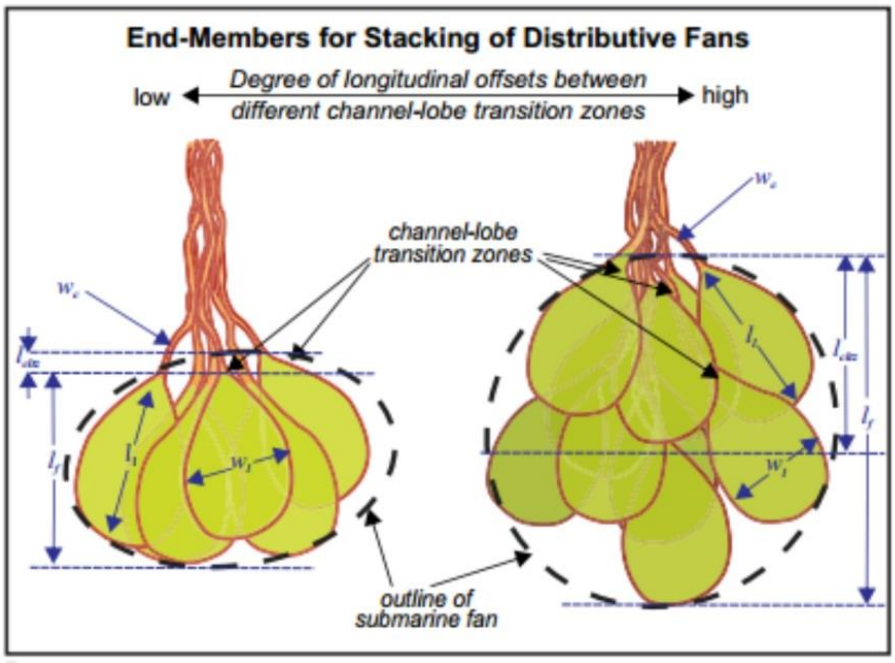

Figure 2.4 *End-member models for distributive submarine fans. One end member contains CLTZs that are located at a common longitudinal position on the fan (left), whereas the other end member contains CLTZs that are located at variable longitudinal locations on the fan (right) (from Pyles et al., 2015)*

2.3 Base-of-slope and CLTZ sedimentary process record

2.3.1 Flow divergence

Unconfined basin-floor environments are dominated by lobe deposition (e.g. Shanmugam and Moiola, 1991; Shanmugam et al., 1995; Bouma et al., 2000; Johnson et al., 2001; Hodgson et al., 2006; Prélat et al., 2009; Flint et al., 2011) and lower slope settings are characterised by channel-levee systems (e.g. Peakall et al., 2000; Posamentier, 2003; Posamentier and Kolla, 2003; Kane et al., 2007; Wynn et al., 2007; Di Celma et al., 2011;

Hodgson et al., 2011). Therefore, the area in between the slope and basin-floor (the base-of-slope) is prone to the development of CLTZs (e.g. Gardner et al., 2003; Hodgson et al., 2006; Brunt et al., 2013a; Van der Merwe et al., 2014). Flow expansion is expected at the base-of-slope, as divergent flow behaviour will result from the gradient and confinement changes in this region (Kneller, 1995). 'Non-uniform' flow behaviour (velocity changes over distance) is predicted at slope changes, where a decrease in slope can result in depletive and divergent flow (Kneller and Branney, 1995). Fluctuations in flow velocity over time are typically classified as 'unsteady' (Fig. 2.5), where waxing flows occur when velocity increases over time and waning when velocity decreases.

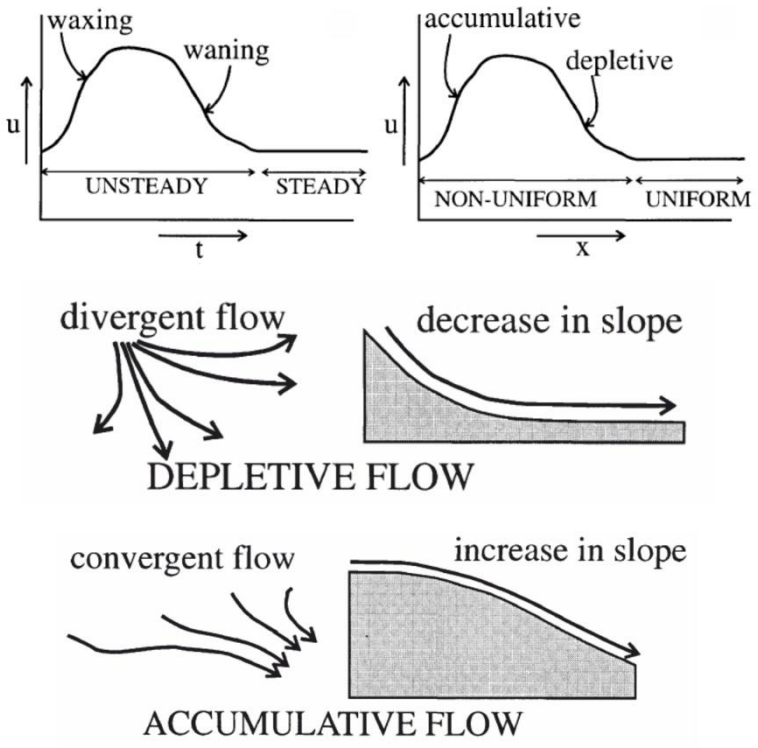

Figure 2.5 *(top) Graphs showing time (t) versus flow velocity (u) and distance (x) versus flow velocity (u) and the different terminology used to describe unsteady and non-uniform flow behaviour. (bottom) Diagram illustrating variance in flow behaviour depending on the type of gradient change. At the base-of-slope a decrease in slope is expected and therefore diverging and depletive flow behaviour (from Kneller et al., 1995)*

2.3.2 Froude-related fluctuations

Due to the diverging and depletive character of flows reaching base-of-slope and CLTZ environments, many have related sedimentary and bedform characteristics of these zones to Froude number (1) fluctuations (Mutti and Normark, 1987; 1991; Mulder and Alexander, 2001; Postma et al., 2009; Ito et al., 2014; Pemberton et al., 2016; Postma et al., 2016), and in particular around the critical Froude number (Fr = 1).The Froude number (1) is related to flow velocity (U), flow height (h) and the reduced gravity (g'), where the gravity constant (g) is influenced by the density difference between the flow mixture (ρ_{mix}) and the ambient fluid (ρ).

$$\mathrm{Fr}' = \frac{U}{\sqrt{g'h}} \quad g' = g\frac{\rho_{mix}-\rho}{\rho}\left[\frac{m}{s^2}\right] \qquad (1)\ (\textit{From Postma et al., 2009})$$

Some deposits within CLTZ settings have been associated with supercritical flow (Fr>1) conditions. For example, coarse-grained deposits within the canyon-fill (Ito et al., 2014) of the Boso Peninsula were interpreted to be formed under supercritical flow conditions from high-density turbidity currents.

Other features, and in particular bedforms (Alexander et al., 2001; Lang and Winsemann, 2013; Cartigny et al., 2011; 2014), are associated with a decelerating supercritical turbidity currents undergoing a hydraulic jump: The transition from supercritical conditions (Fr > 1) to subcritical conditions (Fr < 1) result in flow expansion and the formation of a standing wave. The development of backset bedding within scour-fills has been associated with flows undergoing a hydraulic jump (e.g. Ito et al., 2014; Postma et al., 2015). The accumulation of mudstone clast and pebbly sandstones has been linked to erosive turbidity currents generated by increased turbulence in association with the occurrence of a standing wave (Ito et al., 2014). A range of different bedforms (Cartigny et al., 2014), including cyclic steps, antidunes and chute-and-pool structures, have been experimentally linked to variance in the amplitude of Froude number fluctuations. It has been emphasised

that sediment waves are initially formed as antidunes (Morris et al., 1998; Wynn and Stow, 2002) or as net-depositional cyclic steps (Symons et al., 2016), defined by upstream migration. Upstream migrating scour trains (Fildani et al., 2006; Covault et al., 2014) have been interpreted as net-erosional cyclic steps and linked to channel formation. Differences in the architectural style of the CLTZ, as an area of channel-lobe juxtaposition, has also been related to the criticality of incoming flows (Postma et al., 2016). Postma et al. (2016) suggested that systems, which have been fed by supercritical flows, are architecturally much more complicated. They state that these systems are characterised by erosive channels, offset stacked lobes, hydraulic jump related mouth bars and upslope onlapping backfill deposits. Systems which are fed by subcritical flows are dominantly characterised by depositionally-confined channel systems and more simple architectures.

2.3.3 Rheological flow transformations

Next to Froude-related flow transformations, rheological flow transformations (Fig. 2.6) have also been proposed to occur at channel-mouth settings (Talling et al., 2007; Ito, 2008). The existence of hybrid event beds or linked debrites (Haughton et al., 2003; 2009; Hodgson, 2009; Baas et al., 2011) among submarine fan systems, representing a co-genetic sandy turbulent flow and muddy laminar flow is not well understood.

It has been suggested (Talling et al., 2007; Ito 2008) that these deposits are the result of downfan rheological transitions of turbidity currents to debris flow at CLTZ settings (Fig. 2.6). This transformation was interpreted to be triggered by the incorporation of many finer-grained clasts and sediments into a passing turbidity current by erosion of a muddy substrate, suppressing turbulence and increasing sediment concentrations in the near-bed flow layer. As intensive scouring is occurring at the CLTZ, the incorporation of muddy substrate and consecutive flow transformation is likely to occur in this region.

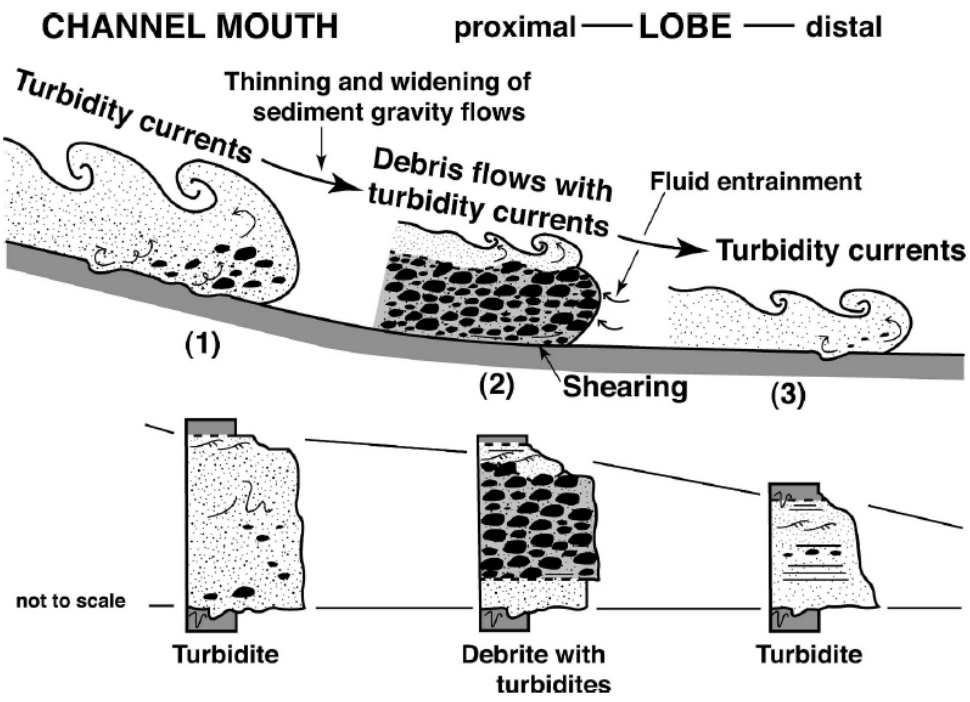

Figure 2.6 *Schematic model for a downfan rheological transition from the channel mouth towards a distal lobe setting, proposed for the Lower-Pleistocene Otadai Formation. In the proximal Lobe setting, a stratified flow exists with a relative dilute turbidity current overriding a clast-rich debris flow (from Ito, 2008)*

2.3.4 Sediment bypass record

Turbidity currents generally become depletive when diverging at channel-mouth settings (Kneller,1995) and may show rapid deposition due to the occurrence of a hydraulic jump (e.g. Russell and Arnott, 2003; Kostic and Parker, 2006; Postma et al., 2009). However, the existence of a transition zone (CLTZ) in between a channel/canyon and a lobe indicates an area dominated by sediment bypass (Wynn et al., 2002a; Stevenson et al., 2015). Evidence of sediment bypass is recorded in the sedimentary characteristics and bedform assemblage of this zone. In this thesis, we define sediment bypass (Stevenson et al., 2015) as a net state of no or a negligible amount of deposition/erosion by a flow, being the result of either a single or multiple flows. Downdip bed thickness increase and a general lack of siltstones have been linked to active bypassing processes of turbidity currents at proximal environments (Ito et al., 2014). Mud-drapes within scour-fills have been related to the

bypass of high-density turbidity currents and subsequent deposition of fine-grained materials by depletive waning flows (Mutti and Normark, 1987; 1991; Morris and Normark ,2000; Kane et al., 2009; Ito et al., 2014; Stevenson et al., 2015). Furthermore, the presence of isolated dunes has been interpreted to be created by sediment reworking of lag deposits by bypassing turbidity currents (Ito et al., 2014).

2.3.5 Flow efficiency

The character of the CLTZ has also been related to other basic flow factors, except for the criticality of the incoming flows (Postma et al., 2016), such as grain size distribution or sediment concentration, said to be controlling the efficiency of the flows exiting the channel-mouth (Mutti and Normark, 1987; Wynn et al., 2002a; Gardner et al., 2003). In high-efficiency systems, the CLTZ is predicted to be widely developed (Mutti and Normark, 1987; Wynn et al., 2002a), while in non-efficient systems lobes may be directly connected to their feeder channels. Gardner et al. (2003) linked the limited development of CLTZ features in the Brushy Canyon Formation (Texas, USA) to low-concentration and low-volume sandy flows, representing low-efficient conditions. Experimental studies looking at depositional bodies linked to a sudden loss in confinement, performed by Baas et al. (2004) suggested a strong relationship between grain size and CLTZ development. Flows containing a significant mud-component resulted in a much better developed CLTZ (Fig. 2.7) with clear disconnection of the lobe and the channel. The CLTZ varied laterally from showing gradual thickness changes towards the lobe at the levees and quite an abrupt transition at the central sections of channels. In general, grain size decreased gradually in the down-current direction, but near the CLTZ grain size decreased rapidly.

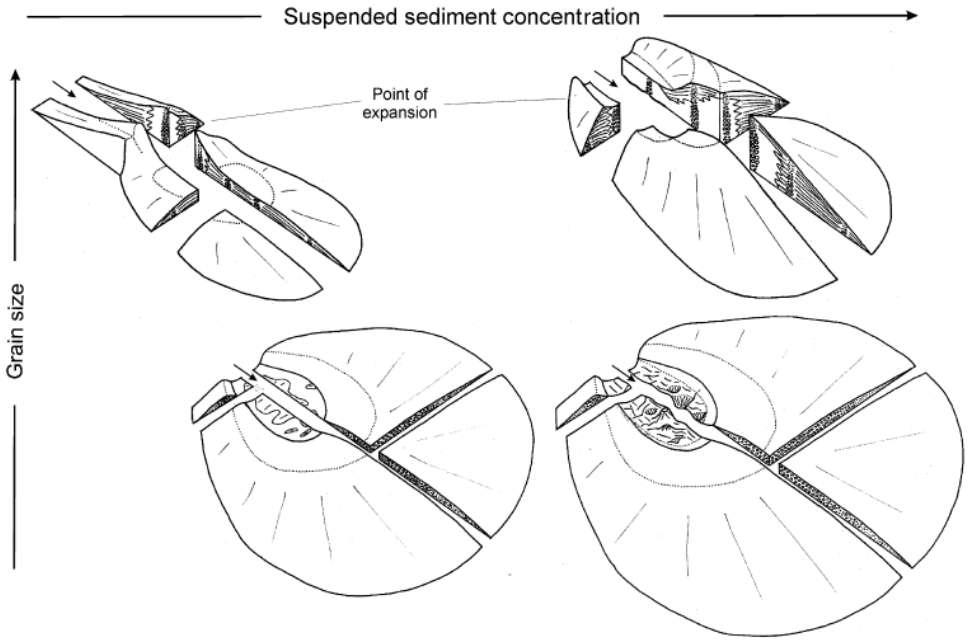

Figure 2.7 *Model for fan morphology from depletive flows, separated by grain size and initial sediment concentration. A clear wedge-shaped expansion point can be observed with coarse-grained low-concentrated flows, whereas fine-grained flows result in more extensive CLTZ development (from Baas et al., 2004)*

2.4 Inconsistencies between ancient and recent system datasets

As the CLTZ is a physiographic area, its expression in the modern as an assemblage of erosional and depositional bedforms is well constrained (e.g. Palanques et al., 1995; Wynn et al., 2002a; Bonnel et al., 2005). However, the transfer of this snapshot configuration into the rock record is an ongoing area of investigation. Our current understanding of the stratigraphic expression of CLTZs (Mutti and Normark, 1987; 1991; Ito et al., 2014) shows clear inconsistencies with elements characteristic of modern CLTZs (Fig. 2.8). Most elements recognised in recent systems are an order of magnitude larger compared to similar examples from the rock record (Fig. 2.8) (Wynn et al., 2002a; Ito et al., 2014). A wider variety of elements are known from the modern (Wynn et al., 2002a), of which some have not yet been described from the ancient. This includes mounds, reworked sands, lineations, variable scour geometries and there are only vary scarce observations of

sediment waves from ancient CLTZ settings (Vicente Bravo and Robles, 1995; Ito et al., 2014; Pemberton et al., 2016), mostly lacking detail or the wider lateral constraint . The big scale of the bathymetric and acoustic backscatter datasets allows a thorough examination of channel to lobe transitions and submarine fans in general, but is also directly a limitation due to the lack of resolution for imaging high-resolution deep-water bedforms. Therefore, our understanding of the modern expression of the CLTZ is mostly limited by the resolution of sonar and shallow seismic datasets (Wynn et al., 2002a), which explain why sub-metre scale features have not been described among modern systems.

Some reasons have been given why larger features, such as amalgamated scours and sediment waves recognised within the modern, have not yet been described from the rock record. The lack of large scour-fills within the outcrop record has been related to the difficulty to differentiate them from channel-fills in purely 2D-transect views (Mutti and Normark, 1987; Wynn et al., 2002a). Modern systems have revealed complicated scour-fill histories where laterally adjacent scours do not necessarily evolve simultaneously and may show different infill patterns (Macdonald et al., 2011a).

Furthermore, scour-fill sedimentation can be typically out-of-phase with external areas (Macdonald et al., 2011a). Clear recognition criteria are, however, still lacking for the differentiation of scour-fills from channel-fills. A lack of sediment waves within the outcrop record has been primarily related to their large wavelength (Piper and Konopoulos, 1994), making it difficult to recognise these bedforms within laterally limited outcrop expressions.

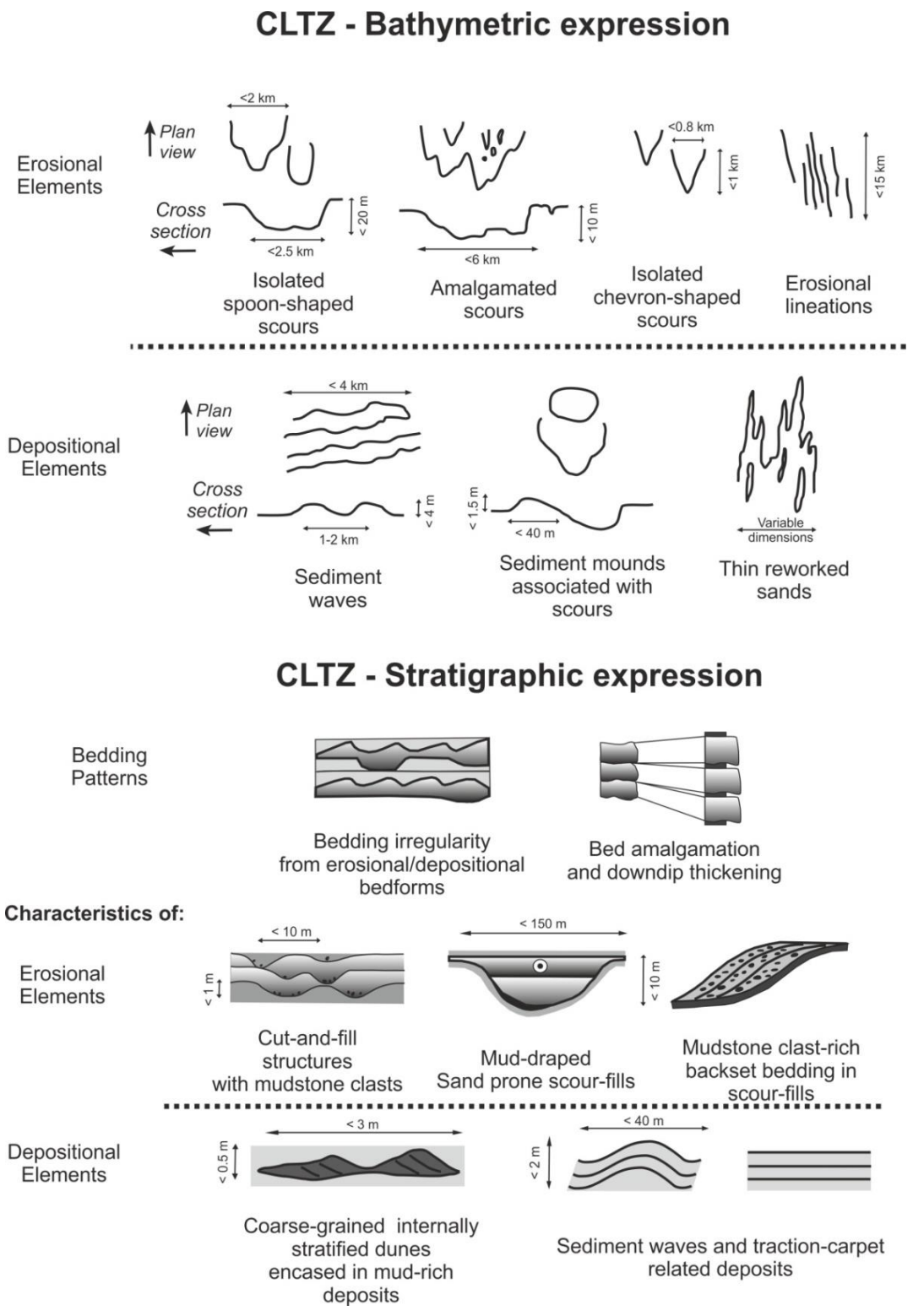

Figure 2.8 *Comparison between stratigraphic expression (from Mutti and Normark, 1987; Ito et al., 2014) and bathymetric expression of CLTZ with division in erosional and depositional elements (from Wynn et al., 2002a). There is clear inconsistency in both dimensions as well as the type of elements.*

2.4.1 Lack of spatial constraint in the CLTZ stratigraphic record

The modern expression of CLTZs only provides a timeslice of a dynamic and evolving system and is therefore not sufficient for understanding responsible processes and how CLTZs are transferred into the rock record. There is a significant on-going discussion into the importance of distinguishing between stratigraphic surfaces that are time transgressive and composite, and geomorphic surfaces that are rarely preserved in the rock record (e.g. Strong and Paola, 2009; Sylvester et al., 2011; Holbrook and Bhattacharya, 2012; Blum et al., 2013; Hodgson et al., 2016). This distinction between physiographic snapshot and stratigraphic transfer is important in understanding the preservation potential of CLTZs. The existing stratigraphic studies (Mutti and Normark, 1987; 1991; Ito et al., 2014) summarise elements associated with these zones, but fail to cover the relationship between different elements and their relative spatial and temporal distribution. It remains unclear how the spatial distribution of elements, such has been observed in the modern (Wynn et al., 2002a), is recorded in the stratigraphic record when the CLTZ is likely migrating and changing in character. When key facies criteria and stacking patterns can be defined due to the recognition of such features in outcrop, it will aid the recognition of CLTZs within 1D core records.

Chapter 3:
Tectonostratigraphy of the SW Karoo Basin and deep-water architectural and facies framework

The tectonostratigraphic development of the Western Cape, and the whole of the southern African continent, can be related to the evolution of western Gondwana (Grunow et al., 1996; Unrug, 1997; Tankard et al., 2009; Flint et al. 2011) (Fig. 3.1). Much of the late Palaeozoic tectonostratigraphic record has been removed in the southern parts of present South Africa, due to large-scale exhumation during regional Mesozoic strike-slip and extensional tectonics. The record in the Western Cape is therefore less complete than in other parts (Fig. 3.1) of western Gondwana, including South America and Antarctica (Flint et al., 2011).

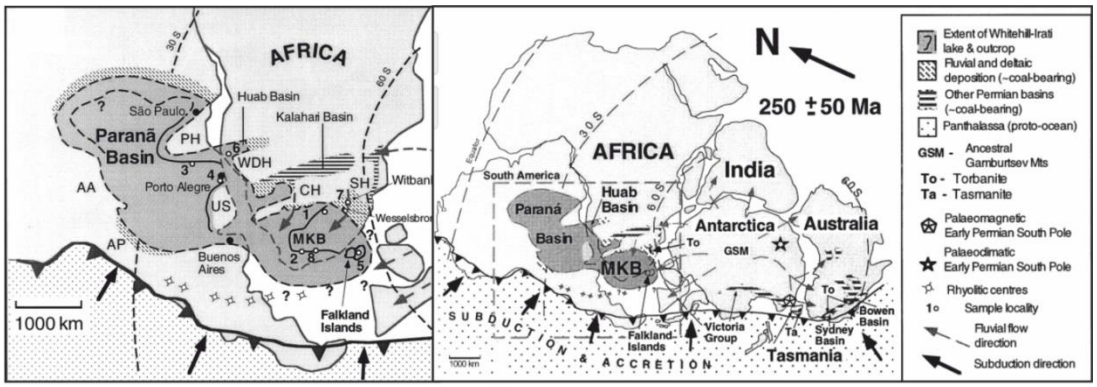

Figure 3.1 *Overview of the extent of the Paraná, Huab and Main Karoo Basin (MKB - here referred to as Karoo Basin) and the Falkland Islands in southwestern Gondwana, in a 250±50 Ma palinspastic position (modified from Faure and Cole, 1999).*

Two sedimentary mega-successions (the Cape and Karoo Supergroups) from the Early Ordovician to Early Jurassic are separated by a major unconformity and were deposited in two laterally offset sedimentary basins in southern Africa, the Cape and Karoo Basins (Visser, 1997; Tankard et al., 2009): The Cape Supergroup (Fig. 3.2) comprises an 8 km-thick succession of Early Ordovician to Early Carboniferous shallow marine, deltaic and

fluvial deposits (Veevers et al., 1994) that was derived from a cratonic source to the north (Tankard et al., 1982). The Karoo Supergroup (Karoo Basin) (Fig. 3.2) overlies the Cape Supergroup and comprises 5.5 km of deep-marine to fluvial deposits that spans the Late Carboniferous to the early Jurassic. It was deposited in a series of smaller interconnected marine basins, linked to regional large-scale subsidence.

Initially the major southern Gondwana basins, including the Karoo Basin, were interpreted to have developed in the late Palaeozoic in response to accretionary tectonics along the southern margin of Gondwana (De Wit and Ransome, 1992; Veevers et al., 1994; López-Gamundi and Rossello, 1998). It was considered that the Karoo Basin developed as a retroarc foreland basin due to flexural subsidence driven by loading of the Cape Fold Belt (Fig. 3.2) lying along the southern margin of the basin (De Wit and Ransome, 1992; Cole, 1992; Veevers et al., 1994; Visser and Praekelt, 1996; Catuneaunu, 2004; Catuneaunu et al., 1998). More recently, the Cape Fold Belt has been interpreted as a younger feature with the help of provenance analyses (Johnson et al., 1997; Andersson et al., 2004; Van Lente, 2004) and tectonostratigraphic analyses (Tankard et al., 2009). Only the youngest sediments of the Beaufort Group and above match up with the Cape Fold Belt as a sedimentary source, according to sedimentary provenance data (Van Lente, 2004). Therefore the subsidence of the Karoo Basin during its deep water phase is more likely to have been controlled by dynamic topography related to subduction (Pysklywec and Mitrovica, 1999) and has been linked to mantle flow influenced by foundering of basement blocks (Tankard et al., 2009). At the time of deposition of the Ecca Group, these basement blocks may have acted as a buried basin boundary, influencing the position of the shelf edge (Tankard et al., 2009).

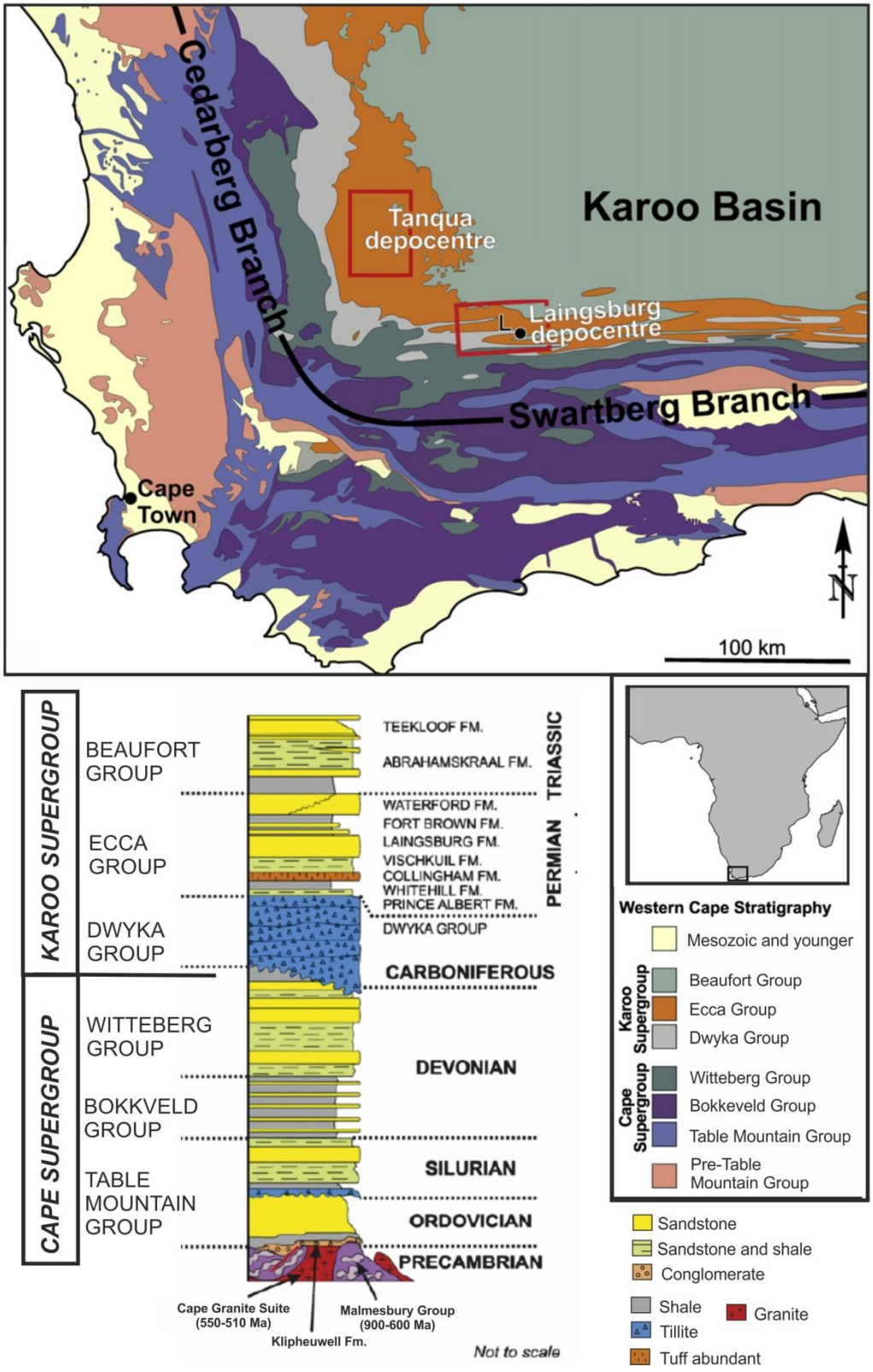

Figure 3.2 *(top) Regional geology of the Western Cape Province, showing location of the Laingsburg and Tanqua depocentres (red boxes), inboard of the post-depositional Cape Fold Belt. The Cape Fold Belt is subdivided into the Cederberg Branch and Swartberg Branch. The 'L' indicates the location of the town of Laingsburg. (bottom) Lithostratigraphy of the Western Cape area showing the division between the Cape Supergroup and the Karoo Supergroup (modified from Flint et al., 2011)*

3.1 Stratigraphic framework of the Karoo Supergroup

The late Carboniferous Dwyka Group is the oldest succession of the Karoo Supergroup (Fig. 3.2) and marks the onset of the Karoo Basin sedimentation, being comprised of an 800 m thick package of diamictites, varves and glacio-fluvial deposits (Visser, 1989; Visser and Young, 1990). A northern sediment source has been interpreted and the glacial sedimentation of the Dwyka Group coincided with the positioning of Gondwana around the South Pole (Visser, 1997) (Fig. 3.1). The Ecca Group is comprised of a 2 km-thick succession of Permian age and initiated post-glacial maximum, being predominantly composed of siliciclastic deposits (Wickens, 1994; Flint et al., 2011). The basal succession of the Ecca Group is slightly carbonaceous, being composed of claystones and cherty claystones with tidal carbonates of the Prince Albert Formation (< 180 m thick), overlain by organic-rich claystone of the Whitehill Formation (~30 m thick). The condensed nature of both these formations indicates low clastic supply rates during deposition (Flint et al., 2011). The overlying Collingham Formation (< 70 m thick) shows an increase in siliciclastic input and is composed of dark carbonaceous claystones interbedded with thin-bedded siliciclastic turbidites. These deposits are characterised by a high concentration of ash beds and a regionally extensive 1 metre thick chert bed (the Matjiesfontein chert), which is used as a stratigraphic marker due to its uniform thickness over at least 5000 km^2 (Flint et al., 2011).

The Upper Ecca Group was deposited in two depocentres (Fig. 3.2) within the southwestern Karoo Basin: the Laingsburg depocentre, which comprises the Vischkuil, Laingsburg, Fort Brown, and Waterford formations, and the Tanqua depocentre, which comprises the Tierberg, Skoorsteenberg, Kookfontein and Waterford formations (Wickens, 1994; Fig. 3.3). Both show a shallowing-upward succession from distal basin-floor through submarine slope to shelf edge and shelf deltaic settings (Wickens, 1994; Flint et al., 2011).

The deep-water infill of both depocentres show sand-rich fan systems separated by thick (1-20 m) claystones. The majority of these claystones have been interpreted to be of a hemipelagic origin (deposition by a combination of vertical settling and slow lateral advection; e.g. Stow and Tabrez, 1998), due to their regional extensive nature (tens of kilometres). Furthermore the presence of ash beds, lack of siltstone materials and high level of bioturbation in this claystone intervals deviates from the mudstone character as observed at initiation and retreat of submarine fan systems, indicating they have been deposited over long timescales.

3.1.1 Tanqua Depocentre

The Tanqua Depocentre is located in the present-day south-western corner of the Karoo Basin, and its fill is composed of both the Lower and Upper Ecca Group. The Tierberg Formation (> 600 m thick; King et al., 2009) marks the initiation of the deep-water fill of the Upper Ecca Group in the Tanqua depocentre (Fig. 3.3) and mainly comprises dark basinal mudstones (Bouma and Wickens, 1991; Wickens, 1994). The Skoorsteenberg Formation (~400 m thick) forms the main deep-water succession and is comprised of a total of four fine-grained and sand-rich submarine fan systems (Fans 1-4) (Bouma and Wickens, 1991; Wickens, 1994; Wickens and Bouma, 2000; Johnson et al., 2001; Hodgson et al., 2006) and one lower slope to base-of-slope unit (Unit 5) (Wild et al., 2005; Hodgson et al., 2006). Patterns of fan initiation, growth, decay and abandonment was identified within this succession based on basinward and landward movement of fan fringes, common to basin-floor fans (Hodgson et al., 2006). The grain size range is narrow within this formation, varying between mud and fine-grained sand. The Skoorsteenberg Formation is overlain by the Kookfontein Formation (~ 240 m thick) (Fig. 3.3) (Bouma and Wickens, 1991; Wickens, 1994), representing dominantly slope and shelf-edge deltaics (Wild et al., 2009) and the deltaic Waterford Formation (~120 m thick), marking the overall progradation of the sedimentary system to the northeast.

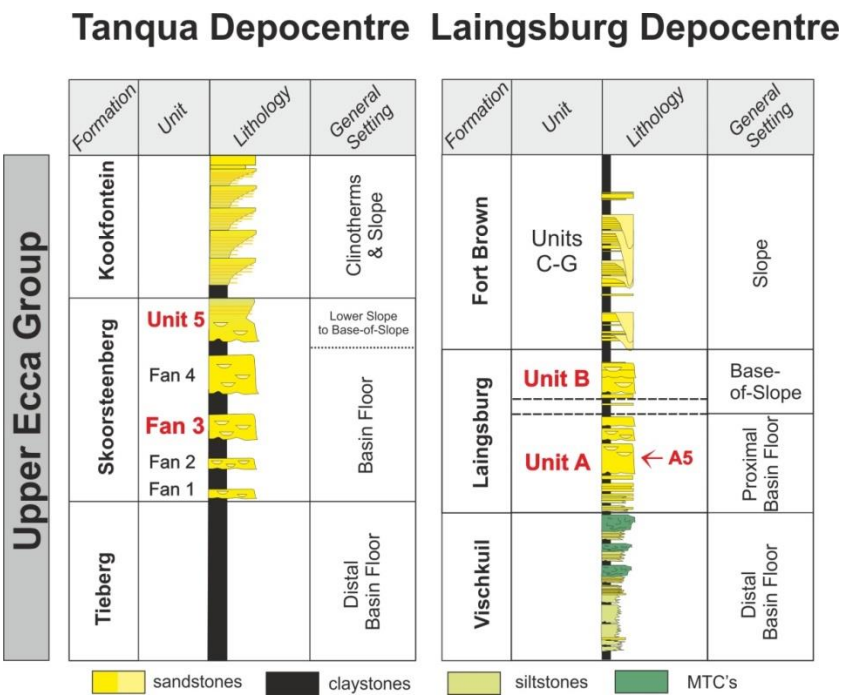

Figure 3.3 *Stratigraphic column of the deep-water deposits from the Laingsburg and Tanqua depocentres. The Fan systems and Units which have been studied in detail within this thesis are highlighted in red (modified from Hofstra et al., 2015)*

3.1.2 Laingsburg Depocentre

The Laingsburg Depocentre, also located in the south-western part of the Karoo Basin (Fig. 3.2), comprises a shallowing upward succession of the Vischkuil, Laingsburg, Fort Brown and Waterford Formations. The deep-water succession was initiated by distal basin plain turbidites, hemipelagic claystones and debrites of the Vischkuil Formation (< 270 m) (Kuenen, 1963; Theron, 1967; Van der Merwe, et al. 2009; 2010; 2011). The contact between the Vischkuil and Laingsburg Formations varies from an unconformity in the north of the depocentre to a correlative conformity in the south, which has been interpreted as evidence for basin-floor topography at this time (Sixsmith, 2000). The Laingsburg Formation (< 800 m) comprises two sand-rich turbiditic intervals (Unit A and Unit B), separated by a 40 m thick hemipelagic claystone interval (Wickens, 1994; Grecula, 2000; Flint et al., 2011). Of these sedimentary units, Unit A is the thickest (150-350 m) and can be subdivided in seven sandstone dominated packages of 15-100 m thickness (A1-A7), separated by regional hemipelagic mudstone and thin-bedded siltstone packages of 1-15 m

thickness. Mudstone units between A3-A4 and between A5-A6 are generally thicker, with a higher fraction of hemipelagic material. Coupled with regional stratal stacking patterns, this mudstone unit hierarchy was used by Flint et al. (2011) to group A1-A3 into a lowstand sequence set with the A3-A4 mudstone interpreted as the related transgressive and highstand sequence set; the combination forming a lower Unit A composite sequence. A4 and A5 were grouped into another lowstand sequence set and, together with the A5-A6 mudstone form a middle Unit A composite sequence. Similarly A6 and A7 are interpreted as a lowstand sequence set, and form an upper Unit A composite sequence with the lower part of the 40 m thick A-B mudstone.

The regional A-B mudstone contains a sharp-based and sharp-topped stratified fine-grained sandstone unit that is up to 15 m thick and lies 10 m below the base of Unit B (Grecula et al., 2003a) referred to as the A-B interfan. Unit B comprises a 50-225m thick sandstone-prone package. A base of slope setting for B in the area west of Laingsburg was interpreted by Grecula et al. (2003a) based on its stratigraphic position overlying the basin-floor fans of Unit A and being overlain by ~500 m of incised and levee-confined slope channel complexes (Grecula et al., 2003a; Flint et al., 2011). Two contemporaneous NE trending channel-levee systems that map down dip (eastward) to distributive deepwater systems are exposed within Unit B over a 25 km dip section, with strike control over some 20 km (Grecula et al., 2003a). Regional mapping combined with sedimentological and stratigraphic analysis indicates that Unit B comprises three depositional sequences (B1, B2, B3) (Grecula et al., 2003a; Brunt et al., 2013a).The overlying Fort Brown Formation is composed of five sand-prone units (Unit C-G) (Fig. 3.2) forming an overlying slope system and mud-prone prodelta succession (Flint et al., 2011; Hodgson et al., 2011; Van der Merwe et al., 2014). The Waterford Formation (< 800 m) (Wickens, 1994; Jones et al., 2013, 2015) comprises the top of the Ecca Group and is mainly defined by sand-prone shelf-edge deltaic deposits.

3.1.3 Sediment provenance

Despite the extent and thickness of the infill of both the Tanqua and Laingsburg depocentres, the sediment source is believed to be very similar throughout the whole stratigraphy (Andersson et al., 2004; Van Lente, 2004). Geochemical analyses have suggested that the deep-water sediments were derived from a felsic igneous source associated with an active continental-margin setting (Van Lente, 2004). Within the claystones between the sand-prone fan systems, a stratigraphic increase of igneous contributions has been observed (Andersson et al., 2004).

The most likely candidates for source terranes for both depocentres are believed to be the Sierra Pampeana granites and schists as well as the Patagonian batholith from the North Patagonian Massif (Van Lente, 2004; Fildani et al., 2007). There may have also been some contribution derived from the late Precambrian Cape Granite Suite (Van Lente, 2004).

The mineral composition of the sandstones is very similar throughout both depocentres with a major component of mono- and polycrystalline quartz (Scott et al., 2000) and minor amounts of feldspar, detrital muscovite and biotite and a wide variety of heavy minerals. Even though the transport pathway is inferred to be long and grain size range is very narrow (clay to fine sandstone), the sediments are still rather immature (Scott et al., 2000), showing mostly subrounded to subangular grains and minimal alteration of micas and feldspars.

3.2 Facies framework

The sedimentary facies of both the Skoorsteenberg Formation (Johnson et al., 2001; Hodgson et al., 2006; Prelat et al., 2009) and the Laingsburg Formation (Grecula et al., 2003a; 2003b; Sixsmith et al., 2004; Flint et al., 2011) have previously been described in detail. A brief summary of the lithofacies encountered within both formations from outcrop and core datasets is here presented. These lithofacies are combined into facies

associations in the following Chapters (4-8), used to define the environment of deposition among various architectural elements.

3.2.1 Structureless sandstone

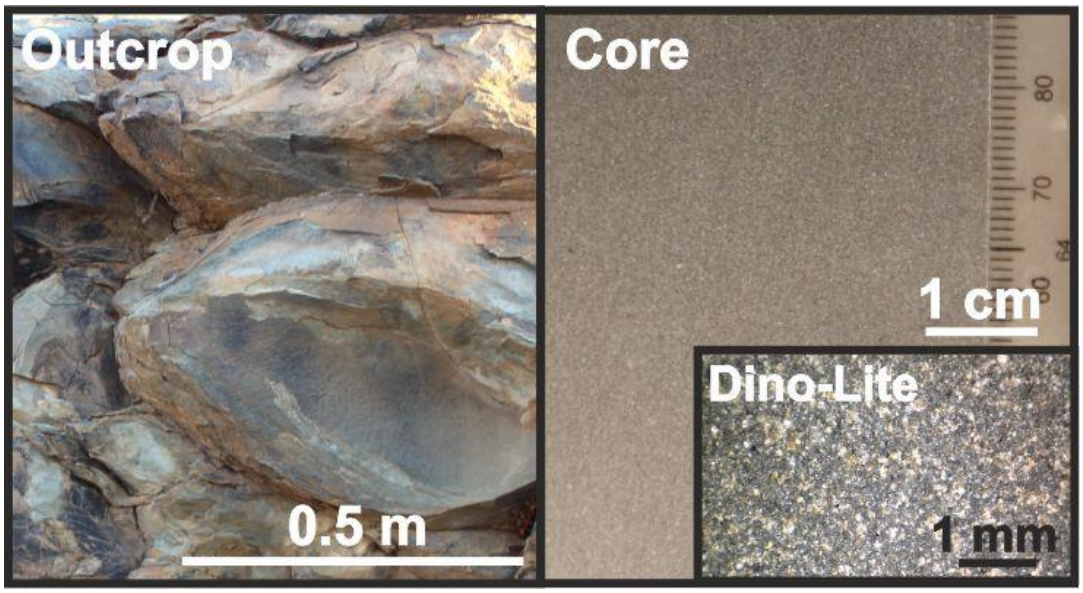

Figure 3.4 *Representative photographs from outcrop (left) and core (right) of structureless sandstone facies. The Dino-Lite image was taken from core.*

Feature	Characteristics and interpretation
Depositional environment	Channel-axis, lobe axis, frontal lobe fringe.
Description	Thick-bedded; Occasional dewatering pipes and dishes that are well preserved in core; widespread amalgamation along erosion surfaces; can contain mudstone chips and carbonaceous material. Grain size ranges from upper to lower fine sand, with rare medium sand.
Basal bounding surface	Sharp, erosive, loading.
Upper bounding surface	Sharp to normally graded.
Bed thickness	Variable <1 m to amalgamated sections of >10 m.
Outcrop width / geometry	Beds can be traced out for several 100s of metres.
Other aspects	Commonly found among Highly amalgamated zones (HAZ) that can pass laterally into stratified successions without bounding erosion surfaces.

Table 3.1 *Summary of the characteristics of structureless sandstone facies and its associated depositional environments.*

3.2.2 Planar-laminated sandstone

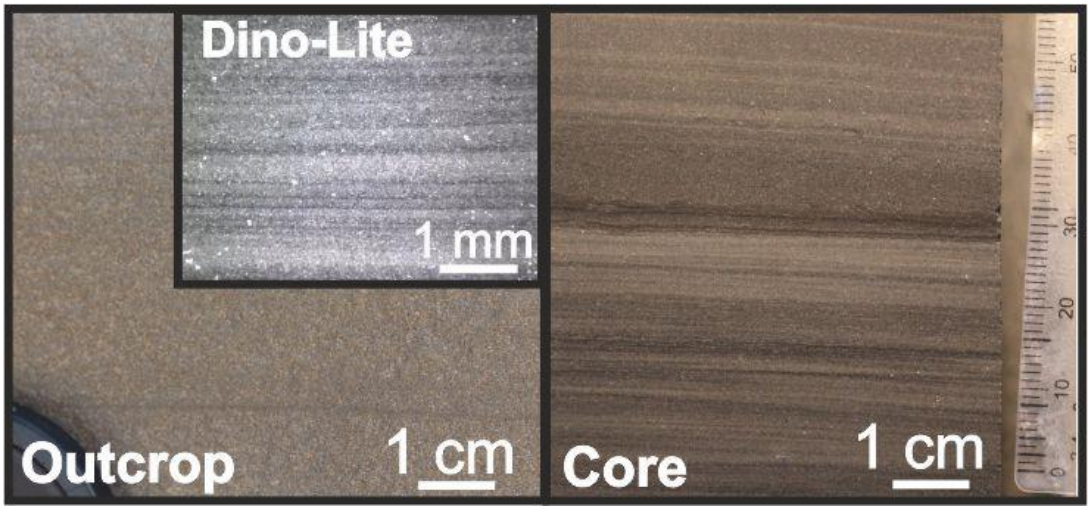

Figure 3.5 *Representative photographs from outcrop (left) and core (right) of planar-laminated sandstone facies. The Dino-Lite image was taken from core.*

Feature	Characteristics and interpretation
Depositional environment	Lobe axis, lobe off-axis, lobe fringe.
Description	Thick to medium bedded; planar parallel laminated; usually normal graded, lower fine sand and very fine sand.
Basal bounding surface	Sharp, loaded.
Upper bounding surface	Sharp to normally graded.
Bed thickness	0.1 m -1 m.
Outcrop width / geometry	Commonly part of lateral facies change to structureless thick-bedded sandstone or medium-bedded wavy ripple laminated sandstone
Other aspects	N/A

Table 3.2 *Summary of the characteristics of planar-laminated sandstone facies and its associated depositional environments.*

3.2.3 Wavy-laminated sandstone

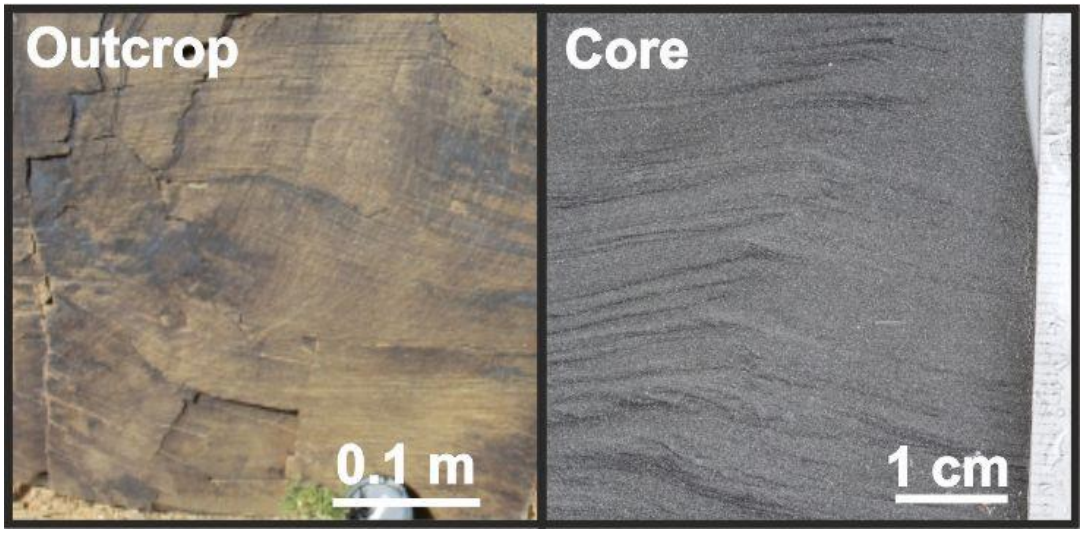

Figure 3.6 *Representative photographs from outcrop (left) and core (right) of wavy-laminated sandstone facies.*

Feature	Characteristics and interpretation
Depositional environment	Lobe off-axis
Description	Medium-to thin-bedded. Wavy/convolute laminated sandstones with wavelengths between 10-50 cm, can be asymmetric with steeper + shallower limbs. Increase upward within individual beds.
Basal bounding surface	Sharp, loaded.
Upper bounding surface	Sharp to gradational.
Bed thickness	0.1 m -1 m.
Outcrop width / geometry	Lateral and stratigraphic transition into current ripple and climbing ripple laminated sandstone.
Other aspects	N/A

Table 3.3 *Summary of the characteristics of wavy-laminated sandstone facies and its associated depositional environment.*

3.2.4 Ripple-laminated sandstone

A: Current ripple-laminated

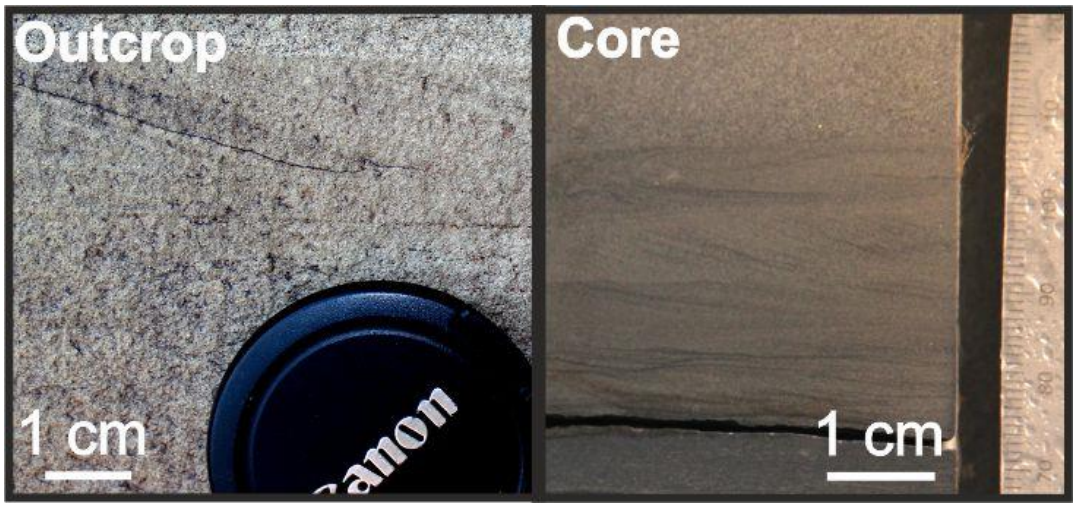

Figure 3.7 *Representative photographs from outcrop (left) and core (right) of current ripple-laminated sandstone facies.*

Feature	Characteristics and interpretation
Depositional environment	Lobe off axis, lobe lateral fringe, external levee/overbank.
Description	Medium to thin-bedded very fine to fine grained sandstone. Low angle to high angle ripple lamination. Stoss-side preservation is common. Grainsize is very fine and lower fine sand.
Basal bounding surface	Sharp.
Upper bounding surface	Sharp to gradational.
Bed thickness	0.05 m-1 m (up to 3.5 m in case of amalgamation).
Outcrop width / geometry	Lateral facies transition to planar laminated sandstone can occur. Extensive for several 100 ms. Amalgamation of multiple beds is common, creating greater (>1 m) bed thicknesses.
Other aspects	N/A

Table 3.4 *Summary of the characteristics of current ripple-laminated sandstone facies and its associated depositional environments.*

B: Climbing ripple-laminated

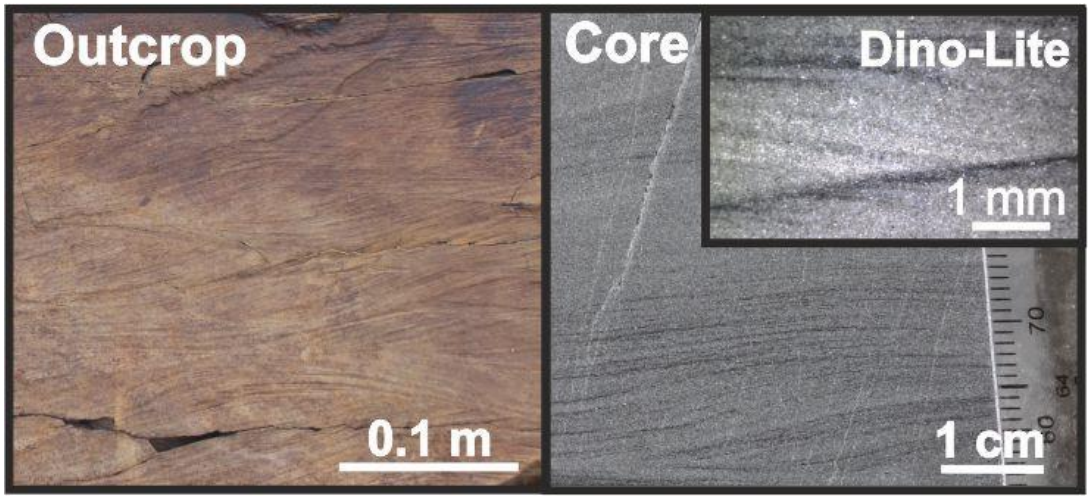

Figure 3.8 *Representative photographs from outcrop (left) and core (right) of climbing ripple-laminated sandstone facies. The Dino-Lite image was taken from core.*

Feature	Characteristics and interpretation
Depositional environment	Lobe off axis, lobe fringe, overbank.
Description	Medium-to-thin-bedded very fine to fine grained sandstone. Ripple foresets can be draped by silt; grainsize very fine and lower fine sand.
Basal bounding surface	Sharp.
Upper bounding surface	Sharp to gradational.
Bed thickness	0.05 m to ~1 m, but commonly 0.1-0.2 m.
Outcrop width / geometry	Extensive for several 10s metres, facies transitions towards climbing ripple lamination or planar lamination.
Other aspects	N/A

Table 3.5 *Summary of the characteristics of climbing ripple-laminated sandstone facies and its associated depositional environments.*

3.2.5 Siltstones

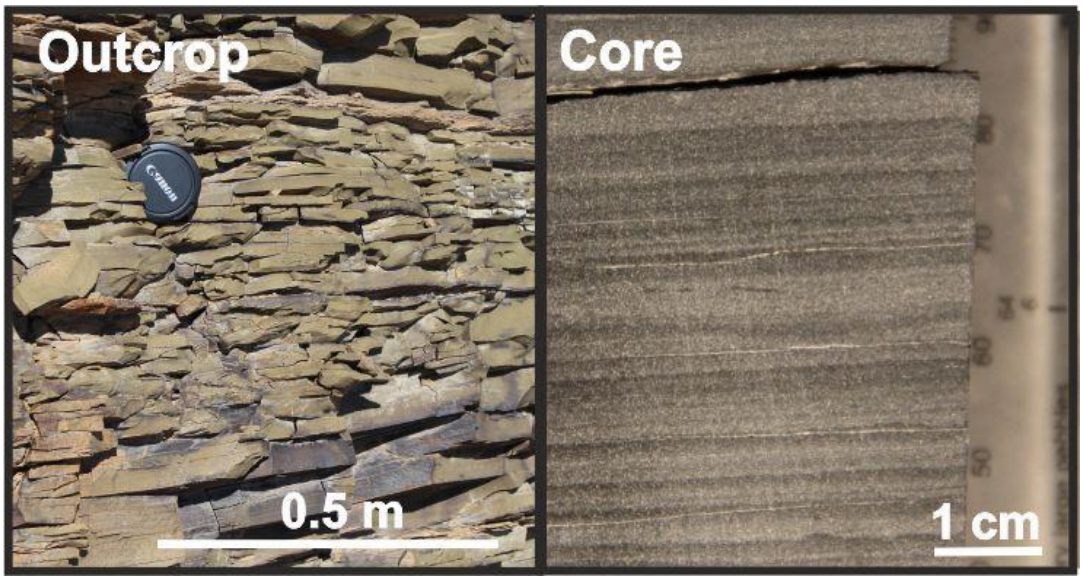

Figure 3.9 *Representative photographs from outcrop (left) and core (right) of siltstone facies.*

Feature	Characteristics and interpretation
Depositional environment	Lobe fringe, bypass-dominated areas.
Description	Normally planar bedded. Rare ripples. Interbedded very fine-grained sandstone beds.
Basal bounding surface	Sharp.
Upper bounding surface	Sharp to transitional.
Bed thickness	Individual beds are typically <0.05 m, Packages that range from 0.1m to >10 m in thickness.
Outcrop width / geometry	Packages can be traced for several kilometres.
Other aspects	Constant sedimentary characteristics throughout the package

Table 3.6 *Summary of the characteristics of siltstone facies and its associated depositional environments.*

3.2.6 Folded siltstones and sandstones

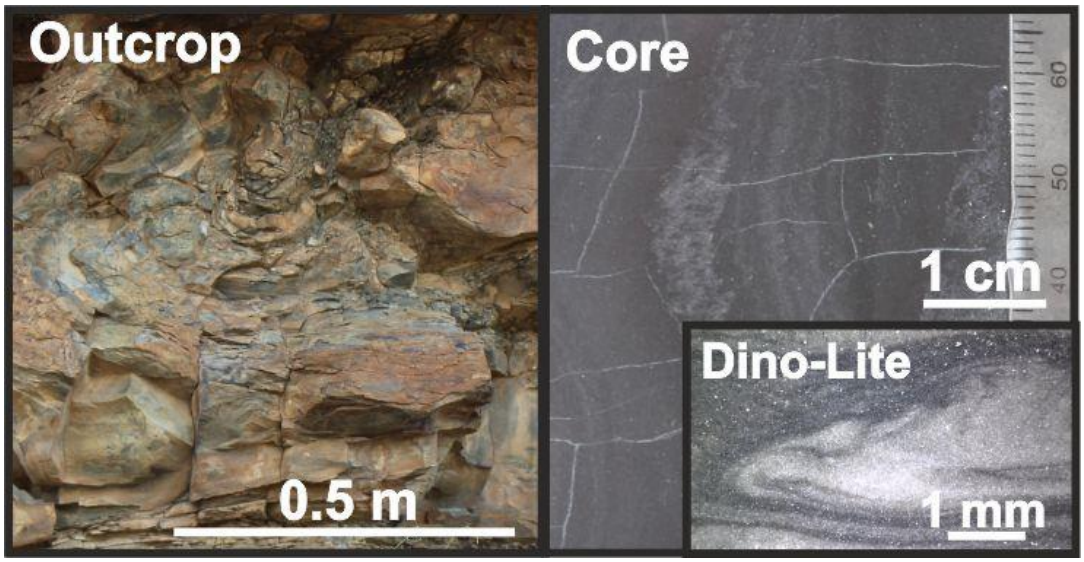

Figure 3.10 *Representative photographs from outcrop (left) and core (right) of folded siltstones and sandstones facies. The Dino-Lite image was taken from core.*

Feature	Characteristics and interpretation
Depositional environment	Slide deposits, channel margin, scour margin.
Description	Weak deformation to highly contoured and folded thin bedded sandstone and siltstone beds.
Basal bounding surface	Sharp to erosional.
Upper bounding surface	Sharp to gradational.
Outcrop thickness	from 10s cm to 10s metres.
Outcrop width / geometry	>5 kms
Other aspects	N/A

Table 3.7 *Summary of the characteristics of folded sandstones and siltstones facies and its associated depositional environments.*

3.2.7 Claystones

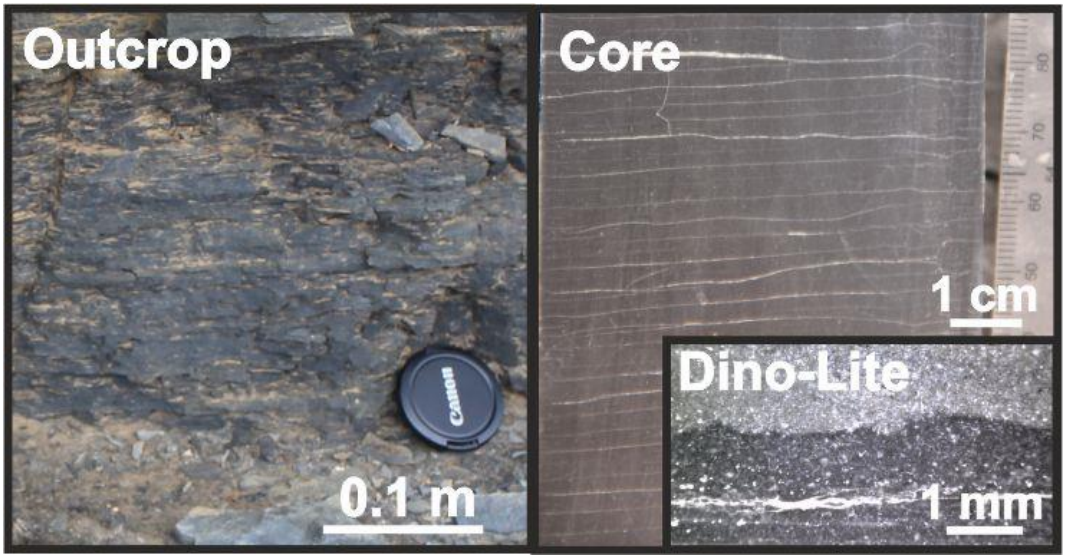

Figure 3.11 *Representative photographs from outcrop (left) and core (right) of claystone facies. The Dino-Lite image was taken from core.*

Feature	Characteristics and interpretation
Depositional environment	Hemipelagic background sedimentation.
Description	Little to no internal stratification seen at outcrop. Thin laminations of very fine silt may be seen in fresh surfaces.
Basal bounding surface	Normally gradational, occasionally sharp.
Upper bounding surface	Sharp, occasionally erosional.
Outcrop thickness	Variable, from 10s cm to several metres.
Outcrop width / geometry	Extensive, locally eroded.
Other aspects	N/A

Table 3.8 *Summary of the characteristics of claystone facies and its associated depositional environment.*

3.2.8 Intraclast conglomerate

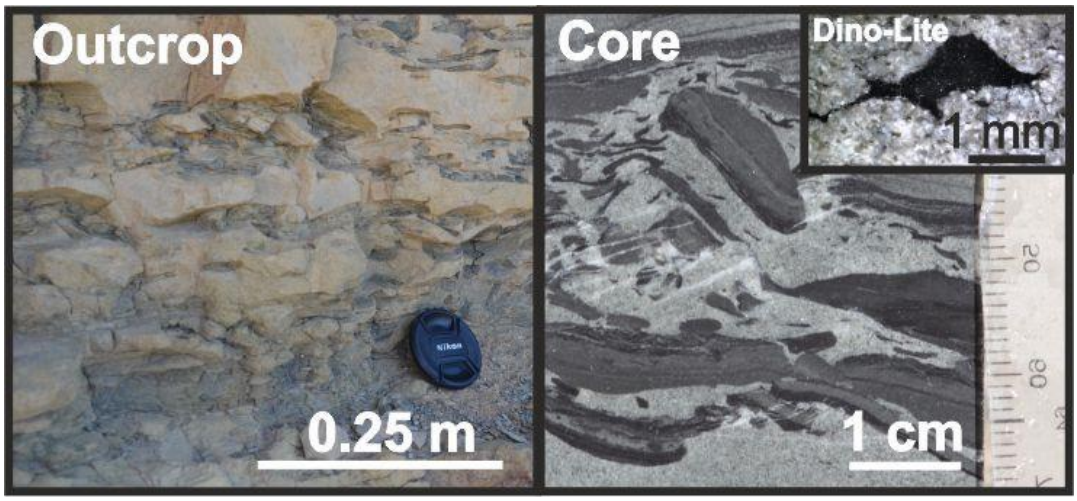

Figure 3.12 *Representative photographs from outcrop (left) and core (right) of intraclast conglomerate facies. The Dino-Lite image was taken from core.*

Feature	Characteristics and interpretation
Depositional environment	Channel-fill, lobe axis, bypass areas.
Description	Angular to sub-rounded claystone and siltstone clasts supported by sandstone matrix. Locally clast supported.
Basal bounding surface	Sharp, erosional.
Upper bounding surface	Sharp.
Outcrop thickness	10s cm to metres.
Outcrop width / geometry	Commonly limited by erosion surfaces, lenticular shaped.
Other aspects	N/A

Table 3.9 *Summary of the characteristics of intraclast conglomerate facies and its associated depositional environments.*

3.2.9 Banded sandstone

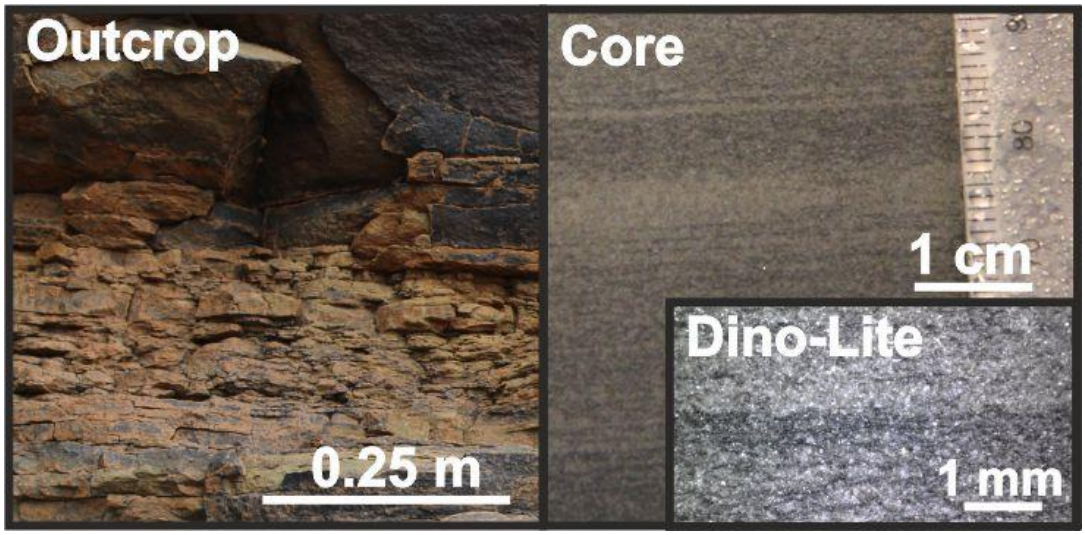

Figure 3.13 *Representative photographs from outcrop (left) and core (right) of banded sandstone facies. The Dino-Lite image was taken from core.*

Feature	Characteristics and interpretation
Depositional environment	Lobe axis, lobe off-axis
Description	Alternating layers of clean and mud-rich sandstone bands. Clean layers can load into the mud-rich ones. Occasionally mud chips, carbonaceous material and/or plant fragments in mud-rich bands.
Basal bounding surface	Sharp to transitional
Upper bounding surface	Sharp, gradational
Outcrop thickness	From 0.1m up to several metres when beds are amalgamated
Outcrop width / geometry	Can be associated with overlying ripple laminations or chaotic sandstone/siltstone. Extensive for 10s metres.
Other aspects	N/A

Table 3.10 *Summary of the characteristics of banded sandstone facies and its associated depositional environments.*

3.3 Architectural element framework

Many deep-water studies within the Karoo Basin have focussed on the identification and characterisation of architectural elements (e.g. Johnson et al. 2001; Hodgson et al. 2006; Grecula et al. 2003a; Prélat et al. 2009; Brunt et al. 2013a). The most important elements within these deep-water fan systems will be briefly discussed.

3.3.1 Lobes

Early lobe models (Mutti, 1977; Mutti and Sonnino, 1981) created a division within two main domains: 'sandstone lobe' (characterised by a high sandstone percentage) and 'lobe fringe' (characterised by a lower sandstone percentage). In the scheme of Mutti (1977), the central 'sandstone lobe' represents approximately one third of the total areal extent of the lobe while the 'lobe fringe' represents the other two thirds. The internal architecture of lobes is commonly described as highly continuous deposits with a parallel-sided bedding style (Chapin et al., 1994; Mahaffie, 1994).

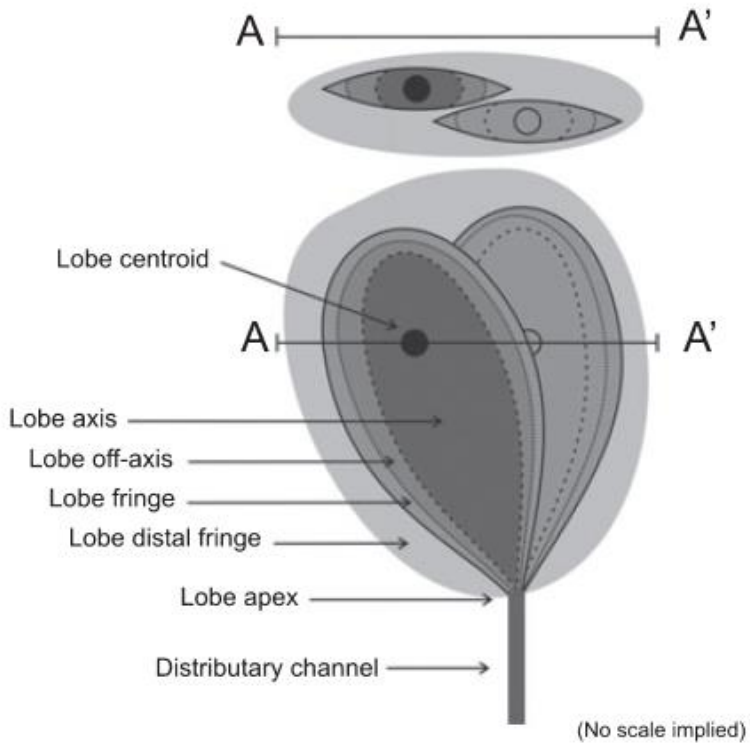

Figure 3.14 *Schematic showing nomenclature used to describe different lobe components and environments (from Prélat et al., 2009)*

Recent work indicates a more complicated depositional architecture (Prélat et al., 2009), with four environments of deposition (Fig. 3.4) in a single lobe: axis, off-axis, fringe, and distal fringe. Among basin-floor lobes, these four depositional environments do not have a simple radial distribution about an apex or from the lobe centroid, but are organised in a complicated finger like distribution. As a result, in dip and strike directions, it is possible to transition back and forth between the same environments of deposition, formed by the stacking of the component lobe elements (Fig. 3.5). Transitions between different environments of deposition occur without passing through erosional surfaces and can take place over short distances (< 100 m) (Prélat et al., 2009). Highly amalgamated zones (HAZs) are prone in lobe apex areas (Hodgson et al., 2006), described as a zone of increased amalgamation of sandstone beds, ranging between 3 and 20 m in thickness, 100 to 400 m in width, and up to 3 km in length, and pass laterally into more stratified deposits. HAZs have been interpreted as the down-dip equivalent of feeder channels, marking the transition from confined to unconfined environments (Hodgson et al., 2006).

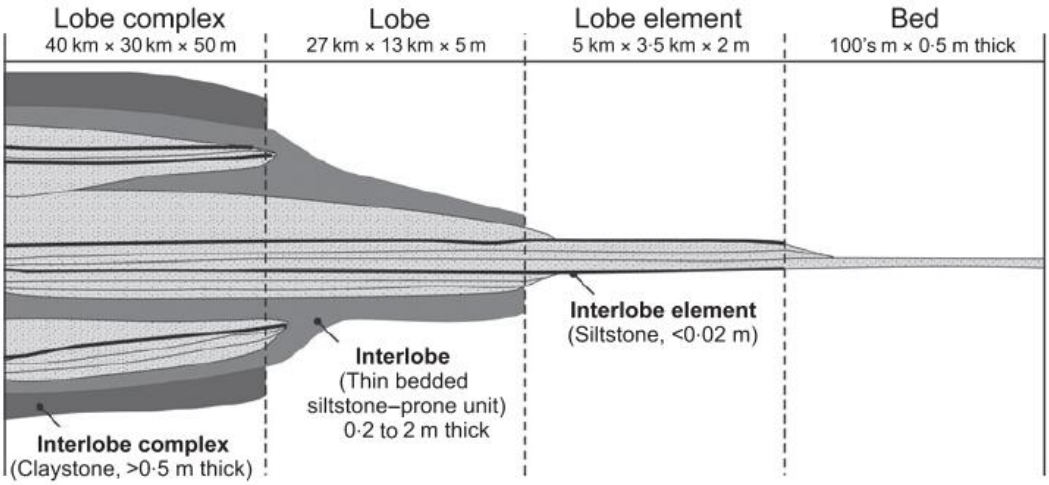

Figure 3.15 *Hierarchical scheme used to differentiate scales within distributive lobe systems (Prélat et al., 2009)*

Within the hierarchical scheme (Fig.3.5) for distributive systems proposed by Prélat et al. (2009), a lobe element (~2 m thick) is formed by a set of multiple event beds. Multiple lobe elements (2-3) typically form one lobe (~5 m thick). Lobes can stack to form lobe complexes (~50 m). Multiple lobe complexes eventually build up a submarine fan system. Different lobes and lobe elements are separated by thin-bedded siltstone-prone units. In the original scheme of Prélat et al. (2009) these were interpreted as interlobes and interlobe elements (Fig. 3.5), but collection of additional data led to their reinterpretation as distal lobe fringes of compensationally stacked lobes, where the abrupt facies changes in 1D-sections mark avulsion surfaces (Prélat and Hodgson, 2013).

3.3.2 Channel-fills

Another important architectural element within submarine fan systems, and in particular within slope and base-of-slope environments, are submarine channels. Channel systems at base-of-slope settings (Fig. 3.6) typically vary between 150- 500 m wide and 8 – 70 m in depth (e.g. Johnson et al., 2001; Van der Werff and Johnson, 2003; Hodgson et al., 2006; Brunt et al., 2013a) and can both be erosionally and constructionally confined, where the latter may show extensive levees over 20 km in width (Fig. 3.6).

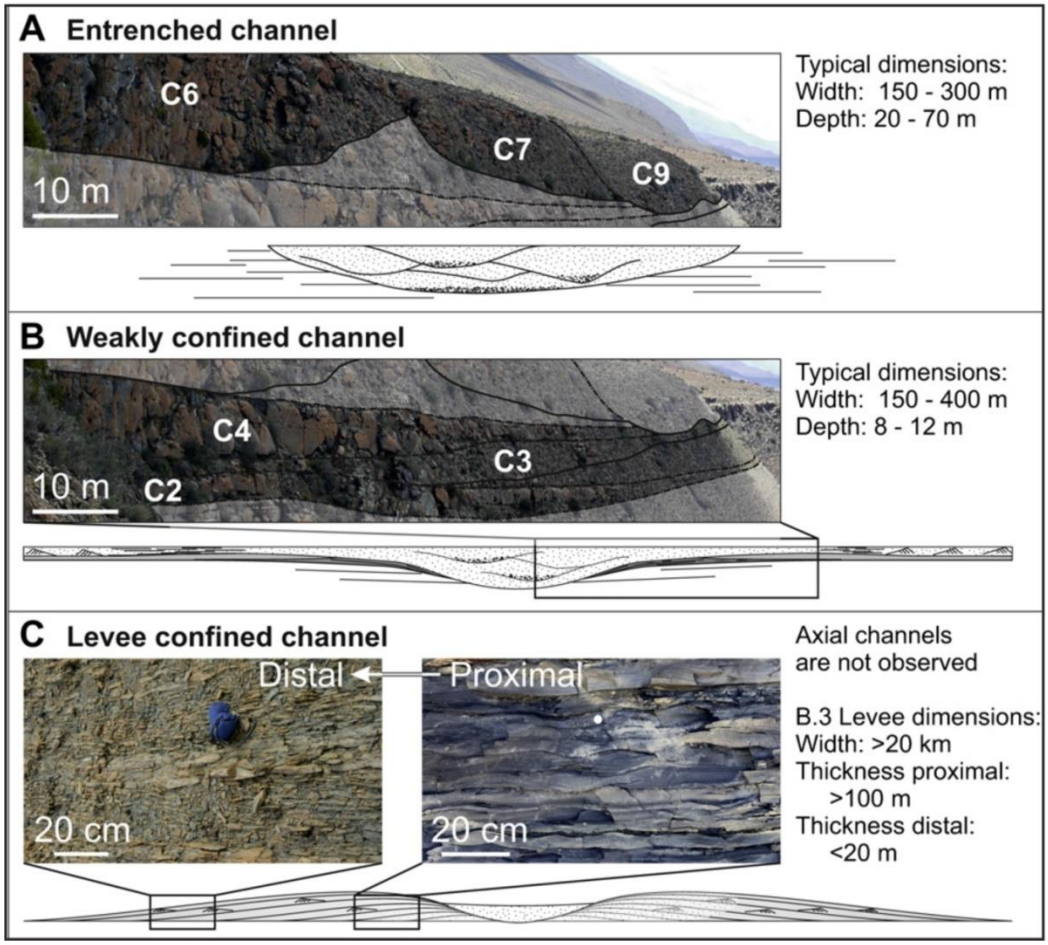

Figure 3.16 *Variance in channel architectures and dimensions among base-of-slope settings (from Brunt et al., 2013a)*

Weakly confined channels contrast with entrenched channels as they show beds thinning away from the amalgamated channel axes and broad channel wings (Brunt et al., 2013a). Axial channel-fills show similar characteristics among the different channel architectures, being dominantly composed of amalgamated structureless sandstones with a basal layer of mudstone clast conglomerates (Johnson et al., 2001; Van der Werff and Johnson, 2003; Hodgson et al., 2006; Brunt et al., 2013a). Channel-margins are more variable in both architecture and facies. The margins of unconfined channels (Fig. 3.6) may show ripple-laminated or planar-laminated thin-bedded sandstones and siltstones, typically thickening and coarsening upward (Grecula et al., 2003a; Brunt et al., 2013a).

Chapter 4:
Giant scour-fills in ancient channel-lobe transition zones: formative processes and depositional architecture

4.1 Summary

Scours are common features of modern deep-marine seascapes, particularly downstream of the mouths of slope channels within channel-lobe transition zones (CLTZs). Their dimensions can easily exceed hundreds in width and length (100-2000 m), and tens of metres in depth (1-100m). However, the stratigraphic architecture of large (>100 m width) scours have not been described in detail from exhumed CLTZs. Here, the infill of two erosional features (0.5-1 km long and 15-20 m thick) from the Permian Karoo Basin succession, South Africa, are presented from palaeogeographically well-constrained CLTZs; one from Fan 3 in the Tanqua depocentre and one from Unit A5 in the Laingsburg depocentre. The basal erosion surfaces of the features are asymmetric with steep, undulating, and composite upstream margins, and low gradient simple downstream margins. The basal infill consists of thin-bedded siltstone and sandstone beds cut by closely-spaced scours; these beds are interpreted as partially reworked fine grained tails of bypassing flows with evidence for flow deflection. The erosional features are interpreted as giant scour-fills. The Unit A5 scour-fill shows a simple cut-and-fill history with lateral and upward transitions from siltstone- to sandstone-prone deposits. In contrast, the Fan 3 scour-fill shows headward erosion and lengthening of the scour surface suggesting temporal changes in the interaction between turbidity currents and the scour surface. This relationship could support the occurrence of a hydraulic jump during scour formation, while the majority of the fill represents deposition from subcritical flows. Different scour preservation mechanisms can be used to explain the style of infill. The architecture, sedimentary facies and palaeoflow patterns of the scour-fills are distinctly different to well documented adjacent basin-floor channel-fills at the same stratigraphic levels. The recognition of scour-fills helps to constrain their sedimentological and stratigraphic

expression in the subsurface, and to improve our understanding of the stratigraphic architecture of channel-lobe transition zones.

4.2 Introduction

Large scours are readily recognised erosional bedforms on modern deep-marine seabeds (e.g., Palanques et al., 1995; Morris et al., 1998; Wynn et al., 2002a; Bonnel et al., 2005; Fildani et al., 2006; Macdonald et al., 2011a; Maier et al., 2011; Shaw et al., 2013; Covault et al., 2014; Paull et al., 2014). Commonly, these scours are concentrated within channel-lobe transition zones (CLTZs), a relatively unconfined area dominated by sediment bypass that separates the mouths of channel feeder systems from lobes (Mutti and Normark, 1987, 1991; Kenyon et al., 1995; Wynn et al., 2002a). Scours commonly form fields consisting of many individual and coalesced scours (e.g., Wynn et al., 2002a; Macdonald et al., 2011a; Shaw et al., 2013). The occurrence of scours is commonly interpreted (Komar, 1971; Mutti and Normark, 1987, 1991; Garcia and Parker, 1989; Garcia, 1993; Macdonald et al., 2011a; Ito et al., 2014), and occasionally demonstrated (Sumner et al., 2013), to be related to flows that have undergone a hydraulic jump (transformation from supercritical to subcritical flow conditions), triggered by changes in flow velocity and/or density. These changes in flow behaviour are predicted to occur in base-of-slope to basin floor transitions where there are abrupt changes in gradient and degree of confinement (e.g., Alexander et al., 2008; Ito, 2008).

Although observations of small-scale scours and megaflutes in ancient systems are abundant (e.g., Macdonald et al., 2011a), large-scale features are not well documented. Megascours associated with Mass Transport Deposits (MTDs) have been constrained by various seismic examples (e.g., Moscardelli, 2006; Sawyer et al., 2009; Ortiz-Karpf et al., 2015) on slope settings and in some outcrop examples from lower slope to base-of-slope deposits (Pickering and Hilton, 1998, their Fig. 63; Lee et al., 2004; Dakin et al., 2012). In

these cases, erosional depressions are tens of metres deep and filled with chaotic deposits. In contrast, large scour-fills in turbidite systems are rarely identified in outcrop, therefore their recognition criteria are poorly constrained. Dimensions of turbidite-filled scours are reported from various outcrop-related studies including: 1) the Ross Formation (Ireland) with typical dimensions of 0.3-3.5 m in depth and 1 to 45 m in length (Chapin et al., 1994; Elliott, 2000a, 2000b; Lien et al., 2003; Macdonald et al., 2011b); 2) the Albian Black Flysch (Spain) with 1-5 m deep and 5-50 m wide scours (Vicente-Bravo and Robles, 1995); 3) the Cerro Toro Formation (Chile) with scour depths of metres and widths of tens of metres (Winn and Dott, 1979; Jobe et al., 2009); 4) the Windermere Group with scours up to several decimetres deep and several tens of centimetres to many tens of metres wide (Terlaky et al., 2015); 5) the composite scours of several metres depth in the Macigno Costiero Fm., Italy (Eggenhuisen et al., 2011); and 6) the Boso Peninsula (Japan) with erosional features filled with backset bedding up to 140 m wide and 10 m deep (Ito et al., 2014). These dimensions are an order of magnitude smaller than the scour dimensions described from modern systems (> 10 m depth and > 100 m width) (e.g., Wynn et al., 2002a; Macdonald et al., 2011a). Scour-fills may be underrepresented in the rock record because outcrop limitations mean that they may have been misidentified as channel-fills due to cross-sectional similarity (Mutti and Normark, 1987, 1991; Wynn et al., 2002a; Normark et al., 2009). Furthermore, the stratigraphic expression of the CLTZ, including scour-fills, is rarely fully exposed or well-constrained in ancient systems (Mutti and Normark, 1987, 1991; Gardner et al., 2003; Ito et al., 2014; van der Merwe et al., 2014).

Here, the morphology and depositional architecture of two exhumed large-scale erosional features from the Permian succession of the Karoo Basin, South Africa, are described in detail: one example from Fan 3 of the Tanqua depocentre and the other from Unit A within the Laingsburg depocentre. Previous mapping has constrained the palaeogeographic context of both locations to areas where there is a down-dip architectural change from

channel- to lobe-dominated deposits (Morris et al., 2000; Van Der Werff and Johnson, 2003; Sixsmith et al., 2004; Hodgson et al., 2006; Jobe et al., 2012; Prélat and Hodgson, 2013). The objectives of this paper are to: i) evaluate the origin of these distinctive erosional features; ii) compare the erosional and depositional history to channel-fills; iii) develop recognition criteria for scour-fills in outcrop; iv) discuss the role of erosional bedforms in improving our understanding of the stratigraphic expression of CLTZs within ancient submarine systems; and v) aid investigations into the role of hydraulic jumps in deep-water bedform development. Accurate recognition and description of large-scale erosional architectural elements has important implications for the robust application of outcrop studies to improve reservoir models and reduce uncertainty in subsurface investigations.

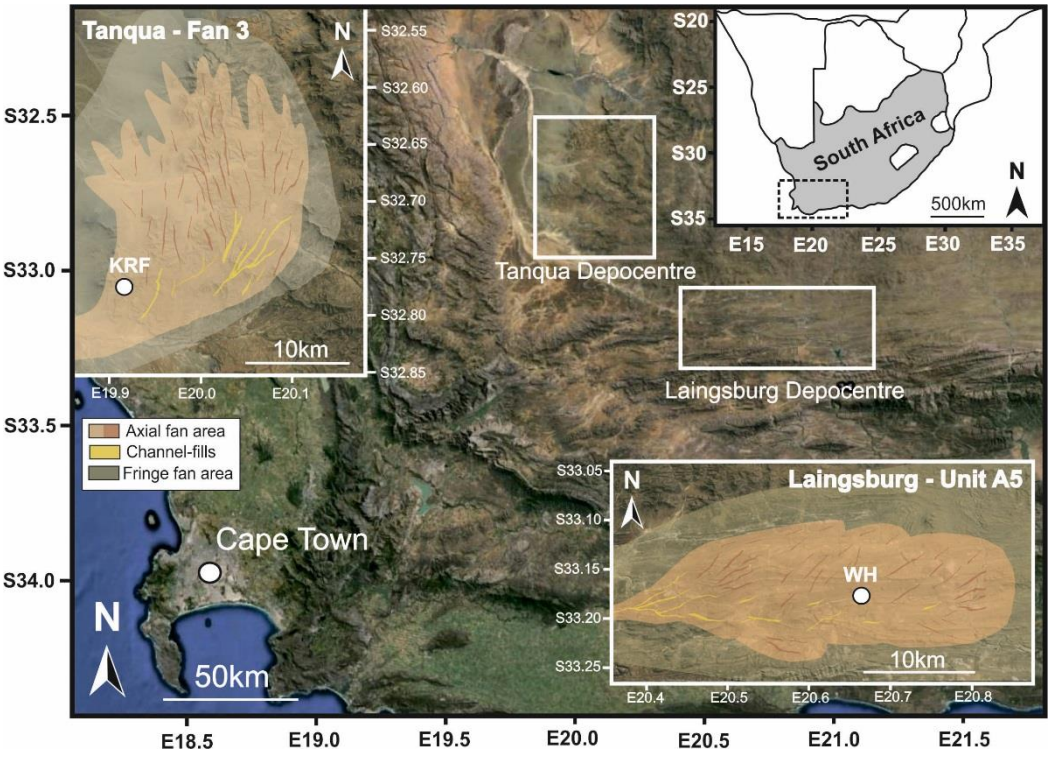

Figure 4.1 *Location map of the Laingsburg and Tanqua depocentres within the Western Cape (South Africa) and schematic interpretations of the Fan 3 and Unit A5 fan systems (based on Sixsmith et al.,2004) and Hodgson et al.,2006). White dots indicate study locations, with KRF = Kleine Riet Fontein and WH = Wilgerhout. Images taken from Google Earth.*

4.3 Regional setting

The Karoo Basin is one of a number of Late Palaeozoic to Mesozoic basins that formed at the southern margin of Gondwana (De Wit and Ransome, 1992; Veevers et al., 1994; López-Gamundi and Rossello, 1998). The Karoo Basin has been interpreted traditionally as a retroarc foreland basin with subsidence purely caused by the loading of the Cape Fold Belt (e.g., Johnson, 1991; Cole, 1992; Visser, 1993; Veevers et al., 1994; Catuneanu et al., 1998). More recent interpretations suggest that subsidence during the Permian was caused by dynamic topography effects due to subduction (Tankard et al., 2009) in a pre-foreland basin stage. The southwest Karoo Basin is subdivided into the Laingsburg and the Tanqua depocentres (Fig. 4.1) of which the deepwater fill of both depocentres is represented by the Ecca Group. The Ecca Group (Fig. 4.2) comprises a 2 km-thick shallowing-upward succession from distal basin-floor through submarine slope to shelf-edge and shelf deltaic settings (Wickens, 1994; Flint et al., 2011).

4.3.1 Tanqua depocentre

This study focuses on part of Fan 3 of the Skoorsteenberg Formation, which is one of four sand-rich basin-floor fan systems (Fig. 4.2) (Bouma and Wickens, 1991, 1994; Wickens and Bouma, 2000; Johnson et al., 2001). Fan 3 is the most extensively studied fan system of the Skoorsteenberg Formation, as it shows the most complete outcrop extent (Hodgson et al., 2006). The Fan 3 study area, Kleine Riet Fontein, is located in the southwestern corner of the Fan 3 outcrop, which is the most updip location (Figs. 4.1, 4.3A). An integrated outcrop and research borehole dataset has established the isopach thickness of Fan 3, and the relative spatial and temporal distribution of sedimentary facies, architectural elements and palaeocurrents (Johnson et al., 2001; Hodgson et al., 2006; Prélat et al., 2009; Groenenberg et al., 2010).

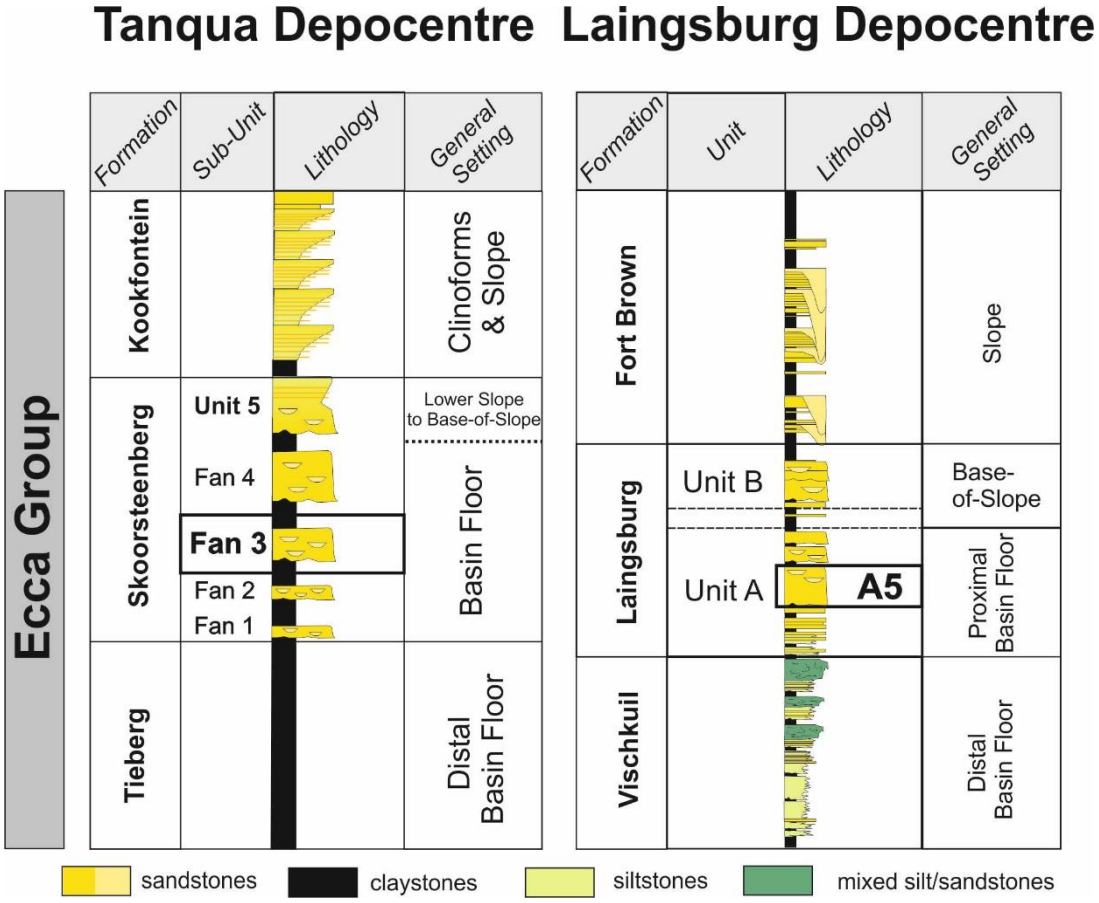

Figure 4.2 *Stratigraphic column of the deep-water deposits from the Laingsburg depocentre and the Tanqua depocentre, based on Prélat et al. (2009) and Flint et al. (2011). The fan systems discussed in this chapter (Fan 3 and Unit A5) are highlighted.*

The axis of the system is located farther to the east along depositional strike in the Ongeluks River area (Fig. 4.3A) and is characterised by distributive basin floor channel systems with overall palaeocurrent to the NNE (van der Werff and Johnson, 2003; Sullivan et al., 2004; Hodgson et al., 2006; Luthi et al. 2006). The distributive character of the channel-systems at Ongeluks River (Fig. 4.3A), the more deeply erosional character of the channels in overlying Fan 4 and Unit 5, and the thinning to the south (Oliveira et al., 2009), all suggest that the southwestern outcrop-limit of Fan 3 is a proximal off-axis base-of-slope setting (Johnson et al., 2001, van der Werff and Johnson, 2003; Luthi et al., 2006; Hodgson et al., 2006; Jobe et al., 2012). The Kleine Riet Fontein area was previously studied in detail

by Jobe et al. (2012) and interpreted as an area receiving unconfined flows, supported by the wide spatial distribution of numerous metre-scale scour features.

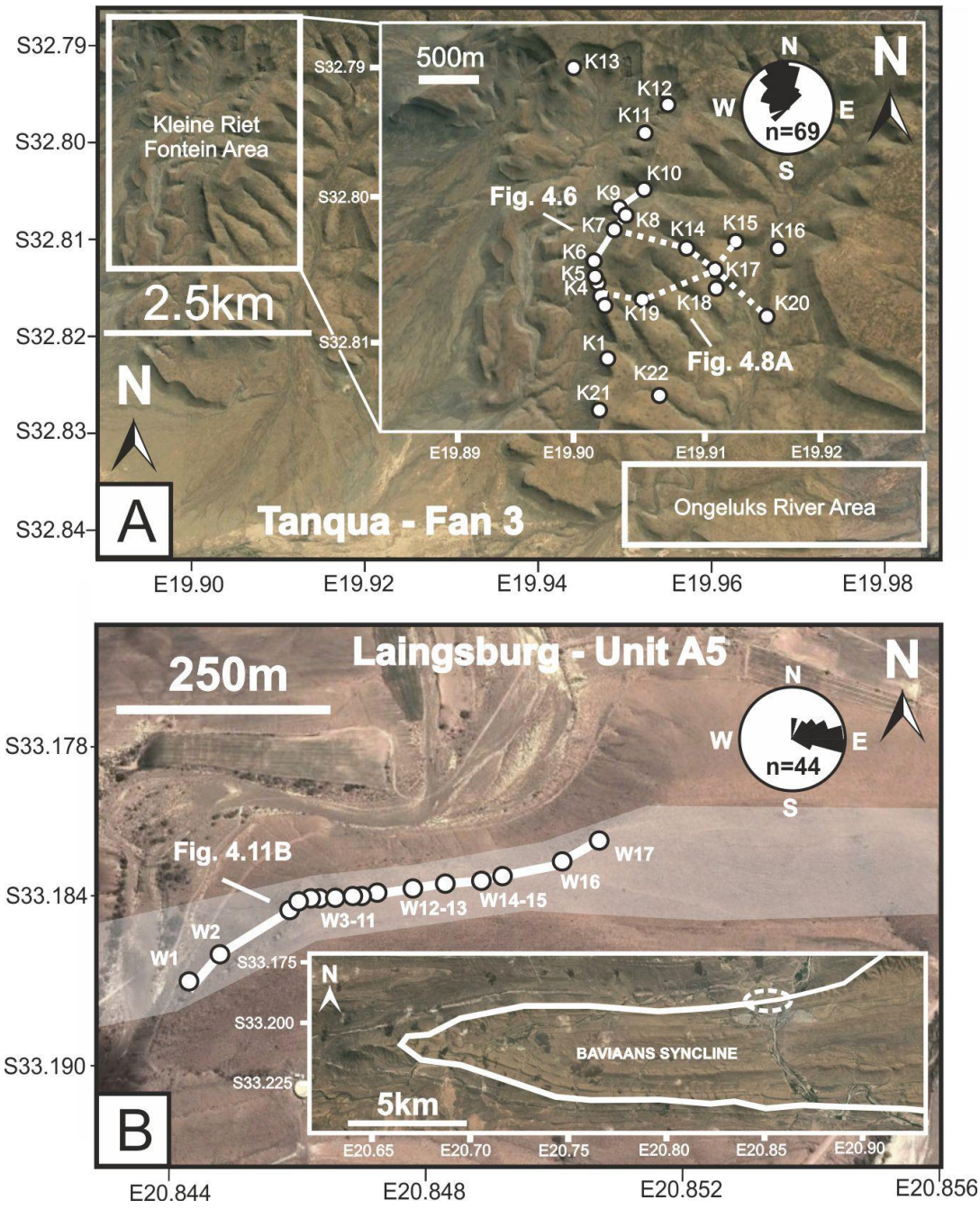

Figure 4.3 *Detailed maps of case study areas with locations of sedimentary logs, and outlines of Fan 3 (A) and Unit A5 (B). Solid line in A indicates the main profile illustrated in Figure 4.6 and the dotted lines indicate the additional profiles of Figure 4.8A. Palaeocurrents are indicated and are taken from thin-beds underlying the erosion surfaces. Images taken from Google Earth.*

4.3.2 Laingsburg depocentre

The proximal basin floor system of the Laingsburg Formation is divided into Units A and B (Sixsmith et al., 2004; Brunt et al., 2013a) (Fig. 4.2). The 350 m thick Unit A comprises sand-prone sub-units A1-A7, which are separated by regionally extensive mudstones (Sixsmith et al., 2004; Flint et al., 2011; Prélat and Hodgson, 2013). The studied outcrop is in the 'Wilgerhout' area within Unit A5, a 100 m thick and more than 50 km long package of sandstones and siltstones on the northern limb of the post-depositional Baviaans syncline (Figs. 4.1, 4.3B), close to the town of Laingsburg. Palaeogeographically, the study area is located in the axis of the A5 system on the basin floor (Sixsmith et al. 2004) (Fig. 4.1). The large number of sand-rich channel-fills that characterise the upper part of A5 in this area point to a location close to the base-of-slope and/or close to the mouths of large distributary channels (Sixsmith et al., 2004; Prélat and Hodgson, 2013).

4.4 Methodology and datasets

Stratigraphic correlations were completed in the field using closely-spaced sedimentary logs (see Appendix B.3), photomontages, and walking out key surfaces with a handheld GPS to construct architectural panels. In the Fan 3 Kleine Riet Fontein study area (4.6 km^2), a total of 20 sedimentary logs was collected (Fig. 4.3A). More than 550 palaeocurrent measurements (See Appendix B.2), primarily from ripple cross-lamination, were collected and tied to specific stratigraphic units. Due to the variability in direction of ripple cross-laminations, a high number of measurements were collected from ripple foresets to ensure an accurate palaeoflow direction. The main outcrop face consists of a 3.5 km long, N-S depositional dip section. Several E-W orientated gullies to the east of the main outcrop face provide additional depositional strike control (Fig. 4.3A). Thin siltstone packages within the regional claystones between Fan 2 and Fan 3 provide local correlation datums.

Within the Wilgerhout area of Unit A5 a total of 17 sedimentary logs along a ~ 500m depositional dip (W-E) section was collected (Fig. 4.3B) (See Appendix B.3). The regional A5 to A6 mudstone (Sixsmith et al., 2004; Flint et al., 2011; Cobain et al., 2015) was used as the datum for all correlations. A total of 44 palaeocurrents was measured (See Appendix B.2) solely from ripple cross-laminations and give an average eastward directed palaeoflow (082°) (Fig. 4.3B). Where the tectonic tilt was > 20° the azimuth of well exposed planar foresets was measured and restored.

4.5 Facies associations

The deep-water deposits of the Karoo Basin show a limited grain size distribution ranging from claystone to fine-grained sandstones. Both Fan 3 and Unit A consist of mainly thin-bedded siltstones and very fine- to fine-grained sandstones. Flow conditions were interpreted from the described facies characteristics. A total of six distinct facies associations was identified based on field observations and are described in detail below. Facies associations are closely based on previous Karoo Basin studies (Johnson et al., 2001; van der Werff and Johnson, 2003; Grecula et al., 2003a; Hodgson et al., 2006; Prélat et al., 2009; Brunt et al., 2013a).

4.5.1 Thick structureless sandstones (Fa1)

Thick (>1 m) fine-grained sandstone beds with little to no internal structure can form amalgamated sandstone packages up to 5 m thick and are tabular (tens to hundreds metres wide). Weak normal grading is observed at bed tops, where planar- and ripple-cross lamination may be preserved. Locally, bed bases and/or tops can show planar laminations (section 4.5.2) and/or banding (section 4.5.3). The sandstone beds can contain a minor amount of dispersed sub-angular mudstone clasts (Fig. 4.4A). Flame structures and tool (drag) marks are observed at bed bases.

These deposits are interpreted as rapid fall-out from sand rich high-density turbidity currents (Kneller and Branney, 1995; Stow and Johansson, 2002) with clasts representing traction-transported bedload (see section 4.5.2 and 4.5.3 for interpretation of planar laminated and banded intervals). Flame structures are associated with syn-depositional dewatering (Stow and Johansson, 2002).

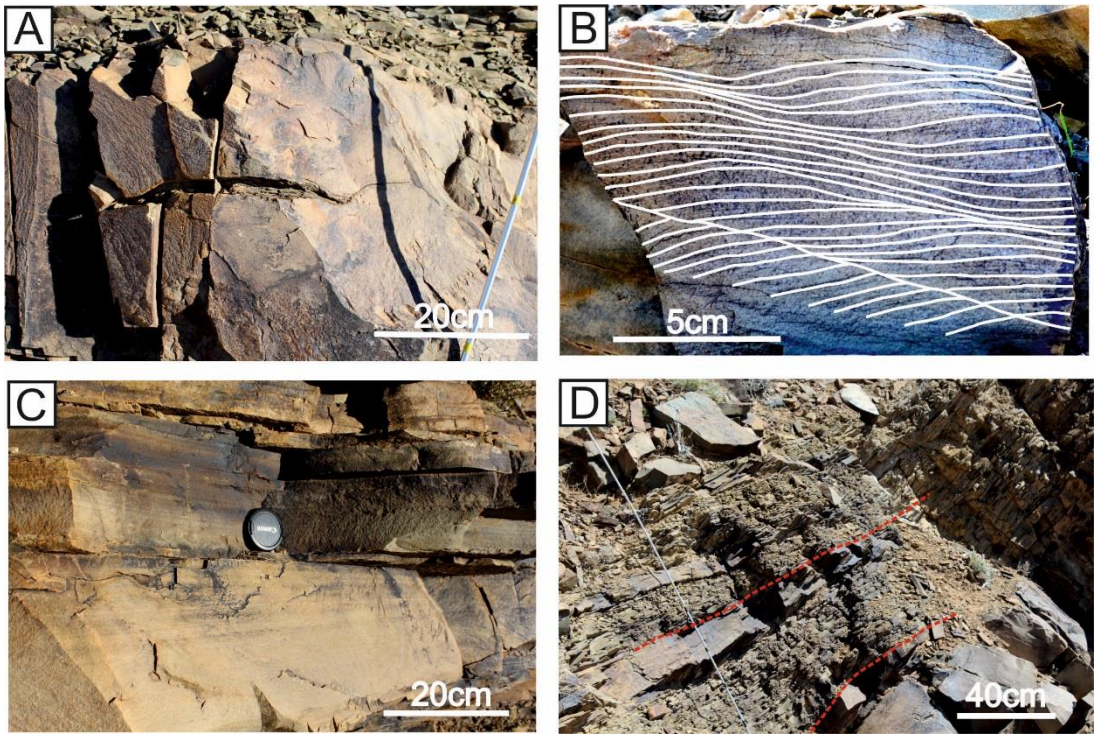

Figure 4.4 *Representative photographs of main sedimentary facies in the case study areas, with (A) structureless fine-grained sandstone with floating siltstone clast (Fa1) – Unit A5; (B) Interpreted photograph showing upward steepening climbing ripple-laminated sandstone bed passing into stoss-side preserved climbing ripples (Fa2) – Fan 3 (C) Banded sandstone (Fa3) – Unit A5; (D) Lateral discontinuous thin-bedded siltstones and sandstones with small-scale erosive marks – UnitA5 (Fa4-2). Difference in scale between pictures has been notified.*

4.5.2 Medium-bedded laminated sandstones (Fa2)

These medium- to thick-bedded (0.2 to 3 m thick), very fine-grained to fine-grained sandstones show various sedimentary structures. Ripple lamination, in particular climbing ripple lamination, is abundant (25-70% of all laminated sandstones), showing high angles of climb with stoss-side preserved lamination (>45° on stoss-side preserved laminae) (Fig. 4.4C). Some beds show a clear upward increase in the angle of climb and proportion of

stoss-side laminae preservation. Where planar lamination is present it is commonly at bed bases. Bases of thicker-bedded structured beds are sharp and the basal part is commonly structureless. Bed tops show abrupt normal grading to fine siltstone. Bed geometries can show lateral thickness variations on tens of metres scale.

High angles of climb and stoss-side preservation in ripple-laminated sandstones are indicative of rapid unidirectional aggradation rates (Jopling and Walker, 1968; Allen, 1973; Jobe et al., 2012; Morris et al., 2014a). When sedimentation rate exceeds the rate of erosion at the ripple reattachment point, the stoss-side deposition is preserved and aggradational bedforms develop (Allen, 1973). This style of tractional deposition is attributed to rapid deceleration of the flow and deposition from moderate-to low-concentration turbidity currents (Allen, 1973; Jobe et al., 2012). The planar laminations within the structured sandstones are interpreted to be deposited under upper stage plane bed conditions (Allen, 1984; Talling et al., 2012).

4.5.3 Banded sandstones (Fa3)

This facies association comprises medium- to thick-bedded fine-grained sandstones (20 to 200 cm, on average 40 cm), with diffuse laminae of over 1 cm thickness (Figs. 4.4B, 4.5A2). This style of lamination is characterised by an alternation between lighter and darker bands, and is referred to as banded sandstones. Lighter bands are well sorted and quartz-rich, whereas organic fragments and/or mudstone clasts and micaceous materials are commonly found within the poorly sorted darker bands. The banding is dominantly planar and parallel to sub-parallel, but can be mildly wavy. Centimetre-scale scour surfaces and loading are common at the bases of lighter bands. Within thicker beds dominated by banded sandstone beds, the bases are structureless and sharp

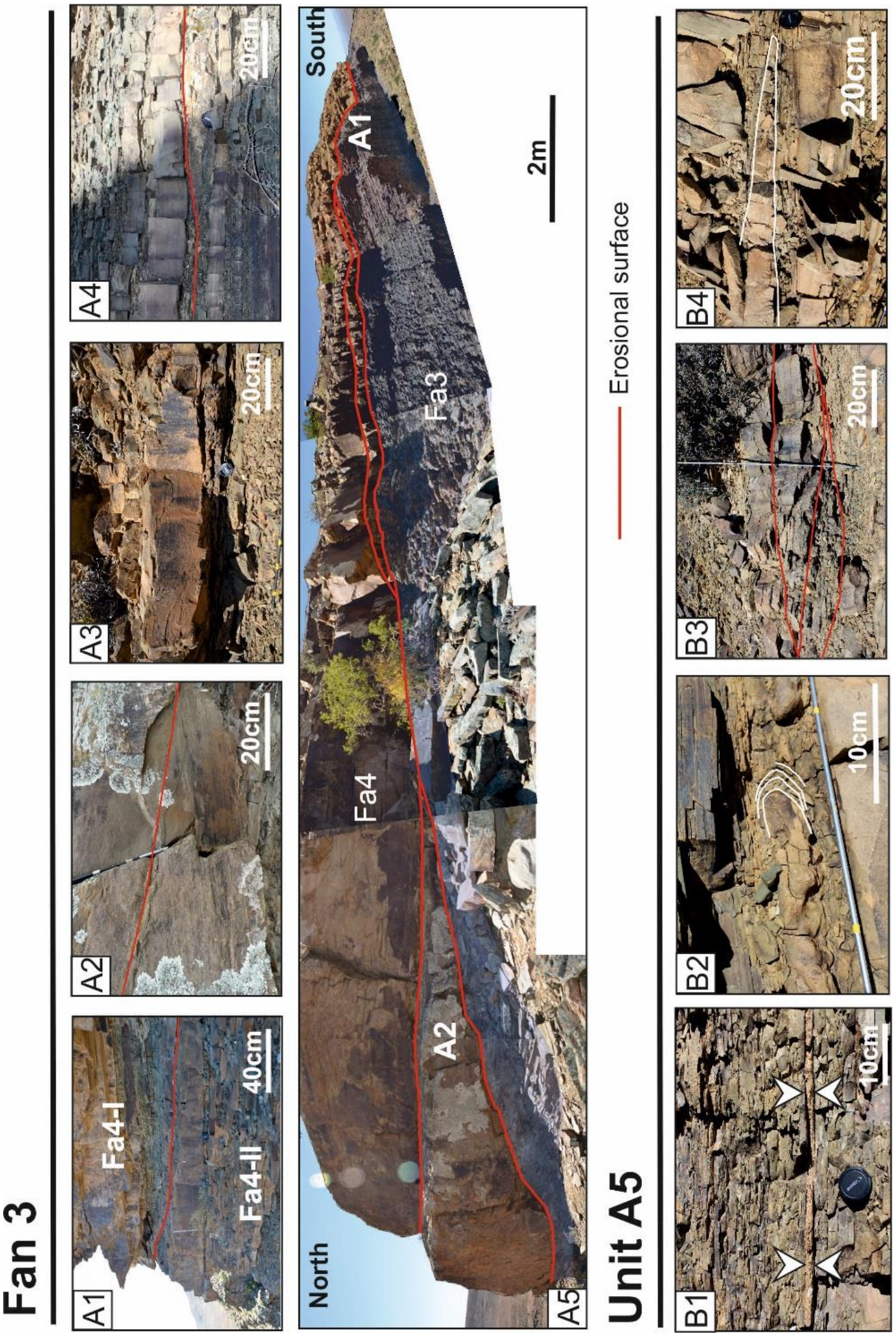

Figure 4.5 *(A) Representative facies photographs from the Fan 3 feature. (A1) Thin-bedded sandstones and siltstones deposits showing the difference in the character below (Fa4-1) and above (Fa4-2) the basal erosion surface. (A2) Internal truncation within medium-bedded banded sandstone. (A3) Truncation surface on top of thin-bedded fine-grained deposits with structured (rippled) sandstone on top with mudstone clast conglomerate at the base. (A4) Undulating basal erosion surface truncating thin-bedded deposits. (A5) Photopanel of the steep stepped southern margin with the locations of A1 & A2 indicated. (B) Representative facies photographs of Unit A5 feature indicated in Fig.4.11C with (B1) Thin-bedded siltstones interbedded with occasional thin coarse-grained sandstone. Individual siltstone beds show thicknesses >3cm (Fa4-2). (B2) Small scale soft-sediment deformed sandstones (Fa6). (B3) Composite erosion surface with initial mudstone clast conglomerate and banded sandstones, with laminae parallel to the erosion surface, on top. (B4) Pinchout of sandstone bed within siltstone thin-beds of the western margin indicated by the white line.*

Banded sandstones differ from planar-laminated sandstones due to the thickness of the laminae (>1 cm), the thickness of the laminated interval within individual event beds (>1 m) and the absence of any major grain size differences between laminae. The observations indicate highly concentrated, aggradational but fluctuating flow conditions. These conditions are present during deposition in traction carpets under high-density turbidity currents (Lowe, 1982; Sumner et al., 2008, 2012; Talling et al., 2012; Cartigny et al., 2013) and have not been linked to a generic flow regime. This is comparable to the H2 division of Haughton et al. (2009) and the Type 2 tractional structures of Ito et al. (2014). Combined with the thickness of individual beds within this facies group, these deposits support an interpretation of high aggradation rate and/or possibly long-duration of individual events.

4.5.4 Thin-bedded sandstones and siltstones (Fa4)

Thin (<20 cm) very fine-grained sandstones are interbedded with laminated siltstones (<1 cm to 5 cm). Ripple lamination, including low-angle climbing ripple lamination, is common within the sandstone beds. This facies association group can be subdivided into 1) tabular sandstones with planar and ripple laminations (Fa4-1), and 2) lenticular sandstones and siltstones associated with numerous centimetre-scale erosion surfaces (Fa4-2; Fig. 4.5A1). Locally, Fa4-2 sandstone beds contain mudstone clasts (<1 cm) (Fig. 4.5A3) and can be associated with mudstone and siltstone clast conglomerates (max 0.5 m thick, 1-2 m long) that are clast-supported with a fine-grained sandstone matrix. Within Unit A5, thin (<5 cm) medium-grained, poorly sorted lenticular sandstone beds that are at least 10 m long (Fig. 4.5B1) are associated with Fa4-2 siltstones. The Fa4-2 siltstones of Unit A5 are thicker bedded (>3 cm) (Fig. 4.5B1).

The tabular bed geometry and predominance of current ripple lamination in Fa 4-1 are interpreted to indicate deposition from lower phase flow conditions within sluggish dilute turbidity currents (e.g., Allen, 1984). The occasional planar laminated sandstone indicates

upper phase flow conditions (Best and Bridge, 1992) but with a transition to lower phase flow conditions due to ripple-laminated tops.

The Fa 4-2 group supports a higher energy environment compared to the FA4-1 group, because of the presence of mudstone clasts and numerous erosion surfaces. The fine-grained siltstone deposits of the Fa4-2 group are interpreted to represent a combination of the tails of bypassing turbidity currents, lag formation and continued reworking of the substrate by long lived turbidity currents, similar to channel-margin deposits (Grecula et al., 2003a, Brunt et al., 2013a; Stevenson et al., 2015). The mudstone clast conglomerates are interpreted as bedload material, derived from a mud-rich substrate, and therefore represent lag deposits of highly energetic bypassing turbidity currents. This facies association shares many similarities to the sediment bypass facies identified within the CLTZs of sand-detached lobe systems in the Laingsburg area (van der Merwe et al., 2014). Fluctuations between depositional and erosional processes results in the interbedding of siltstones and sandstones, including thin and lenticular medium-grained sandstone beds, and multiple erosion surfaces (Stevenson et al., 2015). The presence of unusually thick siltstone beds, and medium-grained sandstones, which are very rare in the Ecca Group, within the Unit A5 Fa4-2 facies group is evidence of localised deposition. The climbing ripple lamination within thin-bedded sandstones indicates rapid aggradation rates (Allen, 1973; Jobe et al., 2012).

4.5.5 Soft sediment deformed (SSD) deposits (Fa5) and claystones (Fa6)

The Fa5 facies group is represented by localised tightly folded and contorted heterolithic units (0.2-0.5 m thick) of thin-bedded siltstones and sandstones (Fig. 4.5B2). Fa5 represents a minor portion of the infill (<1%), the deposits rarely exceed 2 m in length with deformation structures of 10’s of centimetres in width and occurs only within the basal infill towards the margins of both features in close association with Fa4-2. Thick, regionally

extensive units of Fa6 claystones occur as drapes to the deepwater sandstone units in both depocentres.

Due to their marginal location and limited proportions, the contorted thin bed units are interpreted to represent local remobilisations, above erosional relief. Fa 6 represents condensed intervals of hemipelagic deposition, during periods of regional shutdown in coarse-grained sediment supply (Hodgson et al., 2006; Flint et al., 2011).

4.6 Depositional architecture

Both the Fan 3 and the Unit A5 feature are defined by composite and asymmetric basal erosion surfaces that exceed the extent of the exposures (~350 m long in A5; ~1000 m long in Fan 3) and incise 15-20 m into underlying deposits. The palaeoflow directions of underlying and overlying deposits indicate that they are orientated sub-parallel to regional palaeoflow directions and that the updip margins are highly irregular. The Fan 3 exposure is orientated 150-330° with a 340° average palaeoflow at this location (n = 435). The Unit A5 exposure is orientated 075-255° with a 082° average palaeoflow (n = 44). The type and distribution of sedimentary facies and internal stacking patterns differ between the two cases, and are discussed separately.

4.6.1 Fan 3 feature; Tanqua depocentre

The location of the Fan 3 erosional feature (Fig. 4.6) is in the middle of a north-south orientated outcrop in the Kleine Riet Fontein area (Figs. 4.1, 4.6). Mapping of thickness, facies, and system-scale sedimentary architecture with the lack of channel-fills in this area compared to the Ongeluks River area to the south-east supports a proximal off-axis environment (Johnson et al., 2001; Hodgson et al., 2006; Jobe et al., 2012) (Fig. 4.3A). The overall palaeoflow is northwards (Fig. 4.7).

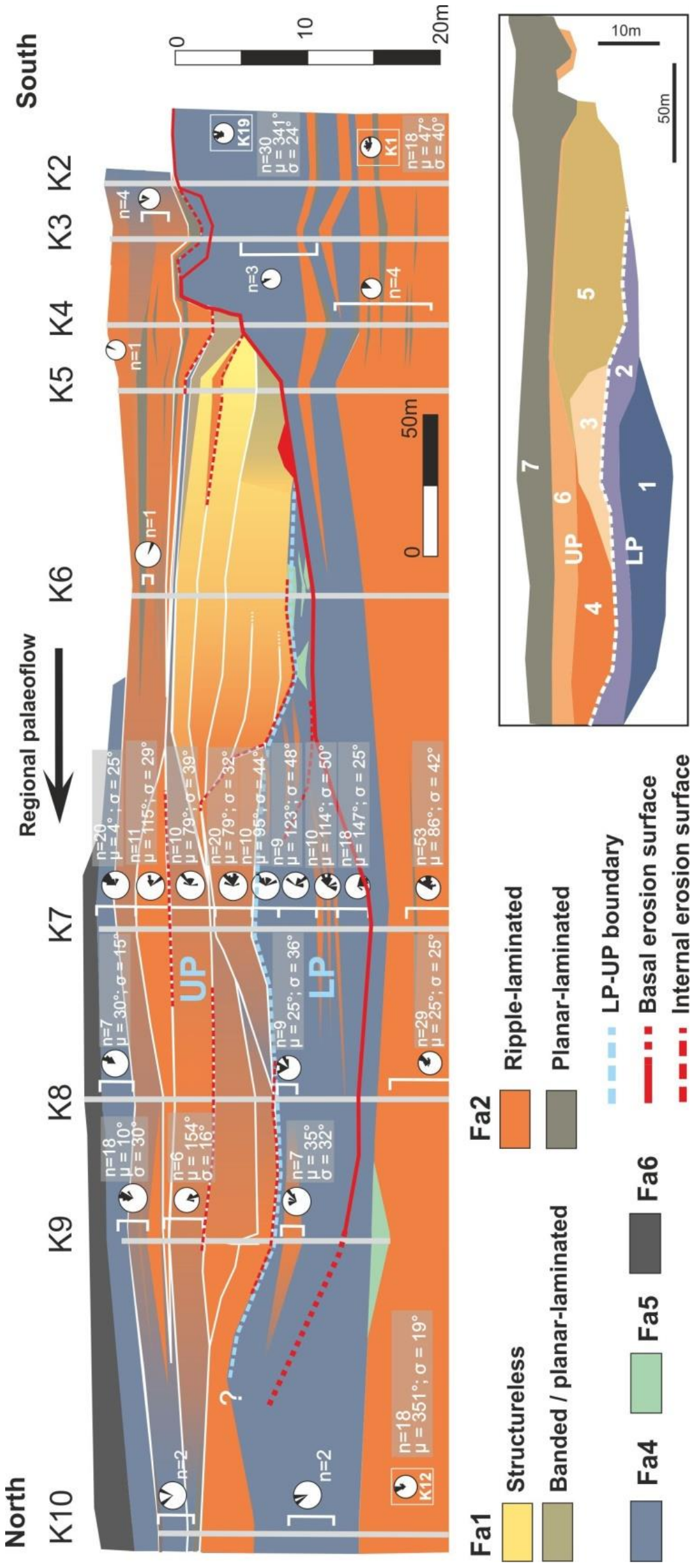

Figure 4.6. *Facies correlation panel of main section (solid line in Fig. 4.3A) of the erosional feature at Kleine Riet Fontein in Fan 3 with palaeocurrents shown, with n = number of measurements, μ = mean palaeoflow and σ = standard deviation. Solid white lines indicate bed boundaries. The fill is divided into a lower (LP) and upper package (UP) and a total of seven infill elements as indicated in the bottom right cartoon. The boundary between the lower and upper package is indicated by a light blue dashed line. Facies association 1 (Fa1) has been subdivided into structureless and banded and/or planar laminated facies; Facies association 2 (Fa2) has been subdivided into ripple and planar laminated facies.*

The underlying deposits can be subdivided into a sandstone-prone package dominated by Fa2 and an overlying siltstone-prone package dominated by Fa4 (Figs. 4.6, 4.7). A minor stratigraphic change in mean palaeoflow is identified between these two packages, from NNE (033°) to NNW (336°) (Fig. 4.7). The feature shows an erosional cut into the siltstone-prone package. All Fan 3 deposits below and above the basal erosion surface extend beyond the study area and are therefore more laterally extensive than the erosional feature itself. The basal erosion surface forms a series of metre-scale steps on the steep (max. 50°) updip southern margin (Figs. 4.5A4, 4.6). The full geometry of the northern margin is obscured, but the overall thinning of the fill suggests a low-angle confining surface (Fig. 4.6). Sedimentary sections taken towards the east (Fig. 4.3A) of the main N-S profile (Fig. 4.6) indicate eastward shallowing of the basal erosion surface and thinning of the infill directed perpendicular to regional palaeoflow (Fig. 4.8A).

The architecture of the fill is established by identification of elements, characterised by abrupt changes in bed thickness and facies across bounding surfaces (Figs. 4.6, 4.9, 4.10). The infill is subdivided into seven elements that are grouped into two distinct packages based on difference in facies proportions and across a composite erosion surface (Figs. 4.6, 4.8B). The lower package is up to 6.5 m thick and comprises elements 1 and 2 separated by an internal truncation surface and abrupt changes in bed thickness (Fig. 4.6). Both elements comprise (Fig. 4.8B) thin-bedded siltstones and climbing ripple laminated sandstones (Fa4-2) containing small (1-4 cm) mudstone-chips and minor (20-40 cm thick) folded thin-bedded deposits (Fa5). The lower package is only present in the northern part of the fill. The upper package is up to 12 m thick and comprises elements 3-7 (Figs. 4.6, 4.9, 4.10). The upper package elements are predominantly medium- to thick-bedded laminated sandstones (Fig. 4.8B) including beds with upward steepening climbing ripple-lamination with increasing stoss-side preservation (Fa2) (Fig. 4.4C).

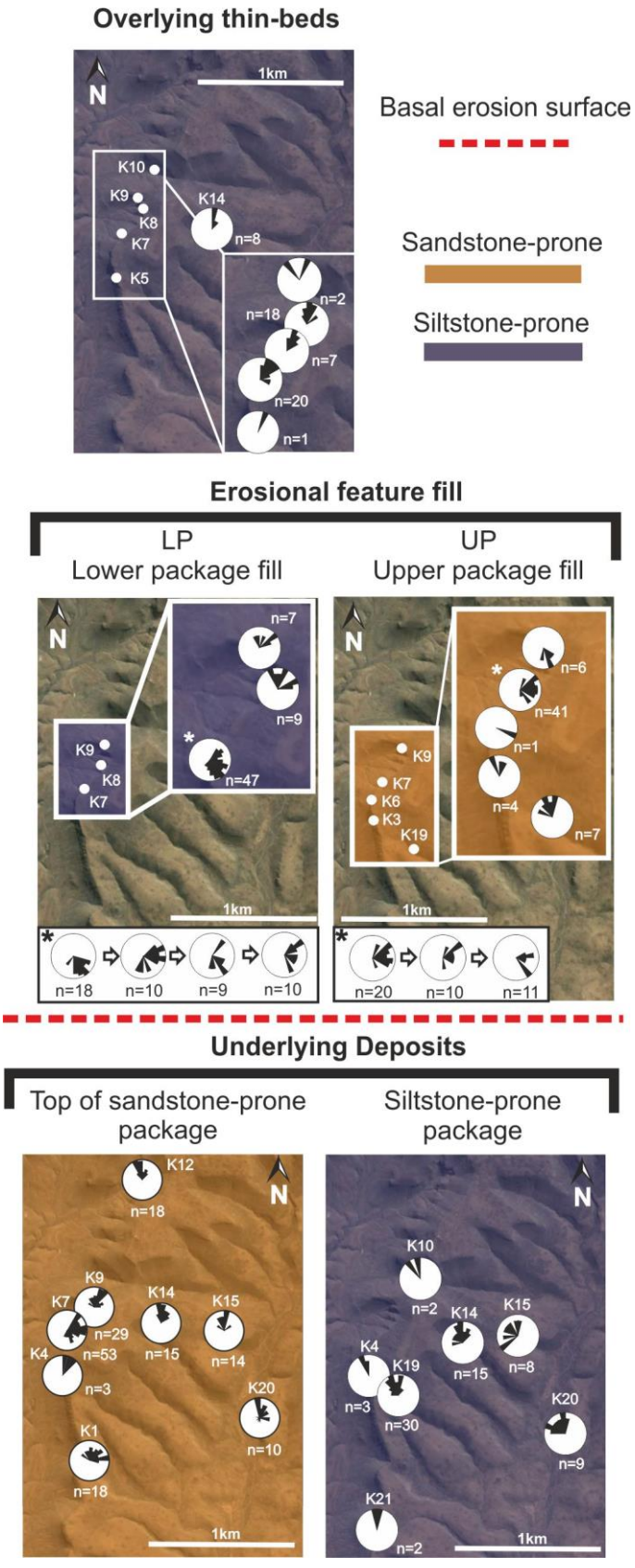

Figure 4.7. *Palaeocurrent distribution within the Kleine Riet Fontein area (Fan 3) subdivided into underlying, fill and overlying deposits. The asterisk shows the more detailed stratigraphic change in palaeoflow direction as also indicated in the main correlation panel of Fig. 4.6 (K7). Background image taken from Google Earth.*

Each of these elements shows lateral thickness changes (scale of metres) and there is a transition to more thinly-bedded deposits (Fa4) towards the margins of all elements (Fig. 4.6) which were not truncated. Elements 3, 4 and 5 are more laterally restricted (Figs. 4.9, 4.10) and show more substantial bed thickness variability compared to the upper elements (6 and 7). Element 4, and to a lesser extent element 6, thicken where the underlying elements thin (Figs. 4.6, 4.9). Elements 5 and 7 contain some banded sandstones (Fa3) directly overlying the basal erosion surface at the southern margin (Fig. 4.5A2), which show a northward facies transition to structureless sandstone (Fa1). Elements 3, 4 and 5 (Figs. 4.9, 4.10) show bedsets (3-7 m thick) that comprise four to five 0.5 to 2.0 m-thick dominantly climbing-ripple laminated sandstone beds, which are interbedded with thin siltstones (<0.1 m). They are thickest near the southern margin, and pass into thin siltstones (<5 cm) in a northward direction (over 50-150 m). Successive pinchouts occur southward, such that the beds shingle updip. Where normally graded sandstone beds thicken they amalgamate, as can be seen in element 5 (Fig. 4.10B). Due to accessibility issues, the exact orientation of the bedding is difficult to measure directly, but outcrop sections of elements 3 and 5 (Figs. 4.9, 4.10) indicate a shallow southward (updip) depositional dip (a few degrees). In addition, beds in element 3 dip upstream approximately 2-4° relative to the underlying laterally extensive bedding (Fig. 4.9).

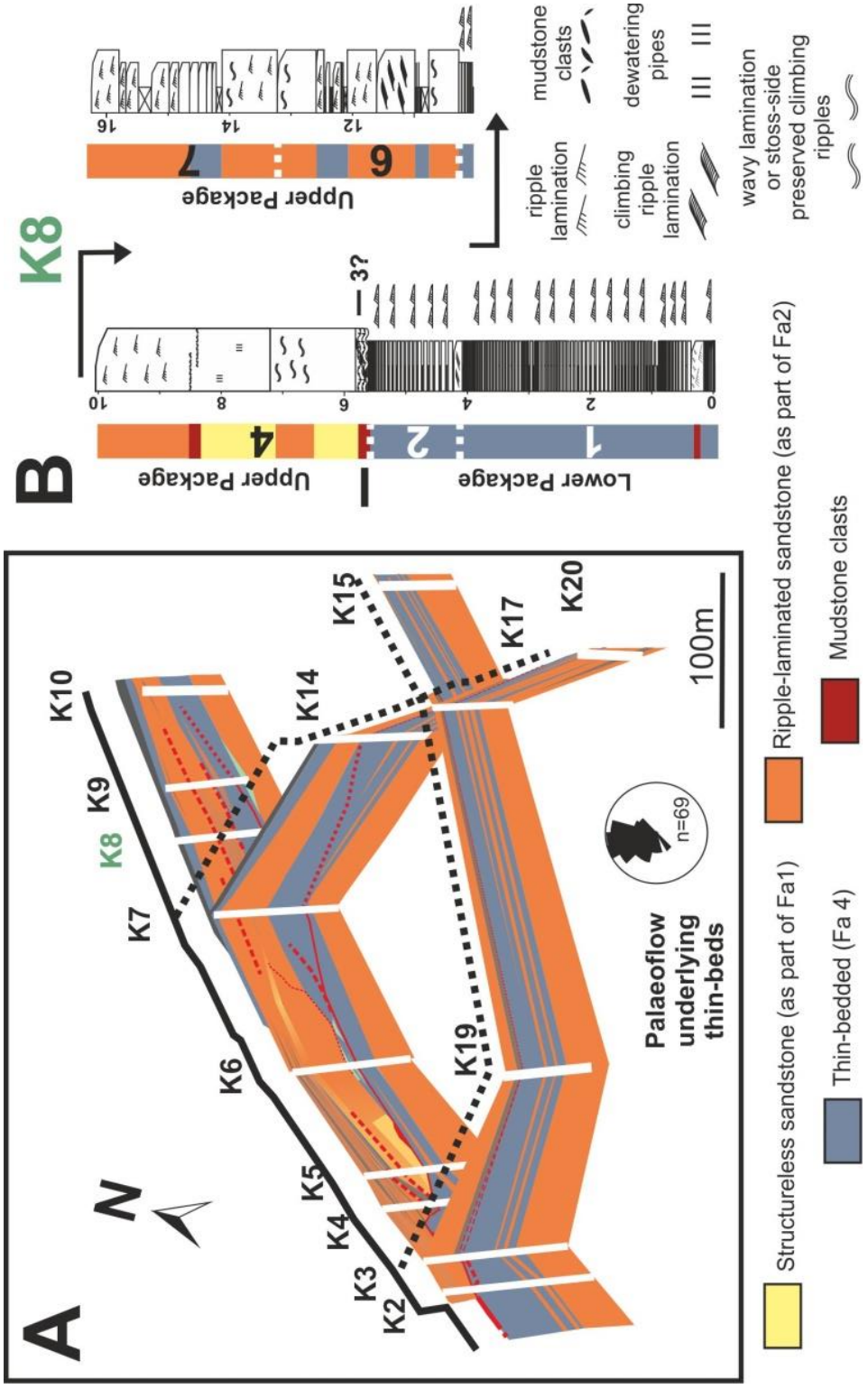

Figure 4.8. *(A) Fence diagram showing the 3D architecture of the Kleine Riet Fontein (Fan 3) erosional feature. Palaeoflow of the underlying thin-bedded deposits is indicated (average = 336°). The infill thins-out both in the eastward and southward directions. See Figure 4.3A for log locations. (B) Detailed log of the fill (K8, see Figs. 4.2,4.6 for location) showing the division in infill elements. Element 3 pinches out at K8.*

Elements 6 and 7 do not preserve clear bed stacking patterns, although lateral variability in bed thickness is observed. Within the individual elements there are no clear vertical trends, however the combination of the upper and lower packages together forms a stepped coarsening and thickening upward profile (Fig. 4.8B) within the axis of the feature.

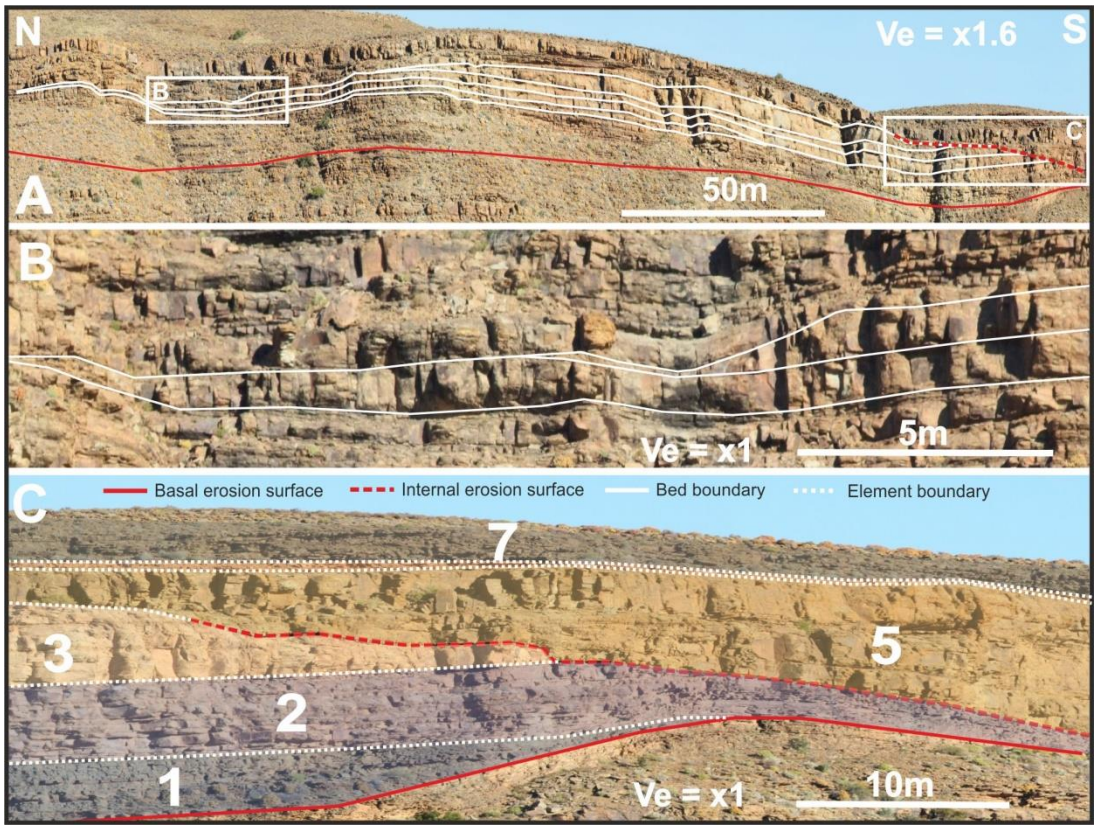

Figure 4.9. *(A)Panoramic view of infill element 3, with (B) Abrupt bed pinch-out in the northern direction, and (C) Truncation of elements in southern direction. Location of (A) is indicated in Figure 4.10.*

The palaeoflow patterns within the erosional feature in the Kleine Riet Fontein area are diverse and show lateral and stratigraphic variations. The lower package preserves a dominant south-easterly orientation (134°) within element 1 at its most southern limit, which becomes more eastward (093°) within element 2 (Fig. 4.6, K7). About 200-300 m to the north, element 2 has a dominant NNE to NE (025° – K8, 035° – K9; Figs. 4.6, 4.7) palaeoflow direction. In the upper package, there is a NE to SE spread (average = 096°) except for element 7, which shows an overall NE direction (028°) at its northern limit and a

more NNW direction (345°) near its southernmost limit (Fig. 4.6). The thin-bedded deposits above the fill of the feature have a NNE palaeoflow (028°, n=57), which is more closely aligned to the underlying deposits (Fig. 4.6) and the regional trend.

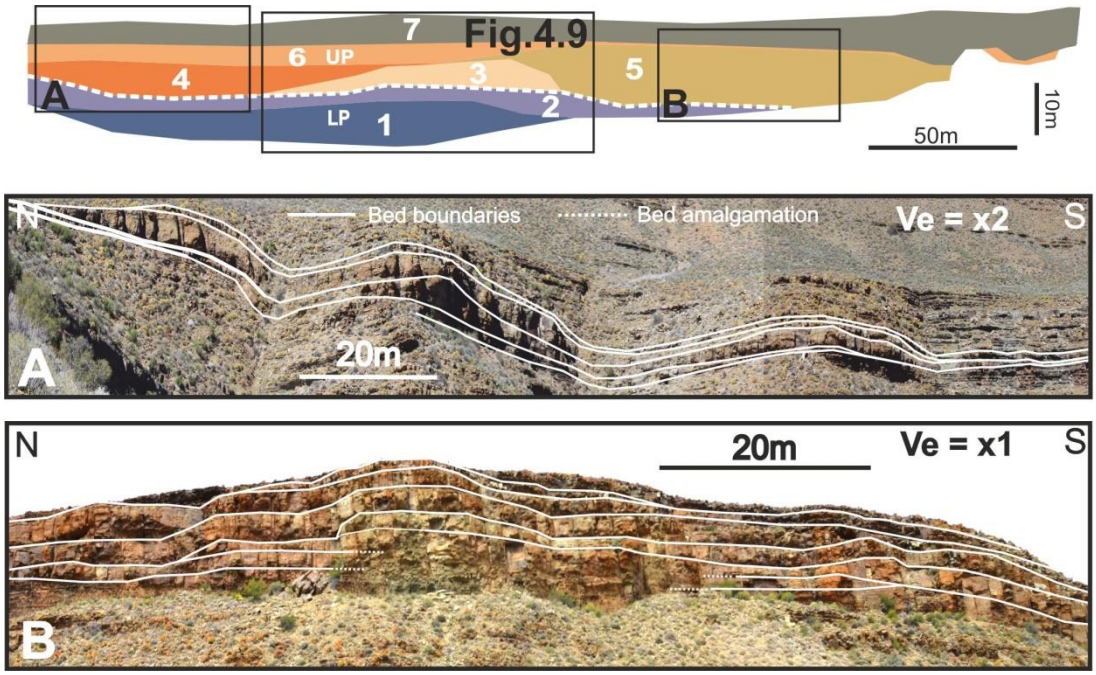

Figure 4.10. *Panoramic photopanels and division of infill elements, displaying the internal architecture within the Kleine Riet Fontein erosional feature (Fan 3). The seven elements have a complicated bed geometry and stacking patterns with abrupt pinch-outs southwards and northwards. Element 4 (Inset A) and 5 (Inset B) both show stacked bedsets with depositional dips in an overall southern (updip) direction. The boxes show the locations of inset A, B and Figure 4.9*.

A second large-scale erosional feature 800 m to the north (around K13, Fig. 4.3A) is situated at the same stratigraphic level in Fan 3, and shares many similarities in architecture and infill facies. The infill of this erosional feature exhibits an average NNW-directed (330°) (n=17) palaeoflow, similar to the underlying thin-bedded deposits. An irregular erosion surface (~15°) has a measured ENE orientation (070°), which is in dip direction to palaeoflow and is overlain by structured sandstones. Three hundred metres to the east, another erosion surface (~6°) is approximately orientated NNW (335°), which is parallel to the palaeoflow, and is evident from discordance in bed dips within the thin-

bedded deposits. The basal surface has a minimum width of 500 m perpendicular to palaeoflow and cuts at least 10 m into underlying deposits. Close to the western margin the fill consists solely of Fa2 facies, but eastwards where the fill thickens, it consists of a lower package of thin-bedded siltstones and sandstones (Fa4-2) and an upper package of structured sandstones (Fa2) that are locally amalgamated.

4.6.2 Unit A5 feature; Laingsburg depocentre

The erosional feature at Wilgerhout lies in the upper half of Unit A5 (60-70 m from the base) within a succession of stacked lobes locally cut by sand-rich channel-forms (Prélat and Hodgson, 2013). A large channel (>600 m wide and >15 m deep) filled by amalgamated structureless sandstones (Fa1) is present at the top of the A5 succession in this location. The association of channels and lobes in this area supports a base-of-slope setting, within the upper part of the Unit A5 system based on regional mapping (Sixsmith et al., 2004; Prélat and Hodgson, 2013). The exposure is limited to a 1 km long E-W orientated section. Regional palaeoflow patterns are towards the ENE (Sixsmith et al., 2004), which is consistent with measurements from the infill deposits (Fig. 4.11). The section shows a steep (2-50°) and stepped western (updip) margin.

The fill consists of three distinct sedimentary packages. A lower package (1.5-5 m thick) comprises thin-bedded siltstones with rare banded or ripple laminated fine-grained sandstone beds (Fa4-2) (Fig.4.11). Locally, thin (<30 cm) mudstone clast conglomerates directly overlie the basal erosion surface. Multiple small-scale (<20 cm deep) cross-cutting erosional surfaces incise into thin-bedded siltstones in the basal ~0.5 m of the fill, but decrease towards the top. Thin (2-3 cm) and lenticular moderately sorted medium-grained sandstones are present within the siltstones and individual normally graded siltstone beds are thick (> 3 cm) (Fig. 4.5B1). The middle package (0.5-10 m thick) comprises medium-bedded banded (Fa3) and structureless sandstones (Fa1) interbedded with siltstones, which pass abruptly from sandstone-dominated to siltstone-dominated (Fa4-2) associated

with bed pinch-out at the western margin (Fig. 4.5B3). Some minor tightly folded deposits (Fa5) (Fig. 4.5B2) occur within the siltstone dominated western margin succession. The upper package (3-8.5 m thick) comprises thick-bedded sharp-based structureless partially amalgamated fine-grained sandstones (Fa1) interbedded with the occasional banded sandstone and thin-bedded siltstone (Fig. 4.11).

This package extends beyond the limits of erosional confinement, but increases in thickness above the deepest point of the basal erosion surface. Within all three infill packages no clear vertical stratigraphic trends have been observed. However, the combination of the three infill packages together (Fig. 4.11B –W15) shows a stepped coarsening- and thickening-upward trend above the basal surface. Above the upper package a 4 m-thick fining- and thinning-upwards unit is present (Fig. 4.11). As these siltstone-prone deposits are tabular, they are not considered to be part of the fill.

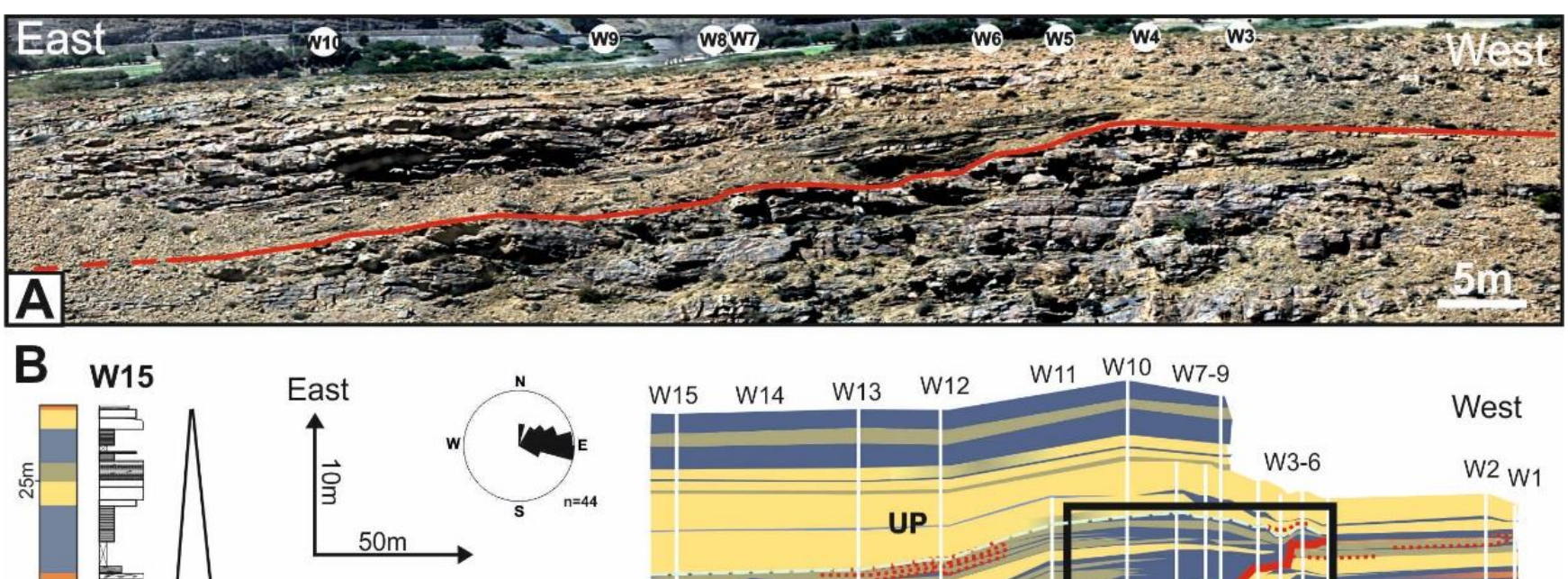

Figure 4.11. *(A) Panoramic view of the Unit A5 case study showing the undulating western (updip) margin. (B) Facies correlation panel of the Unit A5 feature and W15 sedimentary log of scour-fill showing a coarsening- and thickening-upward pattern within the infill and a fining- and thinning-upward trend above the fill. (C) Zoomed-in section of the western margin. Locations of the Unit A5 facies photos within Figure 4.5 are indicated.*

4.7 Discussion

4.7.1 Origin and infill of erosional features

The average palaeocurrents from underlying and overlying deposits indicate that the large asymmetric erosion surfaces described from Fan 3 (Tanqua) and Unit A5 (Laingsburg) are dip-sections (Figs. 4.3, 4.6, 4.11). The steeper upstream surfaces dip at angles of 4-50° (Fan 3) and 2-50° (Unit A5), with prominent metre-scale steps and multiple erosion surfaces indicating the composite nature of the basal surface. In the Kleine Riet Fontein area (Fan 3), the transverse to downstream section is shallow (~3.5°) and smooth (Fig. 4.6), and shows prominent asymmetry in three dimensions with shallowing of the basal surface perpendicular to the regional palaeoflow (Fig. 4.10A). Palaeocurrents within the basal infill are more diverse (ranging from N to SE) than the underlying and overlying deposits (NNE-NNW), with palaeoflow differences of up to 180° (Fig.4. 7).

An asymmetric and composite basal erosional surface with stacked smaller-scale elements could support interpretation of a sinuous submarine channel-fill. However, in a cut through a sinuous channel-fill, the general palaeocurrent is expected to be dominantly parallel to channel banks (dip sections) (Parsons et al., 2010; Wei et al., 2013; Sumner et al., 2014) and are only rarely found to be at high angles to the basal surface (Pyles et al., 2012). Known exhumed examples of outer bank deposits have relatively higher energy facies such as conglomerates, and coarse-grained and/or amalgamated sandstones (e.g., Young et al., 2003; Labourdette et al., 2007; Hodgson et al., 2011; Janocko et al., 2013) compared to inner bank deposits, which does not match with the observed distribution of facies and the relatively low-energy character of the Kleine Riet Fontein infill. Furthermore, channel sinuosity is predicted to be low for the slope gradients of base-of-slope and basin-floor channel bends (e.g., Clark et al., 1992 – close to 1.0 sinuosity at 1:1000 slope angles), especially in sand-prone systems without levee confinement and at mid-high palaeolatitudes (50-60°S) at which the Karoo system formed (Peakall et al., 2012, 2013;

Morris et al., 2014b; Cossu et al., 2015). Consequently, given the low predicted sinuosities it is unlikely that channel bend facies would be at high angles to the regional slope. In contrast, the morphology of the basal surface, the palaeocurrent pattern, and distribution of sedimentary facies support interpretation of large-scale scour-fills, with prominent steep headwalls and lower-angle downstream margins. Basin-floor channel-fills in the Ecca Group have been described by several authors (e.g., Johnson et al., 2001; Sixsmith et al., 2004; Sullivan et al., 2004; Brunt et al., 2013a), and are dominantly characterised by structureless sandstone, highly amalgamated in the axis of the fills and more thin-bedded towards the margins and top of the fills. Where well preserved, the basal erosion surface and facies distribution of basin-floor channels are symmetrical (Sullivan et al., 2004; Luthi et al., 2006), and typically ~250-350 m wide and 15-20 m thick (Pringle et al., 2010; Brunt et al., 2013a). The large-scale scour-fills described, therefore, are distinctly different to the published examples of basin-floor channel fills from the Karoo Basin in terms of their architecture, facies types and distributions, and relationship of palaeoflow to the bounding surface, as well as to sinuous channels from other settings. The erosional feature within the Kleine Riet Fontein area of Fan 3 has been previously interpreted as a channel-fill. Morris et al. (2000) classified it as a crevasse channel-fill, whereas van der Werff and Johnson (2003) interpreted it as the distal depositional part of an overbank channel-fill with a SE-NW orientation. Implicit in both interpretations was that the depositional architecture is different to the basin-floor channel-fills, at the same stratigraphic level 7-8 km to the east in Ongeluks River (e.g., Sullivan et al., 2004; Luthi et al., 2006).

The basal fine-grained fill (Fa4-2) in both scour-fills is interpreted to indicate sediment bypass and the deposition of low-energy tails of flows. The interpretation of thin-bedded deposits indicating sediment bypass has been previously made for channel-fills (e.g., Beaubouef and Friedmann, 2000; Grecula et al., 2003a; Brunt et al., 2013a; Hubbard et al., 2014; Stevenson et al., 2015). However, the thicknesses of individual siltstone beds (>3 cm)

within Unit A5 fill is distinctive, and is interpreted to indicate the capture of flow tails in a scour depression, in a similar manner to thick siltstones in internal levee successions (Kane and Hodgson, 2011). In the Kleine Riet Fontein feature (Fan 3), the diverse palaeoflow directions in the basal siltstone units suggest deflection and spreading of flow at the upstream end. Complex flow patterns are known to be associated with flutes and scours (e.g., Eggenhuisen et al., 2011) with flows exhibiting a recirculating separation cell that forms downstream of the scour lip as the basal high velocity part of the flow is jetted over the depression (Allen, 1971; Farhoudi and Smith, 1985; Karim and Ali, 2000). This may occur in both subcritical and supercritical flows. When the palaeoflow patterns of element 2 (at K7, K8, K9) are compared with the streamline patterns of the spindle-shaped erosional marks of Allen (1971), and assuming a scour orientated with the flow direction of the underlying deposits (336°), there is a close fit in terms of variance and spread (Fig. 4.12). Therefore, the observed palaeoflow patterns can be explained by the presence of a flow separation cell and the generation of reversed bedload transport at the bottom of the flow when passing through the depression (Fig. 4.12).

The second erosional feature located 800 m downstream of the Kleine Riet Fontein scour is similar in architecture and fill. It shows erosion and downcutting surfaces both perpendicular and parallel to regional palaeoflow. The morphology suggests this second erosional feature is also a large composite scour-fill (>300 m wide). As this northern scour is at the same stratigraphic level, it indicates there may be a larger area of erosional bedforms present. This supports Jobe et al. (2012), who interpreted Kleine Riet Fontein as an area that received unconfined flows. A spatial distribution of multiple scour-fills in this proximal off-axis area adjacent to distributive channels in Ongeluks River (Fig. 4.3) supports interpretation of a channel-lobe transition zone close to the base-of-slope.

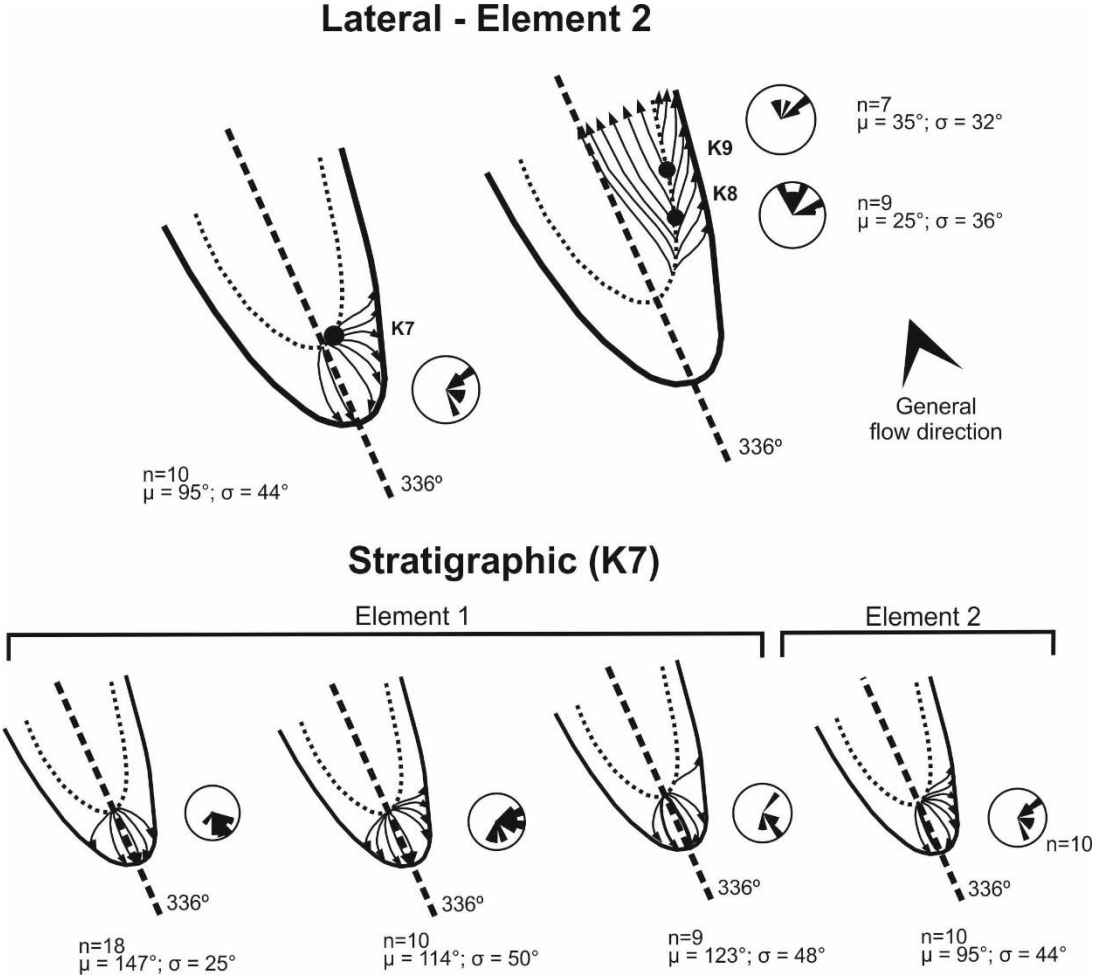

Figure 4.12. *Streamlines based on Allen (1971) and possible linkage to lateral and stratigraphic variance observed at K7, K8 and K9 with n = number of measurements, μ = mean palaeoflow and σ = standard deviation. These streamlines account for an idealised megaflute morphology with an orientation of 336° (based on underlying deposits). See Figure 4.6 for log location and exact stratigraphic intervals.*

4.7.2 Flow-scour dynamics

The merging of multiple erosion surfaces at the steep and stepped upstream margin of both scour-fills point to their composite origin, with multiple flows shaping the morphology of the basal surface. The basal successions of both scour-fills are similar. However, bed architecture, stacking patterns, erosion surfaces, and facies of the upper elements (3-7) in the Kleine Riet Fontein feature point to a more complicated interaction between flow and seabed relief in a later stage of scour evolution.

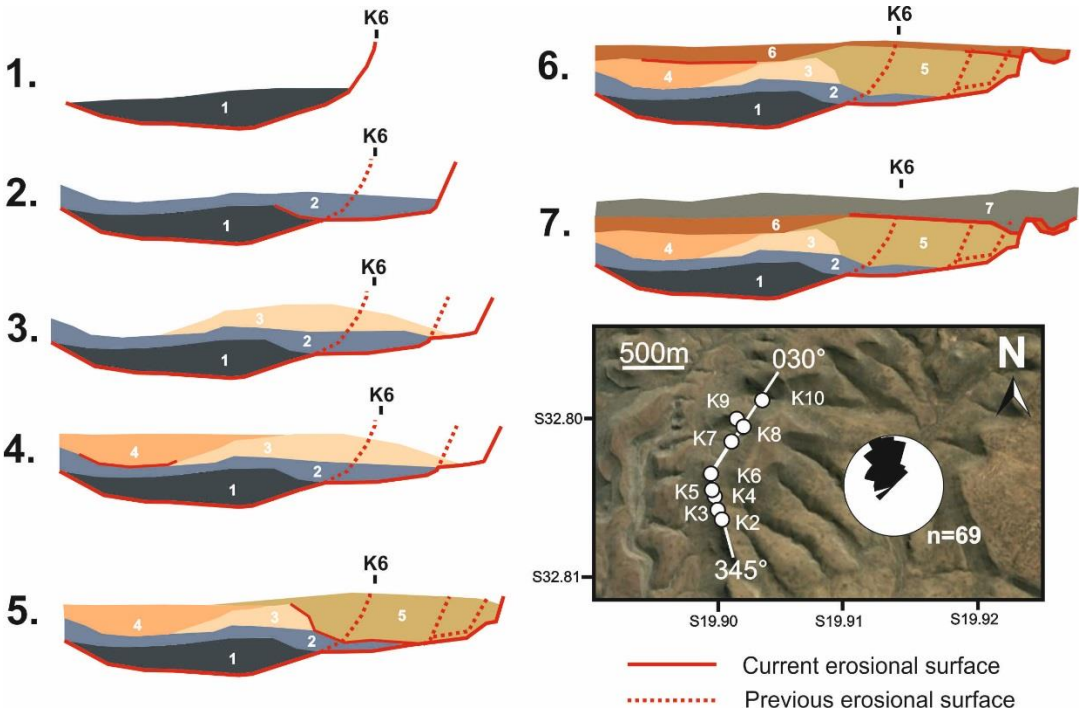

Figure 4.13. *Interpretation of the Kleine Riet Fontein (Fan 3) erosional feature based on the infill elements. It is unknown how far the deposits of element 1, 2 and 3 extended on the southern margin as the basal surface of element 5 modified the previous infill. The palaeocurrent distribution of the underlying thin-beds is orientated to the NNW (336°). It must be noted that this section includes a significant change in orientation around log K6 from 345° (almost parallel to the underlying palaeoflow) to 030° (transverse to the underlying palaeoflow), indicated within the map at the bottom right. Image taken from Google Earth*.

In the Unit A5 feature, the irregular basal surface suggests that, after initial development of the scour, the upstream margin was weakly modified, with little evidence of headward erosion. Minor internal erosion surfaces exist, but generally beds taper towards the upstream margin. The stratigraphic transition from the siltstone- to sandstone-prone deposits points to initial sediment bypass (multiple erosion surfaces and medium-grained sandstone lenses) followed by a period of aggradation (structureless Fa1 and banded sandstones Fa3) as the depression filled. The tabular nature of the bedding and the lack of clear supercritical bedforms, suggests a subcritical nature for the infill.

In the case of the Kleine Riet Fontein scour, the evolution of the scour is assessed from the architecture and stacking patterns of the elements (Fig. 4.13). The position of the upstream

margin of the scour during deposition of element 1 was downstream of the current position of element 2, which was deposited after another phase of erosion, evident from the stepped basal erosional surface (Fig. 4.6). Element 3 shows a similar southward migration after reshaping of the updip margin and only partial infill of the depression. Element 4 is interpreted to have largely filled the accommodation in the downstream and lateral part of the scour. This was truncated by another erosional event that reshaped the updip margin and removed large parts of element 2 and 3. Element 5 and 6 have slightly erosional bases, but mostly infill available accommodation by stacking in a downstream direction. Element 7 has a more uniform thickness but modified the updip margin (Figs. 4.6, 4.13). The interpreted evolution of the basal surface suggests that the initial scouring phase(s) may not be preserved due to sequential deepening and widening of the scour. The stacking of the elements and internal erosion surfaces in the Kleine Riet Fontein scour-fill indicate upstream migration (Fig. 4.13) and lengthening of the original scour surface through headward erosion. Headward erosion, or backward incision, occurs in both supercritical and subcritical flows (e.g., Izumi and Parker, 2000; Hoyal and Sheets, 2009). The sedimentary facies and bed geometries of the elements in the upper package are characterised by stoss-side preserved steep climbing-ripple dominated sandstones that indicate rapid localised fallout from relatively low-concentration turbidity currents. Climbing ripple lamination extends across almost the whole length of the scour-fill until in close proximity of the upstream head of the scour. The shallow (a few degrees) upstream depositional dip observed in a number of the infill elements (3, 4, 5) resemble backset bedding (Fig. 4.9). Backset bedding has been linked to abrupt changes in confinement (Ito et al., 2014), associated with the occurrence of a hydraulic jump (Jopling and Richardson, 1966; Lang and Winsemann, 2013; Cartigny et al., 2014; Ito et al. 2014). The backset deposits, and the majority of the scour-fill, are characterised almost exclusively by climbing ripple-lamination (Fa 2). These deposits may be either the product of rapid settling from the downstream parts of hydraulic jumps as the scour migrated headward, or the products

of subsequent infill by subcritical currents after being previously cut by flows that underwent a hydraulic jump. The measurements of hydraulic jumps over giant scours in a natural gravity current demonstrate, however, that the hydraulic jump enhances upward fluid movement for large distances downstream of the hydraulic jump (Sumner et al., 2013), and therefore minimises sedimentation within the scour. Additionally, the presence of climbing ripple lamination very close to the head of the scour suggests that this final phase was the product of depositional subcritical flows. In combination with the lack of evidence for any depositional features typical of supercritical conditions, other than the backset bedding in elements 3-5, the fill of the scour was predominantly by subcritical flows. Thus the inception, deepening, and sediment bypass phases of these giant scours may have been associated with hydraulic jumps in supercritical flows, whereas their infill was dominantly the product of later subcritical flows. This contrasts to the supercritical deposits interpreted in other examples of backset bedding (Jopling and Richardson, 1966; Lang and Winsemann, 2013; Cartigny et al., 2014; Ito et al., 2014).

The infill character of the scour to the north of the main Kleine Riet Fontein scour is very similar, with a lower siltstone-prone package and an abrupt change into an upper climbing-ripple dominated sandstone package. This suggests both features share a similar depositional history, which could be due to an internal control linked to an updip avulsion, or an external control such as a substantial change in turbidity current energy and/or size. Existing local seabed depressions consisting of partially filled scours could have triggered hydraulic jumps and subsequently reshaped their morphology in a similar manner in both scours, followed by lower energy subcritical flows, explaining the similarity in infill character.

4.7.3 Preservation of giant scour-fills

Within scour fields in modern systems, coalescence of scours is a common phenomenon (e.g., Parker, 1982; Macdonald et al., 2011a; Fildani et al., 2013; Shaw et al., 2013). It has

been emphasized that changes in the behaviour of flows as they pass over the erosional relief of small-scale scours leads to the development of larger depressions (e.g., Shaw et al., 2013). This could be due to either the development of flow separation zones, enhancing erosion, or the triggering of a hydraulic jump (Sumner et al., 2013).

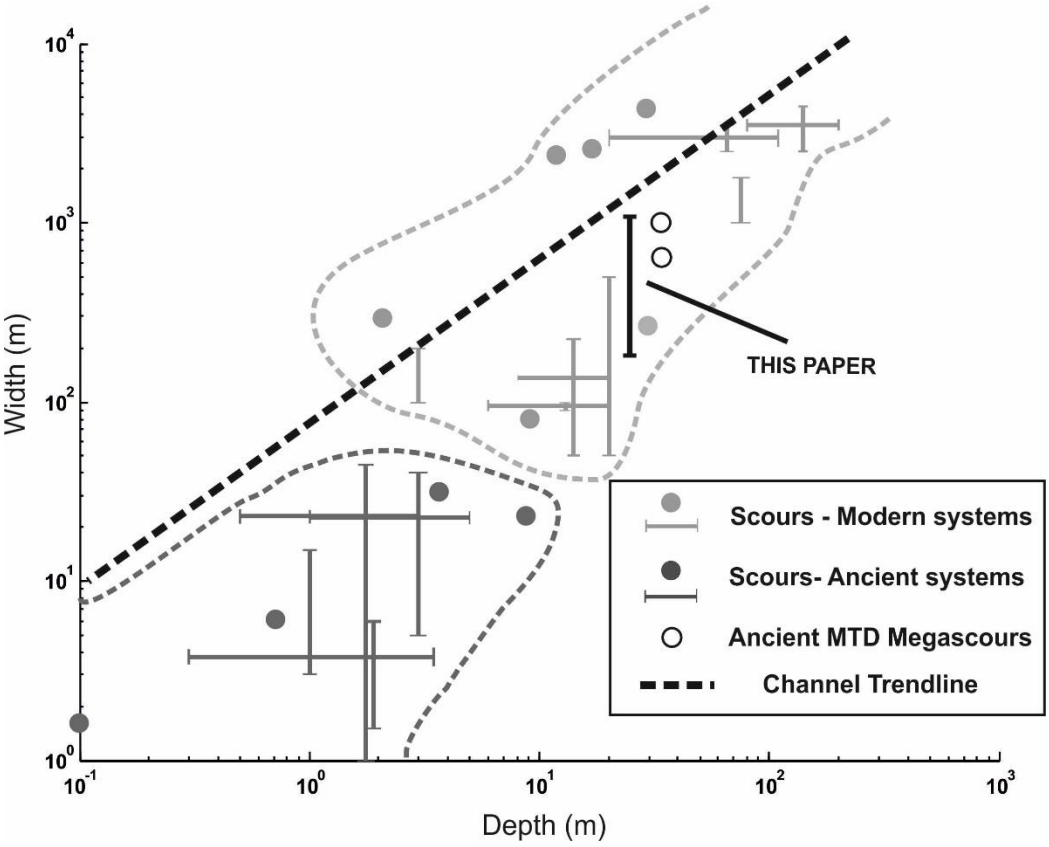

Figure 4.14. *Cross plot of width and depth data of scours and megaflutes from ancient (outcrop) and modern systems. Scour data from Macdonald (2011a). Channel trendline is based on Clark and Pickering (1996).*

A scale gap remains, however, between scours documented from the modern seabed and megaflutes and scours interpreted from outcrop studies (Fig. 4.14). Exhumed scours of the scale described here, and filled with turbidites, have not been described in detail previously. However, the scale of these scour-fills coincides with the range known from modern-day scours (Fig. 4.14) in CLTZs (e.g., Kenyon et al., 1995; Wynn et al., 2002a; Macdonald et al., 2011a), which are able to reach significant dimensions due to their

composite character and upstream migration. This study shows that within sand-rich turbidite systems, such as in the Karoo Basin, scour-fills of dimensions documented from modern system can be preserved, and care is needed to discriminate them from submarine channel-fills.

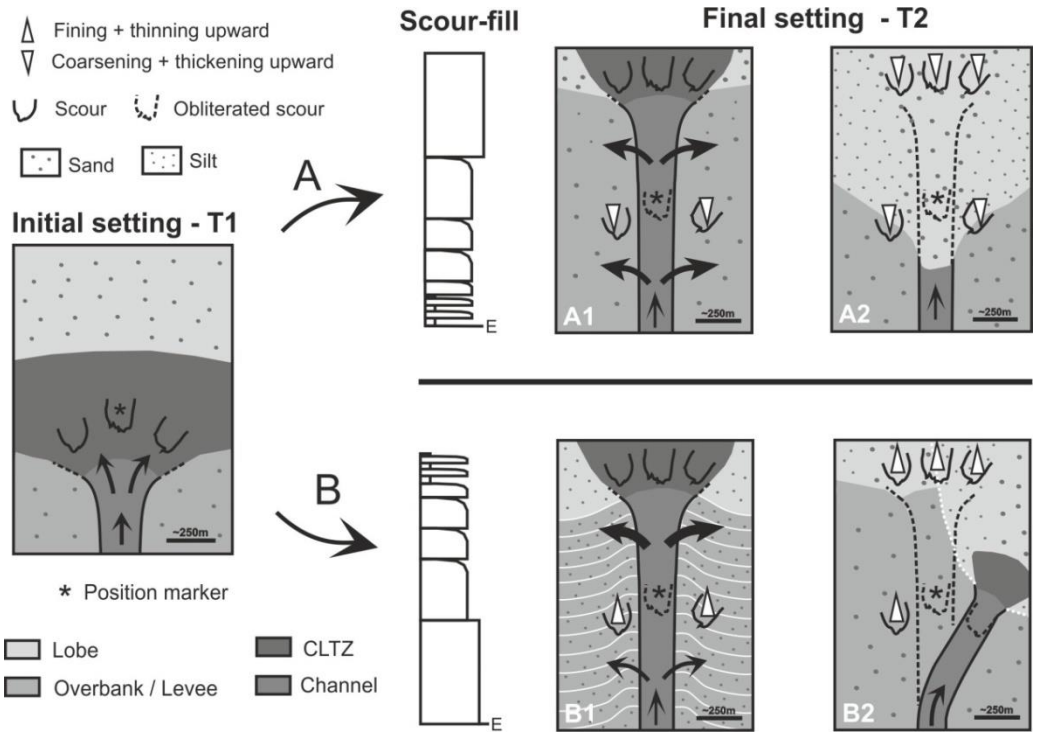

Figure 4.15. *Conceptual model to explain different mechanism of long-lived composite scours preservation from the initial formation (T1) to final depositional configuration (T2) depending on the character of the infill: coarsening and thickening upward (A) or fining and thinning upward(B). Two scenarios are proposed for coarsening- and thickening-upward infills (A): A1 – Scour preservation due to a position adjacent to an erosional channel during propagation with increased overbank deposition; A2 – Scour preservation at the maximum extent of channel propagation followed by infill by lobe retrogradation with decreased overbank deposition. Two scenarios are proposed for finning- and thinning-upward infills (B): B1 – Scour preservation due to a position adjacent to a leveed channel during propagation; B2 – Scour preservation due to channel avulsion and successive infill of scour by lobe fringe materials.*

Scours can be obliterated as channels propagate (Macdonald et al., 2011a) over lobes (Jegou et al., 2008; Macdonald et al., 2011b; Morris et al., 2014a). However, several mechanisms can be invoked to explain the preservation of large-scale composite scour-fills: i) large-scale avulsion of the main feeder system prior to channel propagation into the scoured CLTZ area; ii) the presence of scours at the maximum extent of channel

propagation into the basin; and/or iii) lateral position during channel propagation. The character of scour fills will differ by the mechanism of preservation (Fig. 4.15). CLTZs are more laterally extensive areas (in modern systems ~500km - >10,000 km^2) (Wynn et al., 2002a) compared to channel systems, so that scours can be preserved adjacent to propagating channel-levee systems. The infill signal will depend on the nature of the channel system. During propagation of a leveed channel a fining- and thinning-upward infill will develop as higher parts of density stratified flows are stripped off during levee growth (Fig. 4.15 B1). In contrast, propagation of channels without levees could result in a coarsening- and thickening-upward profile due to the increasing volume of overspill as the channel propagates over the CLTZ (Fig. 4.15 A1). The exact infill style of scours adjacent to channels will depend on the rate of channel propagation to rate of scour infill. In the case of maximum channel propagation (Fig. 4.15 B2), coarsening- and thickening-upwards would be expected as the scour fills by sands during retrogradation of lobes. In the case of channel avulsion prior to complete fill of the scour, a fining- and thinning-upward profile would form from lobe fringe deposits (Fig. 4.15 B2). Both examples described here have a stepped coarsening- and thickening-upward infill (Figs. 4.6, 4.11). Within (A) of Figure 4.15, their depositional history is most likely related to (one of) the two presented preservation mechanisms (A1 and A2).The simple cut-and-fill character of the Unit A5 scour-fill, which is linked to initial bypass succeeded by increasing deposition that fits best with maximum channel propagation (Fig. 4.15 A2). In contrast, the composite infill of the Fan 3 scours indicates proximity to a high energy setting, such as adjacent to an erosional channel (Fig. 4.15 A1).

4.8 Conclusions

This study reports the first detailed documentation of exhumed giant (>1000-1500 m long) turbidite-filled scours from deep-marine settings. Palaeogeographically, both scour-fills are constrained to base-of-slope channel-lobe transition zone settings. The scour-fills exhibit

composite and downstream-asymmetric basal erosion surfaces, with internal erosion surfaces. The sedimentary infills show stepped coarsening- and thickening-upwards trends, with the basal fine-grained deposits being associated with low-energy tails of bypassing turbidity currents and subsequent reworking. The simple infill architecture of the Unit A5 scour suggests a rather straightforward cut-and-fill history, possibly preserved by being situated at the maximum extent of channel propagation. Palaeoflow patterns within the Fan 3 Kleine Riet Fontein scour indicate complicated deflected flow patterns, which supports interpretation of headward recirculation and downstream flow expansion. The facies and architecture of the Fan 3 Kleine Riet Fontein scour-fill, however, points to a more dynamic history of interactions between flows and the relief of the scour, resulting in a more complicated architecture with evidence for headward erosion and a series of large internal erosion surfaces. This is interpreted to be due to scour preservation adjacent to an erosional channel during propagation.

The steep updip margins, stepped coarsening- and thickening upward successions of dominantly subcritical flow deposits, and internal palaeocurrent dispersal patterns contrast with laterally and stratigraphically adjacent basin-floor channel-fills. Despite their palaeogeographic setting and evidence for formation by hydraulic jumps, their fills, including backset deposits, do not support deposition from supercritical flows. Documenting the facies and architecture of scour-fills is important for the identification and description of areas dominated by sediment bypass in the rock record, and has consequences for the accurate geological modelling of CLTZs.

Chapter 5:
Architecture and morphodynamics of sediment waves in an ancient channel-lobe transition zone

5.1 Summary

In modern systems, submarine channel-lobe transition zones (CLTZs) show a well-documented assemblage of depositional and erosional bedforms, however their stratigraphic record is poorly constrained. Several locations from an exhumed fine-grained base-of-slope system (Unit B, Karoo Basin) show exceptional preservation of sandstone beds with distinctive morphologies and internal facies distributions. The regional stratigraphy, lack of confining surface, wave-like morphology, size and facies characteristics support an interpretation as sediment waves within a CLTZ setting. Some sediment waves show steep (10-25°) unevenly spaced (10-100m) internal truncation surfaces that are dominantly upstream-facing, which suggests significant spatio-temporal flow fluctuations. Their architecture indicates individual sediment wave beds are formed by upstream accretion, where each swell grows individually due to differential deposition rather than simultaneously as a sinusoidal wave. These depositional processes do not correspond with known bedform development under supercritical conditions. A combination of compensation-driven lateral switching of the flow and fluctuations around the critical Froude number are suggested to be responsible for their complicated architecture and facies patterns. A scale and formative process-based classification is applied for these sediment waves, as stacking behaviour may vary depending on the scale of observation. Differences in bedform characteristics between the two study areas are related to the position within CLTZ settings. The depositional architecture of turbidite bedforms highlights the importance of understanding the influence of dynamic erosional and depositional processes commonly present in channel-lobe transition zones.

5.2 Introduction

Modern submarine fan systems are characterised by a wide range of depositional and erosional bedforms at channel-lobe transition zones (CLTZs) (Mutti and Normark, 1987; Normark and Piper, 1991; Palanques et al., 1995; Morris et al., 1998; Wynn et al., 2002a; 2002b; Macdonald et al., 2011a). Bedforms are rhythmic features that develop at the interface of fluid flow and a moveable bed (e.g. Southard, 1991; Van der Mark et al., 2008; Baas et al., 2016).

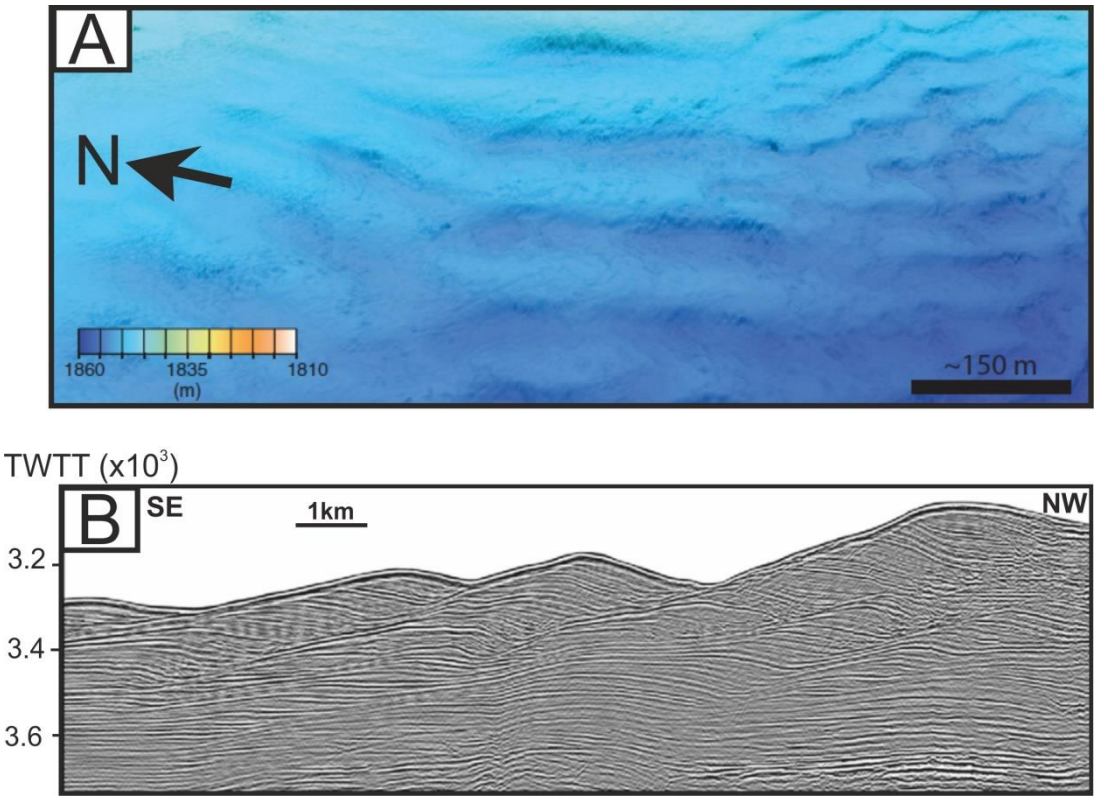

Figure 5.1 *A) A planform view of crescent-shaped sediment waves on the Monterey Canyon floor from autonomous underwater vehicle-collected multibeam data. Modified from Paull et al. 2011. B) High resolution seismic-reflection profile collected across the Var Sediment Ridge in the Var Turbidite System showing kilometre-scale sediment wave architectures. Modified from Migeon et al. 2012.*

Sediment waves are commonly identified bedforms within CLTZs (Wynn and Stow, 2002; Wynn et al., 2002b), and have been extensively described from modern systems (Fig. 5.1) (Normark and Dickson, 1976; Damuth, 1979; Lonsdale and Hollister, 1979; Piper et al., 1985; Malinverno et al., 1988; Praeg and Schafer, 1989; Howe, 1996; Kidd et al., 1998; Morris et al., 1998; McHugh and Ryan, 2000; Migeon et al., 2001; Normark et al., 2002;

Wynn and Stow, 2002; Wynn et al., 2002a; Heinïo and Davies, 2009). Few examples have been identified in ancient deep-marine settings (Winn and Dott, 1977; Piper and Kontopoules, 1994; Vicente Bravo and Robles, 1996; Ito and Saito, 2006; Ito, 2010; Campion et al., 2011; Ponce and Carmona, 2011; Morris et al., 2014b; Postma et al., 2014; Pemberton et al. 2016) (Fig. 5.2). Sediment waves show significant variation in grain size (from mud- to gravel-dominated), which has been linked to their depositional setting (Fig. 5.2B) (Wynn and Stow, 2002), where the coarser-grained sediments typically concentrate within channels and channel/canyon mouth settings. Furthermore, ancient sediment waves are dominantly coarse-grained (coarse-grained sand to gravel), whereas modern examples are dominantly fine grained (silt to mud) (Figs. 5.2A, 5.2C). The lack of exhumed fine grained sediment waves has been ascribed to their long wavelength (Fig. 5.2C) (Piper and Kontopoulos, 1994).

Some finer grained exceptions have been described from the Cerro Toro Formation by Campion et al. (2011) with 35% sandstone volume, and the Karoo Basin by Morris et al. (2014b) with shingled very-fine-grained sandstone beds, both from (proximal) external levee settings (*sensu* Kane and Hodgson, 2011).

The stratigraphic record of sediment waves from CLTZ and channel-mouth settings is not widely documented (Figs. 5.2A, 5.2B). Vicente Bravo and Robles (1995) described hummock-like and wave-like depositional bedforms from the Albian Black Flysch, NE Spain. The hummock-like bedforms showed a sinusoidal pattern in transverse and longitudinal sections, which could be isolated but more likely form bedform fields with wavelengths ranging from 5 to 40 m and heights from a few decimetres to 1.5 m. The hummock-like bedforms were inferred to be genetically related to local scours and probably developed within a CLTZ setting. The wave-like bedforms seen in longitudinal sections exhibit symmetric to slightly asymmetric gravel-rich bedforms with wavelengths ranging between 5 and 30 m and amplitudes from a few cm to 0.7 m.

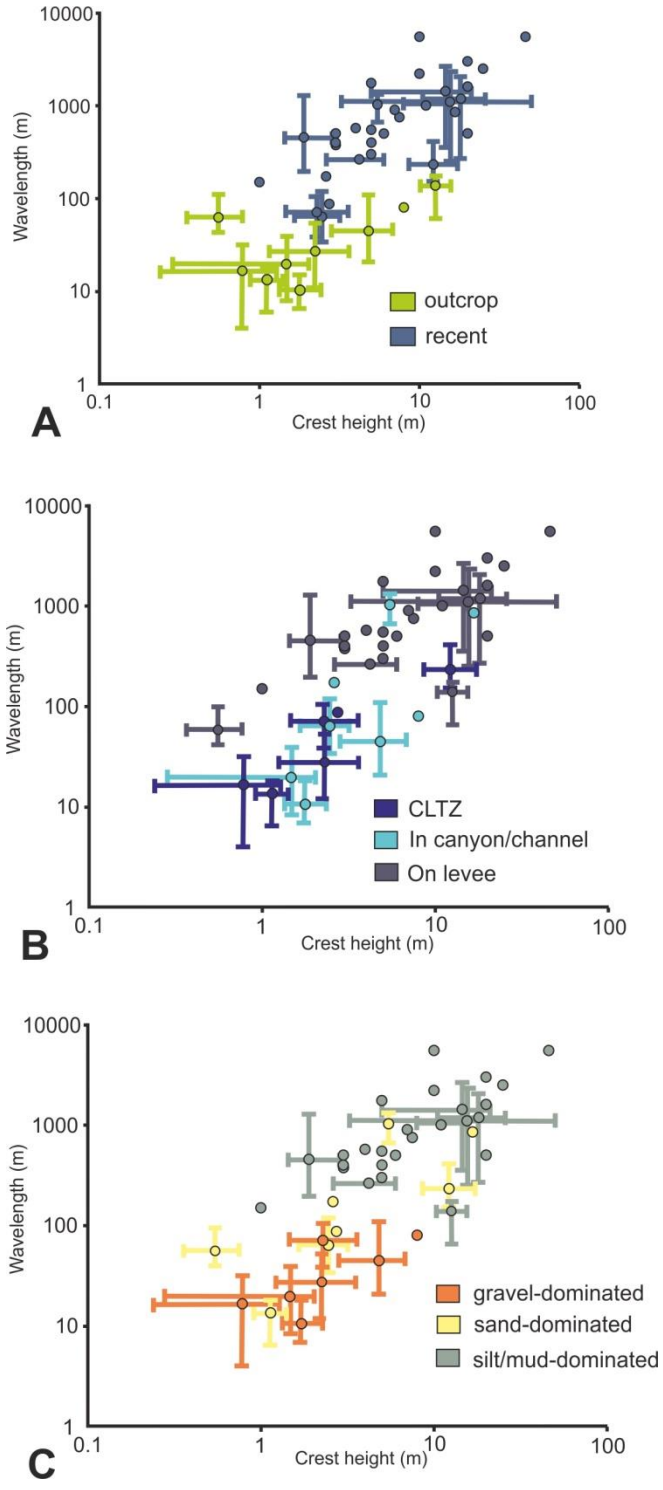

Figure 5.2 *Sediment wave dimensions (crest height versus wavelength) from modern and ancient systems grouped on the basis of type of dataset (A), setting (B) and grain size (C). Data taken from Normark and Dickson (1976); Winn and Dott (1977); Damuth (1979); Lonsdale and Hollister (1979); Piper et al. (1985); Malinverno et al. (1988); Praeg and Schafer (1989); Piper and Kontopoulos (1994); Vicente Bravo and Robles (1995); Howe (1996); Kidd et al. (1998); Morris et al. (1998); Nakajima et al. (1998); McHugh and Ryan (2000); Migeon et al. (2001); Wynn et al. 2002a; 2002b; Normark et al. (2002); Ito and Saito (2006); Heinïo and Davies (2009); Ito (2010); Campion et al. (2011); Ito et al. (2014); Ponce and Carmona (2011); Morris et al. (2014b); Postma et al. (2014).*

Ponce and Carmona (2011) identified sandy conglomeratic sediment waves with amplitudes up to 5 m and wavelengths ranging between 10 to 40 m at the northeast Atlantic coast of Tierra del Fuego, Argentina. Ito et al. (2014) described medium- to very coarse-grained sandstone tractional structures from a Pleistocene canyon-mouth setting within the Boso Peninsula, Japan, with wavelengths up to 40 m and crest heights up to 2 m.

These coarse-grained examples from Japan, Argentina and Spain lack detailed internal facies descriptions and structure. Consequently, the recognition and detailed description of finer-grained sandstone-dominated depositional bedforms in channel mouth settings is lacking. Furthermore, it remains unclear which processes are responsible for the formation of sediment waves within CLTZ settings, as both initial deposition from highly-concentrated turbidity currents and subsequent reworking by lower concentration flows have been proposed (Wynn et al., 2002b). Here, multiple stratigraphic sections from well-constrained base-of-slope systems (Unit B, Karoo Basin) are documented in detail. These sections contain distinctive fine to very-fine sandstone depositional bedforms with complicated architectures, facies and stacking patterns associated with submarine channel-mouth settings. The aims of this chapter are: 1) to improve understanding of their depositional architecture and facies patterns, 2) to investigate bedform hierarchy and stacking patterns, and 3) to constrain their formative processes.

5.3 Regional setting

The southwest Karoo Basin is subdivided into the Laingsburg and the Tanqua depocentres. The Ecca Group comprises a ~2 km-thick shallowing-upward succession from distal basin-floor through submarine slope to shelf-edge and shelf deltaic settings (Wickens, 1994; Flint et al., 2011). The deep-water deposits of the Karoo Basin have a narrow grain size range from clay to upper fine sand. Within the Laingsburg depocentre, Unit B, the focus of this study, is stratigraphically positioned between underlying proximal basin-floor fan deposits

of Unit A (e.g. Sixsmith et al., 2004; Prélat and Hodgson, 2013) and the overlying channelised slope deposits of the Fort Brown Formation (Unit C-G; e.g. Hodgson et al., 2011; van der Merwe et al., 2014). Unit B comprises a 200m thick section at the top of the Laingsburg Formation (Grecula et al., 2003a; Flint et al., 2011; Brunt et al., 2013a), and is subdivided in three subunits, B.1, B.2 and B.3 (Flint et al., 2011; Brunt et al., 2013a). Unit B is well-exposed for more than 350km^2 providing both down dip and across strike control (Brunt et al., 2013a) with over 15km long exposed sections along the limbs of the Baviaans and Zoutkloof synclines and Faberskraal anticline (Fig. 5.3A). The stratigraphic context, and the documented downdip transition from sandstone-prone channel-fills to lobe complexes (Grecula et al., 2003a; Pringle et al., 2010; Brunt et al., 2013a), supports an interpretation of a base-of-slope setting for Unit B in the study area.

Brunt et al. (2013a) presented a depositional model for the complete Unit B based on data from 38 different localities. Subunit B.1 was interpreted to comprise two distinct base-of-slope systems supplied by flows that entered the basin from the south. The base of subunit B.2 shows progradation in the most southern system, whereas a switch of feeder area from south to west is implied in the other. In the overlying subunit B.3, the extent of fining- and thinning-upward thin-bedded deposits incised by channel-complexes, is interpreted to represent an extensive channel-levee system on the lower slope (Brunt et al., 2013a).

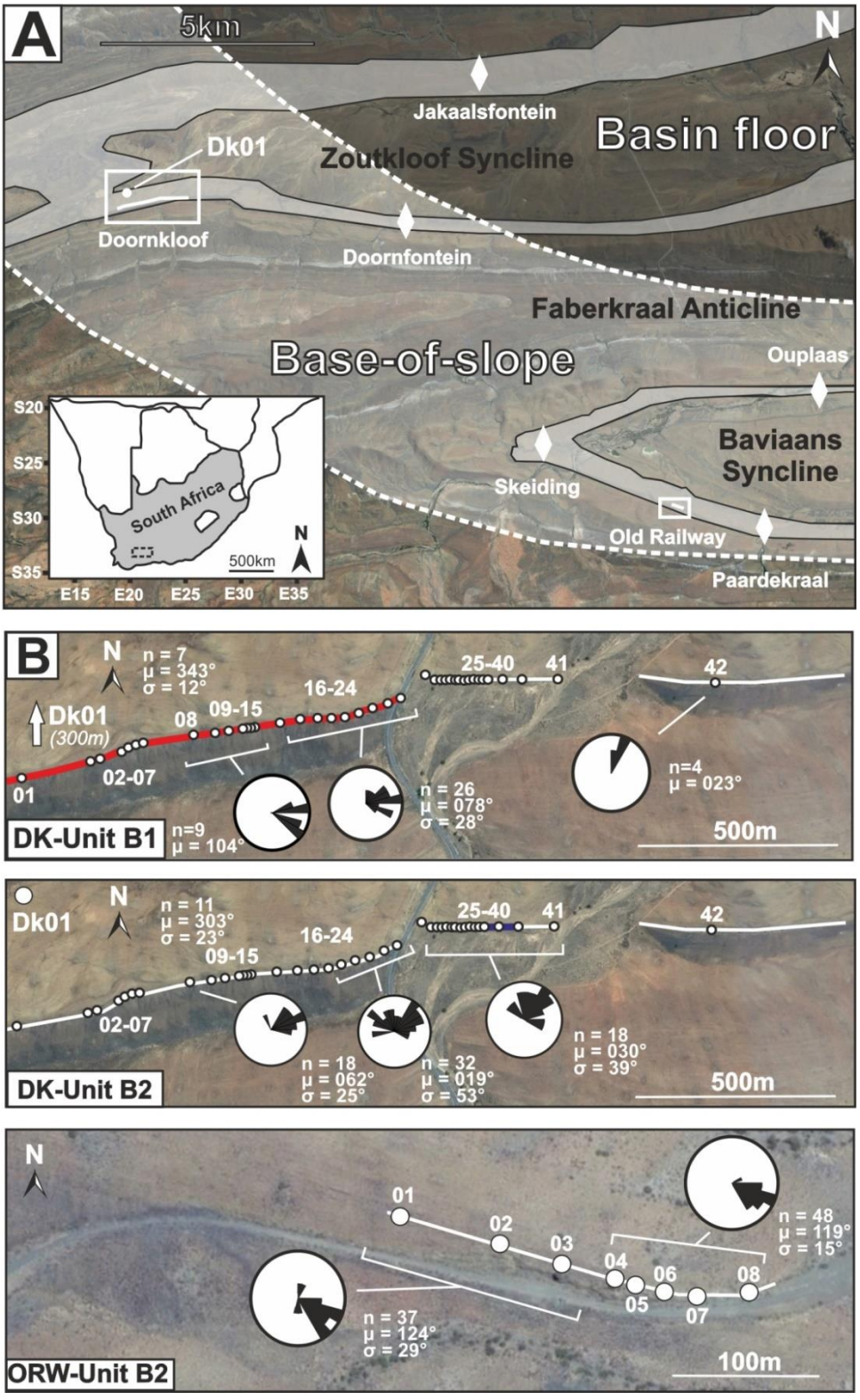

Figure 5.3 *A – Location map of the Laingsburg depocentre within the Western Cape. The transparent overlay with black lining indicates the total exposed area of Unit B. Important outcrop areas are highlighted, including the sections studied in this chapter: Doornkloof and Old Railway. B – Zoomed-in maps of the two sections including palaeocurrent distributions. The outcrop outlines are indicated by solid lines. Red line indicates Section I (Figure 5.4), blue line on DK-unit B2 represents Section II (Figure 5.6).*

5.4 Methodology and dataset

Two areas were studied in detail (Fig. 5.3B): one located in the southern limb of the Zoutkloof Syncline (Doornkloof) and one located in the southern limb of the Baviaans Syncline (Old Railway) (Fig. 5.3). Stratigraphic correlations using closely-spaced sedimentary logs, photomontages, and walking out key surfaces and individual beds with a handheld GPS enabled construction of architectural panels. Where the exposure allowed sub-metre-scale sedimentary logs, individual beds could be correlated over multiple kilometres. Within the Doornkloof area (Figs. 5.3B, 5.4), 11 long (>20-200m) sedimentary logs, supported by 31 short (<5 metres) detailed sedimentary logs were collected along a 2 km long E-W section (See Appendix B.3). Particular emphasis was placed on bed-scale changes in facies to construct detailed correlation panels. Additionally, a research borehole drilled 330 m north of the studied outcrop section (DK01) intersected the lower 92 m of Unit B (Fig. 5.3). Within the Old Railway area (Fig. 5.3B), eight short and closely spaced (5-20m distance) detailed sedimentary sections were collected. Palaeocurrents were collected purely from ripple-laminated bed tops, with 117 palaeoflow measurements at Doornkloof and 87 from the Old Railway area (See Appendix B.2).

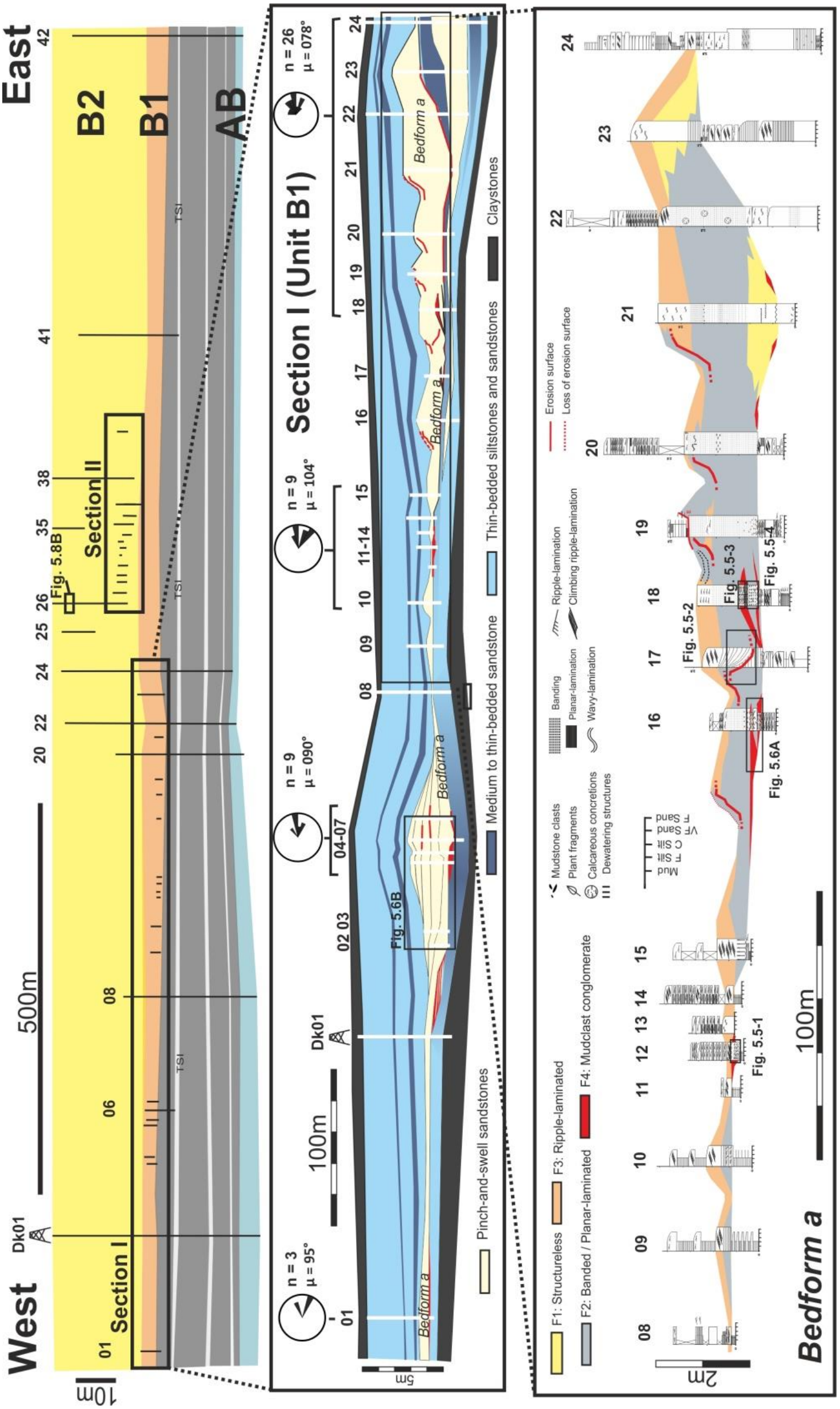

Figure 5.4 *Complete stratigraphic panel of the Doornkloof section showing the subunit subdivision and the location of the two detailed sedimentary sections (I, II) indicated and the position of the DK01 core. The TSI-silt (Brunt et al. 2013a) between the AB interfan and subunit B1 has been used as a stratigraphic datum. The middle correlation panel shows section I of Unit B1; the position of Bedform a and the palaeoflow patterns have been indicated. The bottom correlation panel shows the detailed facies distribution within Bedform a and its internal truncation surfaces. Outcrop photograph locations shown in Figure 5.5 (1-4 on the lowermost sub-panel) and Figure 5.6A have been indicated as well as location of correlation panel in Figure 5.6B.*

5.5 Facies and architecture

Both study areas contain sandstone-prone packages that comprise bedforms with substantial downdip thickness and facies changes without confinement by an incision surface. The rate of thickness change and the range of sedimentary facies are markedly different from that documented in basin-floor lobes (e.g. Prélat and Hodgson, 2013). Depositional bedforms in both study areas are present within a sandstone-prone (>90%) package of dominantly medium-bedded structured sandstones, interbedded with thin-bedded and planar-laminated siltstones. The grain size range is narrow, from siltstone to fine-grained sandstone, with a dominance of very-fine sandstone.

5.5.1 Facies characteristics

The sedimentary facies within the bedforms are subdivided into four types: structureless (F1), banded to planar-laminated (F2), ripple-laminated (F3), and sandstone and mudstone clast conglomerates (F4).

F1: Structureless sandstones show minimal variation or internal structure and are uniform in grainsize (fine-grained sandstone). Locally, they may contain minor amounts of dispersed sub-angular mudstone clasts (1-10 cm). These sandstones are interpreted as the deposits from rapid fall-out from sand rich high-density turbidity currents (Kneller and Branney, 1995; Stow and Johansson, 2002; Talling et al., 2012) with mudstone clasts representing traction-transported bedload. Flame structures at the bases of structureless beds are associated with syn-depositional dewatering (Stow and Johansson, 2002).

F2: Banded and planar-laminated sandstones show large variations in character. The differentiation between planar-laminated and banded facies is based on the thickness and character of the laminae. In banded sandstones, laminae are 0.5-3 cm thick and defined by alternations of clean and dirty sand bands, rich in mudstone chips and/or plant fragments.

Planar-laminations show <1 cm thick laminae that are defined by clear sand-to-silt grain-size changes. Furthermore, bands can be wavy or convolute, show substantial spatial thickness variations (<1 cm) at small (<1 m) spatial scales, and exhibit subtle truncation at the bases of darker bands. Banded facies are mudstone clast-rich when close to underlying mudstone clast conglomerates. Several banded sandstone beds could be traced upstream into mudstone clast conglomerates.

Planar-lamination and banding are closely associated, and in many cases are difficult to distinguish. This suggests that their depositional processes are closely related and are combined here into a single facies group. Planar laminated sandstones are interpreted to be deposited under upper stage plane bed conditions (Allen, 1984; Best and Bridge, 1992). The banded facies are interpreted as traction carpet deposits from high-density turbidity currents (Lowe, 1982; Sumner et al., 2008; Talling et al., 2012; Cartigny et al., 2013) and are comparable to the Type 2 tractional structures of Ito et al. (2014) and the H2 division of Haughton et al. (2009). It has been emphasised that deposits related to traction carpets can show large variation in facies characteristics (e.g. Sohn, 1997; Cartigny et al., 2013).

F3: Climbing ripple-laminated sandstones, commonly with stoss-side preservation. Ripple lamination is most common at bed tops, but occasionally at bed bases, overlain by an amalgamation surface. Climbing ripple-lamination is interpreted as high rates of sediment fallout with limited tractional reworking from flows within the lower flow regime (Allen 1973; Southard and Boguchwal, 1990). Locally, mudstone clasts (<1-4 cm) have been observed within ripple-laminated segments. These mudstone-clasts are interpreted to be the result of overpassing of sediments on the bed (Raudkivi, 1998; Garcia, 2008). When sedimentation rate exceeds the rate of erosion at the ripple reattachment point, the stoss-side deposition is preserved and aggradational bedforms develop (Allen, 1973). This is indicative of high rates of sediment fallout (Jopling and Walker, 1968; Allen, 1973; Jobe et

al., 2012; Morris et al., 2014a), attributed to rapid flow deceleration from moderate-to-low concentration turbidity currents (Allen, 1973).

F4: Mudstone clast conglomerate deposits form discrete patches (<20 m long and <0.3 m thick), which commonly overlie erosion surfaces. Mudstone clasts (<1 cm – 10 cm) vary from subangular to well-rounded. They are dominantly clast supported with a matrix of fine-grained sandstone. Mudstone clast conglomerates are interpreted as lag deposits (e.g. Stevenson et al., 2015) from energetic and bypassing high-density turbidity currents.

5.5.2 Bed architecture: Doornkloof – Subunit B.1

At Doornkloof (Fig. 5.3), subunit B.1 has an average thickness of ~5 m (Fig. 5.4) and is composed of thin- to thick-bedded sandstones, thin-bedded siltstones and lenticular mudstone clast conglomerates (0.1-0.3 m thick, 1-70 m wide) (Figs. 5.5-1, 5.5-2, 5.6). There are substantial lateral variations in bed thicknesses and sandstone-to-siltstone proportions along the 1.5 km long dip section (Fig. 5.4). Locally, medium- to thick-bedded sandstones occur, which comprise bedforms within a package of thin-bedded siltstones and sandstones. These bedforms show lateral changes to more tabular thin-bedded sandstones and siltstones (log 01/log 08 Fig. 5.4). Within the exposed section (~ 2 km), there are three sandstone-prone bedform-dominated sections (200 m to 300 m in length) separated by more siltstone-prone sections (150 to 400 m in length), which have an overall tabular appearance (Fig. 5.4). The Dk01 core (Fig. 5.4, 5.5) is located 330 m to the north of the western limit of Section I where Unit B.1 is a ~5 m thick package of interbedded thin structured sandstones and laminated siltstones (Fig. 5.4). Multiple erosional surfaces are present at the base, and overall in the DK01 core the Unit B.1 succession fines- and thins-upwards. Palaeoflow of the B.1 subunit is dominantly ENE-orientated (082°) (Fig. 5.2B) but shows some deviation within the eastern part of the section (42 – Fig.5.4) towards the NNE (023°).

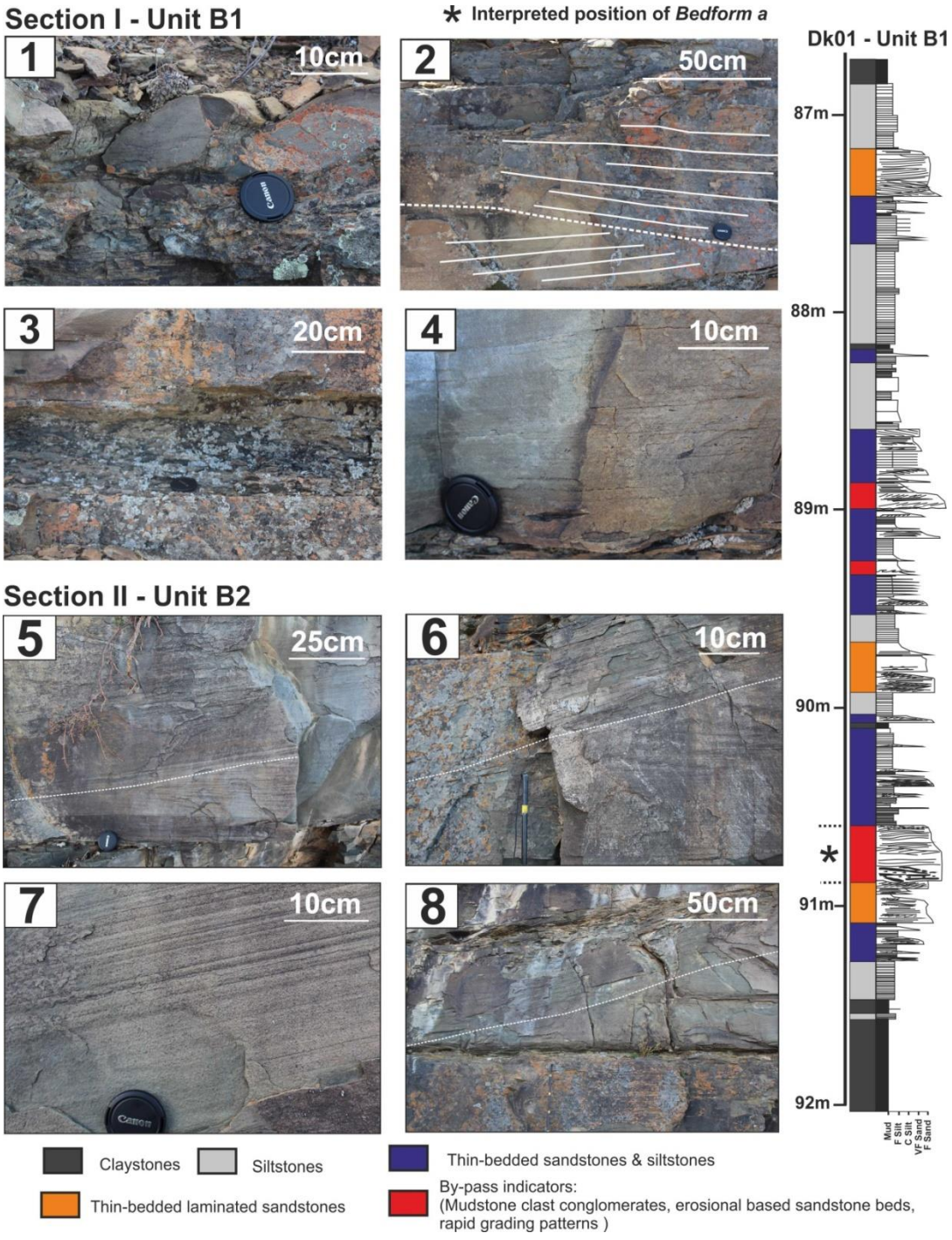

Figure 5.5 *Representative outcrop photographs from Section I and II and descriptive DK01 core log of Unit B1, with 1) Bedform a with ripple-top morphology on top of a local mudstone clast conglomerate deposit; 2) Internal truncation surface (dotted line) in banded division within Bedform a; 3) Mudstone clast conglomerate layer below Bedform a ; 4) Mudstone clast-rich banded section of Bedform a. 5) Lower section of westward orientated truncation surface in Bedform b; 6) Upper section of westward orientated truncation surface in Bedform b; 7) Banded sandstone division in Bedform b; 8) West-facing truncation surface in Bedform c. See Figure 5.4 and Figure 5.6 for locations. Interpreted position of Bedform a is indicated within the DK01 core log.*

The medium- to thick-bedded sandstones within the sandstone-prone sections of Section I, orientated (079°-259°) subparallel to palaeoflow, show large lateral variations in thickness and facies. The bedforms comprise structureless (F1), planar-laminated to banded (F2), and ripple-laminated (F3) sandstones. The facies, architecture and thickness changes of one particular amalgamated bed (*Bedform a*) is described in detail (Fig. 5.3). *Bedform a* thickens (up to 2.5 m) and thins (<20 cm) multiple times, forming a down-dip pinch-and-swell morphology. *Bedform a* shows shallow erosion (<0.5m deep; <30m long) locally at the bed base and occasionally amalgamates with the underlying stratigraphy (Fig. 5.6A). Where it exceeds 0.5 m thickness, banded (F2) sandstone is dominant, occasionally underlain by structureless (F1) divisions, or with climbing ripple-lamination at the bed top (F3). Where *Bedform a* is thin (<0.5 m thick), it is dominated by climbing-ripple lamination (F3). Below *Bedform a,* mudstone conglomerate patches (<30 m long; 5-30 cm thick) can be observed at various locations over the complete section. In some locations (e.g. 16/18, Fig. 5.4) banded sandstone (F2) beds (Fig. 5.5-4) can be observed within the mudstone clast conglomerate patches. These banded beds pinch out or show a transition towards mudstone clast conglomerates upstream, and amalgamate with *Bedform a* downstream (Fig. 5.6A). At the same stratigraphic level as *Bedform a*, the DK01 core shows one 20 cm thick bed with angular mudstone clasts (<1-5cm), here correlated as the same unit.

In *Bedform a,* six truncation surfaces (10-25°) are identified within the eastern limit of the section (Fig. 5.4), where it exceeds 1 m in thickness. All truncation surfaces are sigmoid-shaped and flatten out upstream and downstream within the bed. Sigmoidal truncation surfaces are most dominant in the upper portion of the bed, where they are westward (upstream) facing. The five westward (upstream) orientated truncation surfaces are spaced 15-20 m apart, and are associated with abrupt local upstream thinning. They cut banded (F2) and ripple-laminated (F3) sandstone facies, and are sharply overlain by banded sandstone facies (F2) with bands aligned parallel to the truncation surface.

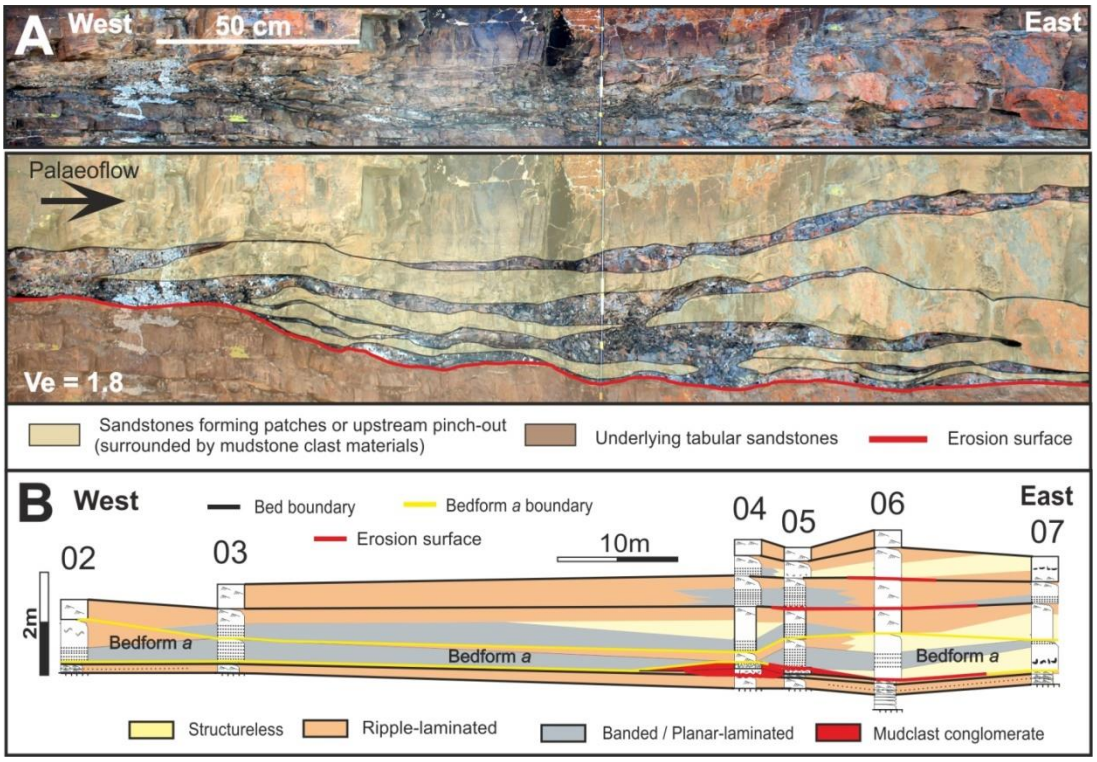

Figure 5.6 *A - Mudstone clast conglomerate patch at the bottom of Bedform a, with clean true-scale photopanel (top) and interpreted vertical exaggerated (Ve = 1.8) photopanel (bottom). It shows a basal erosion surface overlying thin-bedded sandstones, multiple 'floating' sandstone patches, upstream orientated pinch-out and downstream orientated amalgamation. Location of photograph is shown in the lowest panel of Figure 5.4. B – Facies correlation panel of local swell in Unit B.1. Bedform a is located at the base of the sandstone package. See middle panel of Figure 5.4 for location and lower panel of Figure 5.4 for symbol explanations.*

One eastward (downstream) orientated truncation surface (Fig. 5.5-3) in the lower part of the bed is observed at log 17 (Fig. 5.4). The abrupt upstream thinning (SW) and more gradual downstream thickening (NE) gives *Bedform a,* an asymmetric wave-like morphology in dip section. At abrupt bed thickness changes associated with steep truncation surfaces (>15°) (16/19/21 Fig. 5.4), shallow scour surfaces (<0.35 cm) can be observed cutting into the top surface of *Bedform a*, overlain and onlapped by thin-bedded siltstones and sandstones. Within the banded facies (F2), isolated lenses of ripple-lamination (F3) are present (up to 30-40 cm long and 10 cm thick) (Fig. 5.4 – log 19). Mudstone and siltstone clasts (0.2-5 cm diameter) dispersed throughout structureless (F1) sections are typically

well rounded, and rarely sub-angular. At the eastern limit of Section I stratigraphically below *Bedform a*, another 'pinch-and-swell' sandstone bed abruptly increases in thickness downstream and amalgamates with *Bedform a* (Fig. 5.4 – Log 21). Where this bed thickens, *Bedform a* thins abruptly (Fig. 5.3 – Log 23/24). The thin-bedded and siltstone-prone deposits overlying *Bedform a* show more laterally constant geometries, thicknesses and facies. However, around log 02/07 (Fig. 5.4), a package of sandstone beds thickens locally (>100 m long, <5 m thick) above *Bedform a (*Fig. 5.6B). *Bedform a* pinches and swells multiple times within this interval to a maximum of 0.5 m and comprises similar facies as downstream (F1, F2, F3), but lacks internal truncation surfaces. The bed directly above *Bedform a* thickens where *Bedform a* thins and *vice versa* (Fig. 5.6B). The sandstone beds in the top of the package show much more limited thickness variations (~10 cm) and dominantly comprise climbing ripple-laminated sandstone (F2). All sandstone beds above *Bedform a* either pinch-out or show a facies transition towards fine siltstone in both western and eastern directions (Fig. 5.4).

5.5.3 Bed architecture: Doornkloof – Subunit B.2

The sandstone bed morphology and facies characteristics at the base of subunit B.2 share many affinities with the deposits described within subunit B.1 (Fig. 5.7B). Palaeoflow of subunit B.2 is generally NE-orientated (040°) and shows a shift from NE (046°) in the western part of the section, which deviates northwards in the eastern part of the section (030°) (n=47, Figs. 5.2, 5.7B), indicating the section is subparallel to palaeoflow (dip section). Subunit B.2 dominantly comprises medium-bedded structured sandstone (Fig. 5.7A). Closely spaced-logs collected from the main face at the base of B.2 (Section II – Fig. 5.4) are used to trace out individual beds over a distance of 230 m and track internal facies changes. Two beds (*Bedform b* and *Bedform c*) change in thickness (0.5- 2 m for *Bedform b* and 0.3-1.2 m for *Bedform c*) and contain multiple internal truncation surfaces of which six are westward (upstream) facing and one is eastward (downstream) facing.

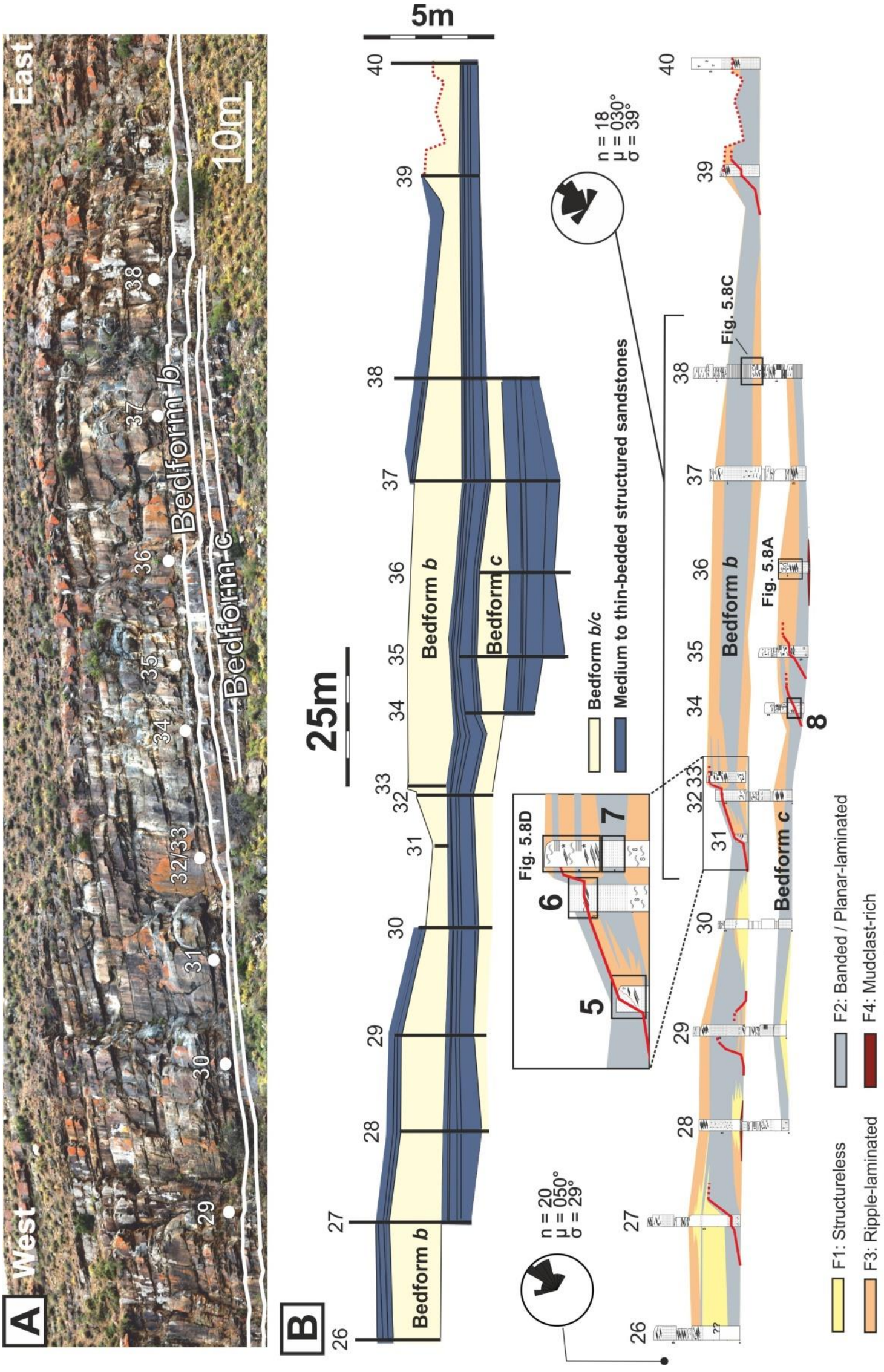

Figure 5.7 *A – Panoramic view of the base of subunit B.2 at the DK-section. B – Facies correlation of the II-section with Bedform b and c. The top panel shows the thickness variability of these beds and the surrounding stratigraphy; the lower panel shows the internal facies distribution of Bedform b and c. Rose diagrams show palaeoflow measurements around Section II. Internal truncation surfaces and location of the facies photos shown in Figure 5.5 (5 to 8) and Figure 5.8 have been indicated. See Figure 5.4 for meaning of log symbols.*

Truncation surfaces cut climbing ripple-laminated facies (F3) with maximum angles varying between 20-30° that shallow out and merge with the base of the bed. They flatten out in the downstream direction within the bed and are overlain by banded sandstone facies (F2). In *Bedform b*, the rate of westward thinning is more abrupt than eastward, giving an asymmetric wave-like morphology (Fig. 5.7B). This abrupt westward thinning is coincident with locations of westward (upstream) orientated truncation surfaces. In the eastern part, 110 m separates two truncation surfaces, in an area associated with bed thinning. However, towards the western part of *Bedform b*, there is only 25-30 m between the westward (upstream) orientated truncation surfaces, and these are not accompanied with abrupt bed thinning.

There is a high degree of lateral and vertical facies variability within *Bedform b* and *c* (Figs. 5.7B, 5.8). Commonly, lateral facies changes are accompanied by bed thickness changes. Locally, within the thicker parts of beds, bases are mudstone clast-rich. Bed tops show climbing ripple-laminated facies at most locations. Banded sandstone facies overlie the truncation surfaces. Some of the ripple-laminated facies (F3) within the middle or lower parts of *Bedform b* and *c* indicate flow directions that deviate (NW to N) from the regional palaeoflow (NE) (Figs. 5.8A, C, D). Detailed analysis of well-exposed sections (Fig.5.8) indicates that many laminated and banded sections are wavy and separated by low angle truncation or depositional surfaces. Ripple-laminated facies are present locally (Fig. 5.8C, D) (<10 cm thick; couple of metre wide patches) within the dominantly banded/planar-laminated facies (F2), as well as flame structures (Fig. 5.8D). *Bedform b* is topped in the easternmost exposure by a scour surface that cuts at least 0.5 m into *Bed b* and amalgamates with an overlying pinch-and-swell bed (Fig. 5.7B). Medium- to thin-bedded structured sandstones are present above and below *Bedform b* and *c*, which do not show any facies or thickness changes over the exposed section.

A

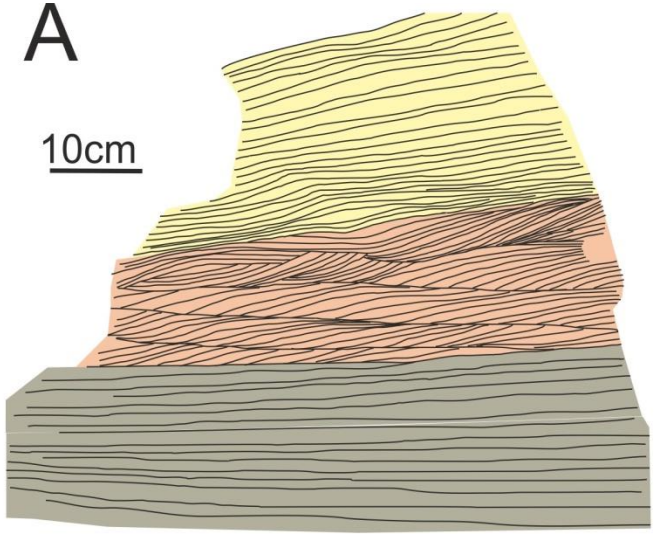

Planar banding/lamination Wavy banding/lamination Ripple-lamination

B

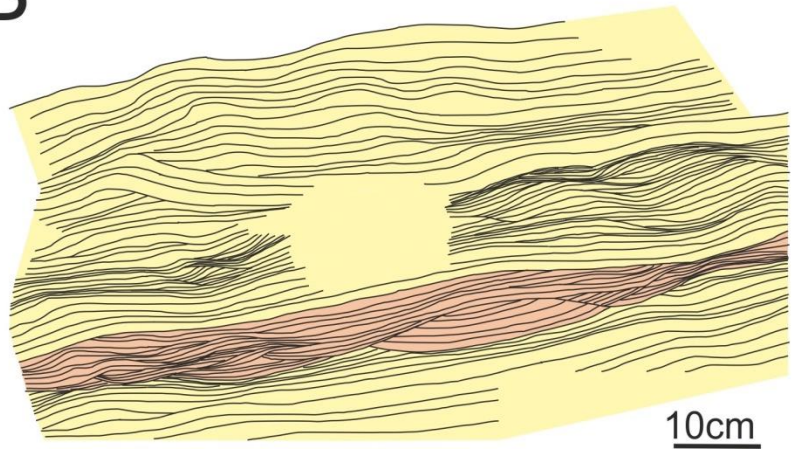

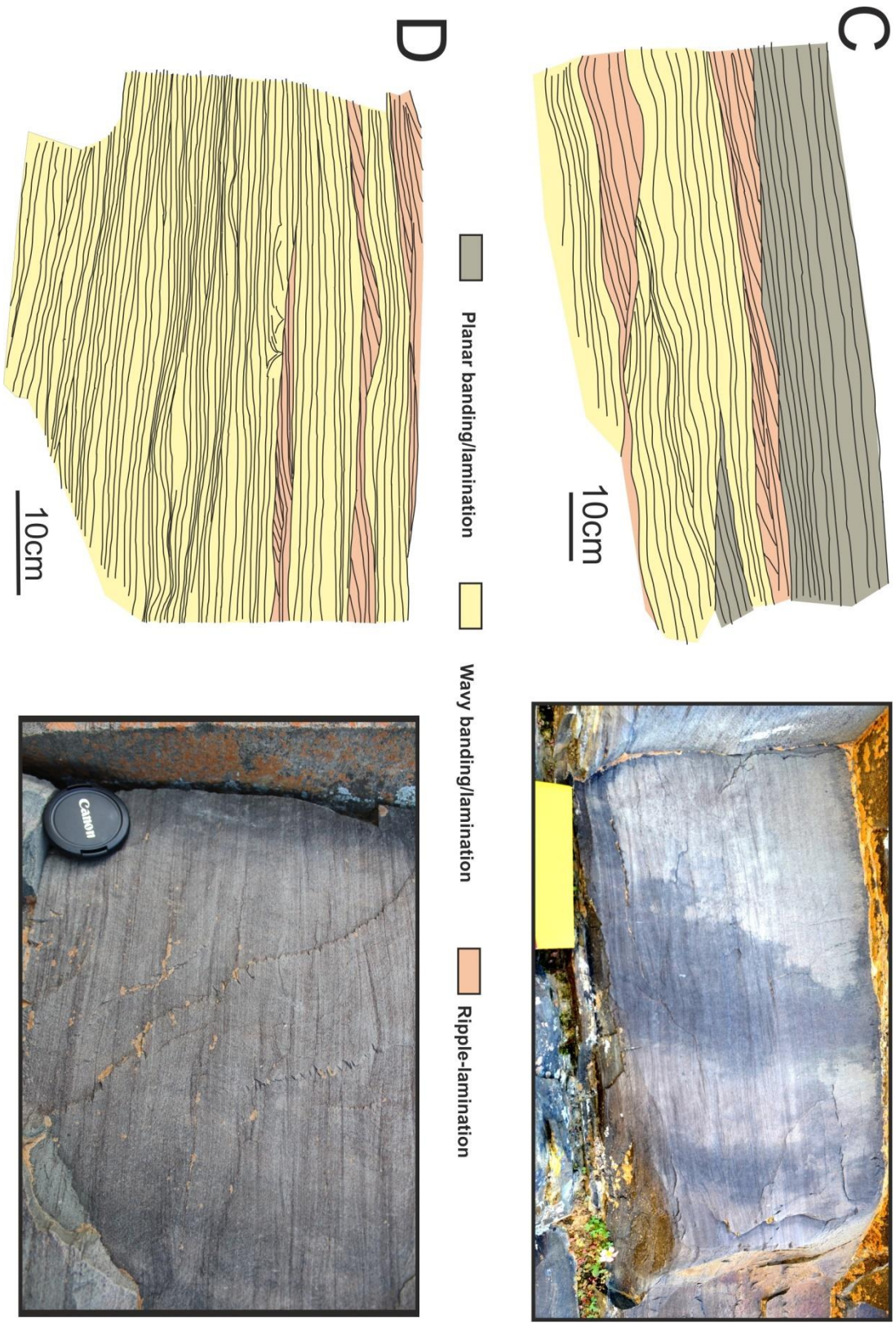

Figure 5.8 *Examples of Internal bed structure and facies changes within Unit B2 (Doornkloof), with one example from Bedform c (A), two from Bedform b (C and D) (see Figure 5.4 and Figure 5.7 for locations) and one (B) from a structured bed at the top of the Doornkloof section within log 24 (see Figure 5.3 for location). All these examples show vertical internal facies changes, which include planar-lamination, wavy-lamination/banding and ripple-lamination.*

The base of subunit B.2 in the DK01 core, at the same stratigraphic level as *Bedform b* and *c*, comprises thick-bedded structureless (F1) to banded (F2) (>3 m) sandstones. Bed bases are sharp and structureless and contain a variable amount of mudstone clasts (<1 cm). The middle to upper parts of these beds show banded facies (F2) with clear mudstone clast-rich and -poor bands, which pass through wavy lamination to climbing ripple (F3) and planar lamination at bed tops.

Above Section II, a 15 m thick sandstone package shows a substantial increase in bed thicknesses (max 4.5 m), mainly due to bed amalgamation (Fig. 5.7A). Some of these beds show a wave-like (asymmetric) morphology, similar to that observed in *Bedforms b and c.* Abrupt bed thinning or pinch-out is common. These pinch-outs are primarily associated with deposition, with rare examples of bed truncation by erosion surfaces. Bounding surfaces can be identified within the sandstone package, which are defined by successive upstream depositional bed pinchout points (Fig. 5.9), with local (<2 m long) shallow erosion (<0.3 m) surfaces. The bounding surfaces separate at least two different depositional elements, which show downstream bed shingling of three to four sandstone beds. The two elements are stacked in an aggradational to slightly upstream orientated manner (Fig. 5.9). These elements are topped by a >60m thick package of tabular and laterally continuous medium- to thin-bedded structured sandstones. The Dk01 core shows a transition from thick- to medium-bedded, dominantly banded (F2), sandstones towards more medium- to thin-bedded structured (F3) sandstones at the same stratigraphic level where the transition to the >60m thick package is observed in outcrop.

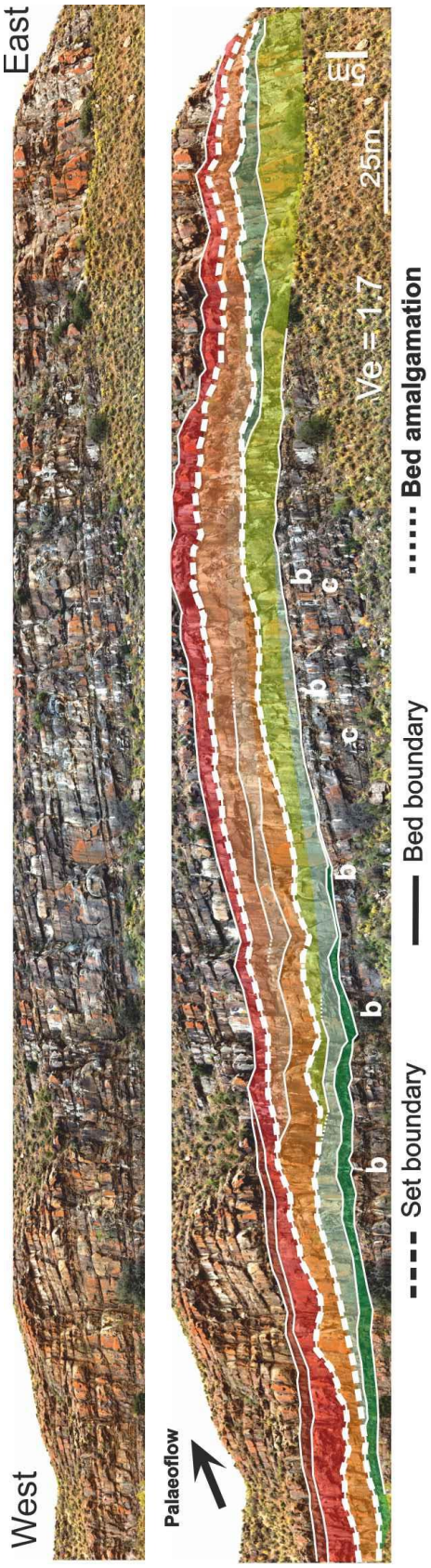

Figure 5.9 *Bedset architecture within the main Unit B2 outcrop face at the Doornkloof area. Key bounding surfaces have been defined based on successive bed pinch-out (set boundaries) with multiple (3-4) downstream-orientated stacked and weakly amalgamated bedforms. While the internal bed configuration is downstream orientated, the bedform sets stack with an upstream orientation.*

5.5.4 Bed architecture: Old Railway – Subunit B.2

At this locality on the southern limb of the Baviaans Syncline the lower 10 m of subunit B.2 is exposed for 100 m EW (Fig. 5.3B). Here, B.2 is a medium- to thin-bedded sandstone-prone unit that shows substantial lateral thickness changes without evidence of a basal erosional confining surface (Fig. 5.10). Mean palaeoflow is ESE (121°) (Fig. 5.3B), indicating the exposure is sub-parallel to depositional dip. The sandstone beds are dominantly climbing ripple laminated, with some banded/planar laminated and structureless divisions.

Multiple climbing ripple laminated beds contain dispersed small mudstone and siltstone clasts (Fig. 5.10-1). The section is characterised by an alteration of beds showing typical pinch-and-swell geometries (0.5-2 m) and more tabular thin-bedded (<0.5 m) sandstones. Locally, individual beds pinch-and-swell multiple times over a distance of ~40m, with wavelengths varying from 15 m to >40 m. Where there are swells, bed bases are erosional (Fig. 5.10-2). Siltstones comprise only ~10% of the succession and are thin-bedded and planar-laminated, with intercalated thin very fine-grained sandstones (<1 cm).

In the top of the section, a 40 cm thick sandstone bed abruptly fines and thins downstream to a centimetre-thick siltstone bed (Fig. 5.11A). This bed thickens and thins along a 12m length (Fig. 5.11A) forming sandstone lenses, before regaining original thickness (40 cm). Within this zone, the bed laterally grades to siltstone and is perturbed locally by centimetre-scale scour surfaces. At log 04 (Fig. 5.10A), a bed that pinches downstream has a downstream-orientated scour on its top surface, which is overlain by thin-bedded sandstones and siltstones that pass upstream out of the scour surface. A downstream thickening bed with an erosive base truncates these beds.

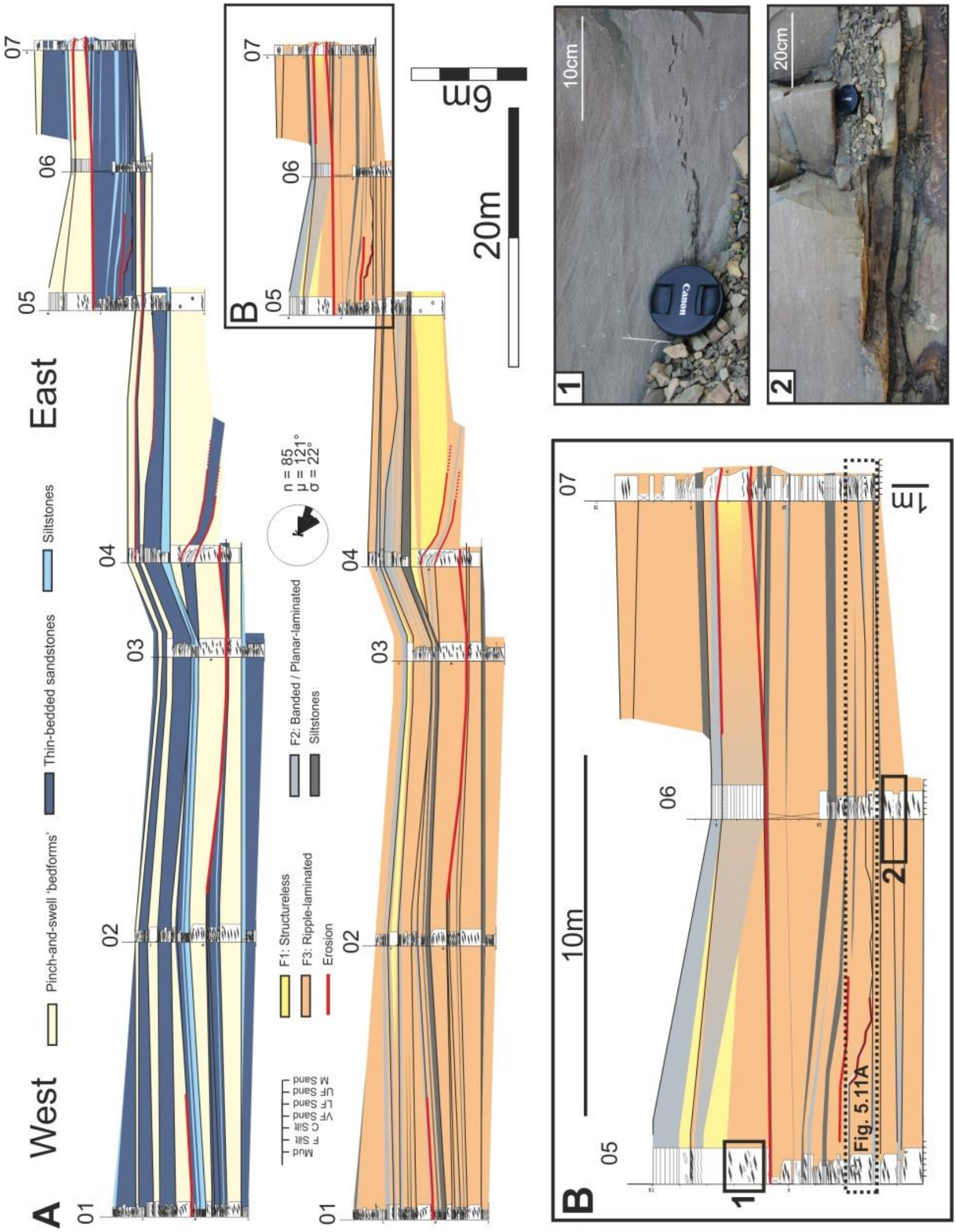

Figure 5.10 *Subunit B.2 within the Old Railway area. A- Facies correlation panels of the section with bedform distribution (top) and facies distribution (bottom). B- Zoomed-in facies correlation panel of most eastern section with 1. – mudstone clasts within a climbing-ripple laminated bed, indicating sediment overpassing, and 2. – bed splitting indicating erosion and amalgamation. See Figure 5.3 for locations and lowest panel in Figure 5.4 for meaning of log symbols. Location of Figure 5.11A is indicated.*

The majority of the observed pinch-and-swell bedforms stack in a downstream direction (Fig. 5.10A). However, occasionally a bed stacks in an upstream manner. This is similar to the stacking patterns observed within subunit B.2 at the Doornkloof section (Fig. 5.9). By following the depositional character, two depositional elements can be identified (Fig. 5.11B), which stack in an overall aggradational manner.

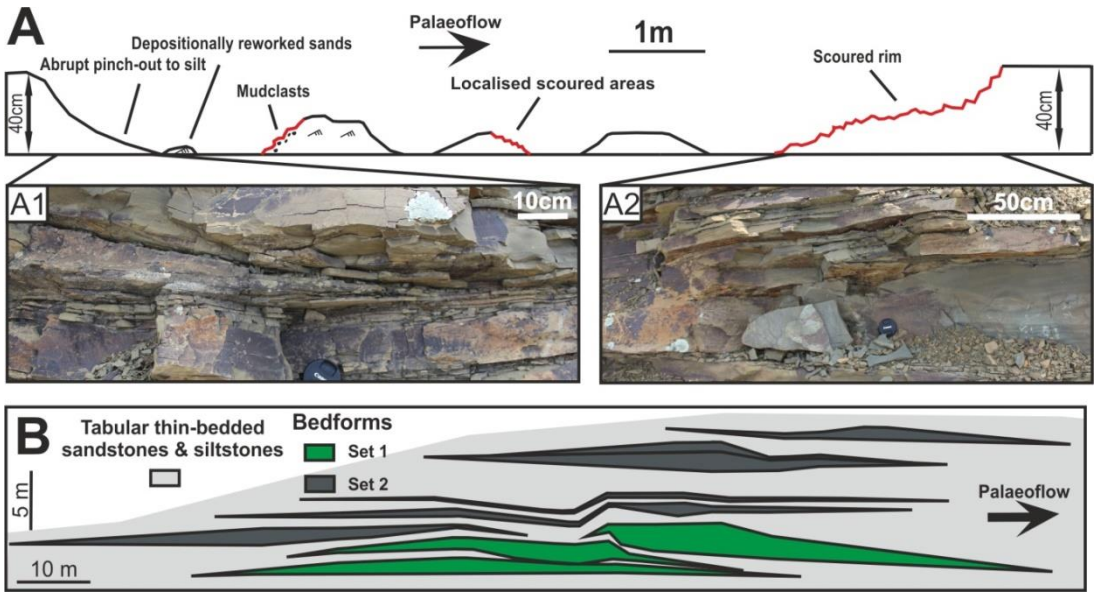

Figure 5.11 *A - Sketch of bed showing transient pinch-out to a thin siltstone bed (see Figure 5.10B for location), with A1 – pinch-out to siltstone and A2 – local scouring of bed top B – Division of the Old Railway section in two depositional elements based on observed stacking patterns.*

5.5.5 Sediment waves within channel-lobe transition zones

Both studied sections show bedforms with clear pinch-and-swell morphology that are subparallel to flow direction. These bedforms developed in a base-of-slope setting without any evidence of a large-scale basal confining surface. Bed-scale amalgamation and scouring are common in the two study areas, however the more significant component of downstream bed thickness changes is depositional. Their geometry and dimensions (>1m height; 10-100m wavelength), support their classification as sediment waves (Wynn and Stow, 2002). The bedforms described from the Doornkloof area (*Beds a-c*) show clear

asymmetric pinch-and-swell morphologies, related to internal upstream-facing truncation surfaces (Figs. 5.4, 5.7). The well-constrained base-of-slope setting, the lack of confining erosion surfaces, and the depositional nature of Unit B downdip are consistent with an interpretation that the sediment waves formed within a CLTZ setting.

5.6 Discussion

5.6.1 Bed-scale process record

The depositional record of sediment wave deposits from CLTZ settings in Unit B are diverse and show significant variations in facies on the sub-metre scale. The characteristics of the sediment wave deposits from the two Unit B datasets will be discussed and compared.

Doornkloof section

Facies of the sediment waves identified at the Doornkloof section are characterised by an assemblage of structureless intervals (F1), banding (F2), and climbing ripple lamination (F3). Local patches of structureless sandstone facies (F1) (Figs. 5.4, 5.7B) at bed bases, suggest periods of more enhanced deposition rates (e.g. Stow and Johansson, 2002), during initiation of deposition. The sediment waves are however dominated by banded and planar laminated facies, related to traction-carpet deposition (Sumner et al., 2008; Cartigny et al., 2013). This suggests net deposition from high concentration flows during most of bedform development. The high degree of variation (band thickness, presence of shallow truncations, wavy nature) in the banded sandstone facies (F2) is explained by either 1) turbulent bursts interacting with the traction carpet, or 2) waves forming at the density interface between the traction carpet and the overlying lower-concentration flow, possibly as a result of Kelvin-Helmholtz instabilities, or a combination of both processes (Figs. 5.5, 5.8) (Sumner et al., 2008; Cartigny et al., 2013). There is a strong spatial and stratigraphic relationship between mudstone clast conglomerates (F4) (Fig. 5.6) and mudstone clasts within banded sandstone facies (F2). As the deposits underlying shallow erosion surfaces are siltstone-prone, the mudstone clast materials must have an origin

further upstream. They are therefore interpreted as lag deposits (e.g. Stevenson et al., 2015), corresponding to low net-aggradation rates from high-concentration flows. The angular mudstone clasts suggest a relative local source area and can possibly be linked to upstream scouring. Scours have been documented upstream of sediment waves in modern CLTZs (Wynn et al., 2002a) and similar relationships have been interpreted in the Albian Black Flysch of NE Spain (Vicente Bravo and Robles, 1995; Wynn et al., 2002a). The transition from banded facies (F2) to climbing ripple-laminated facies (F3), commonly observed at the top of individual beds, represents a transition from net depositional high concentration flows, to steady deposition from moderate to low concentration flows. The dominance of this facies group at bed tops (Figs. 5.4, 5.7) is interpreted as the product of less-energetic and more depositional tails of passing flows.

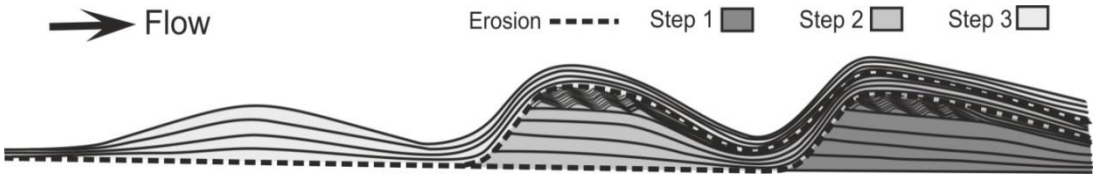

Figure 5.12 *Simplified model showing the upstream accretion process of the sediment waves in the Doornkloof area associated with the banded facies (F2). Due to continuous draping on top of the truncation surfaces, crest height should increase in the downstream direction.*

To better understand the process record and evolution of the Unit B sediment waves, it is important to be able to distinguish the record of a single flow from that of multiple. The Doornkloof sediment waves built depositional relief, although internally they show evidence of erosion (Figs. 5.4, 5.5, 5.6, 5.7). The majority of the observed bed thickness changes within the sediment waves at the Doornkloof section coincide with the presence of steep internal truncation surfaces (Figs. 5.4, 5.7). The preservation of upstream-facing truncation surfaces (Figs. 5.4, 5.7), implies a significant component of bedform accretion at the upstream end (Fig. 5.12) and therefore an upstream younging direction within the area

of observation. To be able to preserve truncation surfaces with angles up to 25° (close to the angle-of-repose), erosion, and the deposition on top of the erosion surface, are likely to be the result of a single flow event. Furthermore, within Unit B.2 all truncation surfaces of *Bedform b* and *c* merge towards the bed base as a single surface (Fig. 5.7), leaving underlying strata untouched and due to the absence of bed splitting suggest a single flow origin for the entire bedform. Within *Bedform a* of Unit B.1, the underlying gravel patches show upstream pinch-out of sandstone beds and downstream amalgamation with *Bedform a* (Fig. 5.6A) reflecting multiple flow events and resulting in marked difference in bedform architecture and bed thickness compared to *Bedform b* and *c*. However, all upstream facing truncation surfaces in the main sandstone body merge, towards a single surface within the deposit, in a similar manner to *Bedform b* and *c*, suggesting a single flow origin for the sediment wave morphology. Furthermore, *Bedform a* can be followed out for ~ 1000 m in upstream direction, showing many small-scale (< 5 m lateral distance) purely depositional undulations in the western end (Figs. 5.4, 5.6B) linked to the deposits on top of the most upstream truncation surface, and therefore is the result of the youngest depositional phase of *Bedform a*. The lack of similar undulating sandstone deposits, below *Bedform a* at this upstream location (Fig. 5.4), suggests that each upstream facing truncation surface in *Bedform a* further downstream, cannot be the result of different flow events. Therefore, within each sediment wave within the Doornkloof section (*Bedform a*, *b* and *c*), the evidence supports the initiation and development of the bedform during the passage of a single flow event. In comparison to *Bedform b* and *c* in Unit B.2, the sediment wave of *Bedform a* appears to have initiated across a series of earlier deposited gravel patches (Figs. 5.6A, 5.6B) and downstream thickening sandstones. Similar steep internal scour surfaces to those observed in these bedforms have been highlighted by Hiscott (1994), which were linked to energetic sweeps from a stratified flow. Consequently, it is suggested that these scour surfaces are the result of spatio-temporal flow fluctuations from a single flow event. A similar depositional history of waxing and waning behaviour

within a single flow was inferred from the sediment waves of the Miocene Austal foreland Basin, Argentina, described by Ponce and Carmona (2011). However the Doornkloof sediment wave architecture can not be explained by the depositional model proposed by Ponce and Carmona (2011), as this model assumes each independent lense-shaped geometry is created and reworked simultaneously, and subsequently draped, linked to flow deceleration. The Doornkloof sediment also show draping over lens-shaped geometries (Fig. 5.12), however the 'lenses' are clearly not disconnected, as is the case in the Austral foreland Basin, but instead directly linked to the draping phase.

The presence of younger bedforms on top of older swells, such as at the upstream location of *Bedform a* (Figs. 5.4 (logs 2-7), 5.5B) or the sediment waves overlying *Bedform b* in Unit B.2 (Fig. 5.9), suggests that initial bedform deposition acts as a nucleus for later sediment wave development. Therefore, larger composite bedform structures can be created as the result of multiple flow events.

Old Railway section

In the Old Railway section (Fig. 5.10), erosional bed bases and bed amalgamation are common, particularly where there is depositional thinning of underlying beds, indicating that the 'pinch-and-swell' bedforms present at this section are the result of multiple flow events. However, the bed amalgamation only has limited impact on bedform thickness as thickness increase dominantly occurs beyond the point of amalgamation and must therefore be of depositional nature. The more uniform facies distribution and lack of internal truncation surfaces within these bedforms (Fig. 5.10) do not suggest spatial-temporal fluctuations of the same order as observed in the Doornkloof area. The Old Railway bedforms classify as sediment waves (Wynn and Stow, 2002) with dimensions of 15 to >40 m wavelength (extending outside outcrop limits) and 1-2m amplitude, however their maximum bed thicknesses (1-1.5 m) is more limited than at the Doornkloof area (>2.5 m), climbing ripple-laminated facies (F3) is more dominant and banded facies (F2) are

almost absent. This F3 dominance indicates that their morphology is primarily controlled by depositional processes, similar to the Doornkloof section but from low concentration turbidity currents compared to high concentration flows at the Doornkloof section.

5.6.2 Spatial variations within a sediment wave field

The differences observed in CLTZ sediment wave character between the Doornkloof and Old Railway sections are most likely related to the feeder channel, including factors such as channel dimensions, magnitude of the incoming flows, and the distance and orientation from the channel mouth.

Previous studies (Brunt et al., 2013a) suggest that all feeder channels within the Unit B base-of-slope system were similar in dimensions, suggesting that the character of sediment waves is unrelated to variations within feeder channels connected to different sediment wave fields (Doornkloof and Old Railway). Alternatively, the facies and architectural differences could be related to their position relative to the channel-mouth. Dominance of lower flow-regime facies (F3) such as climbing ripple-lamination is commonly associated with overbank or off-axis environments (e.g. Brunt et al., 2013a; Kane and Hodgson, 2011; Rotzien et al., 2014).

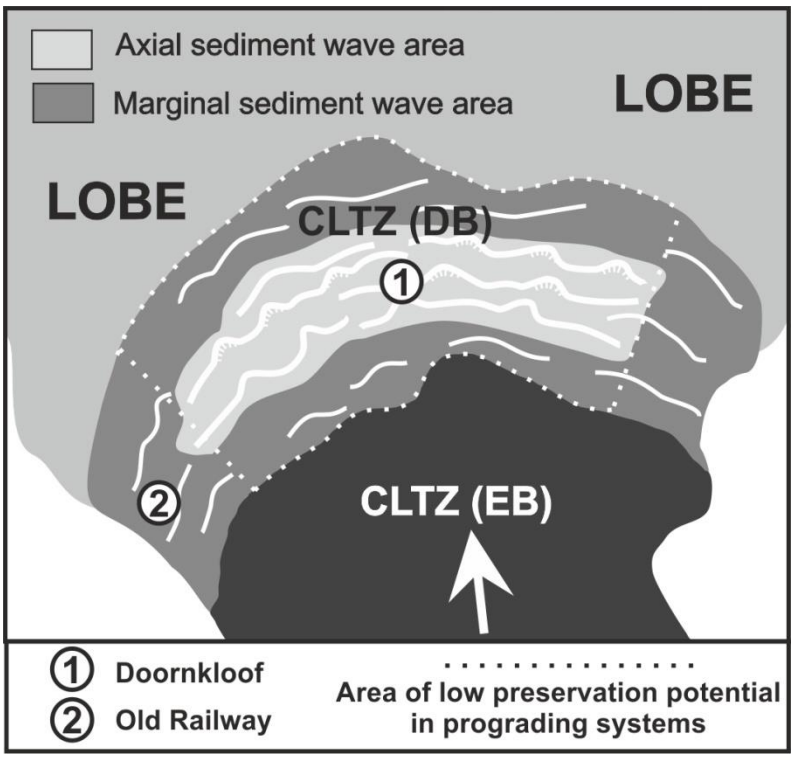

Figure 5.13 *Spatial division within a channel-lobe transition zone between a depositional bedform area (DB) and an erosional bedform area (EB) following Wynn et al. (2002a). Differences in characteristics of sediment waves are explained by spatial differences between the axis and the marginal areas of the deposition-dominated fields (DB) of a CLTZ.*

A similar dominance of lower flow-regime facies (F3) among the flow parallel Old Railway section (Fig. 5.10) could therefore possibly show a more marginal cross-cut through a sediment wave field in comparison to the Doornkloof section (Fig. 5.13). The overall prevalence of more energetic facies (F1, F2, F4) and erosion suggest the Doornkloof area was within a more axial position (Fig. 5.13). Furthermore, within the Doornkloof area, it also shows that climbing ripple deposition (F3) becomes more dominant, where the bedforms significantly pinch (<0.5 m) away from the central areas of deposition (e.g. *Bedform a*; Fig. 5.4), but still with a significant banded sandstone component (Fig. 5.6B).

The differences in expression of the Unit B sediment waves suggest that the stratigraphic record of CLTZ environments exhibit substantial spatial variability. Furthermore, there is evidence to suggest that initial sediment wave architecture can involve both upstream

orientated accretion (Doornkloof area), and downstream orientated accretion (Old railway section) within a single flow, depending on the position with respect to the channel mouth. Even though 3D control on morphology is lacking, it can be expected that this variance in depositional behaviour between axial and marginal areas will have influence on planform crest morphology and will lead to the crest curvatures, which are commonly observed within the modern seafloor (e.g. Wynn et al., 2002b). Furthermore, the preservation potential of the sediment waves such as those from the Doornkloof section is expected to be a lot less than in comparison to sediment wave deposits at marginal positions, like the Old Railway section, due to channel propagation (Fig. 5.13).

5.6.3 Spatio-temporal flow fluctuations

Fluctuations in depositional behaviour in a single flow can be expected in environments where turbidity currents exit confinement (e.g. Kneller and McCaffrey, 1999, 2003; Ito et al., 2008; Ponce and Carmona, 2011), and where flows pass over a rugose seabed (e.g. Groenenberg et al., 2010; Eggenhuissen et al., 2011). Flow non-uniformity does not only affect the loci of deposition but also the depositional facies (Kneller and Branney, 1995; Kneller and McCaffrey, 1999) and can manifest itself within a single event bed at a fixed geographical point (e.g. Kneller and McCaffrey, 2003; Kane et al., 2009; Ponce and Camona, 2011).

When individual flow events are responsible for the facies transitions and steep sigmoidal truncation surfaces within a single bed such as observed at the Doornkloof section (Figs. 5.4, 5.7), it implies significant waxing and waning flow behaviour. Such large fluctuations in flow concentration and depositional behaviour (Fig. 5.14A) can be related to variety of factors acting at CLTZ settings. Waxing and waning behaviour can be induced by flow splitting at the channel-levee system updip, where the primary ‘channelised’ flow may reach the sediment wave field earlier than the secondary ‘overbank’ flow. However, this would imply significant velocity and concentration differences and therefore significant

depositional facies differences between the two stages, which does not fit with what is observed (Fig. 5.14A). Furthermore, it would not explain great number of flow fluctuations interpreted within a single flow event bed. Therefore other mechanisms need to be proposed.

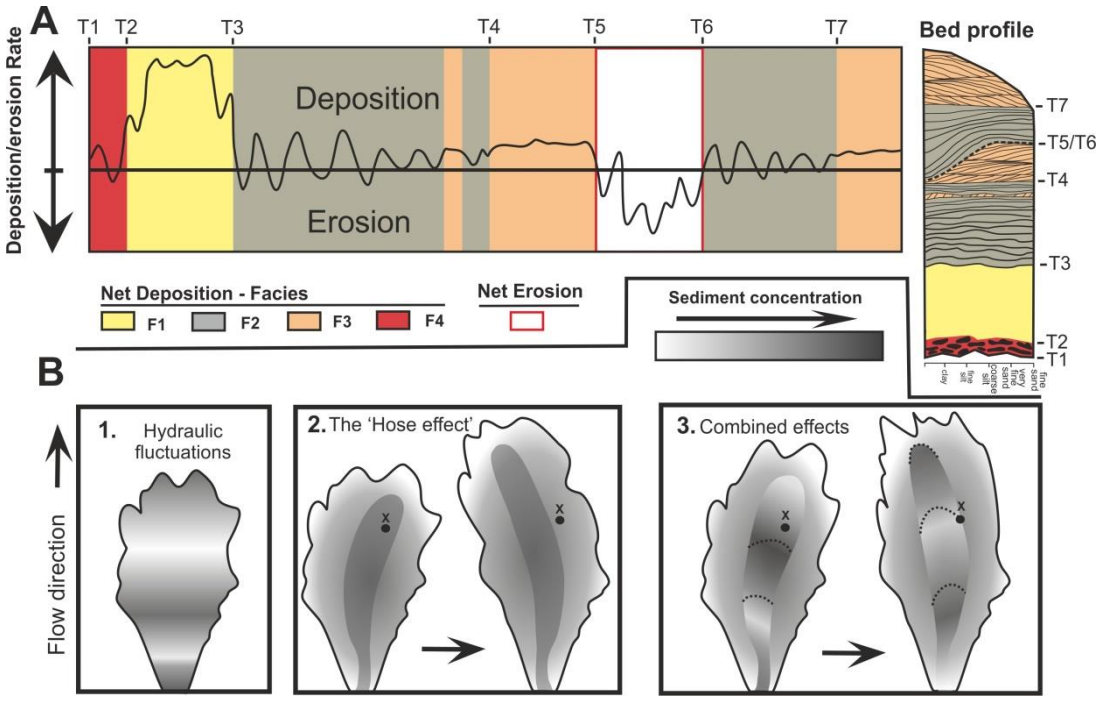

Figure 5.14 *A - Interpretation of flow behaviour and depositional record at a single location by linkage to facies patterns within the Doornkloof sediment waves. The time steps are indicated within the bed profile. B – Different models to explain facies changes linked to large flow fluctuations within the channel-mouth sediment waves with: 1) Hydraulic fluctuations within a single passing flow causing significant density fluctuations; 2) The 'Hose effect' with a high-density flow axis showing inter-flow compensation over the duration of the flow. Reference location (X) would therefore receive the energetic axis of the flow at one point in time (left), but the less energetic off-axis at a later point in time (right); 3) Combined effects, where the more energetic core shows both hydraulic fluctuations and compensational lateral migration behaviour.*

Fluctuations of the Froude number

The net-depositional record of waxing and waning flow conditions (Fig. 5.14A) at a single location (1D) within the Doornkloof sediment waves (Fig. 5.14B-1) could be related to fluctuations around the critical Froude number. Fluctuations of the turbidity current

Froude number are expected in areas of abrupt flow expansion at a break in slope, such as at the base-of-slope (Garcia, 1993; Wynn et al., 2002b). Turbidity currents that undergo transitions from supercritical to subcritical conditions (a hydraulic jump) have been linked to the formation of erosional and depositional bedforms, such as sediment waves (Vicente Bravo and Robles, 1996; Wynn and Stow, 2002; Wynn et al., 2002b; Symons et al., 2016). When supercritical, flow thinning can cause local erosion, which can be followed downstream by rapid subcritical flow expansion and deposition. Sediment waves that show upstream migration of crestlines have typically been associated with supercritical conditions (Wynn and Stow, 2002; Symons et al., 2016), where the stoss-side is defined by deposition and the lee-side by erosion.

Evidence of upstream accretion could support a supercritical nature for the Doornkloof sediment waves, however they do not migrate upstream due to a depositional focus at the stoss-side. The architecture of the internal truncation surfaces resembles the type II and type III antidunal bedforms described by Schminke et al. (1973). However, these antidunes in the Laacher See area are clearly building out at the stoss-side of the bedform. Instead, the Doornkloof sediment waves show truncation and draping at bed swelling locations followed by the deposition of another bed swell upstream, which may or may not be truncated (Fig. 5.12). This means that each swell grows individually rather than simultaneously as a sinusoidal wave. Kubo and Nakajima (2002) observed similar differential deposition for sediment wave development under subcritical flow conditions in physical and numerical experiments. Additionally, consistency in wavelength is lacking for both bed thickness changes (10-100 m) as well as the distance between individual truncations (5- >100 m), which does not comply with the wavelength consistency that is expected when sediment wave development is purely explained by Froude number fluctuations (e.g. Alexander et al., 2001).

<u>The ‘hose effect’</u>

Alternatively, there could be a spatial control on the development of sediment waves, based on flow-deposit interactions and momentum of the flow core (Fig. 5.14B-2). As a turbidity current leaves the confinement of a channel it will not immediately lose its momentum (e.g. Choi and Garcia, 2001), and due to the contrast with the ambient fluid it is not at first instance greatly affected by density gradients. Due to flow-deposit interactions with depositional and erosional relief around the channel-mouth, the flow core may shift around during bedform aggradation. Most studies on flow-deposit interactions focus on temporal changes in flow conditions (e.g. Kneller and McCaffrey, 2003; Groenenberg et al., 2010), but rarely consider lateral changes within a single turbidity currents. A single location within a sediment wave field may receive the energetic flow core at one time linked to erosion and/or deposition from a high concentration flow, and the less energetic and dilute depositional flow margin at other times, comprising a combined record of fluctuating energy levels (Fig. 5.14B-2). Similar behaviour within a single unconfined flow has been described in basin-floor settings of the Cloridorme Formation (Parkash, 1970; Parkash and Middleton, 1970) and at levee settings of the Amazon Channel (Hiscott et al., 1997). The 'hose effect' would result in a composite depositional record as the core of the flow sporadically moves laterally, repeatedly superimposing high energy conditions onto lower energy conditions, therefore explaining the inconsistency in wavelength.

Even though sediment wave architecture does not support depositional behaviour such as that of antidunes or cyclic steps, it is likely that lateral flow movement operated simultaneously (Fig. 5.14B-3) with fluctuations in the Froude number to produce the observed architectures and facies patterns of the Doornkloof sediment waves.

5.6.4 Sediment wave hierarchy

The larger scale architecture of both Unit B sections shows diversity in stacking patterns across different scales of observation (Fig. 5.15). An architectural hierarchy is established (Straub and Pyles, 2012), similar to channel (e.g. Clark and Pickering, 1996; Gardner and Borer, 2000; McHargue et al., 2011) and lobe (e.g. Deptuck et al., 2008; Prélat et al., 2009) systems, based on the recognition of bounding surfaces and depositional geometries. The larger-scale architecture of Unit B.2 of both studied sections (Figs. 5.9, 5.11B) reveals several depositional bounding surfaces, which mark an abrupt upstream shift in the locus of deposition of individual sediment waves.

When an architectural subdivision is applied based on scale and formative processes, distinction can be made between microforms, mesoforms, and macroforms (Jackson, 1975) (Fig. 5.15). Microforms comprise facies-scale bedforms such as ripples, while mesoforms are larger (dune)-scale bedforms (Jackson, 1975). Based on the process interpretations, sediment waves that lack evidence of bed amalgamation (e.g. *Bedform b and c*) are classified as mesoforms in this study. Macroforms represent bedset development by multiple flows, which is evident from bed amalgamation.

Within Unit B.1 of the Doornkloof section, macroform development is limited, but the section shows a ‘macroform’ swell in the upstream end (Figs. 5.4, 5.6B) which is aggradational in nature, while *Bedform a* is defined by upstream orientated thickening as it shows downstream thinning where an underlying bedform is thickening (Fig. 5.4). The much thicker Unit B.2 systems of both sections shows an out-of-phase stacking of mesoforms in a downstream manner (Figs. 5.9, 5.10), as the swells stratigraphically shift downdip.

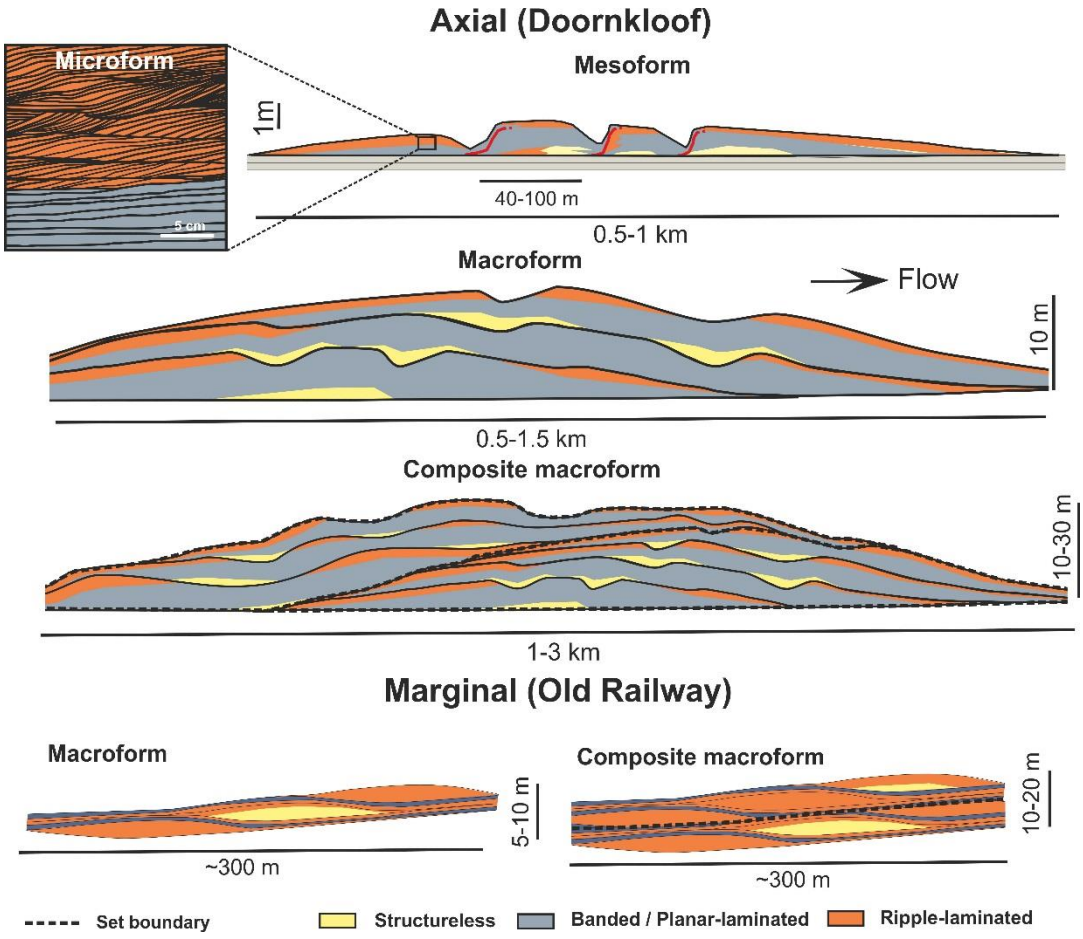

Figure 5.15 *Synthesis model of the Unit B.2 sediment waves based on scale and formative processes, illustrating the hierarchical division into micro-, meso-, macroforms and macroform complexes. The stacking behaviour between the macroform and macroform complex scale is clearly different, but similar within Unit B.2 in both the Doornkloof as Old Railway sections.*

Additional depositional bounding surfaces have been defined that separate multiple bedsets (macroform) and therefore may form larger depositional elements (300 - >1km wavelength, >10 m high, depending on the section), here referred to as composite macroform (Fig. 5.15). Within one composite macroform as defined in both Unit B.2 sections (Figs. 5.9, 5.11B), multiple macroforms stack in an aggradational to slightly upstream orientated manner (Fig. 5.15), as the bounding surfaces are defined by an abrupt upstream orientated shift of depositional swelling.

A downstream orientated shift of mesoform swells as recognised in both Unit B.2 sections could be related to channel system propagation, shifting the focus of sediment wave

formation downstream. However due to limitations on lateral outcrop control, none of the sediment waves have been completely exposed and therefore it remains challenging to fully comprehend the larger scale architecture and the underlying reasons for the observed stacking behaviour.

However, the overall 'macroform complex' stacking patterns within the outcrop window are strongly aggradational, which may explain their preservation as well as the large volume of rock in the record (e.g. Fig. 5.9). In an overall more strongly progradational system, the axis of a sediment wave field is unlikely to be preserved as the feeder channel propagates into the basin (e.g. Hodgson et al., 2016)

A sediment wave hierarchy associated with shifts in depositional focus and stacking behaviour has important implications for the measurement of sediment wave dimensions in other types of data sets (Fig. 5.2). The identification of the bounding surfaces within sediment waves in shallow seismic datasets (Fig. 1B) of modern systems is dependent on data resolution and changes in acoustic impedance are related to lithological boundaries (e.g. Link and Weimer, 1991; Migeon et al., 2001; 2012). The outcrop examples described here, permit the sub-seismic architecture to be identified. We speculate that the inconsistency in migration directions observed within modern coarse-grained sediment waves (Wynn and Stow, 2002; Symons et al., 2016) could also be related to different scales of observation (Fig. 5.15) rather than invoking fundamentally different process origins. This complicated nature reveals that sediment waves represent an important record for understanding flow characteristics and interaction with depositional relief on lower slope to basin-floor settings.

5.7 Conclusions

The architecture of exhumed fine-grained sandstone bedforms from a base-of-slope system are documented in detail. They show complicated lateral and stratigraphic changes in facies comprised of an assemblage of ripple-laminated, banded and structureless sandstone. Due to their setting, lack of confining surface, wave-like morphology and dimensions, they are interpreted as sediment waves. Individual beds can be traced out over significant flow parallel distances (>1 km). The spatial relationships to upstream submarine channel-fills and downstream lobe deposits support their formation in channel-lobe transition zones (CLTZs). In one of the two study areas, the sediment waves show clear steep (10-25°) internal truncation surfaces that are unevenly spaced and dominantly facing in the upstream direction indicating significant spatio-temporal flow fluctuations from a single flow event. Their architecture suggests the depositional processes do not correspond with bedform development under supercritical conditions, as each swell grows individually due to differential deposition rather than simultaneously as a sinusoidal wave. Internal flow compensational behaviour could have a major influence on sediment wave development acting together with Froude-number fluctuations in areas of abrupt flow expansion. Individual sediment wave beds (mesoforms) can show variable stacking behaviour, but commonly stack in a downstream manner, forming larger bedforms (macroforms and composite macroforms). Due to occasional upstream shifts of the depositional focus, the sediment wave packages have an overall aggradational character. Where truncation surfaces are rare, climbing ripple-laminated facies is the dominant facies, and bed thicknesses rarely exceed the 1-1.5 m. Here, the sediment waves are influenced by moulding and deposition of the lower concentrated parts of bypassing flows related to development in a position lateral to the channel-mouth. Sediment waves are a vital component of the bedform assemblage found in CLTZs and represent an important process record for sediment bypass in base-of-slope settings.

Chapter 6:
The stratigraphic record of submarine lobe deposits at base-of-slope settings

6.1 Summary

Commonly in submarine systems, the base-of-slope marks the transition from confined to unconfined flows, which leads to the development of sand-rich lobe deposits. Typically, these proximal deposits are incised during channel avulsion and propagation, which means that their fine-scale architecture and facies characteristics are poorly defined. Multiple integrated outcrop and borehole datasets are presented from base-of-slope successions within the Karoo Basin, South Africa. The recognition of high aspect ratio sandstone-prone packages that are not confined by erosion surfaces indicates that a significant portion of the base-of-slope depositional record is composed of lobes. Downdip thinning and facies transitions suggest that some lobe bodies at the base-of-slope represent discrete bodies, disconnected from basin floor lobe deposits. These lobes are characterised by an abundance of banded sandstones at their axis, climbing-ripple lamination and aggradational bedforms in the off-axis, and sandstone-prone thin-bedded fringes (>75%). This is in contrast with larger, siltier, and more hybrid-bed prone lobes at basin-floor settings. Based on these results and comparisons with other systems, two main lobe types are defined: narrow and simple lobe bodies with a relatively high abundance of banded and ripple-laminated sandstones, dominant in base-of-slope settings, and more radial complicated lobe bodies which may show finger-like geometries and have a relatively high abundance of structureless sandstones, linked debrites and siltstones, dominantly found at basin-floor settings. Flow efficiency is inferred as the primary mechanism controlling differences in both lobe characteristics as depositional locus. The recognition of this variability in lobe character has significant implications for our understanding of the

evolution of submarine fan systems and our understanding of connectivity within deep water reservoirs.

6.2 Introduction

Major advances in the resolution of seismic and seabed datasets have revealed that the architecture of submarine lobes (e.g. Pirmez et al., 2000; Deptuck et al., 2008; Jegou et al., 2008) is much more complicated than previously envisaged. Recent outcrop-related studies have supported the presence of fine-scale lobe architecture and facies distributions (Prélat et al., 2009; Groenenberg et al., 2010; Macdonald et al., 2011b; Straub and Pyles, 2012; Grundvåg et al., 2014; Morris et al., 2014a; Spychala et al., 2015; Terlaky et al., 2016; Masalimova et al., 2016). Many studies have focussed on the most distal parts of the basin floor system (Prélat et al., 2009; 2010; Groenenberg et al., 2010), where, due to the lack of erosional elements, the depositional architecture of lobes is well preserved. In more proximal locations, channel systems can propagate through previously deposited lobe deposits (Gardner et al., 2003; Jegou et al., 2008; Macdonald et al., 2011b; Brunt et al., 2013a; Grundvåg et al., 2014; Morris et al., 2014a), leading to juxtaposition of lobes and channel-levees (Pyles et al., 2014; Hodgson et al., 2016), and partial preservation of lobe deposits.

Base-of-slope regions preserve a complicated stratigraphic record of both depositional and erosional processes (e.g. Gardner et al., 2003; Pyles et al., 2014; Hofstra et al., 2015). Base-of-slope lobe systems are sandstone-rich (80-90%) (Gardner et al., 2003; Berhardt et al., 2011; Brunt et al., 2013a; Morris et al., 2014a; Masalimova et al., 2016) in comparison to more distal basin floor environments (Hodgson et al., 2006; Prélat et al., 2009), making them attractive exploration targets (Prather et al., 2016). System confinement influences lobe dimensions (e.g. Prélat et al., 2010; Spychala et al., 2015, Marini et al. 2015), however lobe properties such as facies characteristics and architecture can also vary between lobes deposited at lower slope to base-of-slope settings preceding channel propagation (Morris

et al., 2014a), and basin-floor lobes (Prélat et al., 2009; Prélat and Hodgson, 2013). Different lobe types within a single system have been identified in the Golo Fan (Deptuck et al., 2008) and the Amazon Fan (Jegou et al., 2008). The reasons for the existence of these differing lobe characteristics are not well understood. However, the fine-scale architecture and sedimentology of lobe deposits in base-of-slope settings and the criteria to differentiate them are poorly constrained.

The objectives of this chapter are to 1) investigate the stratigraphic record of base-of-slope systems, 2) establish recognition criteria to identify submarine lobe deposits within base-of-slope settings, 3) compare the depositional record of lobes across different settings within the same system, and 4) attempt to explain differences in lobe characteristics observed across these settings.

6.3 Regional setting

The Karoo Basin is one of a number of Late Palaeozoic to Mesozoic basins that formed at the southern margin of Gondwana (De Wit and Ransome, 1992; Veevers et al., 1994; López-Gamundi and Rossello, 1998) and is divided into the Laingsburg and Tanqua depocentres. This study focuses on the Tanqua depocentre (Fig. 6.1) in the southwestern part of the Karoo Basin, which shows a deepwater fill, represented by the Ecca Group. The Ecca Group comprises a 2 km-thick shallowing-upward succession from distal basin floor through submarine slope to shelf-edge and shelf deltaic settings (Flint et al., 2011).

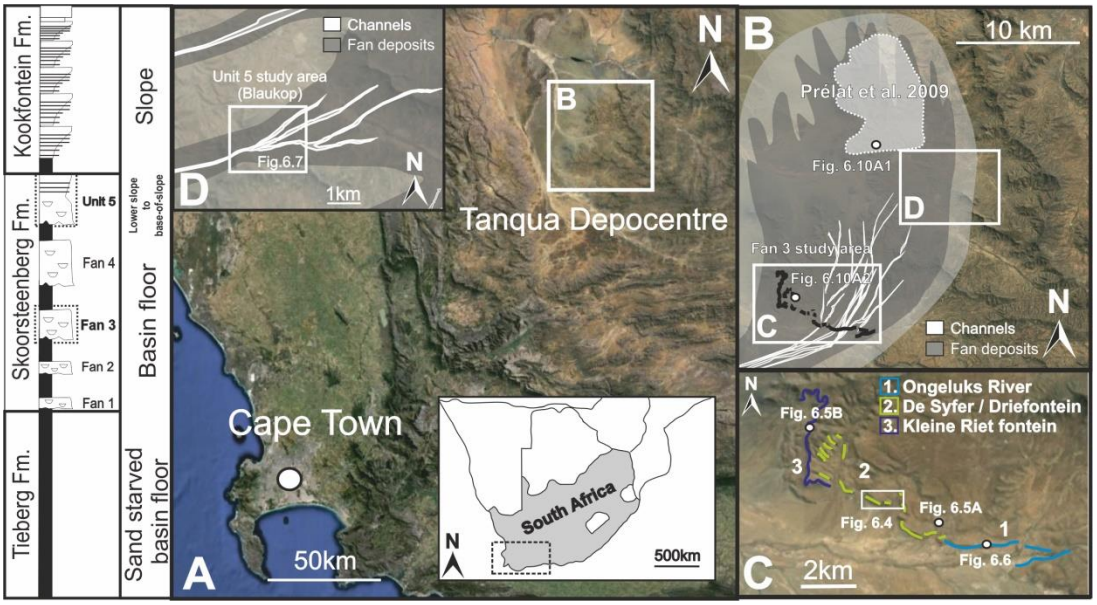

Figure 6.1 *Stratigraphic column on the left shows the deep-water stratigraphy of the Tanqua depocentre. A) Location of the Tanqua depocentre within the Western Cape. B) Location map of Tanqua depocentre with transparent overlay showing a sketch reconstruction of Fan 3 system, light transparent area in the top of the figure indicates where the basin floor lobes have been described by Prélat et al. (2009). C) Subdivision of the most proximal Fan 3 exposures. D) Location map of Unit 5 study area with overlay showing a sketch reconstruction of the Unit 5 system.*

6.3.1 Tanqua depocentre

The focus of this study is on Fan 3 and Unit 5 of the Skoorsteenberg Formation, which are both sand-rich basin floor fan systems (Fig. 6.1) (Bouma and Wickens 1991; 1994; Wickens and Bouma, 2000; Johnson et al., 2001). Fan 3 is the most extensively studied fan system of the Skoorsteenberg Formation, as it shows the most complete outcrop extent (Hodgson et al., 2006). An integrated outcrop and research borehole dataset has established the isopach thickness of Fan 3, and the relative spatial and temporal distribution of sedimentary facies, architectural elements and palaeocurrents (Johnson et al., 2001; Van der Werff and Johnson, 2003; Hodgson et al., 2006; Prélat et al., 2009; Groenenberg et al., 2010). The Fan 3 study area is located in the most proximal outcrop extent of Fan 3 from the Ongeluks River area in the east to the Kleine Riet Fontein area in the west (Fig. 6.1C).

Distributive channel-systems have been previously defined within the Ongeluks River area (Johnson et al., 2001; Van der Werff and Johnson, 2003; Luthi et al. 2006; Hodgson et al.,

2006; Jobe et al., 2012) with an overall palaeocurrent to the north/northeast. The southern outcrops are characterised by the presence of giant scour-fills (Fig. 6.1C) (Hofstra et al., 2015), erosionally-confined channel-fills in overlying Fan 4 and Unit 5, and abrupt thinning to the south (Oliveira et al., 2009). These observations support that the southern outcrops are within a base-of-slope setting (Fig. 6.1C) (Hodgson et al., 2006).

Unit 5 (Fig. 6.1) outcrops mark the transition from a slope to basin-floor environment (Van der Werff and Johnson, 2003; Wild et al., 2005; Hodgson et al., 2006), fed by multiple channel systems (Fig. 6.1D) in contrast to the underlying point sourced fan systems (Hodgson et al., 2006). The presence of slope channel complexes updip (Wild et al., 2005) and unchannelised distributive deposits downdip (Van der Werff and Johnson, 2003), agrees with an interpretation of the Blaukop area as a lower slope to base-of-slope setting. Kirschner and Bouma (2000) interpreted the Blaukop area (Fig. 6.1D) as a distributive channel-levee and overbank system.

6.4 Facies associations

The facies characteristics of the Fan 3 and Unit 5 deposits can be divided into four main facies associations (Fig. 6.2), based on primary observation and facies divisions from previous studies in the Karoo Basin (e.g. Hodgson et al., 2006; Brunt et al., 2013a; Hofstra et al., 2015).

6.4.1 Fa1 – Medium to thick-bedded, amalgamated sandstones

This facies association represents thick fine sandstone beds, which commonly form amalgamated sandstone packages (1 – 20 m) (Fig. 6.2). These deposits show a lot of lateral variability, and can be subdivided into two subgroups based on internal structure, thickness and architecture:

Fa1 Amalgamated and thick-bedded structureless and banded sandstones

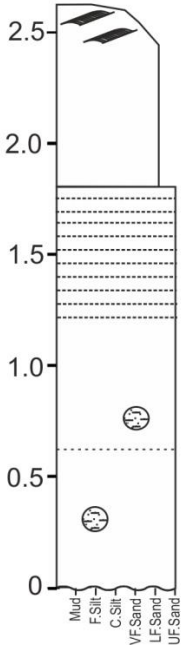

Sandstone percentage

100%

Fa2 Medium to thin-bedded laminated sandstones

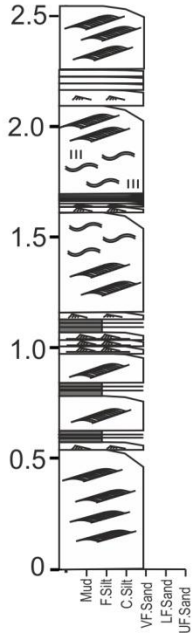

Sandstone percentage

95%

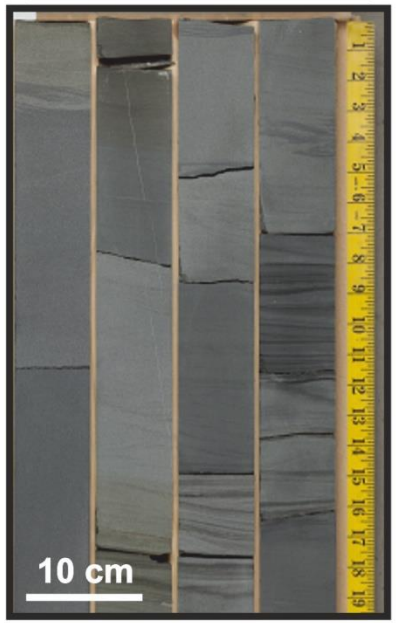

Fa3 Thin-bedded laminated sandstones and siltstones

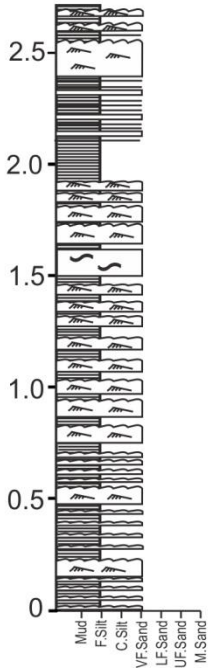

Sandstone percentage

75%

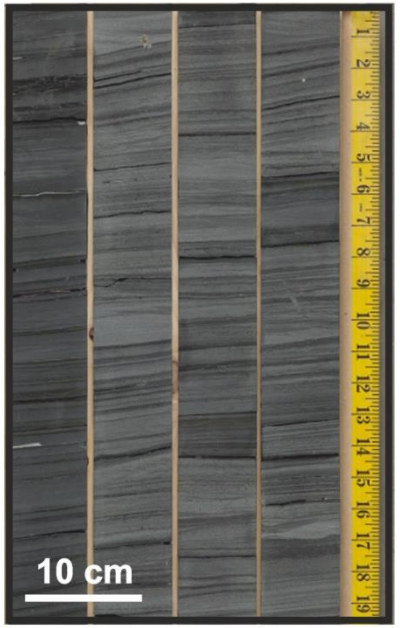

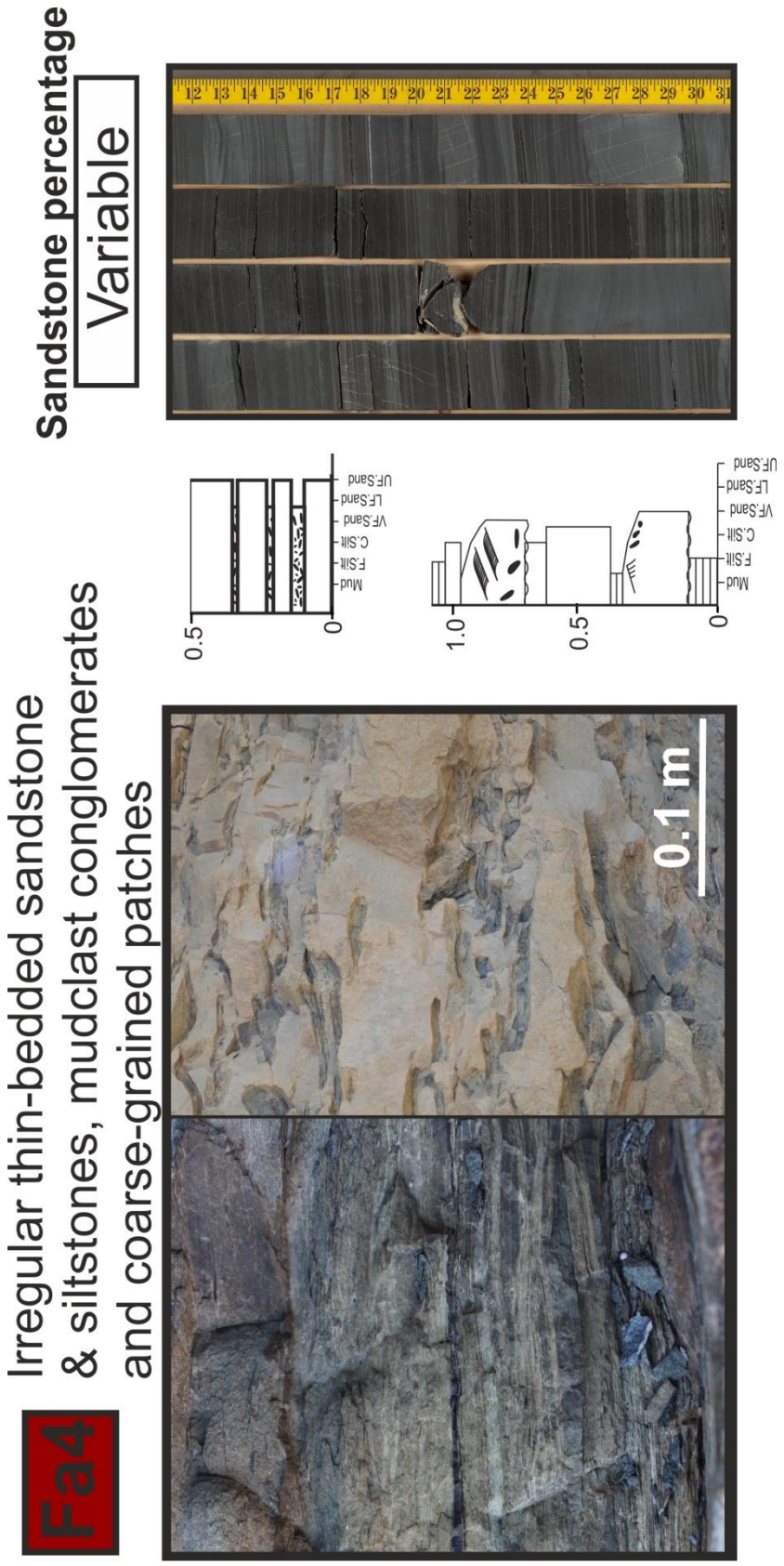

Figure 6.2 *Division of the most common and important facies associations for base-of-slope settings with examples from outcrop and core and representative measured sections from the Fan 3 and Unit 5 systems. See Figure 6.4 for log symbol meaning.*

Fa1A- Amalgamated structureless sandstones with little to no internal structure, which form 5-20m thick low-aspect ratio elements, and < 5m thick high-aspect ratio elements (tens to hundreds metres wide). Where bed tops are preserved, they may show some banding (see Fa1B) and weak normal grading with planar- and ripple-cross lamination. Locally, these sandstone beds contain minor amounts of dispersed sub-angular mudstone clasts and flame structures, and tool marks are observed at bed bases. These deposits are interpreted as rapid fall-out from sand-rich high-density turbidity currents (Kneller and Branney, 1995; Stow and Johansson, 2000) with clasts representing traction-transported bedload (see section Fa1B and 6.4.2 for interpretation of planar laminated and banded intervals). Flame structures are associated with syn-depositional dewatering (Stow and Johansson, 2000).

Fa1B - Medium- to thick-bedded amalgamated fine sandstones (0.2-2.5 m), with a dominance of diffuse cm-thick laminae (Fig. 6.2). These laminae are characterised by an alternation between lighter and darker bands, referred to as banding. The banding is dominantly planar and parallel to sub-parallel, but can be wavy. The light bands are well-sorted quartz-rich laminae and the dark bands comprise poorly sorted sands and silts with organic fragments, mudstone chips and micas. Centimetre-scale scours and loading are common at the bases of lighter bands. The bases of thicker beds dominated by banded sandstone beds are structureless and sharp, showing close affinity with Fa1A.

Banded sandstones differ from planar-laminated sandstones due to the thickness of the laminae (1-4 cm), the thickness of the laminated interval within individual event beds (0.5-2 m) and the absence of any major grain size differences between laminae. The observations support highly concentrated, net aggradational but fluctuating flow conditions. These conditions are present during traction carpet deposition by high-density turbidity currents (Lowe, 1982; Sumner et al., 2008, 2012; Talling et al., 2012; Cartigny et

al., 2013) and have not been linked to a generic flow regime. This is comparable to the H2 division of Haughton et al. (2009) and the Type 2 tractional structures of Ito et al. (2014).

6.4.2 Fa2 - Medium-bedded laminated sandstones

Medium- to thick-bedded (0.2 to 3 m thick), very fine to fine sandstones with various sedimentary structures (Fig. 6.2). Climbing ripple lamination, is abundant (25-70% of all laminated sandstones), showing high angles of climb with stoss-side preserved lamination (up to 45° with stoss-side preserved laminae). Some beds show a clear upward increase in the angle of climb and proportion of stoss-side laminae preservation. Where planar lamination is present it is common at bed bases, and when > 1 m thickness bases are commonly sharp and structureless. Bed tops show normal grading to fine siltstone and bed geometries can vary in thickness on the tens of metres scale.

High angles of climb and stoss-side preservation in ripple-laminated sandstones are indicative of rapid unidirectional aggradation rates (Jopling and Walker, 1968; Allen, 1973; Jobe et al., 2012; Morris et al., 2014a). When sedimentation rate exceeds the rate of erosion at the ripple reattachment point, the stoss-side deposition is preserved and aggradational bedforms develop (Allen, 1973). This style of tractional deposition is attributed to rapid deceleration of the flow and deposition from moderate-to low-concentration turbidity currents (Allen, 1973; Jobe et al., 2012). The planar laminations within the structured sandstones are interpreted to be deposited under upper stage plane bed conditions (Allen, 1984; Talling et al., 2012).

6.4.3 Fa3 - Tabular thin-bedded sandstones and siltstones

This facies association is represented by thin (<20 cm) very fine sandstones, which are interbedded with laminated siltstones (0.5- 5 cm) (Fig. 6.2). Ripple lamination is common, including low-angle climbing ripple lamination. The tabular bed geometry and predominance of current ripple lamination in Fa3 are interpreted to indicate high rates of

sediment fallout with limited tractional reworking from flows within the lower flow regime (Allen 1973; 1984; Southard and Boguchwal, 1990). Rare planar laminated sandstone indicates upper phase flow conditions (Best and Bridge, 1992) but with a transition to lower phase flow conditions due to ripple-laminated bed tops.

6.4.4 Fa4 - Irregular thin-bedded sandstone & siltstones, and mudstone clast conglomerates

Fa4 represents a combination of thin-bedded lenticular (fine to medium) sandstones and siltstones associated with numerous centimetre- to decimetre-deep erosion surfaces and mudstone/siltstone clast conglomerates (Fig. 6.2). Commonly, mudstone clast conglomerates form lenses (max 0.5m thick, 1-2m long), and are clast-supported with a fine sandstone matrix. Locally, very fine sandstone beds contain mudstone clasts (<1 cm) or are unusually coarse (medium sandstone) and show normal grading.

The presence of mudstone clasts and numerous erosion surfaces suggests that Fa4 represents a high energy environment. The mudstone clast conglomerates are interpreted as bedload material, derived from a mud-rich substrate, and therefore represent lag deposits of highly energetic bypassing turbidity currents (e.g. Stevenson et al., 2015). The thin lenticular sandstone deposits are interpreted to represent a combination of the reworking of the substrate by bypassing turbidity currents, and deposition from the tails of these flows. This facies association shares many similarities to the sediment bypass facies identified within the CLTZs of sand-detached lobe systems in the Laingsburg area (Van der Merwe et al., 2014). The climbing ripple lamination within thin-bedded sandstones indicates rapid aggradation rates (Allen, 1973; Jobe et al., 2012).

6.5 Base-of-slope architectures

Previous studies (Johnson et al., 2001; Grecula et al., 2003a; Hodgson et al., 2006; Brunt et al., 2013a), provide a good general constraint on the variety of large-scale elements and architectures that are represented within base-of-slope settings of the Karoo Basin (Fig. 6.3).

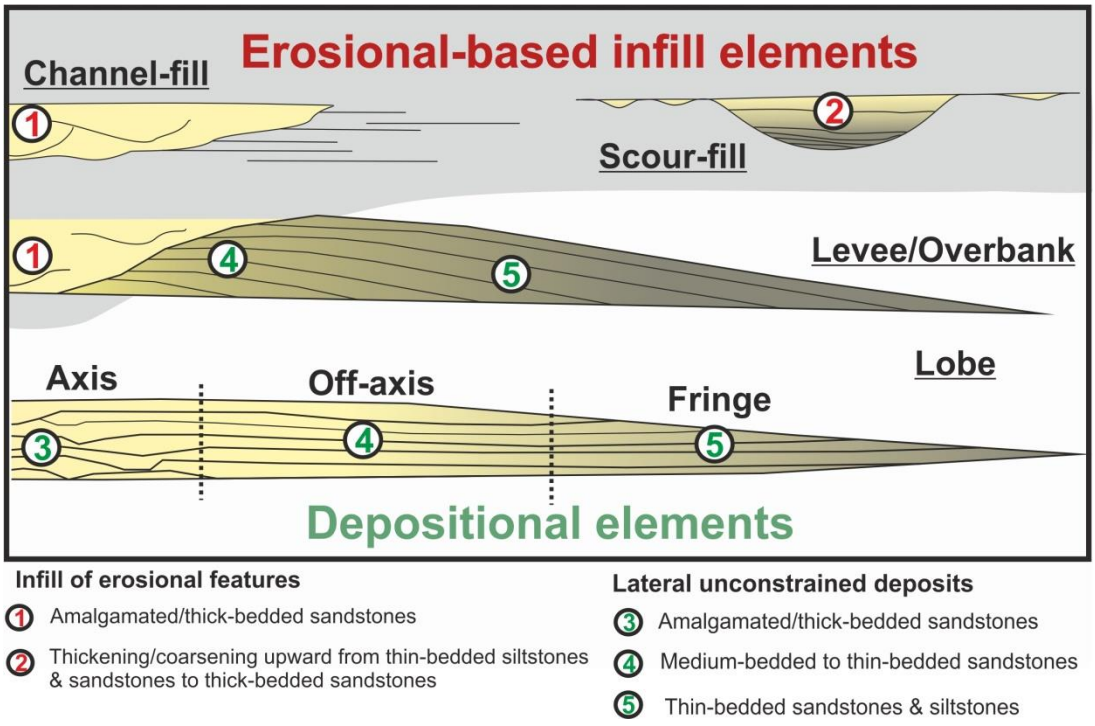

Figure 6.3 *Summary of all large-scale architectural elements expected at base-of-slope settings, divided by erosional or depositional nature (based in part on Brunt et al. 2013a). In a broad perspective, the architecture of infill can be divided into two styles and the architecture of depositional elements can be divided into three different deposit styles.*

6.5.1 Erosional elements

Erosionally-confined channel-fills have been identified within base-of-slope settings in the Karoo Basin (Grecula et al., 2003a; Luthi et al., 2006; Brunt et al., 2013a) with typical dimensions (150-400 m wide; 8-20 m deep) (Fig. 6.3) consistent with other systems around the world (e.g. Posamentier, 2003; Pringle et al., 2003; McHargue et al., 2011). Brunt et al. (2013a) identified entrenched, weakly-confined, and levee-confined channel bodies. Due to a lack of slope on the basin floor, these channel systems tend to show more distributive

patterns (e.g. Van der Werff and Johnson, 2003; Hodgson et al., 2006; van der Merwe et al., 2014). Scour-fills are commonly observed adjacent to channel-fills in base-of-slope settings (e.g. Jobe et al., 2012; Ito et al., 2014; Hofstra et al., 2015; Pemberton et al., 2016), with a range of dimensions (<1 -20 m deep; <1-1500 m long). Making confident distinctions between channel- and scour-fills can be challenging given the 2D limitations of outcrop studies, however some key criteria have been identified (Hofstra et al., 2015) (Fig. 6.3).

6.5.2 Depositional elements

The mapping of high aspect ratio architectural elements based on the identification of bounding surfaces marking abrupt facies changes without significant erosion, and the recognition of distinctive architectural characteristics, such as high-amalgamation zones (HAZs) (Fig. 6.3) (Hodgson et al., 2006; Prélat et al., 2009; Groenenberg et al., 2010), supports identification of lobe deposits. Lobe deposition precedes channel propagation as a system advances (Macdonald et al., 2011b; Brunt et al., 2013a; Grundvåg et al., 2014; Morris et al., 2014a; Hodgson et al., 2016). Commonly, this means that lobe deposits are incised by channels resulting in partial preservation and making their identification more challenging.

A clear distinction between sand-prone deposits that originated from overspilling flows (overbank) and the fringes of lobe deposits can be problematic where the stratal relationship between adjacent architectural elements is unclear (Fig. 6.3). Extensive levee successions have been identified above lobes in base-of-slope settings in the Laingsburg depocentre (Morris et al., 2014a; 2014b; van der Merwe et al., 2014). In the Tanqua depocentre, however, the stratigraphic relationships between channel-fills and surrounding stratigraphy are rarely observed (Fig. 6.3) (Van der Werff and Johnson, 2003; Hodgson et al., 2006). A levee-lobe transition zone has been considered (Morris et al., 2014b; Hodgson et al., 2016), but recognition criteria has not been established. Therefore, given their laterally extensive geometry and incision by channels, we refer to thin-bedded

and sand-rich successions as lobe fringes for simplicity, although it is likely that some of these deposits arise from overspill (Fig. 6.3). Examples of the depositional and erosional elements are provided in the 'Results' section below.

6.6 Results

6.6.1 Fan 3 – base-of-slope system

The focus of this study is on the Syfer and Driefontein area (Fig. 6.1C) between the most south-western outcrop limit of Kleine Riet Fontein and the most south-eastern outcrop limit of Ongeluks River. The Ongeluks River area preserves a distributive channel system in the axis of Fan 3 (Johnson et al., 2001, van der Werff and Johnson, 2003; Sullivan et al. 2004; Luthi et al., 2006; Hodgson et al., 2006), while the Kleine Riet Fontein area shows giant scour-fills that incise into thin-bedded climbing ripple laminated sandstones in an off-axis setting (Jobe et al., 2012; Hofstra et al., 2015). In contrast, the Syfer and Driefontein area is characterised by an abundance of tabular deposits and lack of large-scale erosion surfaces. The tabular deposits comprise thick-bedded structureless and banded (Fa1) sandstones, medium-bedded structured (Fa2) sandstones and thin-bedded siltstones and sandstones (Fa3) (Fig. 6.2).

At two locations (A and B) within de Syfer and Driefontein area (Figs. 6.1C, 6.4), high-aspect ratio sandstone packages are located, which are defined by amalgamated sandstones (Fa1) with shallow erosion surfaces (<0.5 m) at their bases. At *Loc 1* (Fig. 6.4A), thick-bedded structureless sandstones (Fa1A) form an amalgamated 20 m thick package (Fig. 6.4A), with bed splitting in both northern and southern directions. Where sandstone beds are non-amalgamated, they tend to show banded tops (Fa1B). Locally, mudstone clast conglomerates (Fa4) are common (Fig. 6.4A) between structureless amalgamated sandstones. The package shows a transition to more tabular, thin-bedded and fine-grained deposits at the top of the section, and is underlain by thick-bedded tabular sandstones.

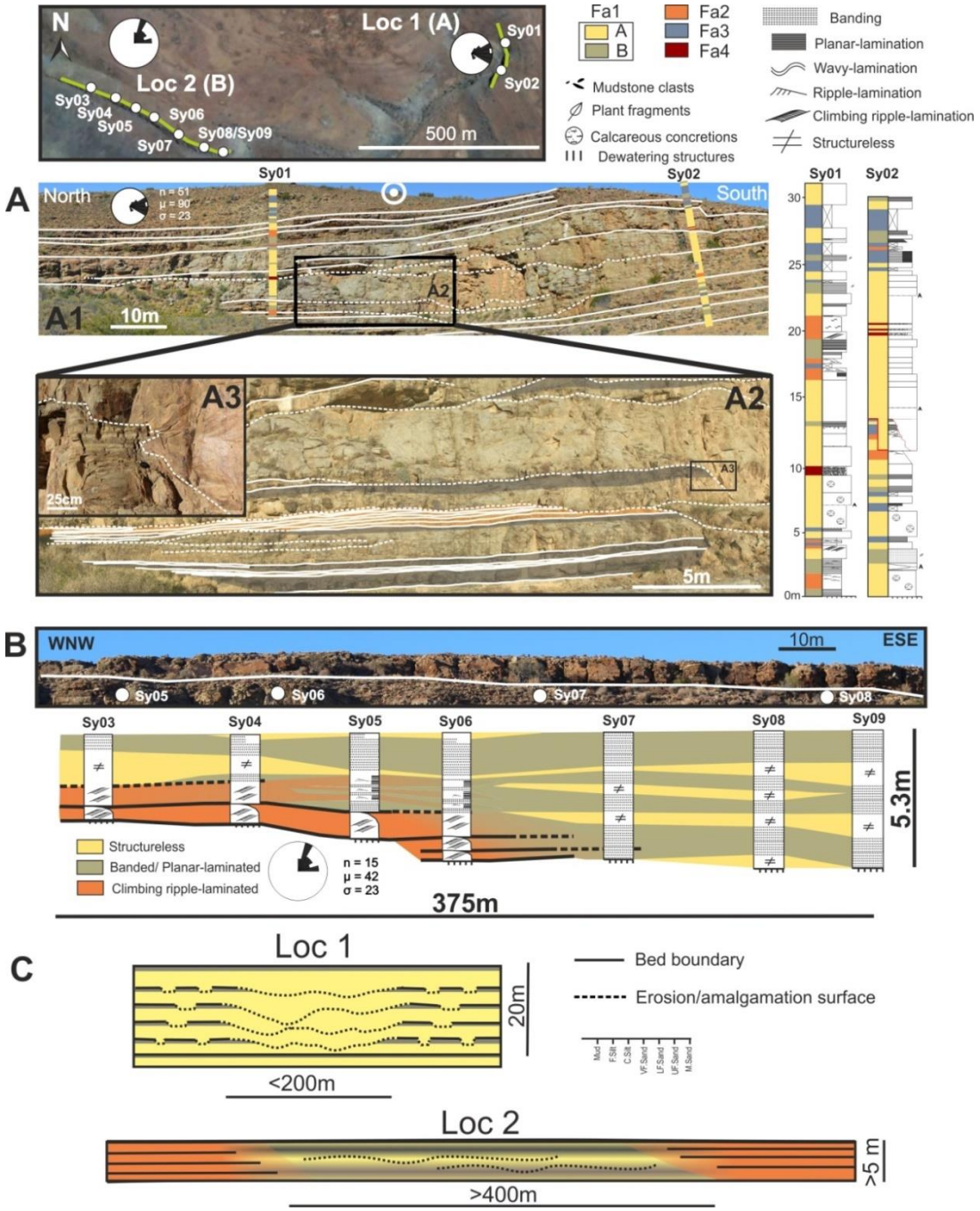

Figure 6.4 *Two localities (Loc 1 and 2) within the Syfer and Driefontein area (see Figure 6.1 for location), with A) strike section of an amalgamated package of dominantly thick-bedded structureless and banded sandstones, showing a 200 m wide zone dominated by bed amalgamation. B) Strike section of an amalgamated package of dominantly banded sandstones, showing bed splitting and facies transitions to climbing-ripple laminated sandstones towards the western margin. C) Cartoons showing the difference in dimensions and facies characteristics between the two amalgamation zones observed within the Syfer/Driefontein area. Palaeocurrents have been indicated, with with n = number of measurements, μ = mean palaeoflow and σ = standard deviation*

Palaeoflow (n=51) is dominantly towards the east (Fig. 6.4A), implying the amalgamated zone is exposed as a strike-section with a maximum width of 200 m.

At *Loc 2* (Fig. 6.4B), the top of the Fan 3 exposure, which is stratigraphically just below (~10 m) the amalgamated sandstone package at *Loc 1*, shows a sandstone package that can be mapped out for approximately 400 m (Fig. 6.4B). The section shows increasing bed amalgamation from WNW to ESE, and the amalgamated facies is dominated by structureless (Fa1A) and banded sandstones (Fa1B). Where bed splitting occurs, abrupt facies changes can be observed from banded sandstones (Fa1B) to climbing ripple-laminated sandstones (Fa2). The position of bed splitting and facies change, shifts westwards up through the section. Palaeoflow (N=15) is NNE-orientated, indicating this is a strike-section of an amalgamated sandstone package with a minimum width of 375m (Fig. 6.4).

The limited amount of erosion and the lack of a confining erosion surface, and the lateral change in bed amalgamation supports both these packages (*Loc 1* and *Loc2*) being High Amalgamation Zones (HAZs) (Hodgson et al., 2006; Prélat et al., 2009; Groenenberg et al., 2010) interpreted as lobe apex settings. Dimensions of HAZs can be variable (3-20m thick, 100-400m wide; Hodgson et al., 2006). The two examples here however, show distinct characteristics (Fig. 6.4C): The amalgamated package at *Loc 1*, has a lower aspect ratio (height: width = 1: 10), is dominated by structureless sandstones (Fa1A) in the axis with more banded sandstone facies (Fa1B) at the margins, compared to *Loc 2*, which shows an amalgamated package with a higher aspect ratio (height: width = 1:75) and a dominance of banded sandstones (Fa1B) in the axis and climbing ripple-laminated sandstones (Fa2) at the margins. There is a strong association between facies transitions and the presence of amalgamation. At *Loc 2*, banded and structureless sandstones (Fa1) amalgamate into a single sandstone package, but where bed splitting occurs there is a facies transition to climbing ripple-laminated sandstones (Fa2) and no erosion at bed bases. At *Loc 1*, the

margins of the HAZ are dominantly composed of structureless sandstones with banded tops (Fa1), with shallow basal scours. The low aspect ratio (Fig. 6.4C) and the similarity in dimensions and facies with nearby channel-fills (e.g. Brunt et al., 2013a) suggests that the amalgamated sandstone package at *Loc 1* may be located closer to up-dip channel-confinement in comparison to *Loc 2*.

Intercalated with the tabular sandstone-prone packages from de Syfer/Driefontein towards the Kleine Riet Fontein area (Fig. 6.1C) are numerous shallow erosional features (< 2 m deep; 10 - >70 m wide) (Fig. 6.5). These smooth-sided features cut into and are filled by medium- to thin-bedded structured sandstones (Fa3) and siltstones (Fa4), which thin beyond the limits of the erosion surface. Both strike (Fig. 6.5A) and dip (Fig. 6.5B) sections have been observed. The dimensions, orientation to palaeoflow, and similarity between the underlying and infill facies supports an interpretation of small-scale scour-fills. The presence of scour-fills among the tabular medium-bedded structured sandstones suggests these features represent a record of both unconfined flow bypass, and rapid deposition from relatively low concentration flows due to the dominance of climbing ripple-lamination. Jobe et al. (2012), who focussed on the Kleine Riet Fontein area (Fig. 6.1C) of Fan 3, noted a wide range of dimensions (10-30m wide, 1-5m deep) and an apparent random stratigraphic distribution of scour-fills.

The Ongeluks River area (Fig. 6.1C) towards the east shows erosionally-confined low-aspect ratio elements that cut into tabular high-aspect ratio elements (Fig. 6.6A). The low-aspect ratio elements are dominantly composed of amalgamated structureless sandstones (Fa1A) with basal mudstone clast conglomerates. The tabular deposits show much more variability within facies characteristics and are composed of a combination of structureless, banded and climbing ripple laminated sandstones, and siltstones (Fa1; Fa2; Fa3), with subtle lateral bed thickness changes.

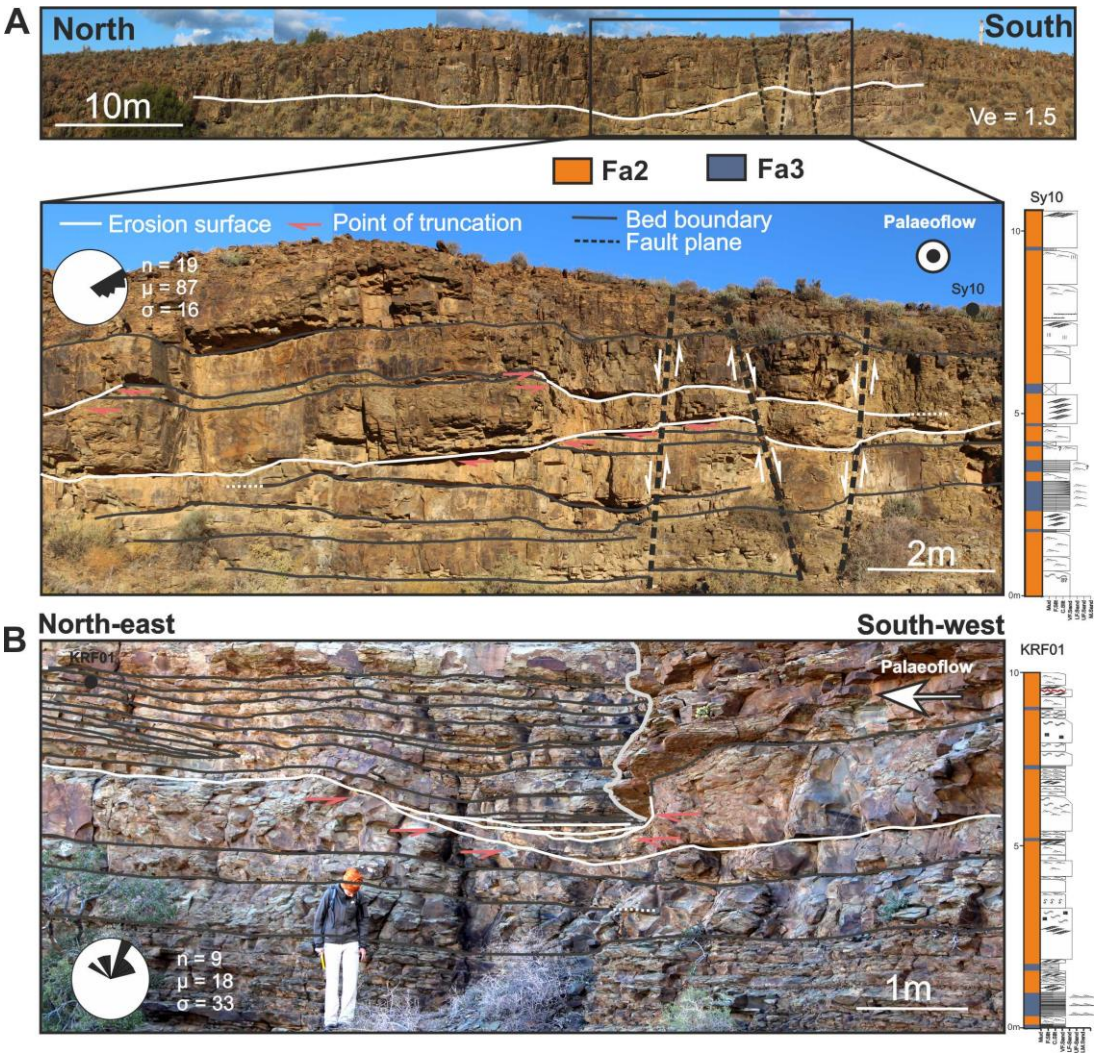

Figure 6.5 *Two examples of small-scale erosional features (< 2 m deep) within medium-bedded laminated sandstones (Fa3) of Fan 3. See Figure 6.1 for locations. A) strike-section through a ~50 m wide smooth erosional surface and B) dip-section through a > 10 m long erosional surface showing a fill with abrupt bed pinch-out. Palaeocurrents have been indicated, with with n = number of measurements, μ = mean palaeoflow and σ = standard deviation*

The low-aspect ratio elements are interpreted as channel-fills, in agreement with previous authors (Johnson et al., 2001; Van der Werff and Johnson, 2003; Sullivan et al. 2004; Luthi et al., 2006; Hodgson et al., 2006). The tabular deposits have been previously referred to as 'inter-channel highs' (Van der Werff and Johnson, 2003), and interpreted as overbank deposits (Luthi et al., 2006). However, they are exceptionally sandstone-prone (Fig. 6.6A2) and share facies affinities with the HAZs (Fig. 6.4) towards the west as well as the lobes identified by Morris et al. (2014a). Therefore, the high aspect ratio thick- to medium-

bedded sandstone packages are here interpreted as lobe deposits incised by channels. Intercalated thin-bedded and relative siltstone-rich (Fa3/Fa4) packages are more challenging to interpret with confidence, and may represent either channel overbank/levee or lobe fringe deposits.

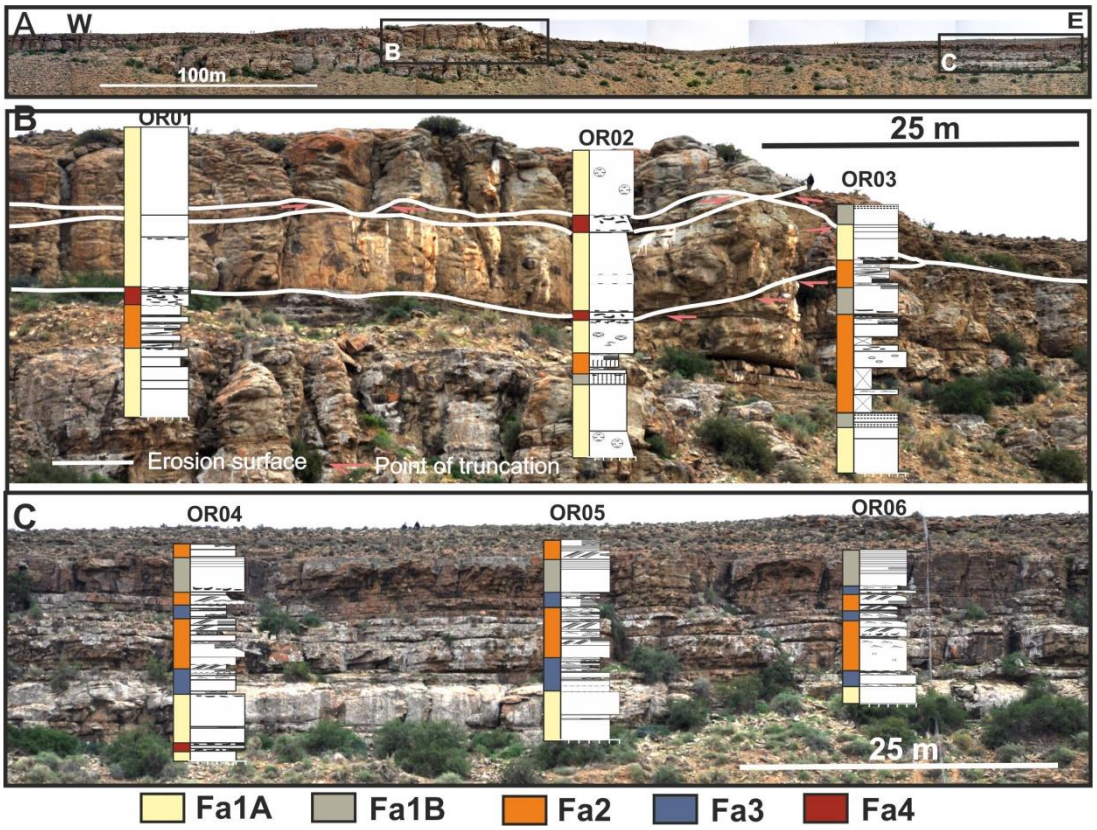

Figure 6.6 *A) Part of the main Ongeluks River outcrop face showing dip sections of: B) erosional-based low aspect-ratio elements, dominated by amalgamated structureless sandstones (Fa1A), previously interpreted as channel-fills (Johnson et al. 2001; Van der Werff and Johnson, 2003; Luthi et al. 2006; Hodgson et al. 2006) cutting into sandstone-prone tabular deposits and C) detailed section of the same sandstone-prone tabular deposits. Main palaeoflow in the Ongeluks River area is ENE orientated. See Figure 6.1 for location.*

6.6.2 Unit 5 – base-of-slope system

The Unit 5 study focuses on a 2 km^2 area (Figs. 6.1, 6.7) where the outcrop provides good constraints on the three dimensional architecture. This is supported by a dataset of 26 closely spaced sedimentary logs (See Appendix B.3), 191 palaeocurrent measurements (See Appendix B.2), primarily from ripple-lamination, and one cored borehole (BK01) sited

150 m away from the nearest outcrop (Fig. 6.7). The core intersects the lower 46.5 m of Unit 5 and allows bed-to-bed correlation to the nearby outcrop (Fig. 6.8A).

The stratigraphy of Unit 5 in the Blaukop area is dominated by tabular beds showing an assemblage of thick-bedded structureless and banded sandstones (Fa1), medium-bedded structured sandstones (Fa2) and thin-bedded structured sandstones and siltstones (Fa3) (Fig. 6.7). Palaeoflow is overall NNE orientated (Fig. 6.7), with a stratigraphic change from NE at the base of Unit 5 towards WNW at the top of the section (Fig. 6.8A)

Thickness changes attributed to depositional (Fig. 6.9A1) and erosional relief (Fig. 6.9A2) are common. Shallow erosion surfaces (<0.5m deep, 10's of metres wide) incise into thick- and medium-bedded sandstone (Fa1 and Fa2) and are overlain by a variety of facies associations (Fa1, Fa2, Fa3). In some cases, these features were filled by a single deposit (Fig. 6.9A2), resulting in depositional relief above an erosional base. Furthermore, medium-bedded laminated very fine sandstones can comprise asymmetric sinusoidal laminations (Fig. 6.9A3). These aggradational bedforms show multiple normal grading patterns and abrupt grain-size breaks (Fig. 6.9A3), indicating they comprise multiple event beds (Fig. 6.9A3). They are similar to the sinusoidal bedforms observed in lobes from base-of-slope and lower slope settings by Morris et al. (2014a). Thick-bedded and amalgamated sandstones (Fa1) comprise ~50% of the sandstone-prone top package and are widespread over the exposed area (>1km wide). They show evidence of widespread shallow (<0.5m) scouring, with strike and downstream thinning, resulting in sharp transitions with underlying deposits. Overall, the proportion of siltstone is limited (<10%) and most thin-bedded sandstones and siltstones (Fa3) are concentrated in the basal 10 m of the ~40 m thick succession. The BK01 core reveals that some thin-bedded sandstones are part of Fa4 as they show irregular and erosive bases (Fig. 6.9B1) with unusually coarse bed bases (medium sandstone) and mudstone clast and chip materials (<1cm - 5cm) at the base (Fig. 6.9B2).

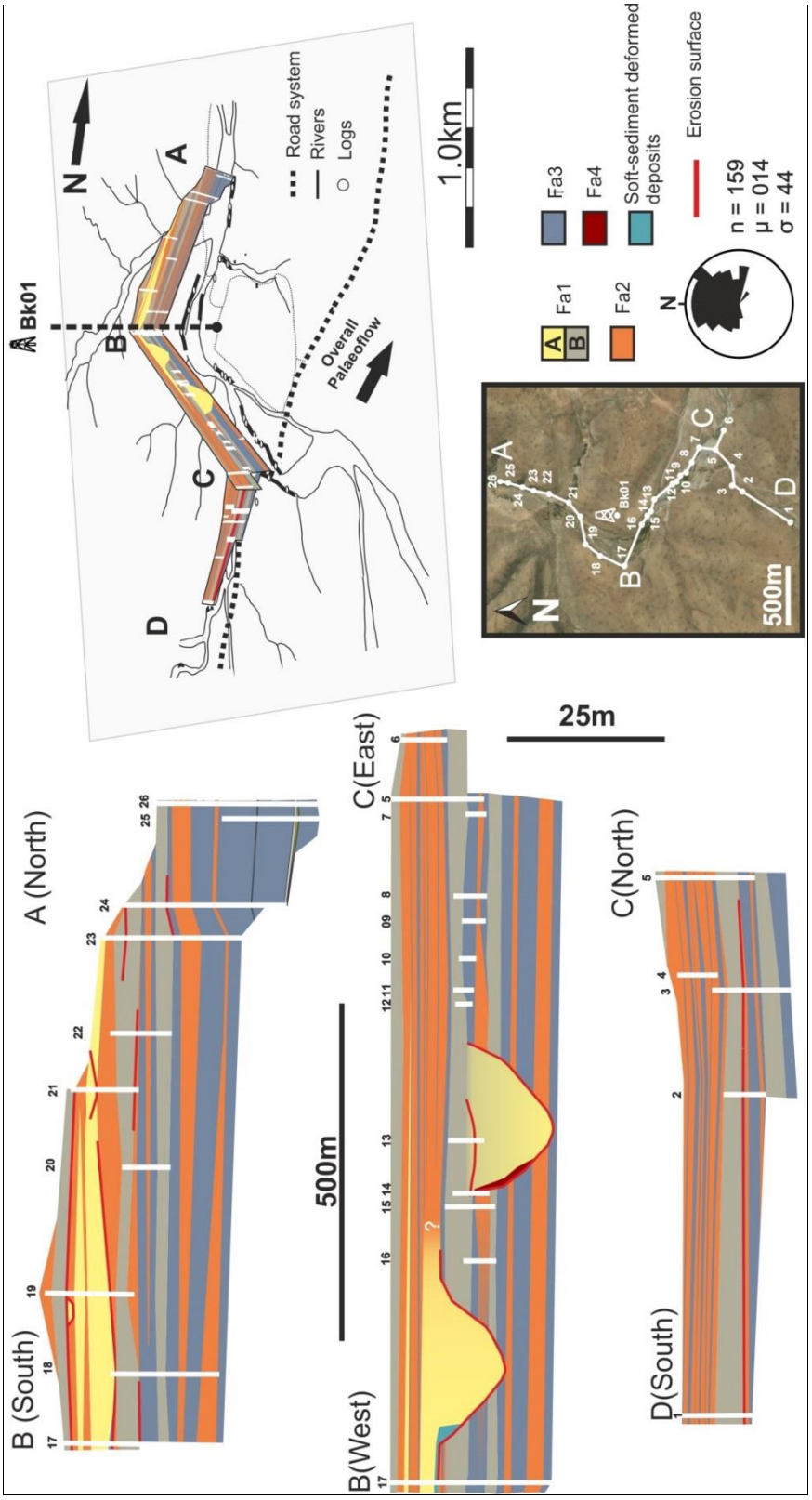

Figure 6.7 *Facies correlation panels and 3D-framework of Unit 5 within the Blaukop area. Log and BK01 core locations are indicated. Palaeoflow is overall NNE orientated. See Figure 6.1 for location*. *Palaeocurrents have been indicated, with with n = number of measurements, μ = mean palaeoflow and σ = standard deviation*

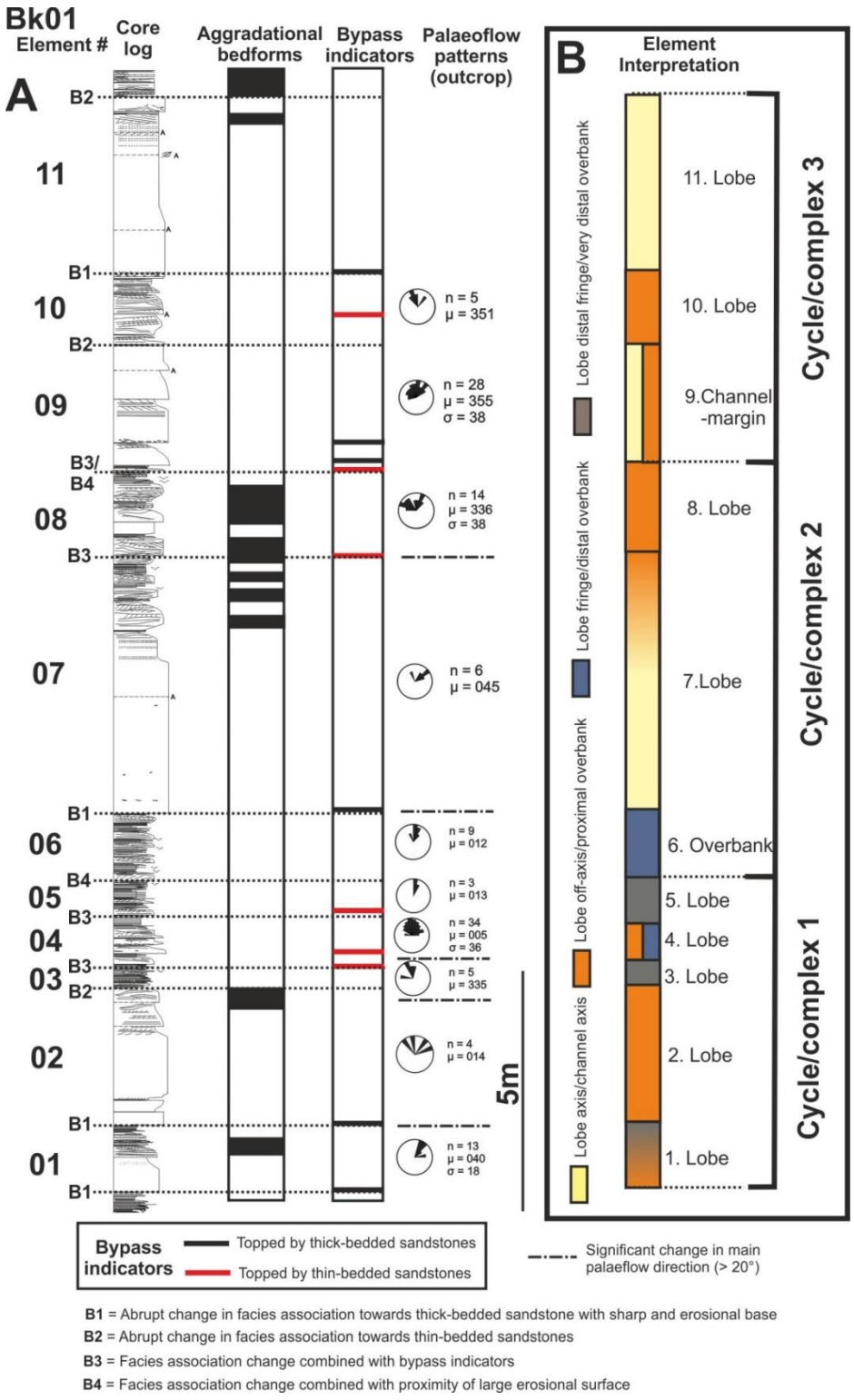

Figure 6.8 *A) Sedimentary log of the top sandstone-prone 25 m of the BK01 core with presence of aggradational bedforms (black bars), bypass indicators and stratigraphic palaeoflow fluctuations (from outcrop - with with n = number of measurements, μ = mean palaeoflow and σ = standard deviation). All eleven depositional elements are indicated as well as the reason behind each element boundary (B1-B4). See Figure 6.4 for remaining symbol explanations. B) Depositional element interpretation and division in three depositional cycles. See Figure 6.11 for further explanation.*

The tabular deposits that comprise most of the stratigraphy (Fig. 6.7) are incised by two erosionally-confined low-aspect ratio amalgamated sandstone bodies (300-350m wide; >10m deep). The basal erosion surfaces of both bodies show steep stepped profiles that cut thin- to thick-bedded sandstones (Fa1, Fa2 and Fa3). The margins show small quantities of mudstone clast conglomerates (Fa4) and soft-sediment deformed deposits (Fig. 6.7). Both bodies are topped by tabular >1 km wide structureless, banded and laminated thick-bedded sandstones (Fa1 Fa2) that form a 'wing'-like architecture (Fig. 6.7).

A simple division can be made between tabular high-aspect ratio bodies and erosionally-confined low-aspect ratio bodies, following a similar approach to the Fan 3 dataset. Due to their dimensions, architecture, facies characteristics of their infill (Fa1) and base-of-slope setting, the low-aspect ratio bodies are interpreted as channel-fills (e.g. Kirschner and Bouma, 2000; Hodgson et al., 2006; Brunt et al., 2013a) (Fig. 6.3). Soft-sediment deformed deposits at the margins of channels represent local margin collapse. Kirschner and Bouma (2000) classified all amalgamated high aspect-ratio sandstone packages also as channel bodies (their Type II), representing a distal variant of the low-aspect ratio channel body. However, due to the minor basal erosion (<0.5 m deep) and high aspect-ratio (>600), a lobe interpretation is here preferred. The low aspect-ratio channel-fills are overlain by high-aspect ratio lobe bodies (Fig. 6.7), resembling 'channel-wings'.

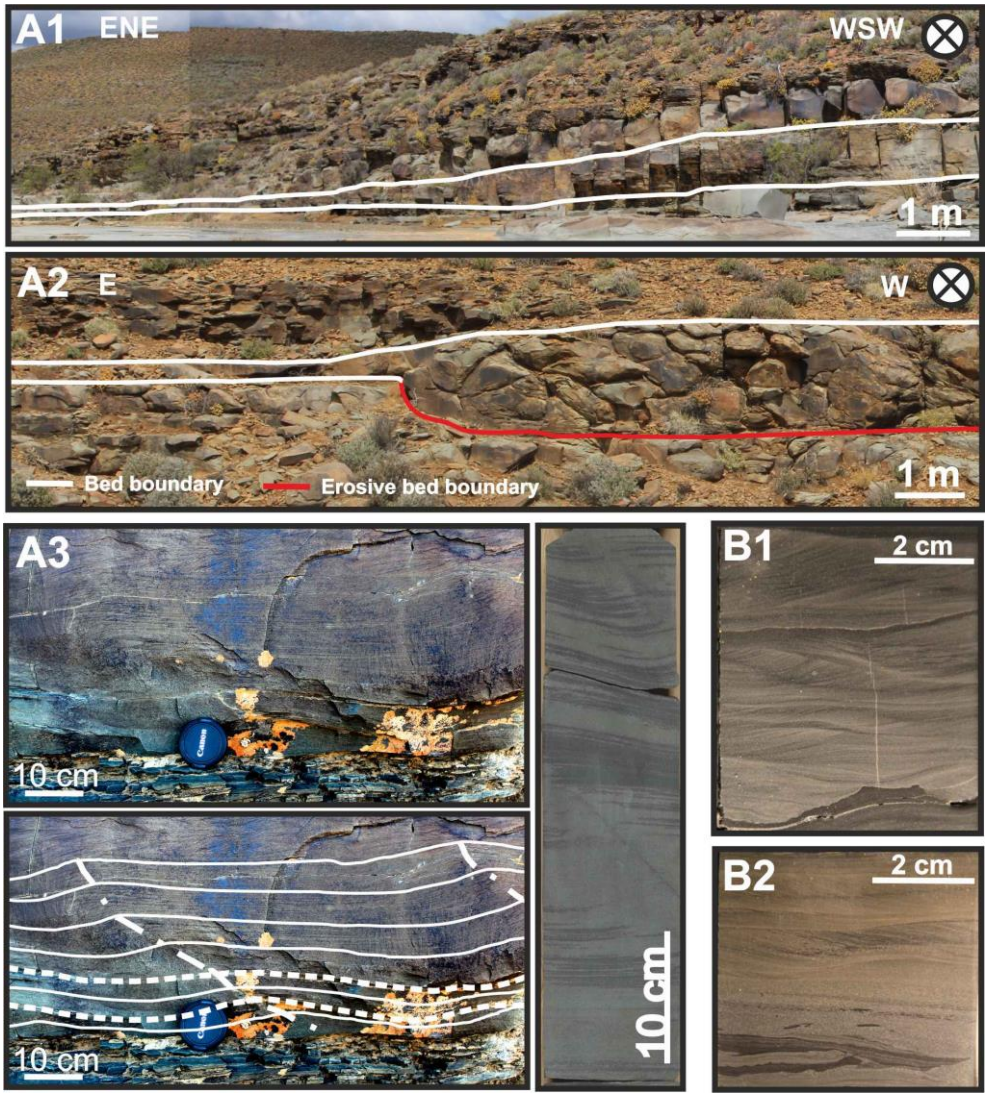

Figure 6.9 *Small-scale architectural elements within tabular deposits from outcrop (A) and bypass indicators (B) within the BK01 core (see Figure 6.7 for location). (A1) Abrupt downstream bed thinning of laminated medium-bedded sandstone; A2) Metre-scale scour feature filled by a single bed showing relative positive relief above the scour-surface. A3) Aggradational bedform composed of multiple beds showing long wavelength (>50 cm) wavy laminations. Top shows uninterpreted and bottom shows interpreted outcrop example; B1) Multiple irregular erosion surfaces among thin-bedded and ripple-laminated sandstones; B2) Abrupt normal grading within thin-bed (6 cm) from medium sandstone to fine siltstone, with irregular mudstone clasts (<1 cm – 5 cm) at the bed base.*

6.7 Defining elements in the base-of-slope stratigraphic record

The Fan 3 and Unit 5 base-of-slope systems are sandstone-prone (80-90%) and show a large diversity in erosional and depositional architectural elements. The stratigraphic variability of facies associations among the base-of-slope stratigraphy of both systems contrasts with that of the more distal reaches (Fig. 6.10A), where basin-floor lobes have

been well-documented (Prélat et al., 2009). In distal areas, the stratigraphy is marked by numerous abrupt stratigraphic alterations between thick-bedded sandstones (Fa1) and siltstones (Fa4), forming packages of 4-8 m and <2 m respectively (Fig. 6.10A). These stacking patterns are interpreted to reflect updip channel avulsion and compensational stacking patterns (Prélat and Hodgson, 2013). In comparison, packages of tabular deposits within base-of-slope successions show more subtlety in stratigraphic facies association changes and are not intercalated with laterally extensive lobe distal fringe deposits, making it more challenging to define individual lobes (Fig. 6.8). In both base-of-slope systems, high aspect-ratio sandstone packages have been interpreted as lobes, due to their sand-prone nature, bed thicknesses (some > 1 m), stratigraphic thickness variability (Figs. 6.6C, 6.7) and minor erosion below bed bases (Figs. 6.6C, 6.7). Furthermore, High Amalgamation Zones (HAZs) (Fig. 6.4) comprise the core of these high aspect ratio elements and are interpreted as the apex of lobe deposits. The juxtaposition of channel systems and lobes at base-of-slope regions (Johnson et al., 2001, van der Werff and Johnson, 2003; Luthi et al., 2006; Hodgson et al., 2006) indicates channel propagation (Pyles et al. 2014). However, alternative criteria have been established to support the identification of lobe deposits in base-of-slope settings.

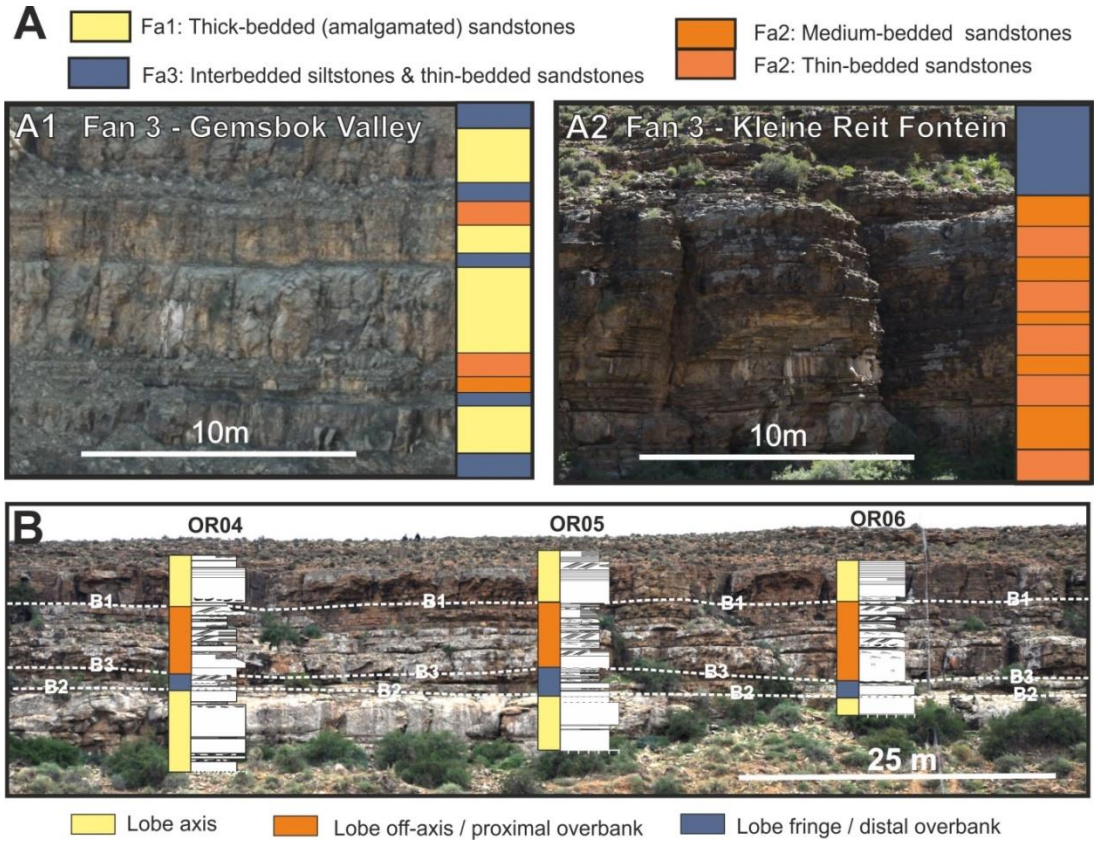

Figure 6.10 *A) Differences in stratigraphic bed thickness and facies variability among tabular deposits between proximal (A1 - Kleine Riet Fontein) and distal (A2 - Gemsbok Valley) locations within Fan 3. See Figure 6.1 for locations. B) Division in depositional elements interpreted as four different lobes within the Ongeluks River area of Fan 3. See Figure 6.8 for explanation of B1-B3*

.

All tabular deposits from both base-of-slope systems can be separated in depositional elements on the basis of stratigraphic facies association changes, bypass indicators, lateral changes in facies and bed thicknesses, changes in palaeoflow patterns and the constrains of basal erosional surfaces of channel-fills (Figs. 6.8A, 6.10B). Based on these criteria, four depositional elements can be defined in the sandstone-prone tabular package of the Ongeluks River area (Fan 3) (Fig. 6.10B), varying in thickness between 1 – 5 m. In the Blaukop area (Unit 5), 11 depositional elements have been identified, varying between 0.5-5.5 m thickness (Fig. 6.8A). Element boundaries were identified based on one of the following factors (Fig. 6.8A): sharp transitions to either thick-bedded sandstones, or thin-bedded sandstones and siltstones, change of facies association with bypass indicators and

change of facies association combined with known proximity of basal erosional channel surfaces.

Depositional elements characterised by thin-bedded deposits are generally thinner (0.5 – 1.5m), compared to depositional elements characterised by thick-bedded and amalgamated deposits (3 – 5.5m). The thin-bedded packages of the high-aspect ratio elements show indictors of sediment bypass (Stevenson et al., 2015) at various stratigraphic levels, in the form of irregular erosion surfaces, mudstone clast materials and unusually coarse bed bases (Fa4) (Figs. 6.8A, 6.9B). The combined record including thin-bedded sandstones and siltstones (Fa3), representing more distal and less energetic flow conditions, suggests substantial variations in flow energy among these thin-bedded packages. Furthermore, the tabular deposits within the Blaukop area (Unit 5), show substantial stratigraphic variations in palaeoflow patterns (Fig. 6.8A), indicating that they likely represent a stack of architectural elements.

The various depositional elements are linked to environment of deposition (Figs. 6.8B, 6.10B, 6.11A) based on the present facies associations (Figs. 6.2, 6.3). Packages of unconfined thick amalgamated (Fa1) sandstones are interpreted as lobe axis locations (Hodgson et al., 2006; Prélat et al., 2009), while medium to thin-bedded laminated sandstones (Fa2) are associated with lobe off-axis or proximal overbank environments (Prélat et al., 2009; Brunt et al., 2013a).

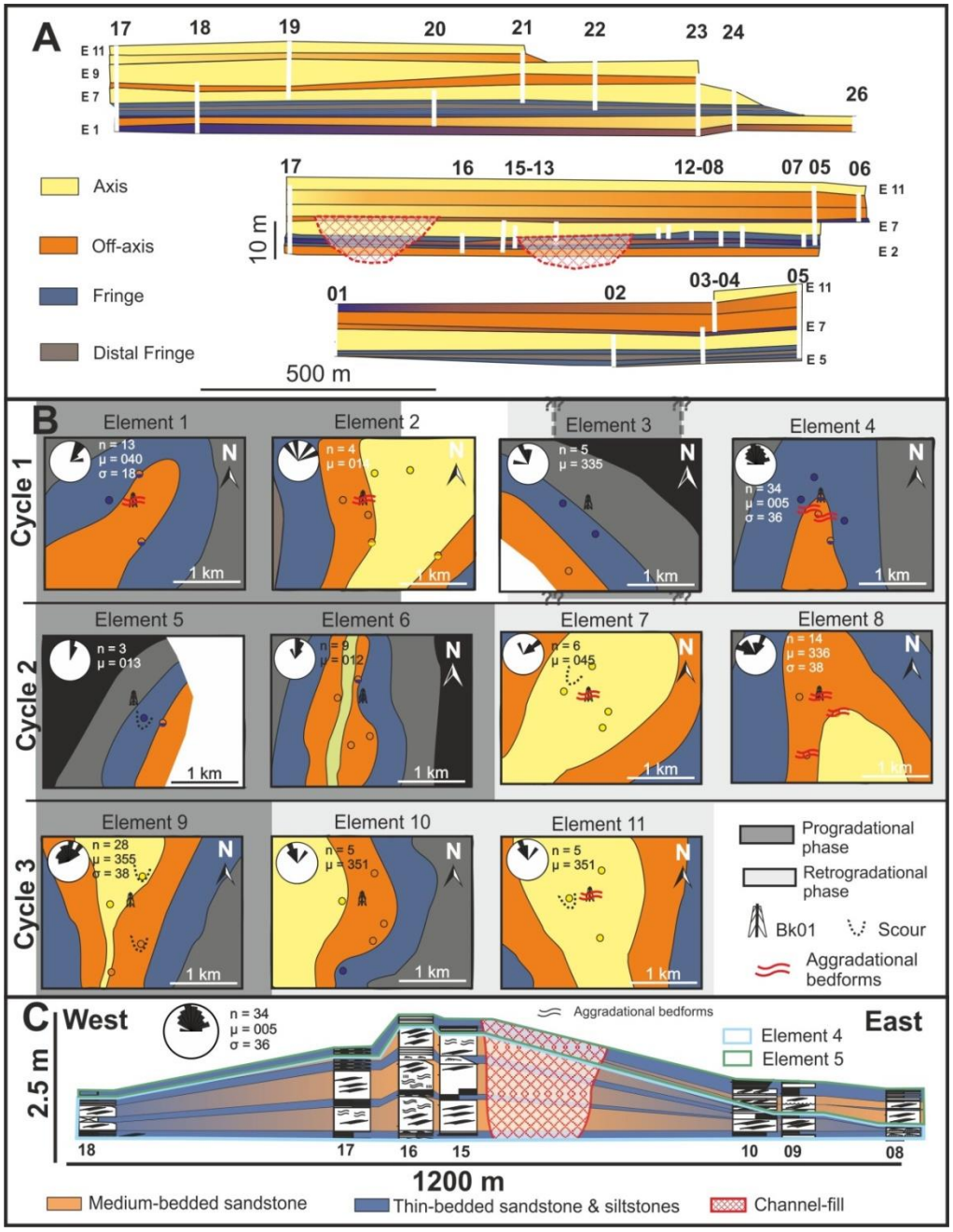

Figure 6.11 *Interpretation of all tabular depositional elements within the Blaukop area of Unit 5. See Figure 6.7 for log locations. With A) Division in depositional elements and the facies variability within B) Planform interpretations and depositional history of the twelve depositional elements with division between lobe and channel-overbank deposits based on palaeoflow patterns and lateral facies transitions. The location of the BK01 core (See Figure 6.8 for interpretation), metre-scale scour features and aggradational bedforms are indicated. The depositional history can be divided into multiple progradational and retrogradational phases (cycles). C) Detailed strike-section through depositional elements 4 and 5, showing thickness/facies changes occurring in multiple directions. The channel-fill is slightly off-centre from the thickest part of element 5. Aggradational bedforms are abundant within the thickest parts of Element 4. See Figure 6.4 for symbol explanation. Palaeocurrents have been indicated, with with n = number of measurements, μ = mean palaeoflow and σ = standard deviation*

Thin-bedded sandstones and siltstones (Fa3) are associated with lobe fringe, but may well represent a transition to levee/overbank deposits (Prélat et al., 2009; Brunt et al., 2013a). The planform expression of the elements (Fig. 6.11B) have been reconstructed for the Blaukop area (Unit 5) based on palaeoflow, thickness patterns and the observed facies transitions. The reconstructions (Fig. 6.11B) show lateral and longitudinal juxtaposition of lobes and channels and indicate a cyclic process of channel propagation and retreat or avulsion, similar to the build-cut-fill-spill model of Gardner et al. (2003). Three main cycles of downdip channel propagation and retreat can be identified (Figs. 6.8B, 6.11B). The first four depositional elements define one cycle, and the younger two cycles include the two identified channel systems (Element 6 and 9 - Figs. 6.7, 6.11), both overlain by younger lobes (Element 7 and 10). Based on stratigraphic palaeoflow patterns (Fig. 6.8A) and lateral facies changes (Figs. 6.7, 6.11), the younger depositional elements indicate less significant lateral shifting behaviour in comparison to the older depositional elements (Fig. 6.11B).

6.8 General characteristics of base-of-slope lobe deposits

The presented Fan 3 and Unit 5 cases demonstrate that lobe deposits comprise a substantial part of the base-of-slope stratigraphy (Figs. 6.10B, 6.11). In Blaukop (Unit 5), the reconstructions (Figs. 6.8B, 6.11B) support the view that the majority of the deposits among high-aspect ratio tabular elements (>75%) are lobe deposits, which permits their key characteristics to be considered (Figs. 6.12, 6.13).

6.8.1 Facies distributions

Within the studied base-of-slope systems, the lobe axis is characterised by a combination of banded (Fa1A) and structureless (Fa1B) sandstones (Figs. 6.4, 6.6C, 6.7), where banding commonly overlies structureless sandstone (Figs. 6.6C, 6.8A, 6.12). The relative portions of banded sandstones and structureless sandstones varies (e.g. Fig. 6.4), which is partially related to eroded bed tops, resulting in dominantly structureless sandstones in the most proximal locations (Fig. 6.12). These axial facies (Fa1) show facies transitions (Fig. 6.4B)

towards medium-bedded dominantly climbing ripple laminated sandstones (Fa2) in the lobe off-axis (Fig. 6.12). Within the Blaukop area, aggradational bedforms (Morris et al., 2014a) (Figs. 6.8A, 6.9A3, 6.11B, 6.11C) are predominantly identified in axial positions, from axis to frontal off-axis lobe environments. Thin-bedded sandstones and siltstones characterise the fringes of lobes in base-of-slope settings (Fa3) (Fig. 6.2). In contrast to the laterally extensive and siltstone-rich lobe fringes in more basinward positions (e.g. Prélat et al., 2009; Prélat and Hodgson, 2013), these fringes are sandstone-rich (75%-95%). Furthermore, lobe fringe elements represent a relative minor part of the base-of-slope lobe stratigraphy (10-15%).

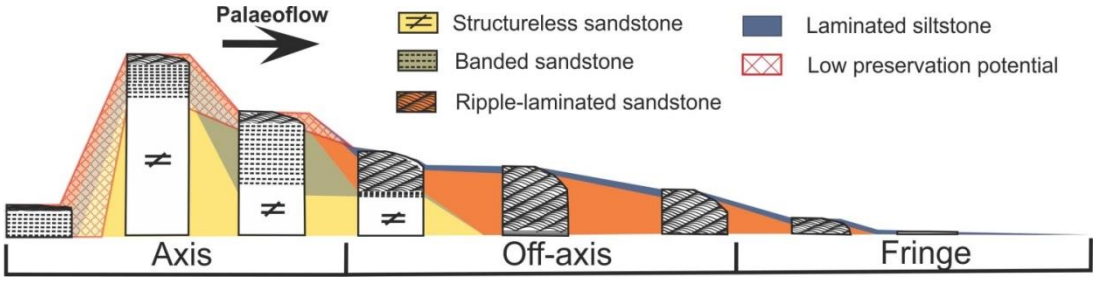

Figure 6.12 *Idealised downstream facies transition of a single depositional flow within a base-of-slope lobe deposit. The upper part of the most proximal deposit has a lower preservation potential due to erosion and amalgamation.*

6.8.2 Lobe architecture

The large dip and strike extent of lobes (e.g. Prélat et al., 2010) and their remnant form where cut by channels, means that quantification of lobe dimensions is challenging. However, the planform reconstructions (Fig. 6.11B) of lobes in the Blaukop area provide some constraint on their size and shape, and suggest that they form simple and narrow architectural bodies (Fig. 6.13). HAZs among the base-of-slope systems show some variation in dimensions and facies characteristics (Fig. 6.4), which in part can be associated with its longitudinal position. Metre-scale scour features are common among lobe deposits in both systems (Figs. 6.5, 6.9A2, 6.13). In the Blaukop area (Unit 5), scour-fills among amalgamated sandstones (Fa1) are related to proximal and axial lobe environments (Fig.

6.11B). Scours within medium- to thin-bedded facies (Fa3; Fa4), are predominantly preserved lateral to the channels that propagated into the basin (Hofstra et al. 2015) (Fig. 6.11B).

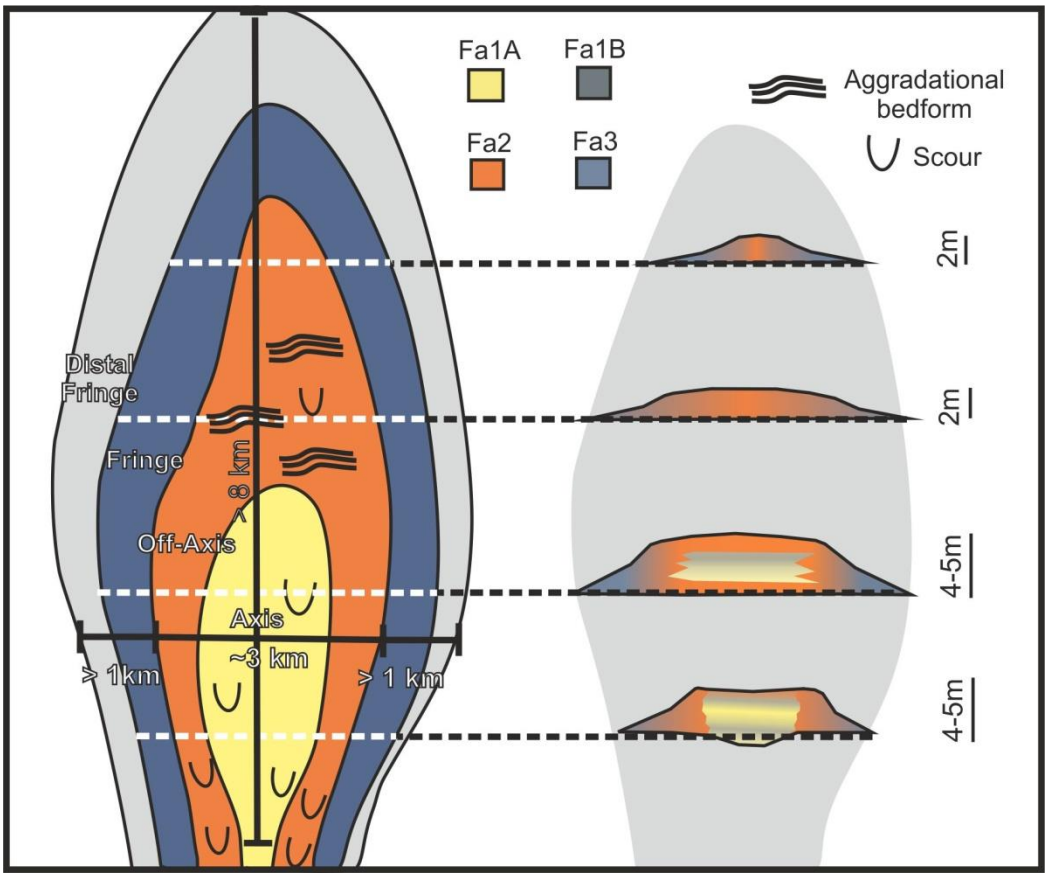

Figure 6.13 *Summary conceptual model of a base-of-slope lobe architecture with the distribution of facies and small-scale architectural elements. The given dimensions are estimates due to the limitations of the used outcrop datasets.*

The thickness of the lobe deposits varies between 5.5 to <0.5 m (Figs. 6.8, 6.10B), depending on its position within the lobe (axis to fringe; Fig. 6.13). Elements 1,2, 4 and 5 show clear thinning in both lateral and downdip directions (Figs. 6.11A, 6.11B). Facies distributions (Figs. 6.11B, 6.11C) indicate that the lobes can comprise multiple across strike transitions over short distances (< 1km). Dip-orientated transitions are not well constrained. The frontal lobe off-axis (Element 1 and 4) (Figs. 6.11B, 6.11C) can be narrow (~ 500 m wide, >3 km long). (Fig. 6.13).

6.8.3 Comparison with existing lobe types

The key characteristics of the lobes defined from the two base-of-slope systems can be compared to well-developed characteristics of different lobe types from various settings (Prélat et al., 2009; Prélat and Hodgson, 2013; Grundvåg et al., 2014; Morris et al., 2014a; Spychala et al., 2015).

In comparison to lobes described from basin-floor settings (Prélat et al., 2009; Groenenberg et al., 2010), the base-of-slope systems differ in lobe facies characteristics, distributions and architecture. The studied Fan 3 and Unit 5 base-of-slope systems (<5.5 m) are limited in thickness compared to the lobe thicknesses recorded on the basin-floor (up to 10-m) (Prélat et al., 2009). The frontal fringes of basin floor lobes are abundant in hybrid event beds (Hodgson, 2009; Prélat et al., 2009), which show an upper argillaceous division, rich in mudstone clast and carbonaceous materials (Haughton et al., 2009; Hodgson, 2009; Kane and Pontén, 2012; Fonnesu et al., 2015). Hybrid event beds are completely lacking within both base-of-slope records. Axial facies of basin-floor lobes are defined by thick packages (~ 5 m) of amalgamated structureless sandstones (Prélat et al., 2009). Banded sandstones (Fa1b), which are common within base-of-slope lobe deposits, have not been reported from the basin floor lobe deposits. The base-of-slope lobe deposits are more heavily modified by erosional features, through juxtaposition of channel systems (Figs. 6.6B, 6.7) and scours (Figs. 6.5, 6.9A2), meaning that the remnant geometries are common. Lobes at basin-floor settings show shallow (m-scale) scouring, but only in axial positions at the base of HAZs (Prélat et al., 2009; Groenenberg et al., 2010).

The lobe deposits from both base-of-slope systems share affinities with frontal lobe deposits, reported from Unit C3 (Fort Brown Formation) and exposed in the adjacent Laingsburg depocentre (Morris et al., 2014a). Frontal lobes, or splays, are lobate bodies deposited ahead of a feeder channel that lengthens into the basin and incises through its

own deposit (Normark et al., 1997; Morris et al., 2014a). They are sandstone-prone and shows an abundance of climbing-ripple laminated sandstones and aggradational bedforms (Fa2), and lack hybrid event beds. Furthermore, the architecture of these lobes is characterised by relatively low-aspect ratios and mounded geometries (Morris et al., 2014a), which is similar to the lobes identified in this study. However, little has been documented on the fine-scale architecture of these frontal lobe deposits (Morris et al., 2014a).

6.8.4 Proximal-to-distal lobe or discrete bodies?

The lobe characteristics of the two base-of-slope systems are clearly distinct from lobes reported from basin-floor settings within the same depocentre (Prélat et al., 2009). However, given the dimensions of lobes (Prélat et al., 2010), it is possible that the studied lobes of the base-of-slope systems represent the updip portion of the lobes studied downdip, and form a physically connected body. However, downdip thinning and facies transitions (Fig. 6.11) have been observed in the lobes at Blaukop (Unit 5) and the frontal fringes differ in character to frontal fringes observed at the basin-floor, where they are characterised by structureless sandstones and linked-debrites. Also, finger-like protrusions observed mostly within basal lobes of the Tanqua fan systems (Prélat et al., 2009; Groenenberg et al., 2010), have not been observed within the base-of-slope systems. In the Central Basin of Spitsbergen (Grundvåg et al., 2014), channel-lobe juxtaposition was also observed within base-of-slope settings and lobes could be traced out towards pinch-out on the basin-floor. However, the most proximal lobe deposits within the Central Basin are much more uniformly thick-bedded and/or amalgamated (Grundvåg et al., 2014) and do not show the same degree of facies variability as observed within the base-of-slope systems (Fan 3 and Unit 5) here described. Furthermore, the similarities in lobe characteristics with lobes from similar settings within the Laingsburg depocentre (Morris et al., 2014a), which have been interpreted as separate bodies from basin-floor (terminal)

lobes downdip, suggests that a large part of the base-of-slope lobes here identified are likely to be disconnected from basin-floor lobes downdip.

The thickness of the channel-fills (5-10 m), however, exceeds that of the maximum lobe thickness (5 m) identified within both base-of-slope systems, which suggest that the (majority of the) channels more likely fed thicker lobes (10 m) downdip on the basin-floor. The difference in character in both dimensions and facies characteristics between HAZs observed in base-of-slope settings (Fig. 6.4C) supports that some elements (Fig. 6.4A) may represent the updip expression of basin floor lobes, while others (Fig. 6.4B) are part of thinner lobes with different sedimentary characteristics. Therefore, the base-of-slope record most likely represents a combination of both the updip expressions of thicker basin-floor lobes as well as the relative more downdip expression of thinner base-of-slope lobes which reach less far basinward. This has important implications for submarine fan architecture and the connectivity within.

6.9 Discussion

Based on facies and architectural characteristics (sand-prone nature, climbing ripple-lamination, aggradational bedforms, lack of hybrid beds, narrow and mounded geometries) the lobes defined from the Fan 3 and Unit 5 base-of-slope systems would classify as frontal lobes (Morris et al., 2014a). However there is no evidence of levee build-up stratigraphically above these lobe deposits, as has been observed in the Fort Brown Formation (Morris et al., 2014a). The reconstructions of one of the two systems has revealed a cyclic process of lobe deposition, channel incision and propagation, and retrogradation (Figs. 6.8B, 6.11B), similar to the BCFS-model of Gardner et al. (2003).

Within such a cyclic process, not all of the lobe deposits are defined by channel propagation, and may well be incised by genetically-unrelated channels that feed basin-floor lobes downdip, and therefore do not correspond with the definition of a frontal lobe

(Normark et al., 1997; Morris et al., 2014a). To be able to uncover the true reasons behind these variations in lobe characteristics within a single system, proper classification is needed.

6.9.1 Submarine lobe classification

Variability in lobe character within a single fan system has been observed in other systems (e.g. Deptuck et al., 2008; Jegou et al., 2008). To cover this variance in lobe character a classification is proposed based on morphological and sedimentary characteristics (Fig. 6.14). Previous lobe classifications made distinctions based on the characteristics of related channels (e.g. Shanmugan and Moiola, 1991), the character of the surrounding stratigraphic package (Pickering, 1981), the geographic position (intraslope) (Spychala et al. 2015) and/or system evolution (frontal, terminal, crevasse) (Prélat et al. 2009; Morris et al. 2014a). However, a system evolution classification is interpretative and precludes making comparisons between ancient and active systems. For example, frontal lobes (Morris et al., 2014a) will be 'terminal' lobes of the system at a certain point during system evolution. Similarly, channel character may evolve over time (e.g. Deptuck et al., 2003; Hodgson et al., 2011; 2016) and not represent the initial state at time of lobe development. Also, lobes cover large areas (Prélat et al., 2010) and may not be constrained to a single geographic zone. Furthermore, if individual lobe bodies are variable within a system, a single geographic area may show a combination of different lobe types and may not be exportable to other systems.

However, lobes have also been classified based on morphological characteristics (Deptuck et al., 2008; Jegou et al. 2008). Within the Amazon Fan (Jegou et al., 2008) a division of two lobe types (Type I and II) was primarily based on morphological differences and dimensions, while within the Golo Fan the division between PILs (Proximal Isolated Lobes) and CMLs (Composite Mid-fan Lobes) was based on lobe size, architecture, feeder channel and setting. Differentiating lobe deposits based on their morphological and

sedimentological characteristics is more valuable, as it is independent of system evolution and geographical position and may be more exportable to different systems and datasets. Through integration of the results presented in this study and previous work from the Karoo Basin (Prélat et al., 2009; Prélat and Hodgson, 2013; Brunt et al., 2013a; Morris et al., 2014a; Spychala et al., 2015), two lobe types are proposed that differ in both architecture and facies characteristics (Fig. 6.14): 'narrow lobes' with lower aspect ratios, smaller surface areas and simple geometries, and 'radial lobes' with higher aspect-ratios, greater surface areas and more complicated fine-scale architecture.

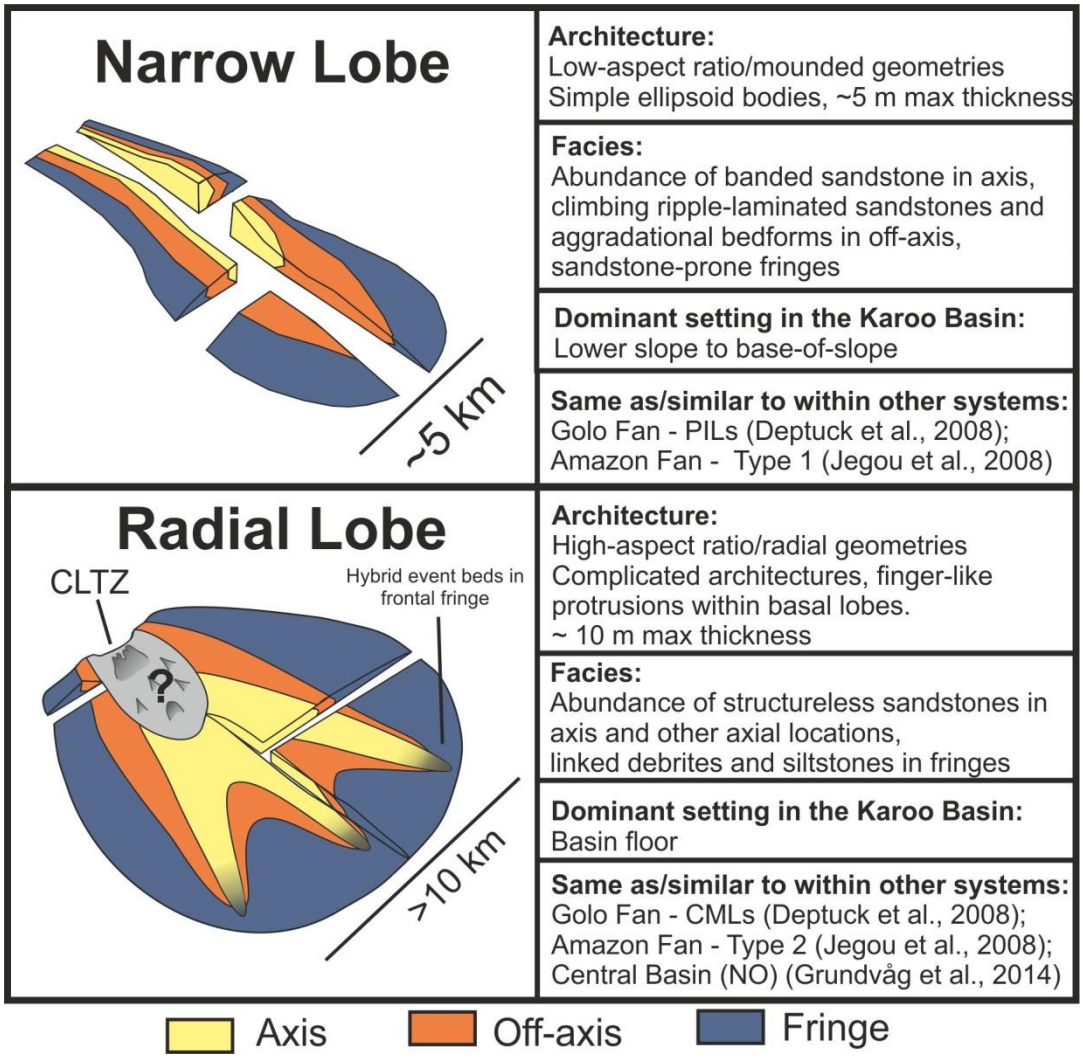

Figure 6.14 *Conceptual models of 'Narrow Lobes' and 'Radial lobes' with associated characteristics regarding architecture, facies and dominant setting within the Karoo Basin. These lobe types are comparable to similar divisions made in the Golo Fan and the Amazon Fan.*

This classification aligns with similar distinctions made in other systems (Fig. 6.14) (Deptuck et al., 2008; Jegou et al., 2008): the PILs at the toe-of-slope from the Golo Fan represent small ellipsoid bodies compared to the larger and architectural complex CML downdip (Detptuck et al., 2008), the 'Type I' lobes of the Amazon Fan form ellipsoid and narrow bodies compared to the more radial morphologies of the 'Type II' lobes which cover larger surface areas (Jegou et al., 2008).

6.9.2 Effect of flow efficiency

The presence of lobes with different characteristics within a single system can be related to an interplay of external or internal factors. External factors such as system confinement (Prélat et al., 2010), could explain the large-scale morphological differences between 'Narrow lobes' and 'Radial lobes' (Fig. 6.14), but not their variance in facies and fine-scale architectural differences. In the Amazon Fan (Jegou et al., 2008), variance in lobe morphology (elongate and radial) between different lobes was observed within the same unconfined basin-floor settings. Therefore, internal factors related to the input flow properties at time of lobe development are more likely to be involved, such as grain size, concentration, volume or flow criticality (e.g. Gladstone et al., 1998; Al Ja'Aidi et al., 2004; Baas et al., 2004; Amy et al. 2006; Postma et al. 2016). These flow parameters have an influence on flow efficiency (e.g. Gladstone et al., 1998; Bouma, 2000; Al Ja'Aidi et al., 2004), which is here defined as the carrying capacity of flows leaving channel confinement. Flow efficiency has been linked both to the expression of channel-lobe transition zones (CLTZ) (e.g. Mutti and Normark, 1987; Wynn et al., 2002a; Gardner et al., 2003; Van der Merwe et al., 2014), as well as the architecture of the deposits downdip (e.g. Al Ja'Aidi et al., 2004; Baas et al., 2004; Hodgson et al. 2016). Therefore, it has to be considered as an important first order control for lobe characteristics. A variety of flow properties can influence flow efficiency, as discussed below.

1) Froude-number

Recent studies have related architectural differences of lobes to the critical densimetric Froude number of turbidity currents (e.g. Lang and Winsemann, 2013; Postma and Cartigny, 2014; Postma et al., 2016) .The more complicated architecture of CMLs in the Golo Fan is explained by Postma et al. (2016) by the supercritical nature of the turbidity currents. The PILs were supplied by inefficient surge-like flows and by subcritical deposition throughout. Within experimental studies, 'supercritical lobes' (Hamilton et al., 2015) are fed by fully erosional 'bypass' channels, which show continuous backfilling before avulsion occurs at the avulsion node. This contrasts to the 'subcritical lobe' (Fernandez et al., 2014) that show channels formed by levee building and lobe deposition occurring directly beyond the slope break (Postma et al., 2016).

Within the systems of the Karoo Basin, the 'narrow lobes' show abundant indications for subcritical flow conditions, due to the abundance of ripple-laminated facies (Morris et al. 2014a). However there have been no observations (Hodgson et al., 2006; Prélat et al., 2009; Prélat and Hodgson 2013; Groenenberg et al., 2010) that support supercritical flow conditions (e.g. Lang and Winsemann 2013; Postma et al. 2014) feeding 'radial lobes' farther downdip. Furthermore, the inferred dominance of levee building within subcritical versus supercritical depositional conditions (Postma et al., 2016) does not comply with the PILs of Deptuck et al. (2008) as they are fed by gullies and erosive channels, instead of the CMLs, which are fed by leveed channels, although outboard of large and stable conduits.

2) Variable flow efficiency related to other basic flow properties

The efficiency of turbidity currents has also been related to flow properties (Mutti and Normark, 1987; Gardner et al., 2003) such as sediment concentration, grain size or flow velocity and size. Deptuck et al. (2008) related differences between PILs and CMLs within the Golo Fan to five factors: 1) sediment properties and flow velocity; 2) the number and frequency of flows; 3) changes in gradient and seabed morphology; 4) lobe lifespan; and 5)

feeder channel geometry. Deptuck et al. (2008) also noted that these factors are inter-related, but mainly depend on the initial flow properties (1) such as concentration, grain size, flow velocity and flow volume. Similarly, Gardner et al. (2003) attributed the Brushy Canyon fan system with relatively inefficient and sand-prone, low-volume flows. The relative impact of these basic flow properties on deposit morphology can however be different. Grain size is considered to have a much more significant impact than sediment concentration on the dimensions and morphology of the deposits (Gladstone et al., 1998; Baas et al., 2004; Amy et al., 2006), and has been inferred as a first-order control on fan system morphology (e.g. Reading and Richards, 1994; Galloway et al., 1998). Differences in length-to-width ratios between depositional bodies were linked to sediment concentration and grain size within experimental studies on the morphology of depletive turbidity current deposits (Al Ja'Aidi et al., 2004; Baas et al., 2004). More efficient flows were predominantly achieved with higher portion of fines, which generated more radial distributive patterns and started depositing at some distance from the point of flow expansion (Baas et al. 2004). In comparison, purely coarse-grained inefficient flows created more elongated morphologies directly at the point of expansion. Increasing flow volume also resulted in more elongated morphologies (Al Ja'Aidi et al., 2004). Differences in facies characteristics between lobe types can be linked to concentration and grain size. Facies characteristics of the 'narrow lobes' among the base-of-slope systems of the Karoo Basin suggest that they were fed by low-concentration and sand-dominated flows, due to the dominance of climbing-ripple lamination and their general lack of silt-grade material (<10%). The limited lobe width is therefore likely related to limitations of flow grain size and concentration.

In comparison, the 'radial lobes' in basin-floor settings are more siltstone-prone, indicating they were fed by efficient flows with a more significant portion of fine-grained materials. Similarly, Deptuck et al. (2008) suggested that flows feeding CMLs periodically had more

suspended mud compared to flows feeding PILs, which supports a greater fine-grained component. A greater mud-component would also fit with hybrid event beds being solely observed within 'radial lobes' (Hodgson 2009; Prélat et al., 2009; Grundvåg et al., 2014).

However, this does not yet explain why in some systems there is a marked relationship between the geographical position and type of lobe present (Deptuck et al., 2008; Prélat et al., 2009; Morris et al., 2014a), and not in others (Jegou et al., 2008; Grundvåg et al., 2014). Grain size distributions and/or flow concentrations can however be altered due to a variety of reasons, either by 1) alteration of the sediment properties at the source, or 2) sediment segregation occurring in between the source and the channel-mouth. 'Narrow lobes' like frontal lobes (Posamentier and Kolla, 2003; Morris et al., 2014a) indicate overall inefficient flow properties, due to deposition near the channel mouth, and are fed by flows with the fine grained component stripped off from density stratified flows into external levee successions (Posamentier and Kolla, 2003; Hodgson et al., 2016). Several mechanisms can however be proposed for limiting the sediment segregation by channel-levee systems and thus maintaining the fine-grained fraction to the channel mouth: 1) an absence of levees or 2) underfit flows in channel-levee systems, where the fines stay confined to the channel. An absence of levees could be caused either by i) being in an early phase of fan development (early lobes), ii) due to an updip avulsion by a levee breach (Brunt et al., 2013b; Ortiz-Karpf et al. 2015), or, iii) as a result of channels being strongly incised.

These different mechanisms that can impact the concentration and grain size of flows implies that both 'narrow lobes' and 'radial lobes' (Fig. 6.14) could develop at all times and geographical positions during the development of the system. However, the inefficient nature of the flows feeding 'narrow lobes', makes it much more likely that they are deposited in and around the base-of-slope (Deptuck et al., 2008; Brunt et al., 2013a; Morris et al., 2014a), when segregation occurs at the slope. Within mud-rich systems like the Amazon Fan (Jegou et al., 2008), 'narrow lobes' may reach further into the basin as

they are still efficient at the base-of-slope but may lose this efficiency due to sediment segregation by basin-floor levee systems. Lobes within the Eocene Central Basin of Spitsbergen (Grundvåg et al., 2014) show most similarities with 'radial Lobes', due to their distribution of linked debrites and siltstone-prone fringes (Fig. 6.14). Their proximal basin-floor to base-of-slope setting does however suggest that 'radial lobes' are not necessarily situated at (distal) basin-floor settings.

6.9.3 Implications for channel-lobe transition zones within the Tanqua fan systems

Variance in flow efficiency will impact connection between the feeder channel and lobe, and therefore the character of the CLTZ (e.g. Baas et al., 2004; Postma et al., 2016). However, within both the Amazon Fan and Golo Fan, none of the lobe types indicates the presence of detachment zones and all lobes appear to be connected to feeder channels. Similarly due to the thickness of the channel-fills within both studied base-of-slope systems (Fan 3 and Unit 5) they are more likely to have fed thicker 'radial lobes' on the basin-floor.

Deptuck et al. (2008) did however suggest that the larger, wider lobes within the Golo Fan (CMLs) were initially supplied by sediment transported beyond the base-of-slope before levees were constructed, which explains why CMLs are located outboard of stable and long-lived feeder channels (Deptuck et al., 2008). This would imply that at time of lobe initiation, lobes fed by efficient flows can be detached from feeder channels but may evolve into an attached lobe due to subsequent channel propagation, resulting in a combined record of unconfined and confined bypass. Some of the inferred morphological differences between radial and elongated lobes could be linked to CLTZ character. Hybrid-bed prone (finger-like) lobe fringes have been linked to updip extensive scouring of muddy substrate at CLTZ settings (e.g. Talling et al., 2007; Ito, 2008), which suggests that the lack of hybrid-bed prone fringes and finger-like morphologies among elongated lobes can be due to their limited CLTZ development.

The presence of features such as large scour-fills (Hofstra et al., 2015) within the Kleine Riet Fontein area (Fig. 6.1B), does indicate there might have been initial periods of non-channelised sediment bypass when more efficient flows reached the base-of-slope, feeding the basin-floor lobes downdip. The stratigraphic position of these giant scour-fills within the top of Fan 3, suggests that part of the basin-floor lobes could have developed either due to updip levee-breach (Brunt et al., 2013b; Ortiz-Karpf et al. 2015) or deepening of the feeder channel, resulting in an efficiency increase of the flows reaching the base-of-slope.

6.10 Conclusions

Several integrated datasets presented from base-of-slope settings within the Karoo Basin indicate that these sand-rich environments dominantly comprise lobe deposits. The character of these base-of-slope lobes varies substantially from basin floor lobes in terms of facies and architecture. They share affinity with frontal lobes, but do not always precede channel propagation. The identification of downstream thinning and facies changes suggests that base-of-slope and basin floor lobe deposits most likely represent different depositional bodies. A division is proposed between small narrow lobes, dominantly found at the base-of-slope and wider, radial lobes at the basin-floor. Narrow lobes are architecturally simple, and show a relative high proportion of climbing ripple-laminated and banded sandstones. In contrast, radial lobes can be architectural more complicated with finger-like protrusions, and show a high proportion of structureless sandstones, hybrid beds and laterally extensive siltstones. Similar divisions have been proposed for the Golo Fan and Amazon Fan. The narrow lobes at base-of-slope settings are defined by channel juxtaposition and metre-scale scour features, while radial lobes show an overall lack of channel incision and predominant compensational stacking behaviour in basin-floor settings. The character differences between narrow and radial lobes are likely to be related to the efficiency of flows that fed the depositional bodies, of which variations in grain size

may be the most significant factor. As differences in flow efficiency can both be related to the degree of flow segregation by channel-levee systems as well as changes to the initial sediment supply, it may explain why different lobe types are not constrained to specific geographical areas in some systems. The recognition of these two lobe types has important implications for understanding the stratigraphic record of CLTZs as well as the evolution and the internal architecture of submarine fan systems as a whole.

Chapter 7:
The impact of fine-scale reservoir geometries on streamline flow patterns in submarine lobe deposits using outcrop analogues from the Karoo Basin

7.1 Summary

Improved prediction of the recovery of oil-in-place in basin-floor fan reservoirs requires accurate characterisation and modelling of multiscale heterogeneities. The use of outcrop analogues is a key tool to augment this process by documenting and quantifying sedimentary architecture, hierarchy, and sedimentary facies relationships. A 3-D geological modelling workflow is presented that tests the impact of fine-scale heterogeneities within basin-floor lobe complexes on reservoir connectivity. Construction of geological models of a basin-floor lobe complex allows realistic depositional architecture and facies distributions to be captured. Additionally, detailed models are constructed from channelised areas within a basin-floor lobe complex. Petrophysical modelling and streamline analysis are employed to test the impact on reservoir connectivity between lobe models with i) vertically-stacked facies with coarsening- and thickening-upwards trends in all locations, and ii) lateral facies changes with dimensions and distributions constrained from outcrop data. The findings show that differences in facies architecture, and in particular lobe-on-lobe amalgamation, have a significant impact on connectivity and macroscopic sweep efficiency, which influence theproduction results. Channelised lobe areas are less predictable reservoir targets due to uncertainties associated with channel-fill heterogeneities. The use of deterministic sedimentary architecture concepts and facies relationships have proven vital in the accurate modelling of reservoir heterogeneities.

7.2 Introduction

Hydrocarbon production targets are moving towards more challenging reservoir types, including offshore turbidite reservoirs in ultra-deepwater settings (>1500 m). Typically, the construction of geological models for these reservoirs uses a combination of subsurface seismic and well data. Well data is particularly sparse during the early phase of projects (Strebelle et al., 2003; Pyrcz and Deutch, 2014) and seismic resolution is inadequate to constrain 3D reservoir connectivity and heterogeneity distribution. Therefore, outcrop analogues and conceptual models are applied to reduce this uncertainty (e.g. Bryant and Flint, 1993; Pringle et al., 2006; Howell et al., 2014).

Application of outcrop data helps to capture architectural complexity and heterogeneities within submarine fan (sheet) systems (e.g. Kleverlaan and Cossey, 1993; Richards and Bowman, 1998; Drinkwater and Pickering, 2001) and to constrain stochastic-based modelling of facies and petrophysical properties (Alabert and Massonnat, 1990; Joseph et al., 2000; Stephen et al., 2001; Amy et al., 2013). A small number of studies have performed stochastic-based modelling of submarine lobe deposits, where individual compensationally stacked flow events were modelled to create lobate geometries or sheet-like splays (Pyrcz et al., 2005; Saller et al., 2008; Zhang et al., 2009). Recent work (e.g. Pirmez et al., 2000; Beaubouef et al., 2003; Deptuck et al., 2008; Prélat et al., 2009, 2010; Macdonald et al., 2011b; Straub and Pyles, 2012) has demonstrated that submarine lobe architecture and facies trends are often not as simple as the classical models (e.g. Mutti et al., 1977; Mutti and Sonnino, 1981) , and involve order and hierarchy (Prélat et al., 2009; Straub & Pyles, 2012) which may not be covered within purely stochastic modelling methods. The planform extent of submarine lobes in the subsurface can be resolved by seismic mapping (Saller et al., 2008), however smaller-scale elements and heterogeneities cannot be seismically resolved. Attributes (Fig. 7.1), such as lobe amalgamation and internal facies transitions (e.g. Stephen et al., 2001; Zhang et al., 2009) have proven to

have a major impact on reservoir model predictions, but their relative impact is poorly constrained. Other attributes such as finger-like geometries within lobe fringe areas (Groenenberg et al., 2010) and the juxtaposition of channels and lobes in Channel-Lobe Transition Zone-s (CLTZs), have never been captured in published reservoir modelling work.

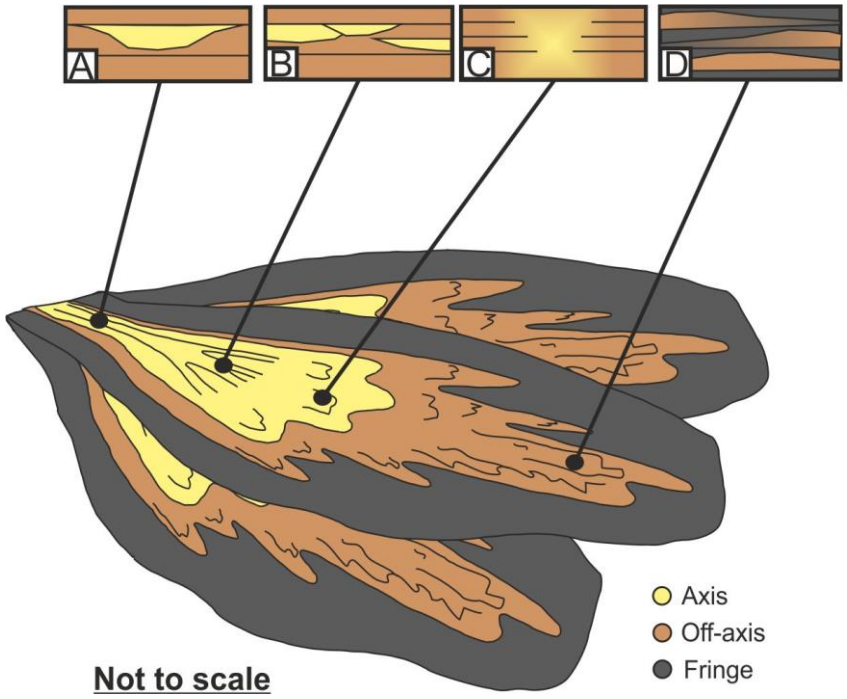

Figure 7.1. *Simplified cartoon of a basin-floor submarine lobe complex showing distinct subenvironments with A – confined channel systems, B – distributive channel network, C – high amalgamation zone (HAZ), D – distal lobe environment. Based on Kane and Pontén (2012).*

The architectural complexity of submarine channel-levee complexes and their influence on reservoir performance (e.g. Clark and Pickering, 1996; Stephen et al., 2001; Larue, 2004; Larue and Friedmann, 2005; Sprague et al., 2005; Mayall et al., 2006; Schwarz and Arnott, 2007; Barton et al., 2010; Pringle et al., 2010; Alpak et al., 2013; Labourdette et al., 2013; Eschard et al., 2014) has been widely studied. The main focus of this work was on the diversity of channel architecture and heterogeneities within channel-fills, such as channel base drapes (e.g. Larue and Friedmann, 2005; Barton et al., 2010; Alpak et al., 2013).

Detailed studies on facies characteristics in turbidite reservoirs (e.g. Stephen et al., 2001; Falivene et al., 2006; Scaglioni et al., 2006) demonstrate that heterogeneities across a range of scales influence connectivity and compartmentalisation of the reservoir. Pore and textural properties in structured and normally graded sandstones will affect flow properties of the bed and the system as a whole (Stephen et al., 2001). The focus on the presence or absence of large-scale baffles and barriers such as shale drapes (e.g. Stephen et al., 2001; Saller et al., 2008; Barton et al., 2010; Pyrcz and Deutsch, 2014) will not capture the whole spectrum of heterogeneities. In contrast to channel-levee complexes, there are only a small number of fine-scale reservoir heterogeneity studies from channel-lobe transition zones, despite being important deep-water reservoir targets. Connectivity of channel-fills with overbank deposits (Eschard et al., 2014), and reservoir performance differences between lobe and channel-fill dominated deposits (Zou et al., 2012) are poorly understood. Zou et al. (2012) noted that sheet-prone sandstones provide more sustained production than channel-prone sandstones due to a significant decrease in sweep efficiency in the latter. Margin connectivity within channel-lobe contacts can be in many cases much better compared to channel-channel or channel-levee contacts (Funk et al., 2012).

In this chapter, the aim is to study and quantify the impact of different conceptual stratigraphic and sedimentological models of deep-marine lobes on reservoir behaviour and fluid flow predictions, and compare these sedimentological and stratigraphic factors to other uncertainties within reservoir modelling. This aim was addressed through the application of both 'hard' (geometric) and 'soft' (understanding) data (*sensu* Howell *et al.* 2014) from outcrop analogues of exhumed basin-floor lobe and channel-lobe transition zone deposits from the Karoo Basin, South Africa. Soft data includes conceptual models, characteristic facies for architectural elements and their lateral or vertical facies relationships. The objectives of this study are to follow a deterministic modelling approach

to investigate the effect of sub-seismic heterogeneities within lobe complex sub-environments (Fig. 7.1) on reservoir connectivity, including 1) lobe amalgamation, 2) facies transitions and distributions and, 3) channelisation. Sensitivity tests on various petrophysical models are performed with the help of 275 single-phase streamline flow simulations.

7.3 Methods

Outcrop datasets from the Tanqua depocentre were used to construct sedimentary facies grid models (Fig. 7.2) within a cornerpoint grid mesh using the commercially available software Reservoirstudio^{TM}. The sketch-based interface and cornerpoint grid of the software permits construction of complicated depositional architectures of lobes and channels, including fine-scale vertical heterogeneity with a low amount of total grid cells. Conventional modelling methods using Cartesian grid meshes are unable to capture small-scale heterogeneities as they are limited to the shape and size of the cells (Aarnes et al., 2008; Jackson et al., 2015).

Separate grid frameworks were used to construct a lobe complex (full lobe-scale models) and two channel-lobe transition zone scenarios (lobe-scale sector models) (Fig. 7.2). Single-phase flow streamline simulations were performed between vertical injector and producer wells, to investigate differences in connectivity and production performance (Fig. 7.2).

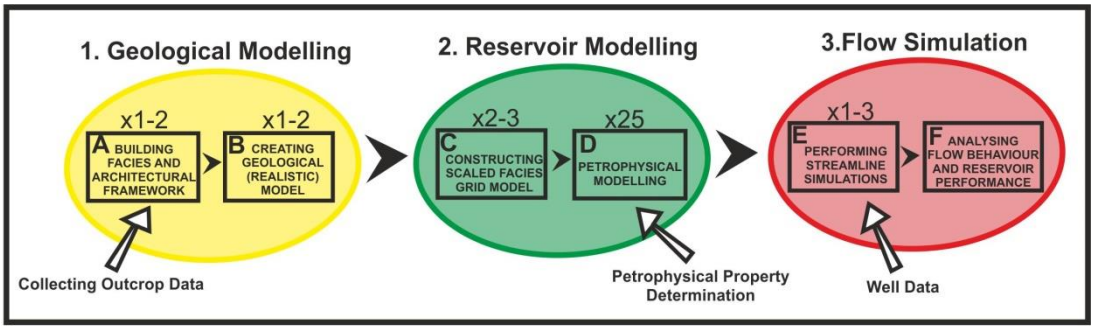

Step	Active input	Main uncertainty	# Models	How uncertainty is covered/ reasons for multiple models
A	Outcrop data (Karoo Basin)	Correctness of sedimentary logs and correlations	CLTZ (2X) BFL (1X)	Different datasets modelled (CLTZ: BK & OR)
B	--	Interpretation of sedimentary architectures	CLTZ-OR (1X) CLTZ-BK (2X) BFL (2X)	Studying the effect of applying different models for lobe facies distributions (BFL: A & B) or the pressence/absence of channel-fills (BK: Ch & no-Ch)
C	--	Level of upscaling	BFL (3X) CLTZ-BK (2X) CLTZ-OR (2X)	Different levels of detail to look at the impact of fine-scale sedimentary architectures on connectivity
D	Petrophysical property data (Glitne Field)	Estimation of petrophysical properties linked to facies groups	25X	Stochastic modelling of petrophysical properties for each facies group - high number of realisations.
E	Well data (Glitne Field)	Well placement	Inj-Prod pairs BFL (2) OR(3) BK(1)	Different injector-producer pairs

Deterministic process Stochastic process

Figure 7.2 *Illustration of the complete workflow that has been followed, including geological modelling, reservoir modelling and flow simulation. All data input is indicated by arrows. The table shows the main uncertainties within each modelling step, the number of submodels produced, how the uncertainties were covered, and why multiple models were required. 'CLTZ' refers to channel lobe transition zone, 'BFL' to basin floor lobe complex model, 'OR' and 'BK' to the 'Ongeluks River' and 'Blaukop' datasets respectively, and 'Ch' and 'no-Ch' to channels and no-channels respectively – see text for further details.*

7.3.1 Regional setting of outcrop analogues

The Karoo Basin is one of several late Palaeozoic to Mesozoic basins that formed on the southern margin of Gondwana in response to convergent-margin tectonism (De Wit and Ransome, 1992; Veevers et al., 1994; López-Gamundi and Rosello, 1998). The southwestern area of the Karoo Basin is divided into two depocentres: the Tanqua and Laingsburg depocentres (Flint et al., 2011). In the Tanqua depocentre (Fig. 7.3), the upper Ecca Group comprises a shallowing-upwards succession from distal basin-floor mudrocks (Tieberg Formation), through basin-floor fans (Skoorsteenberg Formation) to shelf-edge delta deposits (Waterford Formation). The Late Permian Skoorsteenberg Formation (Fildani et al., 2009; McKay et al., 2015) is 400 m in thickness and comprises five distinct

sand-rich submarine fan systems, which are separated by laterally extensive hemipelagic mudstones (Johnson et al., 2001; Van der Werff and Johnson, 2003; Hodgson et al., 2006). Fan 3 is the most extensively studied system (Bouma and Wickens, 1991, 1994; Sullivan et al., 2000; Johnson et al., 2001; Van der Werff and Johnson, 2003; Hodgson et al., 2006; Hofstra et al., 2015), showing the transition from base-of-slope to distal pinch-out. Prélat et al. (2009) and Groenenberg et al. (2010) studied the basin-floor lobe deposits within Fan 3 and showed the importance of autogenic processes that drive compensational stacking patterns. Unit 5 represents the transition from a basin floor to slope environment (Van der Werff and Johnson, 2003; Wild et al., 2005; Hodgson et al., 2006), and was fed by multiple channel systems, in contrast to the underlying point sourced fan systems (Hodgson et al., 2006).

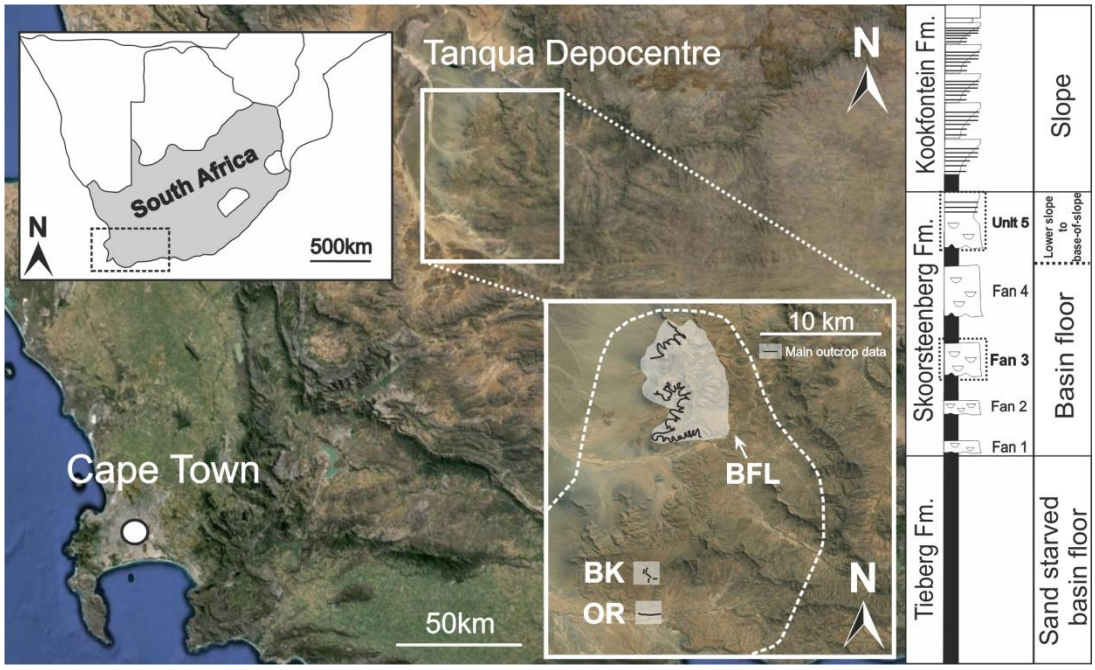

Figure 7.3. *Location map of the Tanqua depocentre showing the outcrop analogues that have been used for facies modelling and the stratigraphic column of the Tanqua deep-water deposits (based on Hofstra et al., 2015). The basin floor lobe complex models (BFL) were based on a large dataset from Prélat (2010) collected within the medial to distal parts of Fan3. For the CLTZ-models two different datasets were used: one from Fan3 (OR) and one from Unit 5 (BK). The dashed outline represents the inferred outline of Fan 3.*

7.3.2 Outcrop data collection and interpretation

Three study areas were used to build facies model frameworks: a distal basin-floor lobe dataset of Fan 3 (BFL) based on Hodgson et al. (2006), Prélat et al. (2009) and Prélat (2010), and two newly collected datasets from CLTZ environments, one from Fan 3 and one from Unit 5 (Fig. 7.3). For reconstructing a full-scale basin-floor lobe complex, the hierarchical scale and sedimentary concepts of Prélat et al. (2009) and Prélat and Hodgson (2013) have been followed. These provide a unique data-set from the medial to distal areas (Fig. 7.3) with closely spaced measured sections across a 150 km^2 study area of Fan 3 with lateral constraints on individual lobes and facies distributions due to good outcrop extent and limited amount of erosion (Fig. 7.4). Lobe facies maps and lobe thickness information (Prélat et al., 2009; Groenenberg et al., 2010) underpin the facies modelling of the basin-floor lobe complex.

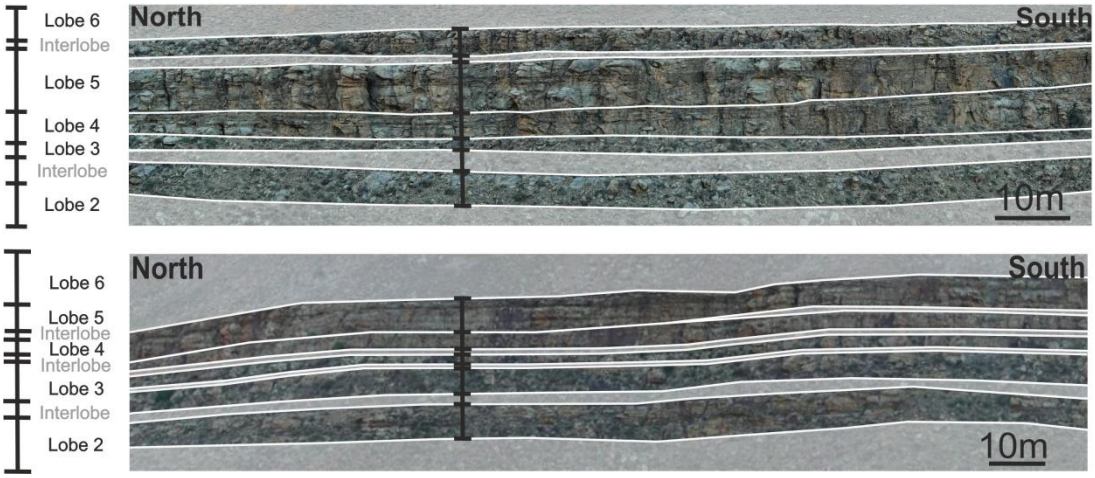

Figure 7.4 *Panoramic views of the Fan 3 lobe complex at two locations at the Gemsbok Valley area. The level of lobe-on-lobe amalgamation is clearly different between both locations. Lobe numbers have been indicated, interlobes and interfan mudstones are presented in greyscale.*

For the CLTZ models, two segments from base-of-slope channelised lobe areas were chosen and sedimentary log data collected: Ongeluksriver (OR) of Fan 3 and Blaukop (BK) in Unit 5 (Fig. 7.3). These study areas augment previous work (Kirschner and Bouma, 2000;

Sullivan et al., 2000, 2004; Van der Werff and Johnson, 2003; Hodgson et al., 2006; Luthi et al., 2006) and show clear differences in the character of channel-fills and channel volumes and their stratigraphic and physical relationship with underlying lobe deposits.

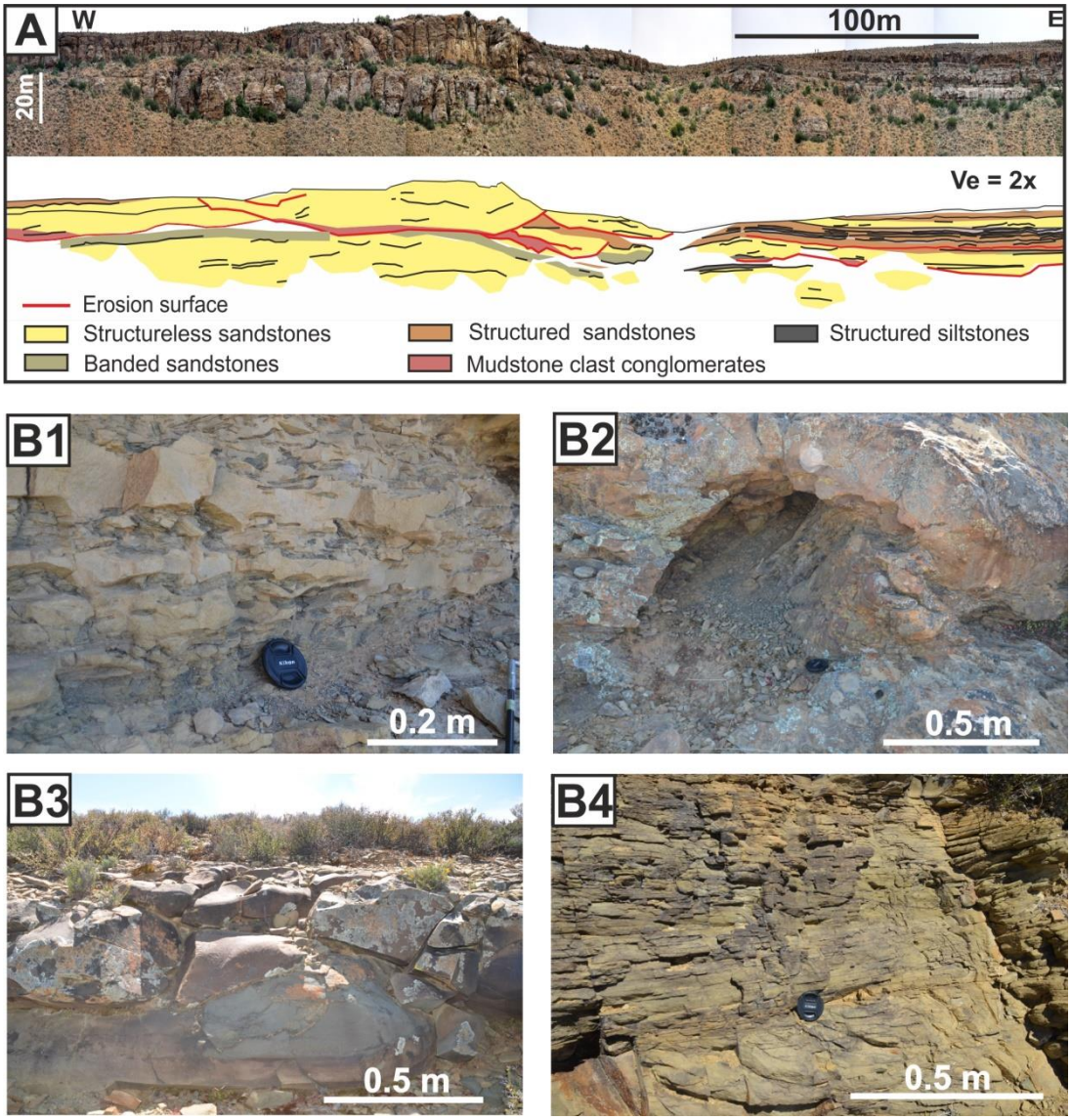

Figure 7.5 *A - Panoramic view of central channelised area of the OR-section and its facies distribution based on log-data. Due to an exposure bias, the most dominant facies that can be observed is structureless sandstone. Red lines indicate erosion surfaces. B - Typical channel-fill facies, with B1 – mud clast conglomerates, both clast-supported (bottom) and matrix-supported (mid to top), B2– Soft-sediment deformed siltstones and sandstones at the channel margin, B3 – Structureless amalgamated sandstones and B4 – Banded argillaceous sandstones.*

The OR area preserves a distributive channel network that incises tabular sand-prone packages which have been referred to as 'intra-channel highs' (Van der Werff and Johnson, 2003; Sullivan et al., 2004; Luthi et al., 2006) (Fig. 7.5). Due to their sandstone-prone

nature and variation in bed thicknesses, they are here interpreted as a combination of lobe and overbank deposits. A new dataset was collected (See *Appendix B.2*) with thirty-four measured sections (25-50 m spacing) within a 2 km wide EW-trending section, which form the basis of the OR model framework. The eight channel-fills show a range of cross-sectional geometries (100-550 m wide, 4-10 m deep), and are vertically and laterally stacked with occasional lateral overlap (Fig. 7.5).

The BLK-section of Unit 5 shows two confined channel systems (~300-350 m wide and >10 m deep) incised into sandstone-rich deposits (Kirschner and Bouma, 2000). Twenty-seven sedimentary logs were collected in a 2 km^2 area with close-spacing (10 to 100 m apart) (See *Chapter 6*, Fig.6.7), permitting the construction of a 3D framework. In addition, one fully cored borehole (BK01) was drilled 150 m away from the nearest outcrop, allowing bed-to-bed correlation with the outcrop dataset (See *Chapter 6*, Fig.6.8).

7.3.3 Basin floor lobe complex (BFL)

The medial to distal part of the Fan 3 lobe complex consists of six lobes, and facies and thickness maps have been constructed for four of them (Fig. 7.6). Thin beds between lobes were originally referred to as interlobes (Prélat et al. 2009), although Prélat and Hodgson (2013) subsequently interpreted these as the distal fringes of other lobes, due to compensational stacking. Facies models were constructed for a lobe complex including the four lobes (Fig. 7.6) and at the scale of the model (20 km x 40 km x 70 m) the interlobes were treated as through-going fine-grained units. Due to this rectangular mesh framework (20 km x 40km), rectangular cells were used, 200 m wide (x) and 300 m long (y) and with variable z cell dimensions (0.25 - 20 m). Reservoirstudio™ permits complicated planform architectures of submarine lobes to be drawn and constructed. The scheme of Prélat et al. (2009) was applied to define four distinct sub-environments of lobe deposition: axis, off-axis, fringe and distal fringe. This subdivision was also applied within the modelling

process; however the fringe and distal fringe were combined to a single 'fringe' sedimentary facies zone. Sedimentary facies associations were attributed to each of the zones within the lobe models, creating realistic facies distributions and vertical stacking patterns. Distinct lobe areas (zones) were created that closely follow the patterns of the original facies distribution (Fig. 7.6) including lobe fingers (Groenenberg et al., 2010). With only three sedimentary facies zones, some simplification of facies modelling was necessary. No distinction was made between frontal and lateral fringes, and hybrid-bed prone areas (Hodgson, 2009) were not included. Lobe and interlobe thickness information were implemented in each individual lobe, and adapted for each lobe zone.

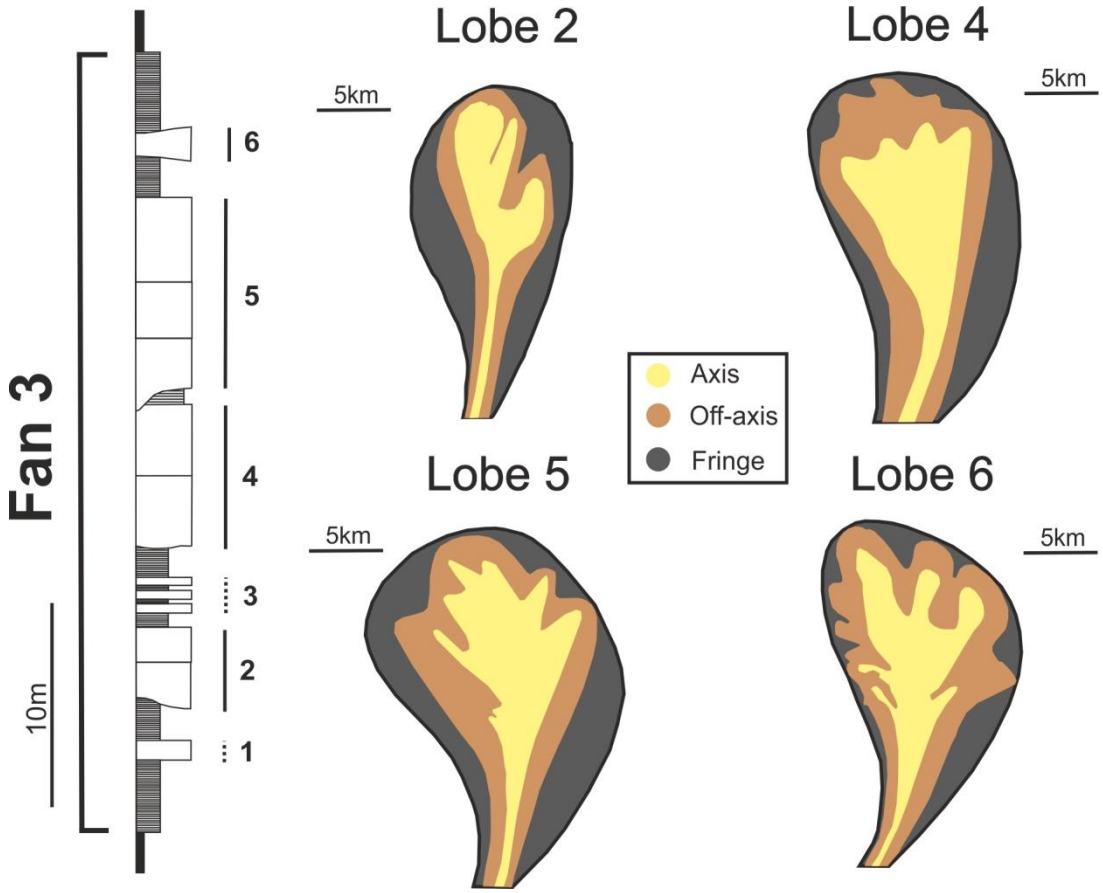

Figure 7.6 *Left - Log showing the Fan 3 basin-floor lobe complex and its division into six different lobes (based on Prélat et al., 2009). Right - Plan view of the simplified facies zones of four lobes used to construct the lobe complex facies models (based on Prélat, 2010). All individual lobes show an irregular 'finger-like' facies distributions in frontal fringe areas.*

Two conceptual models of lobe architecture and facies distribution were tested (Fig. 7.7): Model A, 'classic' lobe model (coarsening- and thickening-upwards at all locations within the lobe) and Model B, the Karoo-based conceptual lobe model (facies transitions from axis to fringe and allowing lobe amalgamation). The classic model (Model A) (Fig. 7.7) follows the Marnoso model of Ricci-Lucchi (1975); Mutti (1977); Mutti and Sonnino (1981); Piper and Normark (1983) or the 'Depositional Lobes' model from Shanmugam and Moiola (1991), in which all facies zones are vertically stacked within each lobe. This implies that fringe zones formed the base of each lobe and covered the whole lobe area. The remaining lobe zones show progressively smaller surface areas, mimicking a stratigraphic pattern of coarsening- and thickening-upwards across the entire volume of the lobe, implying an overall progradational pattern (Prélat and Hodgson, 2013). The facies-transition model (Model B - Prélat et al., 2009) (Fig. 7.7) shows multiple lateral transitions from axis to fringe areas to capture compensational stacking of lobe elements. The axial lobe areas were made slightly erosional, mimicking lobe amalgamation in axial areas (Prélat et al., 2009). Different facies associations have been attributed to each lobe zone based on sedimentary log data. A total of three different facies associations were used for the basin-floor lobe complex models: thick-bedded structureless sandstone (Fa1), medium-bedded structured sandstones (Fa2) and thin-bedded siltstones and sandstones (Fa3).

Within Model A the number of facies groups decreases from axis to fringe, with Fa3 being spread over the complete surface area of the lobe, Fa2 only covering the two inner zones (off-axis and axis) and Fa1 being focused within the axis. All together this resembles a coarsening-upward trend.

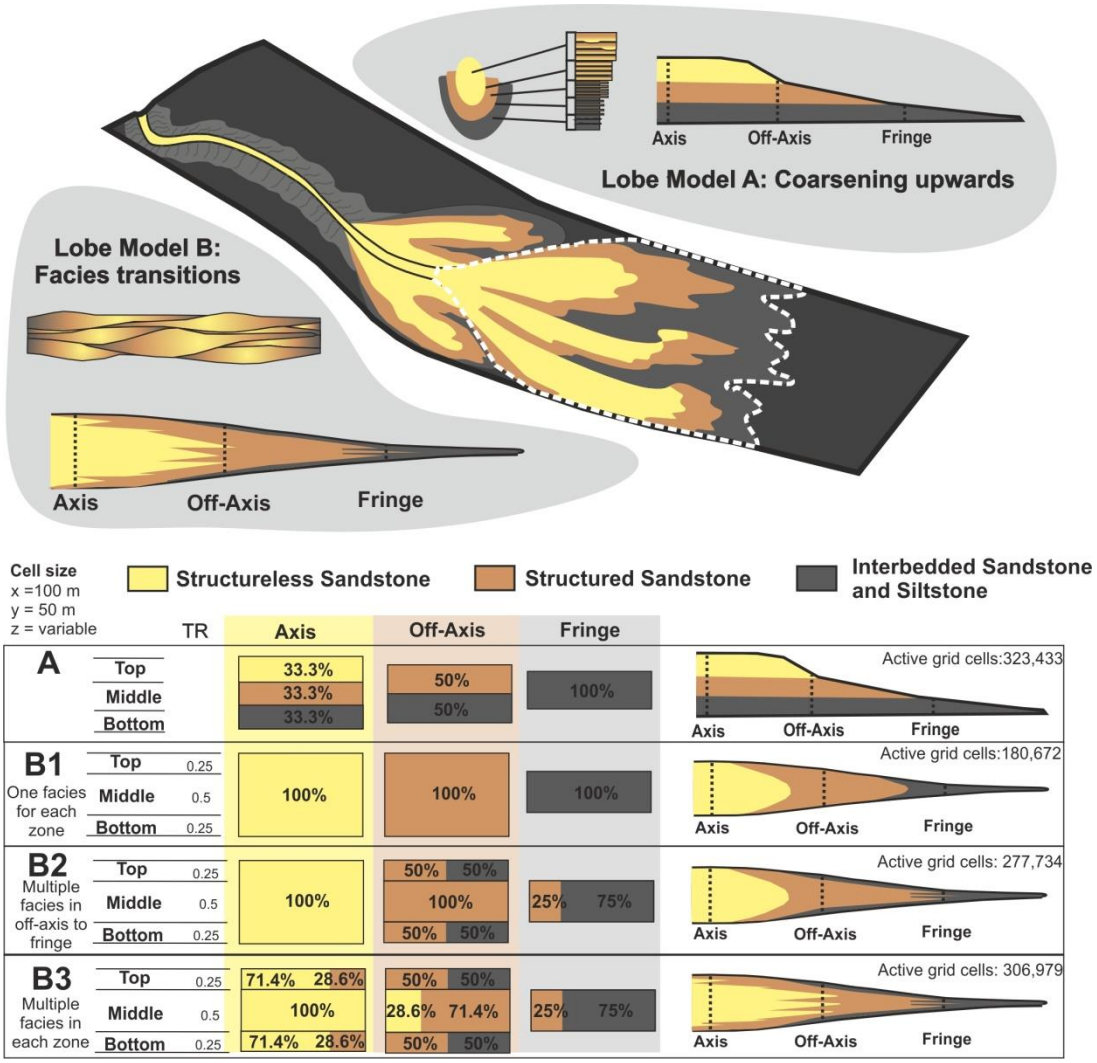

Figure 7.7 *The two lobe construction models that have been applied with Lobe Model A: Stacking of all elements, creating a thickening/coarsening pattern at every single location of the lobe (based on Mutti, 1977), and Model B: Facies transitions from axis to fringe (based on Prélat et al., 2009) with allowance of axial lobe amalgamation. The sketched fan in the middle shows the section (dashed white line) of the system (basin-floor lobe complex) that has been modelled. Different facies submodels were constructed for model B with a division into bottom, middle and top sections. B1: Simplified facies division with a single facies association for each lobe zone and no vertical division; B2: Multiple facies associations in top and bottom within off-axis areas and in fringe areas; and B3: Multiple facies associations within all lobe zones, including middle section of the off-axis areas.*

For Model B, three sub-models were constructed with different proportions of facies associations for the different lobe zones (Fig. 7.7). The vertical lobe structure was divided in three packages (top, middle and bottom) of which the middle portion was twice as thick as the top and bottom portions. The three sub-models represent three different levels of

internal detail with B1 – one facies group for each lobe zone, B2 – multiple facies groups for off-axis and fringe zones, B3 – multiple facies groups for all lobe zones. Due to these differences in facies proportions within the lobe zones, the style of facies transitions that has been modelled from axis to fringe is more abrupt in B1 and B2 than in B3. Attempt was made to keep the overall facies volumes constant between the different BFL models (Fig. 7.7), to prevent major reservoir performance differences due to variance in overall petrophysical properties.

7.3.4 CLTZ environments (OR and BK)

Small-scale sector models (2 km x 2 km x 70 m) were created for the two CLTZ environments (BLK and OR) (Fig. 7.8). All non-channel deposits, including lobes, have been modelled as background layering, representing infinite tabular bodies. This is considered to be sufficient due to the minimal lateral changes in thickness or facies documented at the scale of model in the outcrop data collected from the non-channel deposits. Channel-fills within basin-floor settings of the Karoo Basin dominantly comprise well-sorted structureless sandstones (e.g. Sullivan et al., 2000; Johnson et al., 2001; Van der Werff and Johnson, 2003; Brunt et al., 2013a), and are well exposed at outcrop (Fig. 7.5A). Areas of poor exposure were interpreted as intra-channel overbank and lobe deposits. Sedimentary thicknesses and facies distributions were based on sedimentary log-data (Figs. 7.5, 7.8). Realistic depositional architectures for the channel bodies were based on a combination of outcrop observations and generalised models of base of slope channels within the Karoo (e.g. Van der Werff and Johnson, 2003; Brunt et al., 2013a). Some of the tabular sandstone-prone deposits within the BK study area, have been interpreted as very high-aspect ratio channel-fills (Kirschner and Bouma, 2000). However, due to their uniform thickness over the study area and tabular nature, here they are interpreted as lobes and overbank material and constructed as part of the background layering. Typically, basin-floor channel-fills (200-400 m wide, 5-10 m deep) in the Karoo Basin are comprised of four

main facies groups (Brunt et al., 2013a; Fig. 7.5B): amalgamated structureless sandstone (Fa1), medium-bedded banded argillaceous or 'dirty' sandstone (Fa5), mudstone clast lag conglomerate (Fa4) and soft-sediment deformed deposits (Fa6). Fa 1 is the dominant facies group (>75%; Fig. 7.4A). Typically, with a conventional modelling technique using a regular grid, the channel-fill would be represented by a single facies group , as the incorporation of minority facies would lead to an impractically large number of grid cells. However, the heterolithic character of the facies groups can have significant influence on the reservoir properties. Therefore, two versions of the channel-fills were applied: one with a single-facies fill (Fa1), and one with the addition of the minor facies groups (Fa 1A, Fa4, Fa5 and Fa6). Due to the lack of longitudinal constraint on the channel-fills, standard deviations (0.1-0.5 m) were set for the thickness modelling of each individual facies package. In each CLTZ model, the x and y cell dimensions were set to 100m x 100m, while the z cell was variable between 0.1 to 20 m, depending on the scale of the modelled architecture.

Petrophysical properties are likely to be different in thick amalgamated structureless deposits (Fa 1A) and stratified normally graded sandstones (Fa1B), and therefore a distinction is made. The OR dataset (Fig. 7.8A) was used to construct two alternative sub-models, OR-A and OR-B, with different levels of detail. OR-A represents a simplified (up-scaled) facies model, only including the facies groups that represent the majority of the facies (Fa1A, Fa1B, Fa2 and Fa3) and a more detailed and realistic facies model (OR-B) with the addition of Fa4, Fa5 and Fa6 groups. In addition, some of the background packages were separated into smaller facies packages. Within OR-B the sandstone-rich units were separated into structureless, banded and structured sandstones (Fa1B, Fa2 and Fa4) and the sandstone-poor units into thin-bedded siltstones and structured sandstones (Fa2 and Fa3). The total number of grid cells increased by an order of magnitude (from $70x10^3$ in OR-A to $50x10^4$ in OR-B) with the down-scaling from OR-A to OR-B.

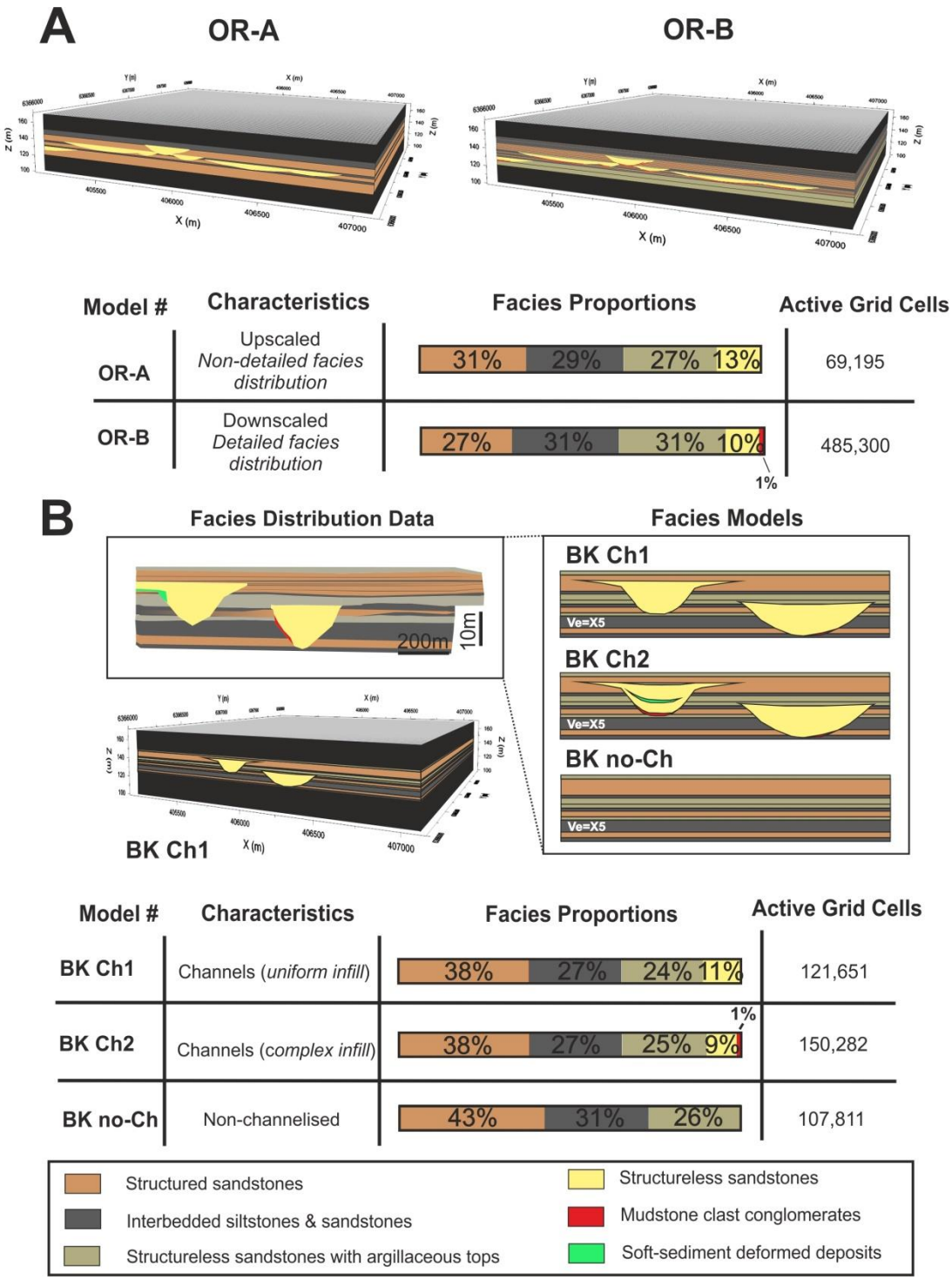

Figure 7.8 *CLTZ reservoir block models with A - OR submodels including a simplified (upscaled) facies distribution (OR-A) and a detailed (downscaled) facies distribution (OR-B); B - BK submodels with two of the three having different levels of detail within channel-fills (BK Ch1 & BK Ch2) and one excluding the channels completely from the model (BK no-Ch). A full block-model of Bk Ch1 is shown as an example. Note that the facies proportion differences between the different submodels are limited.*

Three sub-models were built with the BK-dataset, which were used to understand the influence of channel architecture on reservoir connectivity. The configuration of the background layering was kept constant and consists of a combination of structured sandstones (Fa2), banded sandstones (Fa5) and thin-bedded sandstones and siltstones (Fa3). Two sub-models showed different levels of channel-fill detail: BK-A single facies group for entire channel-fill, and BK-B enhanced channel-fill facies with the addition of Fa4, Fa5 and Fa6. A third sub-model (BK-C) was constructed, where the channel-fills were completely removed and comprised only background layering. In both the OR and BK models, differences within facies proportions of sub-models were minor (Fig. 7.8).

7.3.5 Petrophysical property modelling

No petrophysical property dataset is directly usable from the outcrop analogues which have been altered due to burial metamorphism and weathering (Fildani et al., 2009). Therefore, data were obtained from the Glitne Field, a small oil field within Palaeocene turbidites in the upper part of the Heimdal complex in the South Viking Graben, Norwegian North Sea (Keogh et al., 2008). Previous authors have used geometrical constrains and facies information from the Tanqua submarine systems as an outcrop analogue for the Glitne system (Hodgetts et al., 2004; Keogh et al., 2008).

Therefore, petrophysical properties and production data from this field were used for fluid modelling purposes of this study. Core plug permeability measurements were used from the most central exploration well (15/5-5) within the field (Fig. 7.9A). The well is positioned between two other exploration wells which have been interpreted as a feeder channel (15/5-6) and a lobe fringe environment (15/5-3) (Avseth et al., 2001). Well 15/5 represents a setting where both channel and lobe deposits are interpreted. The core plug measurements were assigned to different facies associations by use of core photographs (e.g. Fig. 7.9A). These data provided a basic understanding of the range in permeability values (1.2-1200 mD/cP) that can be expected from the various facies associations and the

assumption is made that these core plug measurements are representative for the proposed facies groups over their complete cell volume (Ringrose & Bentley, 2015). Remaining permeability values (Fa3; Fa4) were based on Amy et al. (2013). To account for the heterolithic character of some of the facies groups (horizontal *versus* vertical permeability), Kv/Kh permeability factors were applied to certain facies groups (Fig. 7.10) , primarily based on Amy et al. (2013).. A permeability factor was also applied within the banded sandstone facies group (Fa5) as the Glitne core data indicated low permeabilities within argillaceous intervals (Fig. 7.9A) (9 mD/cP compared to >200 mD/cP in non-argillaceous sandstones).

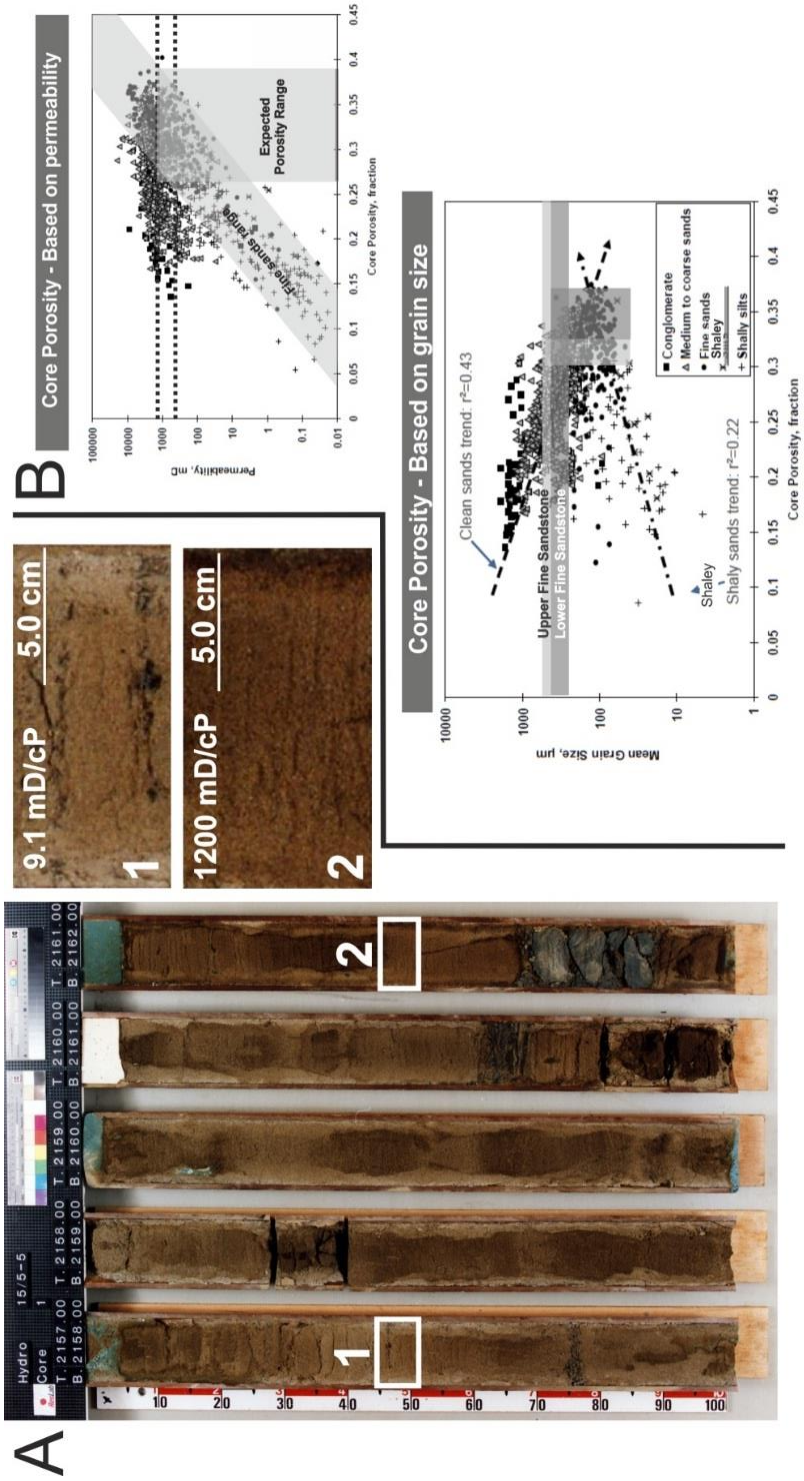

Figure 7.9 *A- Glitne Field core photos from well 15/5. Two core plug permeability measurements (A1 and A2) were undertaken within this sand-prone section (~5m), showing two completely different permeability values, associated with a higher argillaceous content in A1, blocking pore space between individual grains. B - Example of porosity range of the structureless sandstones (Fa1), determined based on the dataset of Bennes and Hamon (2007). Both permeability data from the Glitne field and grain size data from the outcrop record have been used to determine the range in porosity values. The shades of grey indicate the 'fine sands' group range for the associated permeability or grain size range.*

	Fa 1A Structureless Sandstone (AM)	Fa 1B Structureless Sandstone (TB)	Fa 2 Structured Sandstones	Fa 3 Siltstones & sandstones	Fa 4 Mudclast Conglomerate	Fa 5 Banded Sandstones	Fa 6 SSD Deposits
Porosity (fr)							
Mean	0.325	0.325	0.3	0.225	0.145	0.325	0.225
Range	0.26-0.39	0.26-0.39	0.23-0.36	0.16-0.29	0.09-0.20	0.26-0.39	0.16-0.29
Perm KH (mD)							
Mean	1200	800	220	60	2500	800	30
Range	600-1800	600-1200	150-300	1-100	10-5000	600-1200	0-60
Perm KV (mD)							
Mean	1200	800	110	15	2500	10	30
Range	600-1800	600-1200	75-150	1-25	10-5000	7.5-15	0-60
KV/KH	1.0	1.0	0.5	0.25	1.0	0.0125	1.0

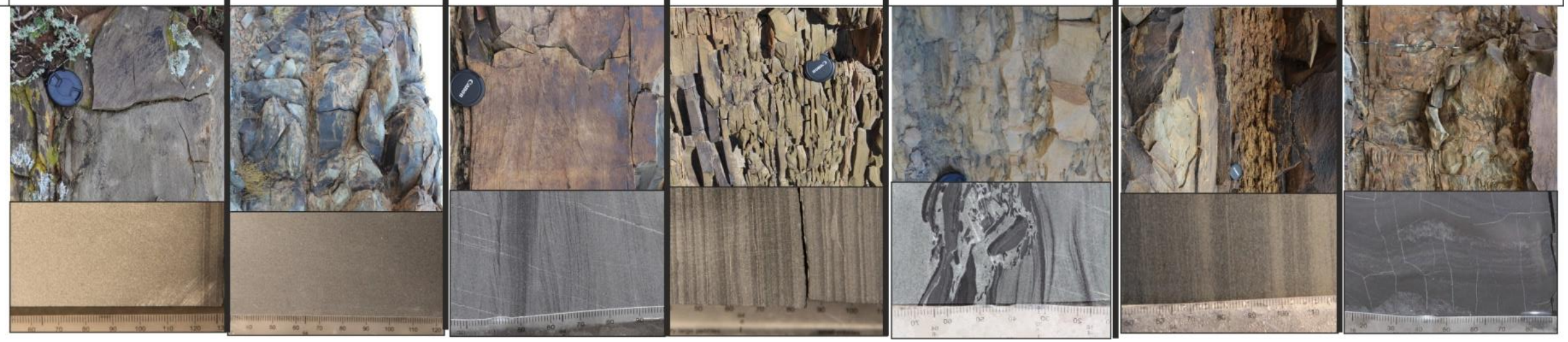

Figure 7.10 *Table showing the range in porosity and permeability values applied within the petrophysical modelling, including core and outcrop examples. For certain facies groups (Fa2, F3 and Fa5) a permeability factor (Kv/Kh) was implemented to account for the expected heterogeneity within them.*

Commonly, banded sandstones show a clean dewatered sandstone base and an argillaceous top (Hofstra et al., 2015), an estimate of 0.0125 Kv/Kh (10/800) was applied for the banded facies group. Highest permeability readings (1200 mD/cP) within the 15/5 core are associated with dewatered (dish and pillar structures) clean sands (Stow and Johansson, 2000). As this value is significantly higher than other structureless sandstone readings (300-600 mD/cP) a division was made between dewatered amalgamated structureless sandstones (Fa1A) and thick-bedded non-dewatered structureless sandstones (Fa1B). For the Fa3 and Fa4 groups, permeability factors (Kh/Kv) have been estimated as the dominance of normal grading and the interbedding with low-permeable siltstones will result in heterogeneous vertical petrophysical properties (Scaglioni et al., 2006).

As porosity data were not available from the Glitne Field, estimations were applied based on the collection of core porosity data from subsurface Tertiary turbidite systems of Bennes and Hamon (2007) (Fig. 7.9B) and Amy et al. (2013). Both 'permeability-porosity' and 'grain size-porosity' cross-plots were used to determine porosity ranges for each sedimentary facies group (Fig. 7.9B). The porosity range was based on the spread of data-points present within this study. To account for the uncertainty within petrophysical properties, ranges were set (Fig. 7.10) and a total of 25 petrophysical property realisations were performed for every submodel within RMS$^{TM}_{2012}$ (Fig. 7.11).

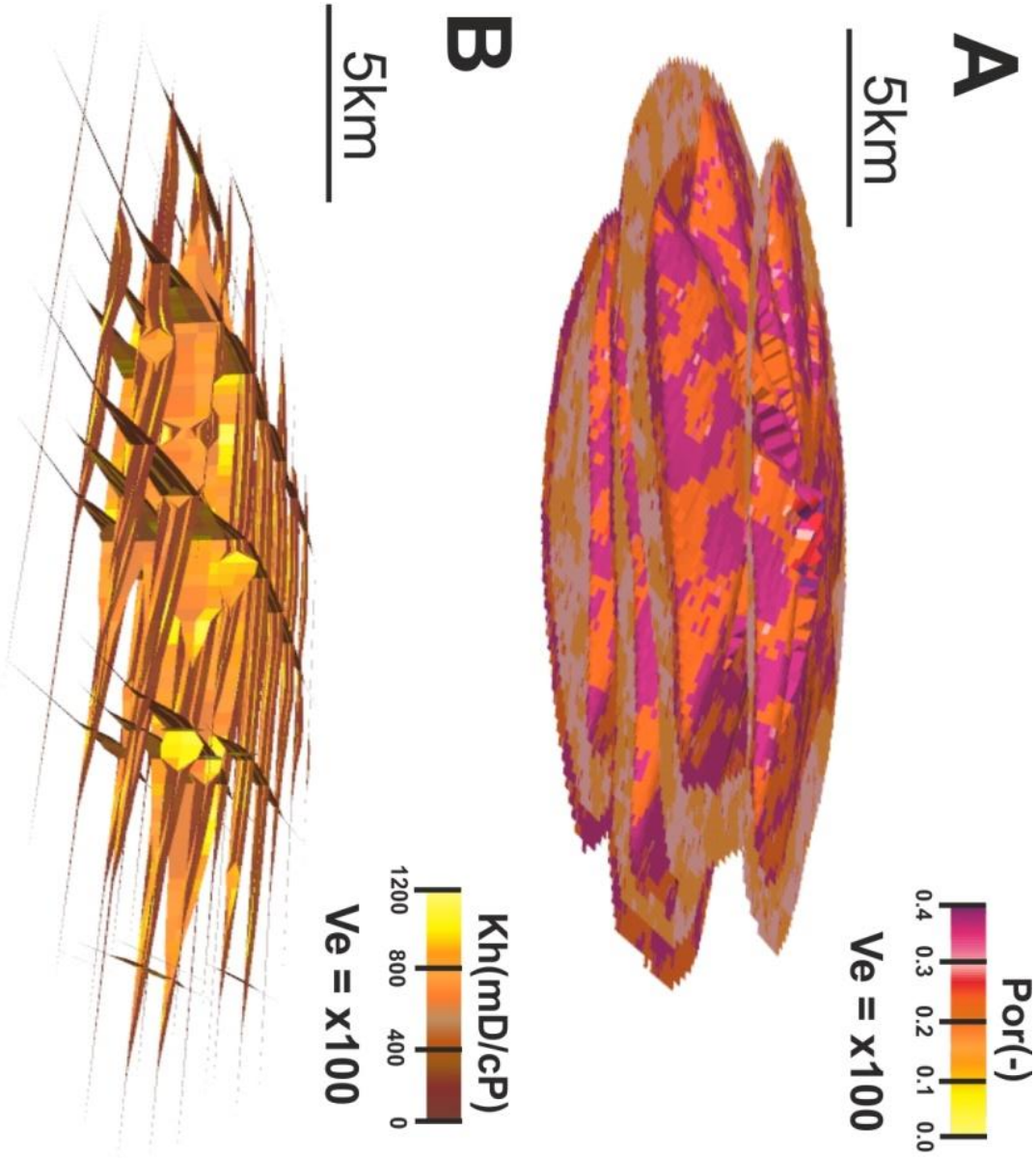

Figure 7.11 *A - Example porosity realisation of BFL-Model B2 showing stacked lobes and a decrease in porosity from axis to fringe. B - Fence diagram of a horizontal permeability (Kh) realisation of BFL-Model B2, showing clear differences between axial and fringe facies. A total of 25 petrophysical property realisations were performed for every submodel.*

7.3.6 Streamline simulation set-up

To test connectivity within the reservoir models, single-phase flow simulations have been performed using the streamline analysis tool in RMS$^{TM}_{2012}$ (blue fluid/red fluid simulation in industry appellation). This simulation tool allows extremely fast analysis of flow patterns within reservoir models, even when the model is complicated and/or large. The main

advantage of this method is that a large number of simulations can be run in a short amount of time (e.g. Brandsæter et al., 2001). This allows the performance of a large number of sensitivity tests to look at the relative impact of various factors on flow patterns. The visual representation of flow patterns, called streamlines, show the path of fluid particles through a reservoir, given constant pressure and reservoir conditions. Within the streamline simulation procedure, the boundary conditions are defined by the well rates and the structural boundaries. Once the pressure distribution is calculated, the velocity field is determined, which forms the basis for the streamlines.

With the help of these streamlines, differences between scenarios in the preferred flow paths can be identified readily. Due to the large number of simulations (275), the tracer breakthrough times (TBT) between injector and producer wells can be used to evaluate the connectivity within the reservoir. A fast tracer breakthrough between injector and producer well is here associated with increased connectivity and/or permeability contrasts (Hovadik and Larue, 2007). As the flow of any fluid or gas in a reservoir is primarily controlled by the spatial distribution of permeability and pressure gradients (Hewett, 1986), contrasts in the permeability due to the presence of different lithofacies will impact reservoir connectivity. For a number of scenarios, drainage functions are performed with the help of generated time-of-flight parameters and pore volumes. These drainage functions give predictions of the production rate using calculated pore volume, time of flight parameters and production/injection regions from the streamline simulation output.

7.3.7 Well set-up

In the basin-floor lobe complex (BFL), two injector-producer pairs (Fig. 7.12) were sited: one in the axis of the complex (Axis) and one in the fringe area (Fringe). Within the OR-models, three injector-producer pairs were placed, longitudinal to the channel orientation (Fig. 7.12), with injectors and producers penetrating the same channel system (Loc1, Loc2 and Loc3). For the BK-models, one injector-producer pair was placed longitudinal to

channel orientation, penetrating both channel systems (Fig. 7.12). Well positions were kept constant between all simulations.

Dynamic rock, dynamic fluid (light oil) and reference pressure were based on data from the Glitne Field. Fluid injection and production occurred over the complete modelled interval. To assure a steady state was reached within each simulation, sensitivity tests were performed and the solution time was set to 10 years (3650 days). The distance between injector and producer was always set to a minimum 1km to ensure active flow. In some cases, where multiple injector-producer pairs are present within a single model, an injector of one pair may interfere with the results of a producer well of another pair. The effects of different injectors on the producer wells could be separated during the streamline simulations and to prevent any possible interference, only the paired-well data (1 km distance) have been included within the results. Flow rates and well pressures from both producers and injectors were based on well data from the Glitne Field and kept the same between different realisations, in order to allow constant pressure and reservoir conditions for the performance of streamline simulations.

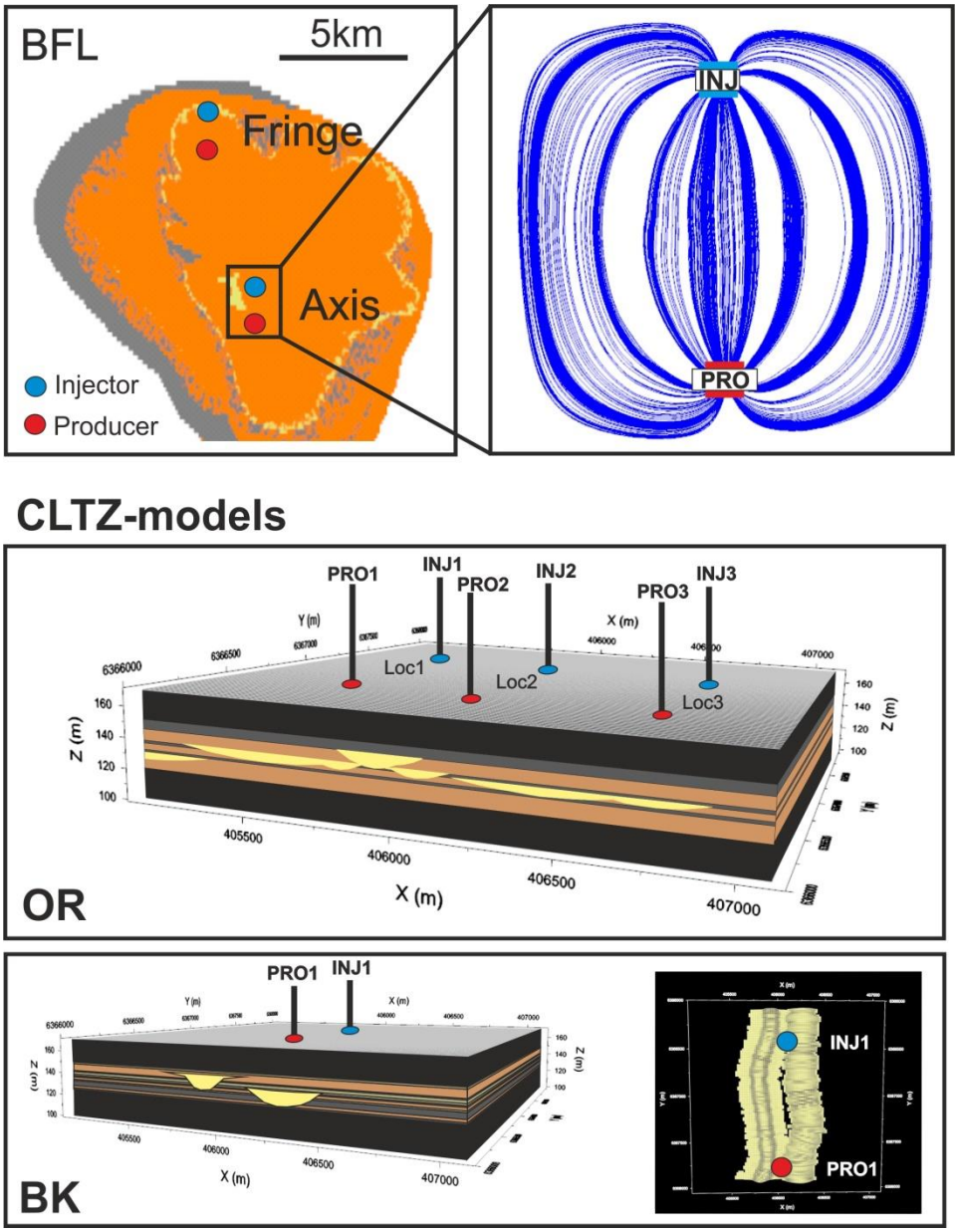

Figure 7.12 *Well setup for BFL, OR and BK models. Injector and producer pairs were set at different locations with a fixed 1 km distance in between. Within the BFL-model two injector-producer pairs were located at different locations within the complex, an example of flow streamlines within a fully heterogeneous reservoir is shown on the right. Within the CLTZ models, the producer-injector pairs were orientated along channel orientation and positioned so that they penetrated the channel bodies. In the BK-model the wells penetrated the margins of both channel systems.*

7.4 Streamline simulation results

7.4.1 Basin floor lobe complex (BFL)

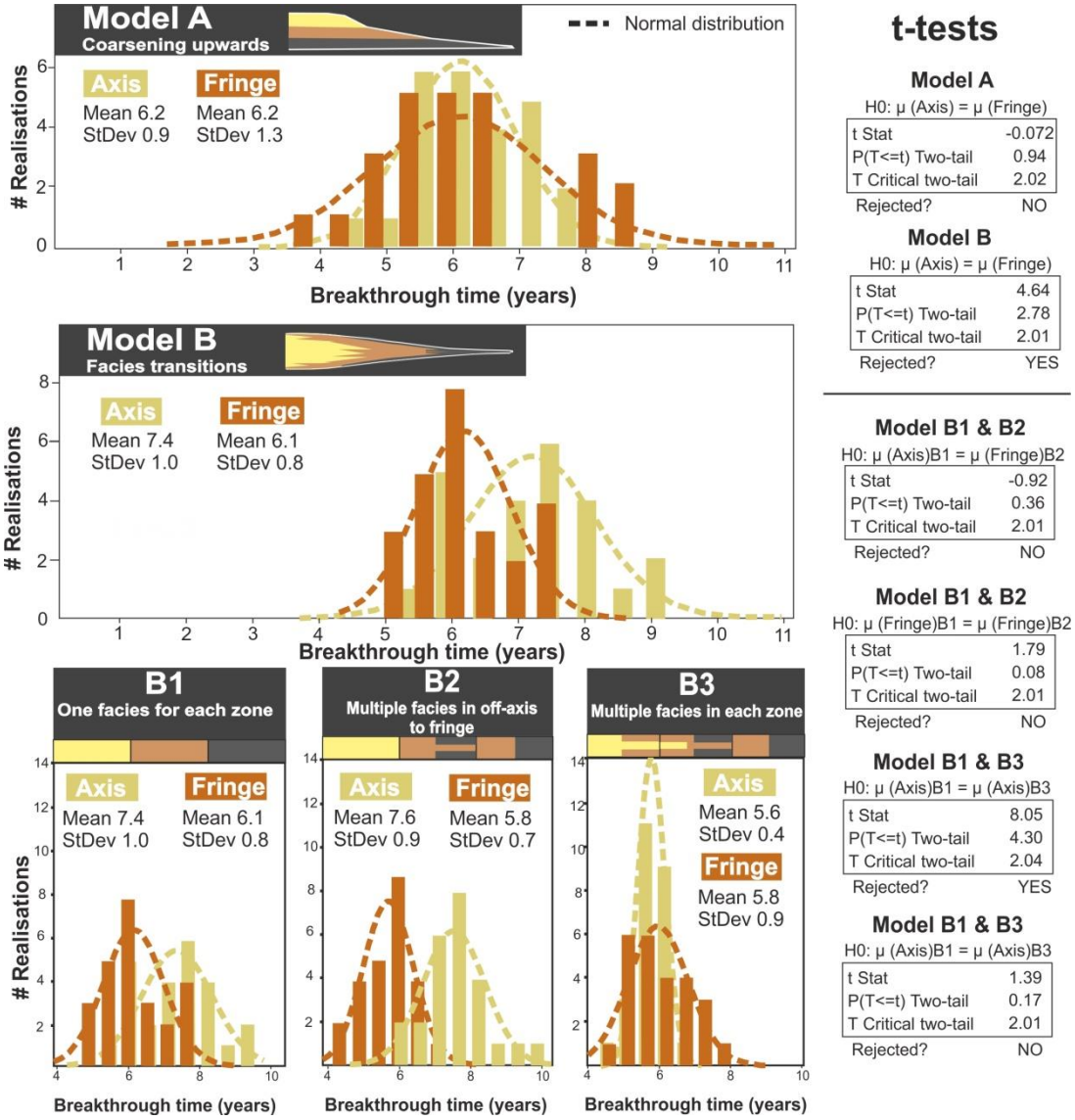

Figure 7.13 *Breakthrough time (TBT) histograms of all performed BFL model streamline simulations. The histograms show the results for the 25 simulations that were run for each well pair. Model A shows similar TBT's for different locations within the system, while Model B clearly shows differences depending on location. The lower three histograms show the difference between the Model B submodels. The results of various two-tailed t-tests have been given to the right.*

Simulation results of Model A (coarsening- and thickening-upwards) and Model B (facies transitions) (Fig. 7.7) are compared using TBT histograms (Fig. 7.13) that show the spread in breakthrough times between injector-producer pairs in different realisations. These different realisations are the result of the stochastic approach on the petrophysical

modelling (Fig. 7.2). Within Model A, the timing of breakthrough is similar for both locations, but with a slightly larger spread at the 'Fringe' location. In Model B, however, the breakthrough at the 'Axis' is on average more than a year (1.3) later than at the 'Fringe'. Two-tail t-tests (0.05 significance level), assuming unequal variances, confirms that the results from both locations are distinctive populations (Fig. 7.13). Drainage functions performed for Model A and B at the 'Axis' (five per model) indicates that within Model B production rates are significantly higher directly from the start of production and that cumulative production is on average over 40% higher (Fig. 7.14) after the first 40 years. Timing of breakthrough between Model B1 and B2 is similar at both well locations, which is confirmed by two-tailed t-tests (Fig. 7.13). However, the TBT results of Model B3 (Fig. 7.13), show a significantly reduced average breakthrough time at the 'Axis' (confirmed by t-test – Fig. 7.13) of 2 years compared to Model B2. The wells at the 'Fringe' within Model B3 on the other hand show very similar results to Model B2. Furthermore, a substantial difference (~60% in 40 years) in cumulative production can be observed between the 'Axis' and the 'Fringe' in Model B (B2) within a lobe complex (Fig. 7.14).

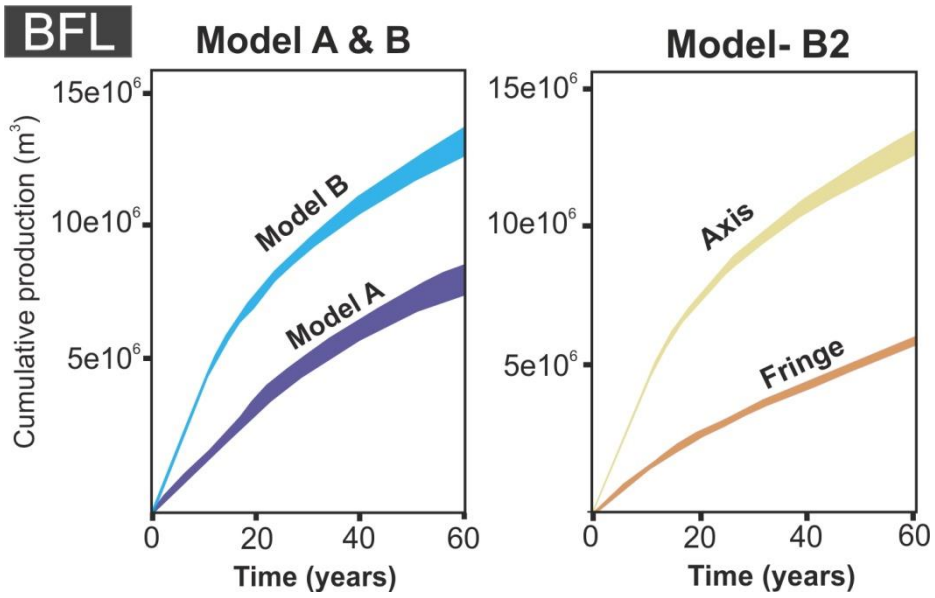

Figure 7.14 *Production curves showing difference in overall cumulative production between Model A and B and between locations within Model B2. The curves are composed from the (limited) spread resulting from a total of 5 different petrophysical realisations for each submodel.*

7.4.2 CLTZ models

The TBT results of the OR and BLK models have been summarised in Figure 7.15. Within the upscaled version of the OR-model (OR-A), breakthrough takes longer (2-3 years) for all well locations compared to the more realistic sub-model (OR-B). Within OR-B, the timing of breakthrough is not only shorter but also more uniform at the different well pairs. Within both the OR-A and OR-B simulations, streamlines from all wells are observed to focus along the main channel-fill sandstones (Fa1A) (Fig.7. 15).

Similar effects on TBT can be observed between BK Ch1 and BK Ch2 with an average decrease of breakthrough time of 4 years. The non-channelised model (BK no-Ch) shows minimal differences with slightly shorter breakthrough timing compared to BK Ch1 confirmed by a t-test (Fig. 7.15). Drainage functions have also been performed and show distinct variation between the submodels after the first 10 years (Fig. 7.15). The lowest production rates are reached within (BK Ch2), while the highest production rates are seen within the non-channelised model (BK no-Ch). However, differences within cumulative production between the submodels are limited (3-8% in 40 years) and only become significant after the first 20 years. Active pore volume has also been calculated for the BK-models, to see if part of the observed production differences could be related to differences in reservoir volume. Active pore volume is the segment of the total pore volume that can be produced from before breakthrough occurs. Differences between BK Ch1 (3.34×10^6 m^3) and BK Ch2 (3.30×10^6 m^3) are minimal. However, by removing the channels completely (BK no-Ch – 3.05×10^6 m^3), active pore volume was reduced by more than 8%. This indicates that total reservoir volume is not the controlling factor as the models with the largest active pore volume (BK Ch1 and BK Ch2) show lower production rates.

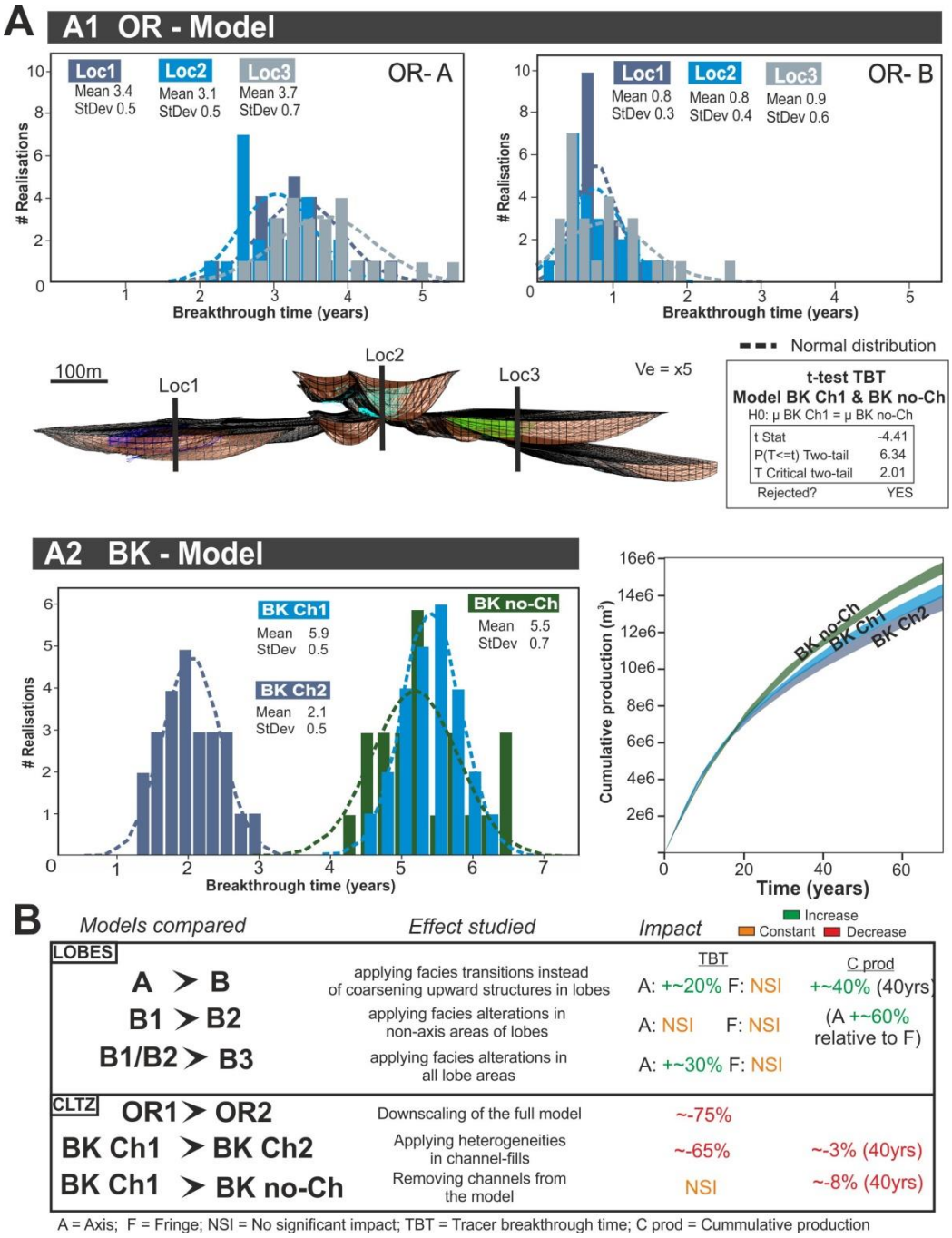

Figure 7.15 (A) *Breakthrough time (TBT) histograms of all CLTZ models (OR and BK). Only limited differences can be observed between locations. A significant shift can be observed between the upscaled version (OR-A) and the downscaled version (OR-B). Streamlines in both models are all focused within the main channel facies (Fa1) as shown in the example below. The BK-model shows a similar shift in TBT from BK Ch1 to BK Ch2. Only a limited reduction (t-test results are given) is observed between BK Ch1 and BK no-Ch in breakthrough time. Production curves are not very different in all three cases, (based on 5 different simulations) but highest cumulative production is reached within the non-channelised model (BK no-Ch). (B) Summary table showing all the model alterations that have been studied and the average results from all performed streamline simulations and drainage functions.*

7.5 Discussion

7.5.1 Interpreting streamline simulation results

The single phase-flow experiments were designed to study the relative differences in connectivity within reservoirs. A slow breakthrough time of the injected fluid within the producer well indicates that the injector and producer are poorly connected within the reservoir, which can have negative consequences for production rates. On the other hand, early breakthrough often has negative implications for recovery factors due to expensive water cycling and low vertical sweep efficiency within the reservoir (e.g. Brouwer et al.,2001; Brouwer and Jansen, 2002; Alhuthali et al., 2006). Therefore, the sensitivity studies and their implications on the timing of breakthrough can help to rank different probable scenarios of reservoir performance. When breakthrough times have proven to be distinct (t-test) between sub-model results, it shows that the effect of the change applied in the facies model is significant enough to be discriminated from the uncertainty associated with petrophysical properties. A higher uncertainty (high standard deviation) within the results is mostly related to the greater impact and uncertainty within the low-permeable deposits on the connectivity of the system, compared to the high-permeable deposits. The use of simplistic reservoir models, before adding more complicated variables is widely referred to as 'top-down modelling' (e.g. Williams et al., 2004). By adding more variables to simplistic models, a large variety of different scenarios can be created which can highlight the most significant uncertainties, called 'procycling' (Larue & Hovadik, 2012). Procycling is considered a useful process for uncertainty analysis, especially for deep-water reservoirs (Larue & Hovadik, 2012; Saikia et al., 2015).

<u>Basin floor lobe complex (BFL)</u>

The modelling results of the medial to distal basin floor lobe complex (BFL) show that the choice of conceptual geological model (Model A or B) has a major influence on the best well placement strategy. Within Model B, there is a clear difference observed in both

breakthrough time and production from the axial lobe complex areas (Axis) compared to more fringe positions (Fringe). This is related to the lateral facies changes that have been implemented within Model B and are not present within Model A. Furthermore, Model B has a significantly better production rate (Fig. 7.14). This is largely related to the petrophysical property differences between the two models as the nature of Model A with all lobe zones stacked in combination with the facies maps will result in different facies proportions. The average permeability of Model B (156 mD) is therefore over 50% higher than within Model A (92 mD), which will impact production results. Reservoir performance differences are therefore related to both the facies structure as well as facies proportions differences related to the conceptual models applied within Model A and B. The B-submodels indicate that facies changes applied within the off-axis/fringe environments do not significantly influence the connectivity of the system (B1 and B2). Changes applied in the axis of the lobes (B3), where lobe amalgamation occurs, have a much more significant impact. In this case, the addition of Fa2 within the axial lobe areas improved the vertical connectivity, even though its volume was limited (14.3% of axis – Fig. 7.7). Also, the results demonstrate that when heterogeneity is increased within the axial areas, performance differences between well locations are less apparent. The adjustments within lobe style modelling of the BFL models prove to have significant impact on predicted reservoir performance. In many cases, this uncertainty in modelling of sedimentary architecture is more significant than the large uncertainties associated with the petrophysical modelling (spread in TBT results).

CLTZ Models

The results from the CLTZ-block model indicate that channel-fills within channelised lobe areas can have a variable effect on reservoir performance. Wells within the coarse, upscaled version of the OR-model (OR-A) take more than 3 times longer to reach breakthrough compared to the downscaled version (OR-B). In both the detailed model

(OR-B) and the upscaled version (OR-A), fluid flow streamlines concentrate within the channel-fills (Fig. 7.15A). However, the heterogeneities of the minor facies associations within OR-B have a major effect on pressure concentration, which results in the compartmentalisation of the reservoir, indicated by the early breakthrough.

The BK-model confirms that heterogeneities within minor facies groups of channel-fills have substantial impact on reservoir connectivity. Differences in performance between BK Ch1 and BK Ch2 are also related to vertical compartmentalisation of the reservoir, resulting in early breakthrough. The similarity in results of BKCh1 and BK No-Ch also indicates that the channel-fills only have a limited influence on the performance of the reservoir. In addition, according to the drainage functions (Fig. 7.15A), the channel fills still have a slightly negative effect on production when they are well-connected (BK Ch1) with the background deposits (lobes and overbank), compared to when no channel fills are present (BK No-Ch). The more favourable petrophysical properties of the channel-fill facies (Fa1A) (Fig.7.10) compared to the sand-prone and volumetrically larger background deposits will in both the BK Ch1 and the BK Ch2 (Fig. 7.8) cases act as a pressure leak, which reduces the drainage area of the reservoir. Production differences between the three cases are mostly due to the full vertical injection and production, which ensures injection and production over the whole vertical interval. Production differences could well become more significant if injection or production would not occur over the complete reservoir interval, as vertical permeability boundaries will become much more important.

7.5.2 Implications on reservoir performances within CLTZ environments

Stratigraphic juxtaposition of basin-floor channels and lobes, such as observed in the Tanqua depocentre outcrops (e.g. Luthi et al., 2006; Fig. 7.4A), has a variable effect on reservoir performance (Fig. 7.15B), and depends on the nature of the lobe deposits and the presence of flow barriers or baffles at the base of and within the channel-fills. With injection over the full vertical thickness of the fan, interlobe (distal fringe) heterogeneities

do not have much effect when the deposits are sufficiently sand-prone. Other factors such as inter-channel barriers have proven to substantially change reservoir predictions (Fig. 7.15). These barriers include channel bases that are at least partly overlain by mudstone clast conglomerates. As these mudstone clast conglomerates could provide high permeability in the case of matrix-supported types but very low permeability in the case of clast-supported types, a wide range in permeability (10-5000 mD) has to be accounted for. Furthermore, the impact of heterogeneities caused by (partly) argillaceous sandstones have been considered. OR-B and BK-B both show a clear overall switch to early breakthrough with the addition of these vertical heterogeneities (Fig. 7.15B). This shows that the combination of multiple heterogeneous facies groups can influence flow pathways within the reservoir.

However, these intra-channel barriers (consistent basal mudstone clast conglomerate layer and argillaceous sandstones in the top of the fill) that have been added in the CLTZ submodels (OR-B and BK Ch2) may represent an end member scenario as basin-floor channel-fills show limited spatial variety and variability between channel-fills (e.g. Brunt et al., 2013a). According to Alpak et al. (2013), the presence of mud drapes, including mudstone clast-conglomerates, at the channel-base is most important when assessing recovery factors. However, the probability of channel bases overlain by mudstones in base-of-slope and basin-floor settings according to Alpak et al. (2013) is significantly less (<10%) than compared to slope channel-fills where mudstone drapes across the base of channels are more common and interpreted to indicate sediment bypass (e.g. Barton et al., 2010; Hubbard et al., 2014; Stevenson et al., 2015). Eschard et al. (2014) observed lenses of matrix-supported (claystone) materials in their study of the basin floor system of the Pab Formation and noted that the lateral extension of these units is commonly limited. In the case of Eschard et al. (2014), the flow streamlines were able to bypass the heterogeneities due to local erosion and therefore only had limited impact. This implies that even though

the channels within a channelised lobe area (CLTZ) are considered to have better connected margins compared to upslope channel-levee systems (Funk et al., 2012; Alpak et al., 2013), there is a great level of uncertainty accompanying the behaviour of these boundaries and associated performance of CLTZ-reservoirs. Due to the combination of relatively low total volumes of channel-fills compared to surrounding deposits including lobes, the distributive character and the uncertainty within channel-fill behaviour, channelised-lobe environments may be considered as a higher risk as an exploration target than conventional ideas might suggest.

Alternative areas of better vertical connectivity are high amalgamation zones (Stephens et al., 2001; Hodgetts et al., 2004; Hodgson et al., 2006) at lobe apexes. Within these areas there is an overall lower chance of reservoir compartmentalisation compared to channelised lobe areas, due to the lack of horizontal flow barriers. Also the impact of abrupt facies changes (in the case of an erosive barrier) compared to gradual facies changes (in the case of facies transitions), may have important consequences for the pressure distribution and fluid migration rates. The BFL model results show that amalgamation of lobe axes has a significant impact on reservoir performance.

7.5.3 Ranking reservoir performance

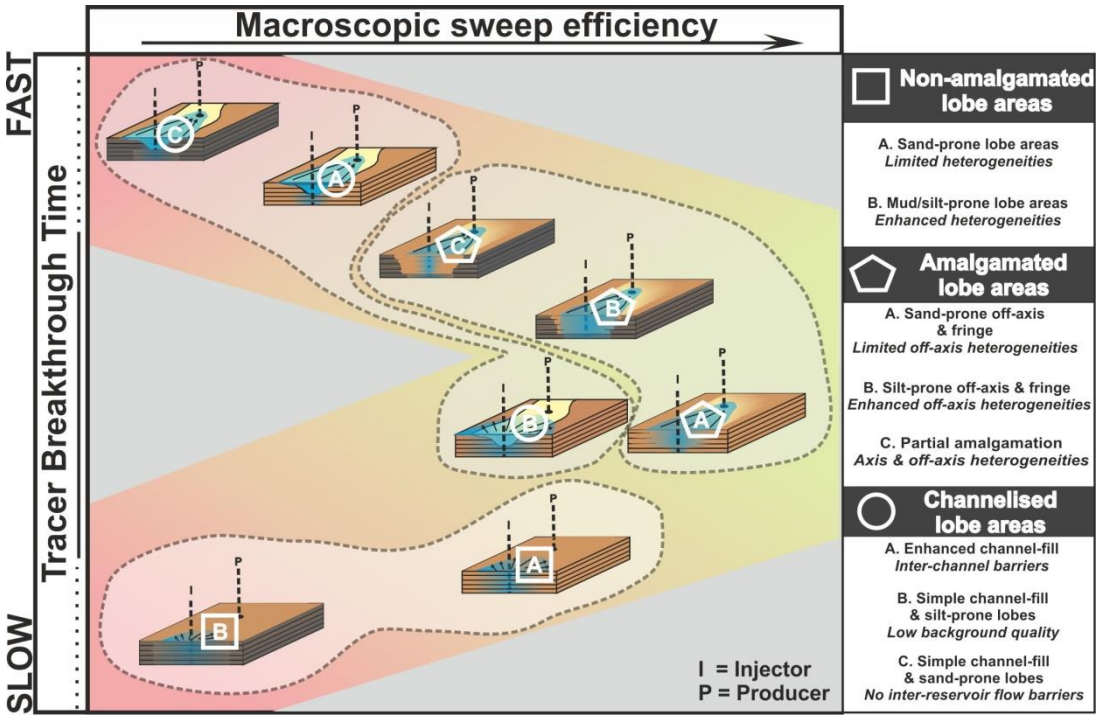

Figure 7.16 *Summary conceptual model of macroscopic sweep efficiency versus tracer breakthrough time (TBT) within different lobe sub-environments. Different scenarios have been plotted and grouped into: non-amalgamated, amalgamated and channelised lobe areas. Both an early and late breakthrough will have negative consequences for sweep efficiency with a slow breakthrough indicating a badly connected injector-producer pair with low production rates and a very early breakthrough or a very well-connected injector-producer pair, but with significant loss of drainage area. Most uncertainty is associated with channelised lobe areas as heterogeneities can possibly cause compartmentalisation of the reservoir, whereas this does not occur within amalgamated lobe (HAZ) areas.*

Streamline simulations are commonly used for ranking reservoir performance before more comprehensive flow simulations are initiated (e.g. Idrobo et al., 2000) and can also be used when complicated grids or high number of grid cells make flow simulation challenging. Comparing the macroscopic sweep efficiency between the different scenarios gives a good indication of problem areas as well as identifying the areas of interest for exploration within deep-marine fan systems. The well-constrained depositional architecture of the Karoo Basin lobe complexes (Hodgson et al., 2006; Prélat et al., 2009), further

understanding from the modelling results of this study, and previous stochastic modelling results (e.g. Stephens et al., 2001; Funk et al., 2012; Alpek et al., 2013), have been integrated to develop a model on recovery (macroscopic sweep) efficiency within basin-floor fan systems. A division has been implemented based on sub-environments (Fig. 7.16): channelised lobe, amalgamated lobe and non-amalgamated lobe areas. Different scenarios have been attributed to each sub-environment linked to heterogeneity differences. Macroscopic sweep efficiency has been linked to the timing of breakthrough. As only for a limited number of models drainage functions (Fig. 7.14; 7.15) were run, the general assumption was made that both slow and rapid breakthrough will result in relatively low recovery with limited drainage areas. A good non-compartmentalised and connected reservoir with good-to-intermediate porosity will result in the best total recovery. The most variability in performance can be seen among the channelised lobe areas (CLTZ) (Fig. 7.16, circles). The possibility of both compartmentalised and non-compartmentalised channelised lobes, makes the prediction of macroscopic sweep efficiency within these environments more challenging. Less uncertainty is associated with amalgamated lobe areas (Fig. 7.16, pentagons) where good vertical and horizontal connectivity are predicted. Amalgamated lobe areas as a reservoir will therefore have higher chances of good recovery rates and will be less of an exploration risk compared to channelised lobe areas.

7.6 Conclusions

A 3-D geological modelling workflow is presented from outcrop data collection, through constructing reservoir models to performing single-phase flow simulations. The workflow highlights the importance of understanding fine-scale sub-seismic sedimentary architecture. Various sensitivity tests were performed by applying geologically realistic scenarios for sedimentary architecture and facies distributions of submarine lobe deposits and channel-fills. Results show that the conceptual model applied for a specific case study can have significant influence on the reservoir connectivity and macroscopic sweep

efficiency, especially when lobe amalgamation is considered. The implications on connectivity by alternations in facies within the high net lobe axis areas are much more significant compared to similar changes within lobe off-axis to fringe areas. Juxtaposition of channel-fills and lobe deposits, which is common in CLTZs, has diverse effects on reservoir performance depending on the presence of inter-channel barriers and the sand-prone nature of the lobes. In CLTZs, due to the high degree of uncertainty of heterogeneities associated with channelised lobe areas, they can be considered a more challenging production target compared to areas of lobe amalgamation where good horizontal and vertical connectivity are more certain. For the construction of geologically realistic reservoir models, it remains vital to collect quantitative data from fine-scale architectures within outcrop analogues, which may form significant reservoir heterogeneities, and to develop and test conceptual models, such as can be done with the well-constrained basin-floor fan systems of the Karoo Basin.

Chapter 8:
Controls on the stratigraphic record of the channel-lobe transition zone

The envisaged configuration of ancient CLTZs is based primarily on observations of modern systems (e.g. Palanques et al., 1995; Nelson et al., 2000; Wynn et al., 2002a; Bonnel et al., 2005) that represent a geomorphic snapshot of an evolving and dynamic part of deep-water systems. The morphological features that are present within such systems can represent large numbers of events operating over long timescales (e.g. Macdonald et al., 2011a).

An assemblage of features associated with CLTZs in modern systems have been identified within the outcrop record of the Karoo Basin in this study (Fig. 8.1), including amalgamated scour-fills (*Chapter 4*), isolated scour-fills (*Chapter 6*) and sediment waves (*Chapter 5*). CLTZs have been identified in ancient successions (Mutti and Normark, 1987; Gardner et al., 2003; Ito et al., 2014; Pemberton et al., 2016); however, the transfer of this geomorphic palimpsest into the stratigraphic record is poorly constrained (Fig. 8.1). The detailed outcrop studies from locations with excellent palaeogeographic control show the preservation of complicated architectures across a range of hierarchical scale of both erosional (*Chapter 4*) and depositional (*Chapter 5*) bedforms. To elucidate the stratigraphic record of CLTZs, it is essential to consider the variance among flow-bedform interactions, and how this may influence bedform preservation.

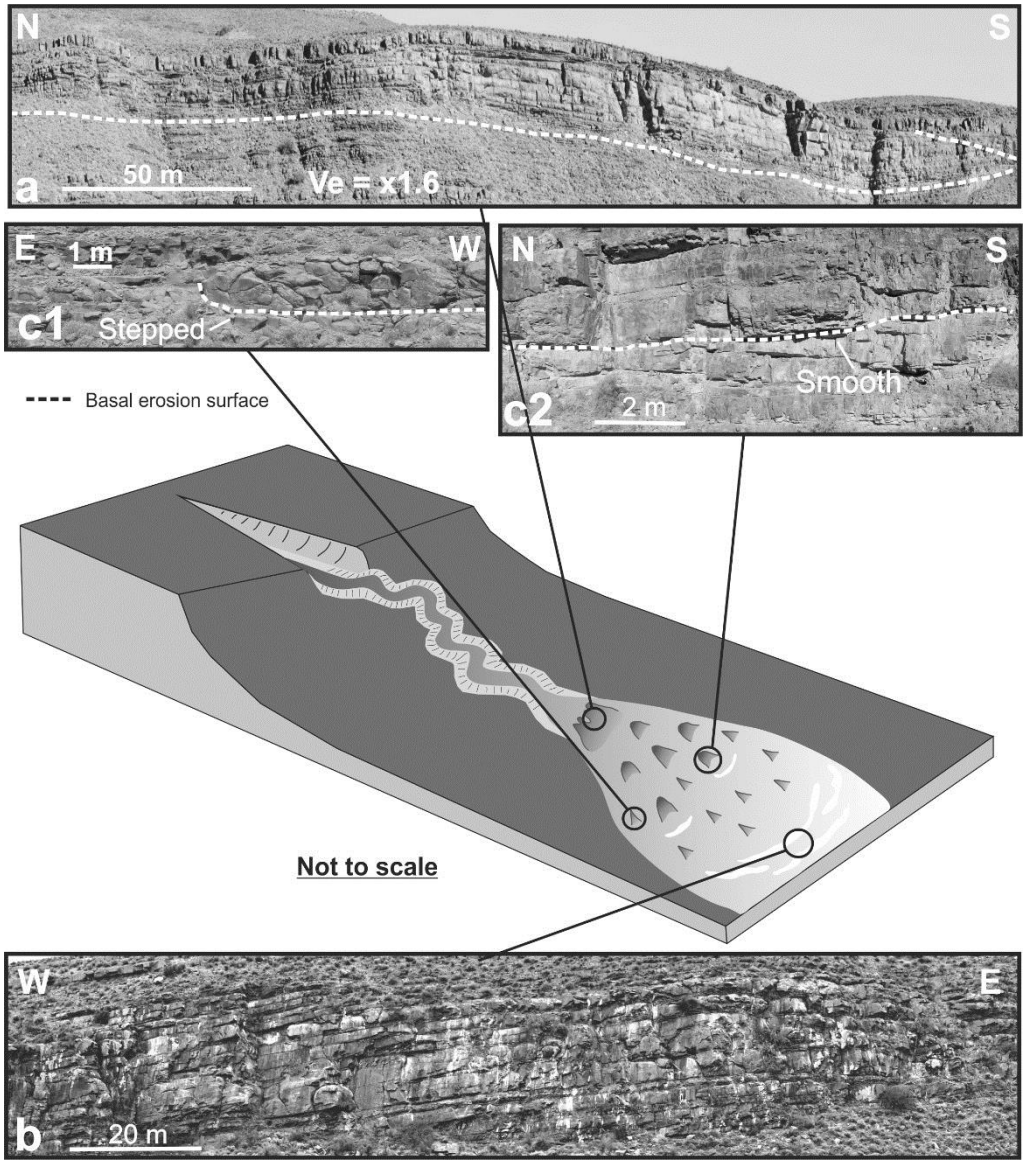

Figure 8.1 *Outcrop expression of major CLTZ elements covered in this study and as defined from modern systems, including giant scour-fills (a) from Chapter 4, sediment waves (b) from Chapter 5 and variable geometries of metre-scale scours (c1 and c2) from Chapter 6.*

8.1 Flow-bedform interaction

The outcrop dataset of this study (*Chapter 4-6*) shows large-scale variability in bedform architecture within CLTZ settings, which is most likely related to the interaction between bypassing flows and existing erosional and depositional bedforms. Irregularities within the substrate may act as 'weaknesses' and bypassing turbidity currents may have a tendency to interact (e.g. Eggenhuisen and McCaffrey, 2012). For example, large-scale scours

(*Chapter 4*) are formed due to the erosion by consecutive flows of existing irregularities in the substrate, by processes such as headward incision.

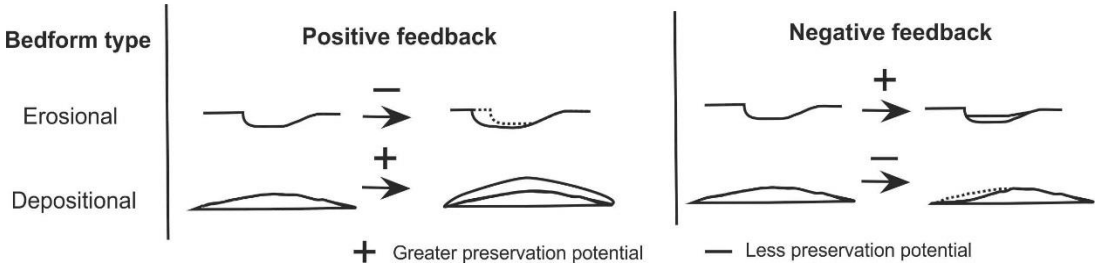

Figure 8.2 *Simplified diagrams showing the variability in flow-bedform interactions that have been observed in this study, with positive feedback to the left (bedforms acting as nucleus) and negative feedback to the right. Palaeoflow is from left to right.*

Furthermore, sediment wave (*Chapter 5*) deposition can form positive relief, acting as a nucleus for further sediment wave development. In both of these examples, the original bedform provided a positive feedback in the development of larger or composite bedforms formed by consecutive flows.

Among modern systems a distinction is often made among small-scale scours between chevron/v-shaped and spoon/u-shaped (e.g. Wynn et al.2002a). The reasons behind the observed differences in planform architecture are however not well understood. It is possible that their architecture is related to the sedimentological properties of the substrate. However, differences in dimensions (<20 m deep, <2 km wide, <2.5 km long for spoon-shaped; few m's deep, <0.8 km wide, < 1 km long for chevron-shaped) may also suggest that their morphological differences can be related to the number of flows responsible for their formation, where chevron-shaped scours may have a single flow origin, while spoon-shaped ones most likely are the result of multiple.

However, scours have also shown to enhance deposition from the tails of turbidity currents (*Chapter 4*) due to 'flow capture', or local scouring at points of abrupt depositional thickness changes within sediment waves (*Chapter 5*). In the latter, successive flows (partly) remove the depositional bedform as an irregularity within the substrate (Fig.

8.2), acting as a negative feedback. Whether turbidity currents interact with bedforms in the CLTZ, through a positive or negative feedback, has implications for the depositional architecture preserved in the rock record. Erosion will modify or remove bedforms, while deposition will increase preservation potential. During the passage of a single turbidity current, these interactions can be highly variable, as variation is expected in different parts of the flow (e.g. erosive flow head, bypassing flow body, depositional tail). Furthermore, within modern systems, such as along the northeast Atlantic continental margin (Macdonald et al., 2011a), interaction between a scoured-substrate and a single flow has been proven to be highly variable, as scour-fill histories of laterally adjacent scours indicate they do not necessarily evolve simultaneously.

The overall manner of flow-bedform interaction is likely to be strongly related to the sedimentary evolution of the feeder channel.

8.2 Preservation potential of CLTZ elements within an evolving fan system

To better understand the stratigraphic record of CLTZs, and to make comparisons with modern systems, it is important to consider the preservation potential of different features in response to system evolution. Submarine fan systems are defined by progradational and/or retrogradational phases (e.g. Posamentier et al., 1991; Richards et al., 1998; Hodgson et al., 2006; 2016). Therefore, the stratigraphic record of CLTZs is highly dependent on the evolution of the feeder channel.

CLTZ development will vary among the different phases of fan system evolution (Fig. 8.3). Within a prograding system, the CLTZ will be incised during feeder channel propagation, partially limiting the development of features and deposits. In a retrogradational phase existing CLTZ elements will be preserved as channels aggrade. However this will eventually prevent further CLTZ development due to direct contact with the lobes downstream. Most extensive CLTZ development can be expected in between the progradational and

retrogradation phases, at the maximum extent of channel propagation. As the system will be static and aggradational, the CLTZ will have more time to develop (Fig. 8.3). Overall, only progradational and static phases in the evolution of a fan system ought to be considered for CLTZ development.

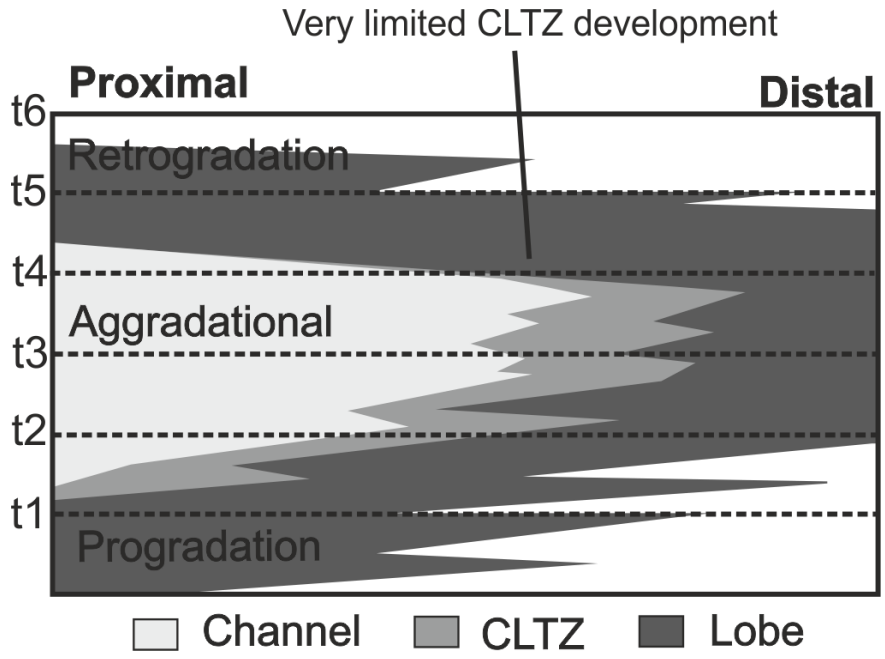

Figure 8.3 *Conceptual Wheeler diagram showing variance in CLTZ development during fan system evolution. During retrogradational phases, CLTZ development will be limited by channel aggradation and physical channel and lobe connection.*

8.2.1 Time and rate of channel propagation

The CLTZ can be preserved as a surface (e.g. *Chapter 6*; Elliott, 2000b; Gardner et al., 2003) and a net-depositional volume of rock (e.g. *Chapter 4*; Pemberton et al., 2016). The style of preservation must be related to time and the number of events that are needed to develop CLTZ related bedforms.

To preserve the deposits associated with the CLTZ during system progradation, accommodation is required. When the system is characterised by rapidly propagating channels, there may not be enough time or accommodation to form substantial features or

deposits, creating a ‘weak’ CLTZ signal where channels appear to be directly juxtaposed with lobes. However, a CLTZ within a stationary to slowly propagating system will have a stronger signal with better developed features, which is more likely to be preserved as a volume of rock. Therefore CLTZ development could be more substantial at a high subsidence rate or at fixed or limited channel propagation,

This is supported by the variance in the volume of CLTZ associated facies within scour-fills (*Chapter 4*). When the scour-fill is preserved adjacent to channel propagation, bypass-related facies only represent a limited quantity of the infill (<25%). However, when the scour-fill is preserved at the maximum extent of channel progradation, a greater portion of the infill can be related to the CLTZ (50%), which can be explained by relative static CLTZ behaviour (Fig. 8.3). Similarly, the preservation of thick packages of sediment waves (*Chapter 5*) is aided by fixed to very slow progradation of the feeder channel.

The CLTZ is not only limited to base-of-slope environments as channels also terminate on the slope or on the basin-floor. However, CLTZs are better developed at base-of-slope settings, as flows reaching the base-of-slope will naturally expand and leave channel confinement (Kneller, 1995). The CLTZ will therefore have a greater tendency to be static or propagate much more slowly in base-of-slope settings, resulting in an enhanced development of CLTZ features and deposits.

8.2.2 Spatial control

In addition to a temporal control, there is also a significant spatial control on the preservation of CLTZ elements. Overall, axial CLTZ areas are less prone to preservation compared to the edges (Fig. 8.4), as CLTZ margins have a tendency to be net-depositional and are less prone to reworking by channel-propagation. In the case of a propagating channel, the preservation potential may vary among the various elements as CLTZs spread out in a radial pattern from the channel-mouth (Fig. 8.4). Elements, such as amalgamated scour-fills, focus close to the channel-mouth (Wynn et al., 2002a) and are therefore most

probably utilised by, and obliterated during, channel propagation. In comparison, depositional bedforms such as sediment waves, tend to be deposited in the distal reaches of CLTZs (Fig. 8.4), and therefore cover a wider lateral extent, making it less likely they are (completely) cannibalised during channel propagation. As proximal elements are more prone to be cannibalised, this could lead to a stratigraphic record where erosional elements are relatively unrepresented compared to depositional elements.

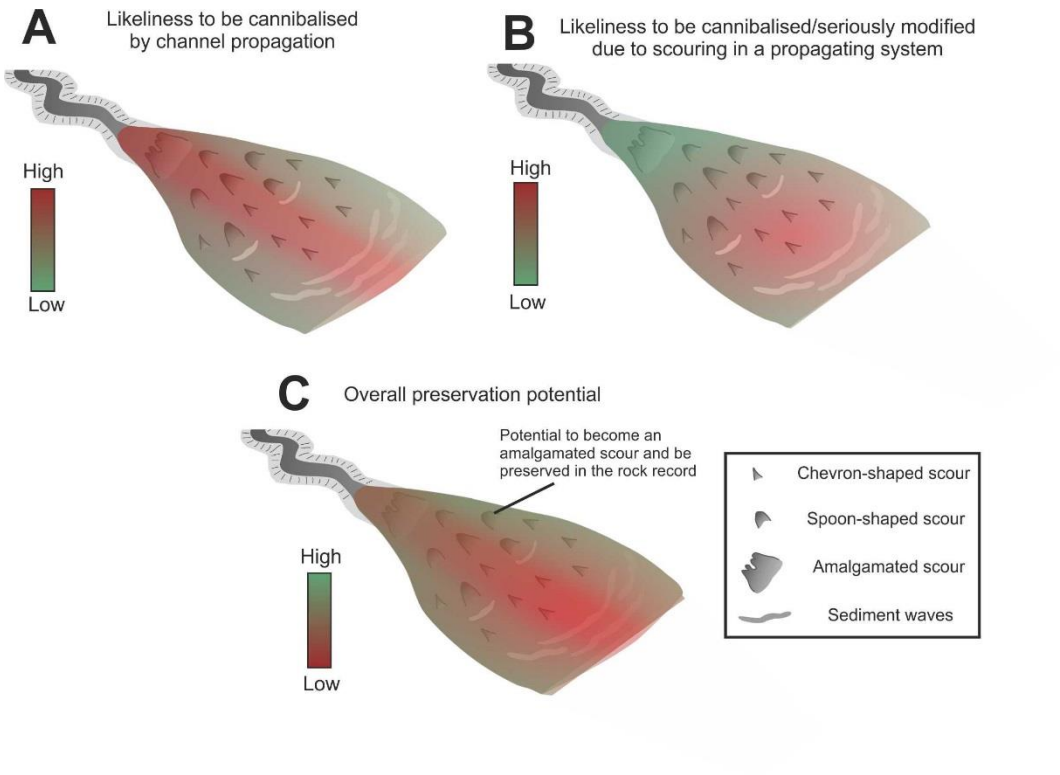

Figure 8.4 *Preservation potential of various elements and areas within the CLTZ stratigraphic record of a prograding system. The overall preservation potential (C) is composed of the likeliness to be cannibalised by channel propagation (A) and the likeliness to be cannibalised or seriously modified due to scouring (B).*

However, the preservation of different elements is also affected by the propagation of erosional elements within the CLTZ (Fig.8.4B) and, in particular, by formation of scours. The elements most proximal within a CLTZ area, which are preserved adjacent to channels that propagated, are not likely to be significantly altered as they will transition abruptly from a

CLTZ to a channel-overbank environment. More distal CLTZ settings will be altered by scouring as the CLTZ migrates down dip, although the margins will in this case also have a greater tendency to be preserved. Large amalgamated scour-fills associated with adjacent channel propagation have been identified (*Chapter 4*) in outcrop, proving that it is possible to preserve these elements within the rock record. This is related to the simultaneous evolution of scours during channel propagation, where initial small-scour features at CLTZ margins (Fig.8.4B) may evolve to larger amalgamated scours as the channel-mouth advances. They are preserved in the rock record through infill by overbank flows as the channel propagates adjacent to these features. This down dip migration of the CLTZ itself will have a negative impact on the preservation of depositional elements, compared to erosional elements. Depositional elements tend to form in the distal reaches of the CLTZ, and therefore may endure a longer phase of CLTZ propagation compared to the most proximal elements. The internal architecture of sediment waves (*Chapter 5*) suggest a first order depositional control on their formation and therefore they are prone to be eroded when the channel extends, instead of migrating further downstream. The overall preservation potential (Fig. 8.4C) of CLTZs and their elements within a prograding system is therefore much more significant at the margins compared to its axis.

8.3 Primary controls on the CLTZ stratigraphic record

The stratigraphic record of CLTZs shows a high degree of variability, especially among the architectures and facies characteristics of the different bedforms (*Chapter 4; Chapter 5*). This raises major complications for the identification of ancient CLTZ settings within purely

1D datasets (core), as there are no clear key recognition criteria established.

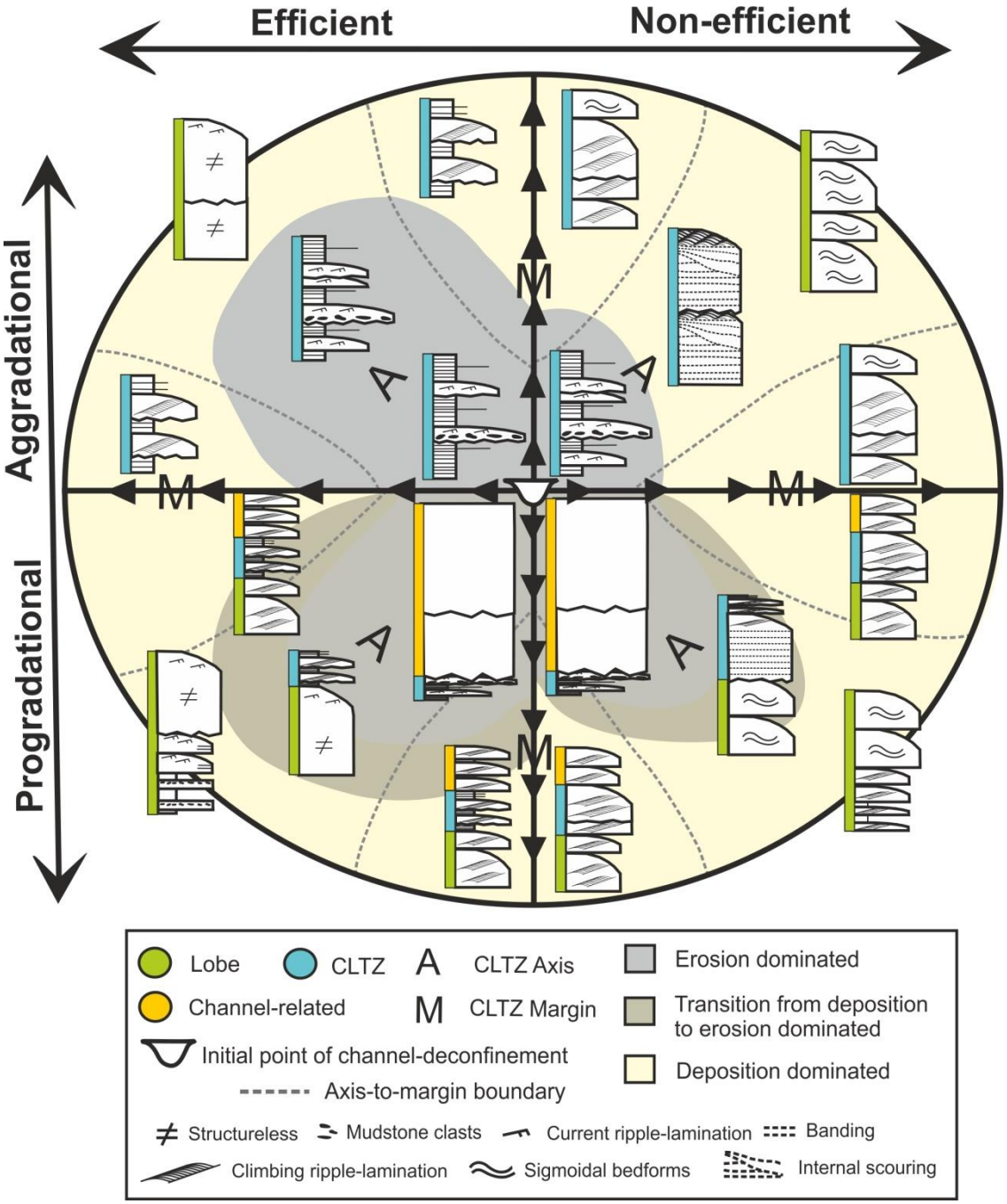

Figure 8.5 *Summary diagram showing the CLTZ stratigraphic record variability. Each quarter represents different depositional conditions as the depositional record can be linked to three first order controls: spatial variability, flow efficiency and channel evolution. The top half represents conditions where channel system is static over time and the lower half an overall progradational system. The left half represents efficient conditions and the right half non-efficient conditions. Within each quarter the axial record is indicated with an 'A', while the marginal record is indicated with an 'M'. The different coloured bars represent associated architectural elements.*

The sedimentary variability of CLTZs can be quantified by assessing the major controls on CLTZ preservation. Based on the results of this study, three primary controls are postulated to influence the depositional character of the channel-lobe transition zone:

1) Spatial variability
2) Flow efficiency
3) Channel evolution

These three controls combined properly cover the variability within the CLTZ record (Fig. 8.5).

8.3.1 Spatial variability

Similar to lobes and channels (e.g. Prélat et al., 2009; Brunt et al., 2013a), variation exists in the depositional record from axial to fringe positions within channel-lobe transition zones (Fig.8.5). Deposition and erosion by the flow axis leads to different stratigraphic patterns compared to deposition and erosion by flow margins. Within CLTZ and base-of-slope environments, axial positions tend to be very prone to banded and structureless sandstones. Marginal positions are more prone to climbing ripple-laminated sandstones and are relatively poor in structureless and banded sandstone (Fig.8.5).

The examination of erosional and depositional bedforms within CLTZs has also revealed that their character is highly dependent on their position (*Chapter 4; Chapter 5*) relative to the feeder channel. Sediment waves show spatial variability in facies dimension and architecture, where axial sediment waves are more dominated by banded sandstones, show internal truncation surfaces and reach greater thicknesses (>1.5 m). In comparison, sediment waves in more marginal positions are dominated by climbing-ripple laminated facies, lack internal truncation surfaces and are more limited in thicknesses (< 1.5 m).

Similarly, giant scour-fills (*Chapter 4*) show significant variations in infill facies and internal architecture, which can be associated with their location relative to the channel-mouth.

Scour-fills preserved adjacent to prograding channels, are dominated by climbing-ripple laminated sandstones compared to scour-fills preserved at the maximum extent of channel propagation, which show more structureless and banded sandstones.

8.3.2 Flow efficiency

Flow efficiency, which is controlled by factors such as flow concentration, volume, grain size and Froude number, has been advocated as a first order control on CLTZ character (Mutti and Normark, 1987; Gardner et al., 2003). In this study, it has also been related to differences in characteristics between the lobes deposited at lower slope to base-of-slope settings and lobes deposited at basin floor settings (*Chapter 6*). In more efficient systems, deposition tends to occur further down dip of the feeder channel-mouth compared to more inefficient systems (e.g. Mutti and Normark, 1987). Therefore, CLTZs are predicted to be much more areally extensive in efficient systems compared to inefficient systems. When looking at lobe (apex) facies (*Chapter 6*), this relates to an abundance of banded and (stoss-side preserved) climbing ripple-laminated sandstones in inefficient systems, and abundance of more siltstones and structureless sandstones in more efficient systems. Overall, the CLTZ is more extensive, thin and widespread when incoming flows are efficient, compared to less extensive and more deposition-dominated when incoming flows are generally inefficient.

8.3.3 Channel evolution

The last major control on CLTZ preservation is the evolutionary behaviour of the feeder channel, which is regarding CLTZ development (Section 8.2) best divided between static and progradational (Fig. 8.5). Within the Karoo fan systems both unattached and attached fan systems have been identified (Van der Merwe et al., 2014). As unattached systems are preserved in the rock record, it implies that feeder channels do not always propagate fully,

to connect with the lobe systems down dip. This could be either due to sudden up dip avulsion, leaving the system underdeveloped, very slow progradation rates in general, or at maximum channel extent within the developing fan system. If a channel is able to propagate (quickly) through the CLTZ, it will significantly alter its stratigraphic record.

8.3.4 Summary of stratigraphic variability in CLTZ expression

Preservation potential, channel evolution and setting are key parameters when considering the transfer of the CLTZ into the stratigraphic record. After initial development of erosional and depositional bedforms, their eventual preservation in the rock record depends on the character of successive flow-bedform interactions. CLTZs can be represented by a single surface or a volume of rock, being highly dependent on the propagation rate of the feeder channel. CLTZs can be dynamic, and migrate, and lengthen or shorten through time. Base-of-slope settings are hypothesized to show better developed CLTZ features, as CLTZs tend to be more static in these settings. Marginal areas are better preserved compared to axial areas where the juxtaposition of channel/levees and lobes may be the expression of the CLTZ. The characteristics of CLTZ deposits and features vary significantly depending on location, flow efficiency and the style of channel evolution. By considering these three first order controls, the stratigraphic record of the CLTZ can be better elucidated.

Chapter 9:
Conclusions

9.1 Addressing the key questions

Here, the key research questions established in *Chapter 1* are addressed within the scope of this study. The answers to the questions lead to recommendation for future research directions.

9.1.1 How is the assemblage of depositional and erosional elements that characterise CLTZs and base-of-slope settings transferred into the stratigraphic record?

A wide assemblage of depositional and erosional elements associated with CLTZs have been identified and presented in this thesis by the use of an integrated core and outcrop dataset. These elements have been tied to observations from CLTZs documented in modern systems including large amalgamated scour-fills (*Chapter 4*) and sediment waves (*Chapter 5*). The elements preserve a high degree of complexity in their facies distribution patterns and a high level of variability in the depositional architecture. Some giant-scour-fills show simple cut-and-fill histories, while others show evidence of headward incision and temporal changes in the interaction with the scour surface. The infill may show variable facies characteristics, but their thickening/coarsening upward structure over the complete fill differentiates them from base-of-slope channel-fills. Sediment wave deposits show clear evidence of upstream migration, but do not resemble known supercritical bedform structures. Hierarchical scales have been identified in both depositional (sediment waves – *Chapter 5*) and erosional (giant scour-fills – *Chapter 4*) bedforms, indicating long time scales for their development. A major part of the depositional record in base-of-slope settings is represented by lobes (*Chapter 6*), which are typically juxtaposed against sandstone-rich channel-fills. These lobes represent simple independent architectural bodies with different characteristics compared to the basin-floor lobes

downdip: They are relatively abundant in banded and climbing ripple-laminated sandstone and poor in linked debrites, structureless sandstone and siltstone. Differences in characteristics can be associated with alterations in flow efficiency that impact both lobe and CLTZ character. The preservation of elements that characterise the CLTZ and base-of-slope in the rock record depends on a number of factors (*Chapter 8*), wherein the style of channel evolution is important to consider. As the features defining the CLTZ suggest long time-scales for their development (*Chapter4; Chapter 5*), the stratigraphic record of CLTZs may be less well preserved within a rapidly propagating channel compared to a system where the channel propagates slowly (*Chapter 8*). How flows interact with erosional and depositional bedforms is highly variable and determines how they are eventually preserved within the rock record. Features that develop at the margins of CLTZ have the largest potential to be preserved (*Chapter 8*), as has been observed with giant scour-fills (*Chapter 4*) and sediment waves (*Chapter 5*). Overall, the assemblage of depositional and erosional elements associated with CLTZs, show very diverse characteristics depending in particular on the location relative to, and the evolution, of the feeding channel.

9.1.2 What are the key representative facies, architectural elements, and stacking patterns that characterize CLTZs in the rock record?

This study has provided a comprehensive description of the characteristics of major channel-lobe transition zone elements, their dominant facies and stacking behaviour. A number of facies groups are particularly prone within CLTZ and base-of-slope environments:

- Banded sandstones
- Structureless sandstones
- Mudstone clast conglomerates
- Climbing-ripple laminated sandstones

- (Laterally restricted) thin-bedded siltstones

Particular facies groups can be more dominant within CLTZ deposits, depending on the architectural element or sedimentary environment that is involved (Fig. 9.1). Facies characteristics vary especially between marginal and axial positions, where margins are dominated by climbing ripple laminated sandstones, while axes show more banded and structureless sandstones. Scour-fills differ from channel-fills as they show thickening and coarsening upward structures over the complete fill, while channel-fills are rather uniform in facies and are dominated by thick amalgamated structureless sandstones (*Chapter 4*). Lobe deposits at the base-of-slope show an abundance of banded and climbing-ripple laminated sandstones (*Chapter 6*). Sediment waves are dominated by banded sandstones when preserved in axial locations, while they are richer in climbing-ripple laminated sandstones at the margins of CLTZ settings (*Chapter 5*).

The stacking behaviour of sediment wave deposits within the studied outcrop sections proves to be complicated, as individual event beds dominantly stack in a downstream manner, but due to abrupt upstream-orientated shift of the depositional focus, the system is aggradational on a larger scale. Lobe deposits at the base-of-slope (*Chapter 6*) show both lateral and longitudinal juxtaposition of lobes and channels, as well as cycles of downdip propagation and retreat. This is in contrast to stacking patterns of basin-floor lobes downdip, which are primarily driven by lateral compensation.

Overall, the CLTZ record in base-of-slope settings is highly variable (*Chapter 8*), depending on channel-evolution, position relative to the channel-mouth and flow efficiency. CLTZ development is expected at progradational and aggradational phases of fan evolution, but is largely prevented at retrogradational phases. CLTZs are better developed at base-of-slope settings, aided by slow propagation rates of channels in these locations.

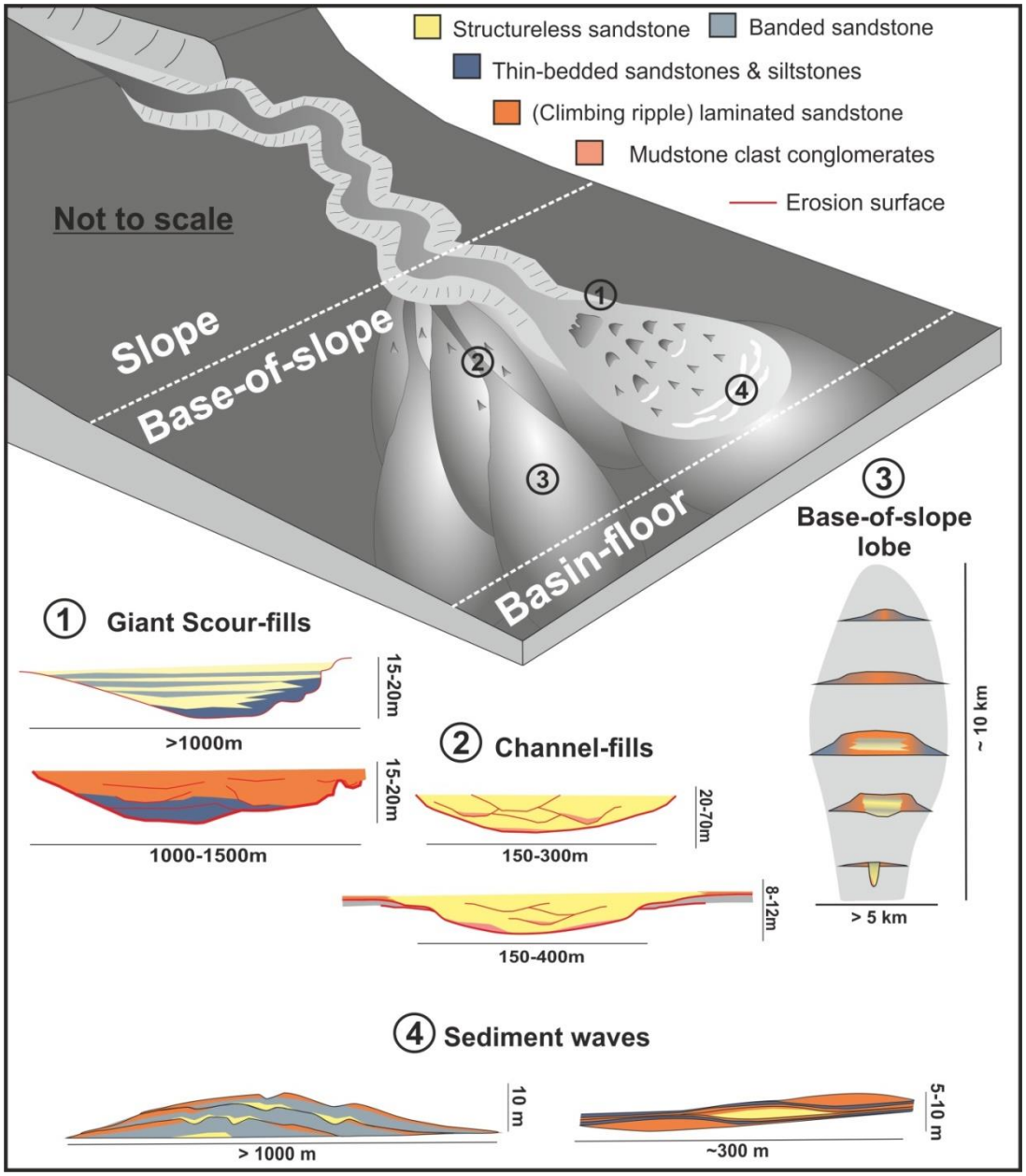

Figure 9.1 *Synthesis of base-of-slope elements showing the variation in facies characteristics and distribution as discussed within this study. Channel fills based on confined and unconfined base-of-slope channels of Brunt et al. (2013a).*

9.1.3 What is the impact of fine-scale sedimentary architecture in lobe complex and channel-lobe transition reservoirs?

A complete modelling workflow has been presented, including field data collection (*Chapter 6*), facies modelling, petrophysical modelling and flow simulations to test the impact of fine-scale architectures within lobe complexes and channelised lobe environments (*Chapter 7*). The simulation results have shown that juxtaposition of

channel-fills and lobe deposits, common at base-of-slope settings (*Chapter 6*), has diverse effects on reservoir performance. This depends on the presence of inter-channel barriers, such as mudstone clast conglomerates and argillaceous sandstones, as well as the sand-prone nature of the channelised lobes. When inter-channel barriers are common, their presence has serious negative consequences for reservoir connectivity (*Chapter 7*). Base-of-slope systems are exceptionally sand-prone (>80%), and lobes represent a substantial part of the stratigraphy (*Chapter 6*). In comparison with slope settings, channel-fills may not represent the largest reservoir volume within base-of-slope systems. Even when there is good connection between channel-fills and surrounding stratigraphy, they may act as 'thief sands' because of their good petrophysical properties (*Chapter 7*). Due to the high uncertainty of heterogeneity distribution associated with channelised lobe areas, they can be considered as challenging production targets. Areas of lobe amalgamation, however, may involve much less uncertainty, always showing both good horizontal and vertical connectivity.

9.2 Suggestions for future work

9.2.1 Giant scour-fill architecture

This study includes the first detailed description of large-scale amalgamated scours from channel-lobe transition zone settings in ancient deepwater deposits (*Chapter 4*). With criteria established to help support the recognition of scour-fills in Hofstra et al. (2015), similar architectures and infill characteristics may be identified from other outcrop records. Additional examples would increase our understanding of how these architectural elements are preserved in the rock record and how they can be differentiated from channel-fills, for example from the Peïra Cava or Ross Formation. Furthermore, this study has revealed that the architecture and infill of these scours can be highly variable, which is related to position relative to the channel mouth and to system evolution. This requires

further investigation to gain a better understanding on what controls both the characteristics and the preservation potential of giant scour-fills.

Experimental and numerical modelling approaches may aid further in the understanding of the formation of the complicated architectures of these features.

9.2.2 The process record of sediment waves

Detailed examination of the architecture and facies distributions of sediment waves within CLTZ settings (*Chapter 5*) has revealed that their process record is much more complex than previously assumed (e.g. Wynn and Stow, 2002; Symons et al., 2016). Similar bedforms have not been described elsewhere, from either outcrop, seismic or experimental studies. Even though along strike variations have been incorporated within these studies, the 3D-architecture of these bedforms is still weakly constrained, which limits our understanding of their process record. In other areas, like the Albian Black Flysch (Vicente Bravo and Robles, 1996) or the Favignana Calcarenites of Sicily (Slootman et al., 2016) 3D-architecture is much better exposed, and detailed study of these areas will massively aid within our understanding.

The Karoo systems are defined by a very narrow grain size distribution and these bedforms may look different in systems with a wider grain-size range (e.g. Neuquen Basin, Peïra Cava), due to the importance of grain size on bedform formation. I have proposed likely primary controls and interactions on their formation, including compensation-driven flow fluctuations. These controls will need further investigation, most ideally by numerical or experimental approaches, to be able to fully comprehend the depositional architecture of these bedforms. Furthermore due to recent advances in imaging and measuring techniques of active submarine systems (e.g. Khripounoff et al., 2003; Xu et al., 2004; Sumner et al., 2013; Talling et al., 2013), it is possible to track the development of sediment waves by individual flow events, which can give vital information for their process record.

9.2.3 Recognition of sand-prone sediment waves in high-resolution seismic datasets

The sedimentary packages in which sediment wave deposits related to CLTZs have been identified in the Karoo Basin (*Chapter 5*) are very sandstone-prone (>90%) (Brunt et al., 2013a). If similar packages would be studied by means of high-resolution seismic, it remains unclear to which level the architectures here described would be recognised within these datasets, as the number of internal reflectors may be highly limited due to the uniform lithology. It would be valuable to restudy existing shallow reflection seismic datasets of sediment waves within CLTZ settings (e.g. Bonnel et al., 2005; Kuang et al., 2014) to gain a better understanding of how the described architectures relate to sediment wave architectures in recent systems.

9.2.4 Differentiation between overbank and lobe environments

It remains very challenging to make clear distinctions between levee/overbank and lobe off-axis to fringe environments within outcrop and core datasets (*Chapter 6*) because the processes operating in both these sedimentary environments are similar. A proper distinction between both environments will aid in defining the stacking behaviour of lobes within submarine fan systems from 1D core. Given that levees have a larger map-view 'footprint' than channels (e.g. Kane and Hodgson, 2011; Morris et al., 2014b), in areas where there is juxtaposition of lobes and channels the 'levee-lobe' transition zone (LLTZ) should be more extensive than the true channel-lobe transition zone. It may be possible to improve this understanding by more detailed identification of all sedimentary features of both environments and, in particular, through the use of integrated datasets where direct correlation of core to architecture is possible.

9.2.5 Understanding submarine mid-fan areas

This study has suggested that the stratigraphic record of fan systems at base-of-slope settings is substantially different to the stratigraphic record at distal basin floor settings,

including the characteristics of the lobe deposits that are present in these settings (*Chapter 6*). However, the work has not covered how the transition between the two areas is characterised. For example, it is unclear if the two described lobe types (basin-floor and base-of-slope) are discrete elements or if a transition exists from one to the other, with 'hybrid' lobes showing characteristics of both. Further investigation is needed to connect the base-of-slope areas with the areas down dip. This will require detailed mapping and characterisation work. Furthermore, it is unclear how these different lobe types may be represented in the case of a stepped slope profile (e.g. McGilvery and Cook, 2003; Prather, 2003; Adeogba et al., 2005), where each flat may act as a small-scale basin-floor.

9.2.6 Quantifying the preservation potential of CLTZs

Key to unraveling the stratigraphic record of CLTZs within outcrop and core is understanding the preservation potential of its different elements (*Chapter 8*). Suggestions have been made for major controls on CLTZ preservation, including flow efficiency influencing CLTZ dimensions and the evolutionary character of the system. Off-axis CLTZ environments have been proposed to be best preserved in the rock record. The development and preservation of CLTZs and their elements could potentially be further improved by experimental and numerical modelling methods by looking in detail on subjects such as the interaction between turbidity currents and irregularities in the substrate or the influence of decreased flow confinement at the channel mouth and a break-in-slope. Also, capturing flow dynamics within modern systems (e.g. Black Sea, Medocino Canyon), such as active measurements of a hydraulic jump (Sumner et al., 2013), may massively improve our understanding of CLTZ preservation.

List of References

Aarnes, J.E., Krogstad, S.,Lie, K-A., 2008. Multiscale mixed/mimetic methods on corner-point grids. Computational Geosciences 12, 297-315.

Adeogba, A.A., McHargue, T.R., Graham, S.A., 2005. Transient fan architecture and depositional controls from a near-surface 3-D seismic data, Niger Delta continental slope. AAPG Bulletin 89, 627-643.

Alabert, F.G., Massonnat, G.J., 1990. Heterogeneity in a complex turbiditic reservoir: stochastic modelling of facies and petrophysical variability. SPE Annual Technical Conference and Exhibition. Society of Petroleum Engineers, SPE 20604.

Andersson, P.O.D., Worden, R.H., Hodgson, D.M., Flint, S., 2004. Provenance evolution and chemostratigraphy of a Palaeozoic submarine fan-complex: Tanqua Karoo Basin, South Africa. Marine and Petroleum Geology 21, 555-577.

Al Ja'Aidi, O.S., McCaffrey, W.D., Kneller, B.C., 2004. Factors influencing the deposit geometry of experimental turbidity currents: implications for sand-body architecture in confined basins. In: Lomas, S.A., Joseph, P. (Eds.) Confined Turbidite Systems. Geological Society of London, Special Publication 222, pp 45-58.

Alexander, J., Bridge, J.S., Cheel, R.J., Leclair, S.F., 2001. Bedforms and associated sedimentary structures formed under supercritical water flows over aggrading sand beds. Sedimentology 48, 133-152.

Alexander, J., McLelland, S.J., Gray, T.E., Vincent, C.E., Leeder, M.R., Ellett, S., 2008. Laboratory sustained turbidity currents form elongate ridges at channel mouths. Sedimentology 55, 845-868.

Alhuthali, A., Oyerinde, A.,Datta-Gupta, A., 2006. Optimal waterflood management using rate controls. SPE Annual Technical Conference and Exhibition. SPE 102478-MS.

Allen, J.R.L., 1971. Transverse erosional marks of mud and rock: their physical basis and geological significance. Sedimentary Geology 5, 167-385.

Allen, J.R.L., 1973. A classification of climbing-ripple cross-lamination. Journal of the Geological Society of London 129, 537-541.

Allen, J.R.L., 1984. Parallel lamination developed from upper-stage plane beds: a model based on the larger coherent structures of the turbulent boundary layer. Sedimentary Geology 39, 227-242.

Alpak, F.O., Barton, M.D.,Naruk, S.J., 2013. The impact of fine-scale turbidite channel architecture on deep-water reservoir performance. AAPG Bulletin 97, 251-284.

Amy, L.A., Talling, P.J., Edmonds, V.O., Sumner, E.J., Lesueur, A., 2006. An experimental investigation of sand-mud suspension settling behaviour: implications for bimodal mud contents of submarine flow deposits. Sedimentology 53, 1411-1434.

Amy, L.A., Peachey, S.A., Gardiner, A.R., Pickup, G.E., Mackay, E., Stephen, K.D., 2013. Recovery efficiency from a turbidite sheet system: numerical simulation of waterflooding using outcrop-based geological models. Petroleum Geoscience 19, 123-138.

Avseth, P., Mukerji, T., Jørstad, T., Mavko, A., Veggeland, T., 2001. Seismic reservoir mapping from 3-D AVO in a North Sea turbidite system. Geophysics 66, 1157-1176.

Baas, J.H., Van Kesteren, W., Postma, G., 2004. Deposits of depletive high-density turbidity currents: a flume analogue of bed geometry, structure and texture. Sedimentology 51, 1053-1088.

Baas, J.H., Best, J.L., Peakall, J., 2011. Depositional processes, bedform development and hybrid bed formation in rapidly decelerated cohesive (mud-sand) sediment flows. Sedimentology 58, 1953-1987.

Baas, J.H., Best, J.L., Peakall, J., 2016. Predicting bedforms and primary current stratification in cohesive mixtures of mud and sand. Journal of the Geological Society 173, 12-45. doi: 10.1144/jgs2015-024.

Barton, M., O'Byrne, C., Pirmez, C., Prather, B., Van der Vlugt, F., Alpak, F.O., Sylvester, Z., 2010. Turbidite channel architecture: Recognizing and quantifying the distribution of channel-base drapes using core and dipmeter data. In: Pöppelreiter, M., García-Carballido, C., Kraaijveld, M. (Eds.) Dipmeter and bore-hole image log technology: AAPG Memoir 92, pp. 195-210.

Beaubouef, R., Friedmann, S., 2000. High resolution seismic/sequence stratigraphic framework for the evolution of Pleistocene intra slope basins, western Gulf of Mexico: depositional models and reservoir analogs. In: Weimer, P., Slatt, R.M., Coleman, J., Rosen, N.C., Nelson, H., Bouma, A.H., Styzen, M.J., Lawrence, D.T. (Eds.) Deep Water Reservoirs of the World. GCSSEPM Foundation, Houston, pp. 40-60.

Beaubouef, R.T, Van Wagoner, J.C., Adair, N.L., 2003. Ultra-high resolution 3-D characterization of deep-water deposits-II: Insights into the evolution of a submarine fan and comparisons with river deltas, AAPG Annual Meeting, Extended Abstracts, May 11-14.

Bennes, M., Hamon, G., 2007. Core petrophysical synthesis carried out at a scale of a basin, some examples from Tertiary offshore reservoirs. Society of Core Analysts SCA, 27, 1-12.

Bernhardt, A., Jobe, Z.R., Lowe, D.R., 2011. Stratigraphic evolution of a submarine channel-lobe complex system in a narrow fairway within the Magallanes foreland basin, Cerro Toro Formaion, southern Chile. Marine and Petroleum Geology 28, 785-806.

Best, J., Bridge, J., 1992. The morphology and dynamics of low amplitude bedwaves upon upper stage plane beds and the preservation of planar laminae. Sedimentology 39, 737-752.

Blum, M., Martin, J., Milliken, K., Garvin, M., 2013. Paleovalley systems: insights from Quartenary analogs and experiments. Earth-Science Reviews 116, 128-169.

Bonnel, C., Dennielou, B., Droz, L., Mulder, T., Berné, S., 2005. Architecture and depositional pattern of the Rhône Neofan and recent gravity activity in the Gulf of Lions (western Mediterranean). Marine and Petroleum Geology 22, 827-843.

Bouma, A.H., 2000. Coarse-grained and fine-grained turbidite systems as end member models: applicability and dangers. Marine and Petroleum Geology 17, 137-143.

Bouma, A.H., Wickens, H.de V., 1991. Permian passive margin submarine fan complex, Karoo basin, South Africa: possible model to Gulf of Mexico. Gulf Coast Association of Geological Societies Transactions 41, 30-42.

Bouma, A.H., Wickens, H.de V., 1994. Tanqua Karoo, ancient analog for fine-grained submarine fans. In: Weimer, P., Bouma. A.H., Perkins, B.F. (Eds.) Submarine Fans and Turbidite Systems: Sequence Stratigraphy, Reservoir Architecture, and Production Characteristics. Gulf Coast Section SEPM Foundation 15th Research Conference Proceedings, pp. 23-34.

Brandsæter, I., Wist, H.T., Næss, A., Lia, O.A., Ole, J., Ringrose, P.S., Martinius, A.W., Lerdahl, T.R., 2001. Ranking of stochastic realizations of complex tidal reservoirs using streamline simulation criteria. Petroleum Geoscience 7, S53-S63.

Brouwer, D.R., Jansen, J.D., 2002. Dynamic optimization of water flooding with smart wells using optimal control theory. SPE European Petroleum Conference, SPE 78278.

Brouwer, D.R., Jansen J.D., Van der Starre, S., Van Kruijsdijk, C.P.J.W., Berentsen, C.W.J., 2001. Recovery increase through water flooding with smart well technology. SPE European Formation Damage Conference, SPE 68979.

Brunt, R.L., Hodgson, D.M., Flint, S.S., Pringle, J.K., Di Celma, C., Prélat, A., Grecula, M., 2013a. Confined to unconfined: Anatomy of a base of slope succession, Karoo Basin, South Africa. Marine and Petroleum Geology 41, 206-221.

Brunt, R.L., Di Celma, C.N., Hodgson, D.M., Flint, S.S., Kavanagh, J.P., van der Merwe, W.C., 2013b. Driving a channel through a levee when the levee is high: an outcrop example of submarine down-dip entrenchment. Marine and Petroleum Geology 41, 134-145.

Bryant, I.D., Flint, S.S., 1993. Quantitative clastic reservoir geological modelling: problems and perspectives. In: Flint, S.S., Bryant, I.I., (Eds.) The geological modelling of hydrocarbon reservoirs and outcrop analogues. IAS Special Publication 15, pp. 3-20.

Callow, R. H., McIlroy, D., 2011. Ichnofabrics and ichnofabric-forming trace fossils in Phanerozoic turbidites. Bulletin of Canadian Petroleum Geology 59, 103-111.

Campion, K.T., Dixon, B.T., Scott, E.D., 2011. Sediment waves and depositional implications for fine-grained rocks in the Cerro Toro Formation (Upper Cretaceous), Silla Syncline, Chile. Marine and Petroleum Geology 28, 761-784.

Cartigny, M.J., Postma, G., van den Berg, J.H., Mastbergen, D.R., 2011. A comparative study of sediment waves and cyclic steps based on geometries, internal structures and numerical modeling. Marine Geology 280, 40-56.

Cartigny, M.J., Eggenhuisen, J.T., Hansen, E.W., Postma, G., 2013. Concentration-dependent flow stratification in experimental high-density turbidity currents and their relevance to turbidite facies models. Journal of Sedimentary Research 83, 1047-1065.

Cartigny, M.J., Ventra, D., Postma, G., Den Berg, J.H., 2014. Morphodynamics and sedimentary structures of bedforms under supercritical-flow conditions: New insight from flume experiments. Sedimentology 61, 712-748.

Catuneanu, O., 2004. Basement control on flexural profiles and the distribution of foreland facies: The Dwyka Group of the Karoo Basin, South Africa. Geology 32, 517-520.

Catuneanu, O., Hancox, P., Rubidge, B., 1998. Reciprocal flexural behaviour and contrasting stratigraphies: a new basin development model for the Karoo retroarc foreland system, South Africa. Basin Research 10, 417-439.

Chapin, M., Davies, P., Gibson, J., Pettingill, H., 1994. Reservoir architecture of turbidite sheet sandstones in laterally extensive outcrops, Ross Formation, western Ireland. In: Weimer, P., Bouma, A.H., Perkins, B.F. (Eds.) Submarine Fans and Turbidite Systems: Sequence Stratigraphy, Reservoir Architecture, and Production Characteristics. Gulf Coast Section SEPM Foundation 15th Research Conference Proceedings, pp. 53-68.

Choi, S.U., Garcia, M.H., 2001. Spreading of gravity plumes on an incline. Coastal Engineering Journal 43, 221-237.

Choux, C.M.A., Baas, J.H., McCaffrey, W.D., Haughton, P.D.W., 2005. Comparison of spatio-temporal evolution of experimental particulate gravity flows at two different initial concentrations, based on velocity, grain size and density data. Sedimentary Geology 179, 49-69.

Clark, J.D., Pickering, K.T., 1996. Submarine channels; Processes and Architecture, Vallis Press, London, 231 pp.

Clark, J.D., Kenyon, N.H., Pickering, K.T., 1992. Quantitative analysis of the geometry of submarine channels: implications for classification of submarine fans. Geology 20, 633-636.

Cobain, S.L., Peakall, J., Hodgson, D.M., 2015. Indicators of propagation direction and relative depth in clastic injectites: implications for laminar versus turbulent flow processes. GSA Bulletin 127, 1816-1830.

Cole, D., 1992. Evolution and development of the Karoo Basin. In: De Wit, M.J., Ransome, I.G.D. (Eds.) Inversion Tectonics of the Cape Fold Belt, Karoo and Cretaceous Basins of Southern Africa. Balkema, Rotterdam, pp. 87-99.

Cossu, R., Wells, M.G., Peakall, J., 2015. Latitudinal variations in submarine channel sedimentation patterns: the role of the Coriolis forces. Journal of the Geological Society 172, 161-174.

Covault, J. A., Romans, B. W., Graham, S. A., Fildani, A., Hilley, G. E., 2011. Terrestrial source to deep-sea sink sediment budgets at high and low sea levels: Insights from tectonically active Southern California. Geology 39, 619-622.

Covault, J.A., Kostic, S., Paull, C.K., Ryan, H.F., Fildani, A., 2014. Submarine channel initiation, filling and maintenance from sea-floor geomorphology and morphodynamic modelling of cyclic steps. Sedimentology 61, 1031-1054.

Crimes, T. R., Hidalgo, J. G., Poire, D. G., 1992. Trace fossils from Arenig flysch sediments of Eire and their bearing on the early colonisation of the deep seas. Ichnos: An International Journal of Plant & Animal *2*, 61-77.

Dakin, N., Pickering, K.T., Mohrig, D., Bayliss, N.J., 2012. Channel-like features created by erosive submarine debris flows: Field evidence from the Middle Eocene Ainsa Basin, Spanish Pyrenees. Marine and Petroleum Geology 41, 62-71.

Damuth, J.E., 1979. Migrating sediment waves created by turbidite currents in northern South China Basin. Geology 7, 520-523.

Deptuck, M.E., Steffens, G.S., Barton, M., Pirmez, C., 2003. Architecture and evolution of upper fan channel-belts on the Niger Delta slope and in the Arabian Sea. Marine and Petroleum Geology 20, 649-676.

Deptuck, M.E., Piper, M.E., David, J.W., Savoye, B., Gervais, A., 2008. Dimensions and architecture of late Pleistocene submarine lobes off the northern margin of East Corsica. Sedimentology 55, 869-898.

De Wit, M.J., Ransome, I.G., 1992. Regional inversion tectonics along the southern margin of Gondwana. In: De Wit, M.J., Ransome, I.G.D. (Eds.) Inversion Tectonics of the Cape Fold Belt, Karoo and Cretaceous Basins of Southern Africa. Amsterdam, Balkema, pp. 15-22.

Di Celma, C.N., Brunt, R.L., Hodgson, D.M., Flint, S.S., Kavanagh, J.P., 2011. Spatial and temporal evolution of a Permian submarine slope channel-levee system, Karoo Basin, South Africa. Journal of Sedimentary Research 81, 579-599.

Drinkwater, N.J., Pickering, K.T., 2001. Architectural elements in a high-continuity sand-prone turbidite system, late Precambrian Kongsfjord Formation, northern Norway: Application to hydrocarbon reservoir characterization. AAPG Bulletin 85, 1731-1757.

Eggenhuisen, J.T., McCaffrey, W.D., 2012. The vertical turbulence structure of experimental turbidity currents encountering basal obstructions: implications for vertical suspended sediment distribution in non-equilibrium currents. Sedimentology 59, 1101-1120.

Eggenhuisen, J.T., McCaffrey, W.D., Haughton, P.D., Butler, R.W., 2011. Shallow erosion beneath turbidity currents and its impact on the architectural development of turbidite sheet systems. Sedimentology 58, 936-959.

Elliott, T., 2000a. Depositional architecture of a sand-rich, channelized turbidite system: the Upper Carboniferous Ross Sandstone Formation, western Ireland. In: Weimer, P., Slatt, R.M., Coleman, J., Rosen, N.C., Nelson, H., Bouma, A.H., Styzen, M.J., Lawrence, D.T. (Eds.) Deep Water Reservoirs of the World. GCSSEPM Foundation, Houston, pp. 342-373.

Elliott, T., 2000b. Megaflute erosion surfaces and the initiation of turbidite channels. Geology 28, 119-122.

Ercilla, G., Casas, D., Estrada, F., Vázquez, J.T., Iglesias, J., García, M., Gómez, J., Acosta, J., Gallart, J., Maestro-González, M., Marconi Team, 2008. Morphosedimentary features and recent depositional architectural model of the Cantabrian continental margin. Marine Geology 247, 61-83.

Eschard, R., Deschamps, R., Dobligez, B., Lerat, O., Langlais, V., Euzen, T., 2014. Connectivity estimation between turbiditic channels and overbank deposits from the modelling of an outcrop analogue (Pab Formation, Maastrichtian, Pakistan). In: Martinius, A.W., Howell, J.A., Good, T.R. (Eds.) Sediment-Body Geometry and Heterogeneity: Analogue Studies for Modelling the Subsurface. Geological Society, London, Special Publication 387, pp. 203-231.

Falivene, O., Arbués, P., Howell, J., Muñoz, J.A., Fernández, O., Marzo, M., 2006. Hierarchical geocellular facies modelling of a turbidite reservoir analogue from the Eocene of the Ainsa Basin, NE Spain. Marine and Petroleum Geology 23, 679-701.

Farhoudi, J., Smith, K.V., 1985. Local scour profiles downstream of hydraulic jump. Journal of Hydraulic Research 23, 343-358.

Fernandez, R.L., Cantelli, A., Pirmez, C., Sequeiros, O., Parker, G., 2014. Growth patterns of subaqueous depositional channel lobe systems developed over a basement with a downdip break in slope: laboratory experiments. Journal of Sedimentary Research 84, 168-182.

Fildani, A., Normark, W.R., Kostic, S., Parker, G. 2006., Channel formation by flow stripping: Large-scale scour features along the Monterey East Channel and their relation to sediment waves. Sedimentology 53, 1265-1287.

Fildani, A., Weislogel, A., Drinkwater, N.J., McHargue, T., Tankard, A., Wooden, J., Hodgson, D.M., Flint, S.S., 2009. U-Pb zircon ages from the southwestern Karoo Basin, South Africa – Implications for the Permian-Triassic boundary. Geology 37, 719-222.

Fildani, A., Hubbard, S.M., Covault, J.A., Maier, K.L., Romans, B.W., Traer, M., Rowland, J.C., 2013. Erosion at inception of deep-sea channels. Marine and Petroleum Geology 41, 48-61.

Flint, S.S., Hodgson, D.M., Sprague, A., Brunt, R.L., Van der Merwe, W.C., Figueiredo, J., Prélat, A., Box, D., Di Celma, C., Kavanagh, J.P., 2011. Depositional architecture and sequence stratigraphy of the Karoo basin floor to shelf edge succession, Laingsburg depocentre, South Africa. Marine and Petroleum Geology 28, 658-674.

Fonnesu, M., Haughton, P., Felletti, F., McCaffrey, W., 2015. Short length-scale variability of hybrid event beds and its applied significance. Marine and Petroleum Geology 67, 583-603.

Funk, J.E., Slatt, R.M., Pyles, D.R., 2012. Quantification of static connectivity between deep-water channels and stratigraphically adjacent architectural elements using outcrop analogs. AAPG Bulletin 96, 277-300.

Galloway, W.E., 1998. Siliciclastic slope and base-of-slope depositional systems: component facies, stratigraphic architecture, and classification. AAPG Bulletin 82, 569-595.

Garcia, M.H., 1993. Hydraulic jumps in sediment-driven bottom currents. Journal of Hydraulic Engineering 119, 1094-1117.

Garcia, M.H., 2008. Sedimentation Engineering: Process, Measurements, Modeling and Practice. American Society of Civil Engineers, Reston, Virginia.

Garcia, M., Parker, G., 1989. Experiments on hydraulic jumps in turbidity currents near a canyon-fan transition. Science 245, 393-396.

Gardner, M.H., Borer, J.M., 2000. Submarine channel architecture along a slope to basin profile, Brushy Canyon Formation, west Texas. In: Bouma, A.H., Stone, C.G. (Eds.) Fine-grained turbidite systems: AAPG Memoir 72, SEPM Special Publication 68, pp. 195-214.

Gardner, M.H., Borer, J.M., Melick, J.J., Mavilla, N., Dechesne, M., Wagerle, R.N., 2003. Stratigraphic process-response model for submarine channels and related features from studies of Permian Brushy Canyon outcrops, West Texas. Marine and Petroleum Geology 20, 757-787.

Gladstone, C., Phillips, J.C., Sparks, R.S.J., 1998. Experiments on bidisperse, constant-volume gravity currents: propagation and sediment deposition. Sedimentology 45, 833-844.

Grecula, M., 2000. Stratigraphy and architecture of tectonically controlled turbidite systems, Laingsburg Formation, Karoo Basin, South Africa. Unpublished Ph.D. Thesis. University of Liverpool, 184 pp.

Grecula, M., Flint, S.S., Wickens, H.de V., Johnson, S.D., 2003a. Upward-thickening patterns and lateral continuity of Permian sand-rich turbidite channel fills, Laingsburg Karoo, South Africa. Sedimentology 50, 831-853.

Grecula, M., Flint, S.S., Potts, G., Wickens, deV, Johnson, S.D., 2003b. Partial ponding of turbidite systems in a basin with subtle growth-fold topography: Laingsburg-Karoo, South Africa. Journal of Sedimentary Research 73, 603-620.

Greene, H. G., Yoklavich, M. M., Starr, R. M., O'Connell, V. M., Wakefield, W. W., Sullivan, D. E., McRea Jr., J.E., Cailliet, G. M., 1999. A classification scheme for deep seafloor habitats. Oceanologica acta 22, 663-678.

Groenenberg, R.M., Hodgson, D.M., Prélat, A., Luthi, S.M., Flint, S.S., 2010. Flow-deposit interaction in submarine lobes: insights from outcrop observations and realizations of a process-based numerical model. Journal of Sedimentary Research 80, 252-267.

Grundvåg, S.A., Johannessen, E.P., Helland-Hansen, W., Plink-Björklund, P., 2014. Depositional architecture and evolution of progradationally stacked lobe complexes in the Eocene Central Basin of Spitsbergen. Sedimentology 61, 535-569.

Grunow, A., Hanson, R., Wilson, T., 1996. Were aspects of Pan-African deformation linked to lapetus opening? Geology 24, 1063-1066.

Habgood, E.L., Kenyon, N.H., Masson, D.G., Akhmetzhanov, A., Weaver, P.P., Gardner, J., Mulder, T., 2003. Deep-water sediment wave fields, bottom current sand channels and gravity flow channel-lobe systems: Gulf of Cadiz, NE Atlantic. Sedimentology 50, 483-510.

Hamilton, P.K., Strom, K.B., Hoyal, D.C.J.D., 2015. Hydraulic and sediment transport properties of autogenic avulsion cycles on submarine fans with supercritical distributaries. Journal of Geophysical Research: Earth Surface 120, 1369-1389.

Haughton, P.D., Barker, S.P., McCaffrey, W.D., 2003. 'Linked' debrites in sand-rich turbidite systems-origin and significance. Sedimentology 50, 459-482.

Haughton, P., Davis, C., McCaffrey, W., Barker, S., 2009. Hybrid sediment gravity flow deposits-classification, origin and significance. Marine and Petroleum Geology 26, 1900-1918.

Heiniö, P., Davies R.J., 2009. Trails of depressions and sediment waves along submarine channels on the continenta margin of Espirito Santo Basin, Brazil. Geological Society of America Bulletin 121, 698-711.

Hewett, T.A., 1986. Fractal distributions of reservoir heterogeneity and their influence on fluid transport. SPE Annual Technical Conference and Exhibition, Society of Petroleum Engineers, SPE 15386.

Hiscott, R.N., 1994. Traction-carpet stratification in turbidites-fact or fiction? Journal of Sedimentary Research 64, 204-208.

Hiscott, R.N., Hall, F.R., Pirmez, C., 1997. Turbidity-current overspill from the Amazon Channel: texture of the silt/sand load, paleoflow from anisotropy of magnetic susceptibility, and implications for flow processes. In: Flood, R.D., Piper, D.J.W., Klaus, A., Peterson, I.C. (Eds.) Proceedings of the Ocean Drilling Program, Scientific Results 155, pp. 53-78.

Hodgetts, D., Drinkwater, N.J., Hodgson, D.M., Kavanagh, J., Flint, S.S., Keogh, K.J., Howell J.A., 2004. Three-dimensional geological models from outcrop data using digital data collection techniques: an example from the Tanqua Karoo depocentre, South Africa. In: Curtis, A.C., Wood, R. (Eds.) Geological Prior Information: Informing Science and Engineering. Geological Society, London, Special Publication 239, pp. 57-75.

Hodgson, D.M., 2009. Distribution and origin of hybrid beds in sand-rich submarine fans of the Tanqua depocentre, Karoo Basin, South Africa. Marine and Petroleum Geology 26, 1940-1956.

Hodgson, D.M., Flint, S.S., Hodgetts, D., Drinkwater, N.J., Johannessen, E.P., Luthi, S.M., 2006. Stratigraphic evolution of fine-grained submarine fan systems, Tanqua Depocenter, Karoo Basin, South Africa. Journal of Sedimentary Research 76, 20-40.

Hodgson, D.M., Di Celma, C.N., Brunt, R.L., Flint, S.S., 2011. Submarine slope degradation and aggradation and the stratigraphic evolution of channel-levee systems. Journal of the Geological Society of London 168, 625-628.

Hodgson, D.M., Kane, I.A., Flint, S.S., Brunt, R.L., Ortiz-Karpf, A., 2016. Time trangressive confinement on the slope and the progradation of basin-floor fans: Implications for the sequence stratigraphy of deep-water deposits. Journal of Sedimentary Research, 86, 73-86.

Hofstra, M., Hodgson, D.M., Peakall, J., Flint, S.S., 2015. Giant scour-fills in ancient channel-lobe transition zones: Formative processes and depositional architecture. Sedimentary Geology 329, 98-114.

Holbrook, J.M., Bhattacharya, J.P., 2012. Reappraisal of the sequence boundary in time and space: Case and considerations for an SU (subaerial unconformity) that is not a sediment bypass surface, a time barrier, or an unconformity. Earth-Science Reviews 113, 271-302.

Hovadik, J.M., Larue, D.K., 2007. Static characterizations of reservoirs: refining the concepts of connectivity and continuity. Petroleum Geoscience 13, 195-211.

Howe, J.A., 1996. Turbidite and contourite sediment waves in the northern Rockall Trough, North Atlantic Ocean. Sedimentology 43, 219-234.

Howell, J.A., Martinius, A.W., Good, T.R., 2014. The application of outcrop analogues in geological modelling: a review, present status and future outlook. In: Martinius, A.W., Howell, J.A., Good, T.R. (Eds.) Sediment-Body Geometry and Heterogeneity: Analogue Studies for Modelling the Subsurface. Geological Society, London, Special Publication 387, pp. 135-151.

Hoyal, D.C.J.D., Sheets, B.A., 2009. Morphodynamic evolution of experimental cohesive deltas. Journal of Geophysical Research: Earth Surface 114, 2003-2012.

Hubbard, S.M., Covault, J.A., Fildani, A., Romans, B.W., 2014. Sediment transfer and deposition in slope channels: Deciphering the record of enigmatic deep-sea processes from outcrop. GSA Bulletin 126, 857-871.

Idrobo, E.A., Choudhary, M.K., Datta-Gupta, A., 2000. Swept volume calculations and ranking geostatistical reservoir models using streamline simulation. SPE/AAPG Western Regional Meeting. Society of Petroleum Engineers. SPE 62557.

Ito, M., 2008. Downfan transformation from turbidity currents to debris flows at a channel-to-lobe transitional zone: the lower Pleistocene Otadai Formation. Journal of Sedimentary Research 78, 668-682.

Ito, M., 2010. Are coarse-grained sediment waves formed as downstream-migrating antidunes? Insight from an early Pleistocene submarine canyon on the Boso Peninsula, Japan. Sedimentary Geology 226, 1-8.

Ito, M., Saito, T., 2006. Gravel waves in an ancient canyon: analogous features and formative processes of coarse-grained bedforms in a submarine-fan system, the Lower Pleistocene of the Boso peninsula, Japan. Journal of Sedimentary Research 76, 1274-1283.

Ito, M., Ishikawa, K., Nishida, N., 2014. Distinctive erosional and depositional structures formed at a canyon mouth: A lower Pleistocene deep-water succession in the Kasuza forearc basin on the Boso Peninsula, Japan. Sedimentology 61, 2042-2062.

Izumi, N., Parker, G., 2000. Linear stability analysis of channel inception: downstream-driven theory. Journal of Fluid Mechanics 419, 239-262.

Jackson, R.G., 1975. Hierarchical attributes and a unifying model of bed forms composed of cohensionless material and produced by shearing flow. Geological Society of America Bulletin 86, 1523-1533.

Jackson, M., Percival, J., Mostaghimi, P., Tollit, B., Pavlidis, D., Pain, C., Blunt, M., 2015. Reservoir modelling of flow simulation by use of surfaces, adaptive unstructured meshes, and an overlapping-control-volume finite-element method. SPE Reservoir Evaluation & Engineering. Doi: 10.2118/163633-PA.

Janocko, M., Nemec, W., Henriksen, S., Warchol, M., 2013. The diversity of deep-water sinuous channel belts and slope valley-fill complexes. Marine and Petroleum Geology 41, 7-34.

Jegou, I., Savoye, B., Pirmez, C., Droz, L., 2008. Channel-mouth lobe complex of the recent Amazon Fan: The missing piece. Marine Geology 252, 62-77.

Jennette, D., Wawrzyniec, T., Fouad, K., Dunlap, D.B., Meneses-Rocha, J., Grimaldo, F., Muñoz, R., Barrera, D., Williams-Rojas, C.T., Escamilla-Herrera, A., 2003. Traps and turbidite reservoir characteristics from a complex and evolving tectonic setting, Veracruz Basin, southeastern Mexico. AAPG Bulletin 87, 1599-1622.

Jobe, Z.R., Bernhardt, A., Fosdick, J.C., Lowe, D.R., 2009. Cerro Toro channel margins, Sierra del Toro. In: Fildani, A., Hubbard, S.M., Romans, B.W. (Eds.) Stratigraphic Evolution of Deep-Water Architecture: Examples of Controls and Depositional Styles from the Magallanes Basin, Southern Chile 2009. SEPM Field Trip Guidebook 10, pp. 31-33.

Jobe, Z.R., Lowe, D.R., Morris, W.R., 2012. Climbing-ripple successions in turbidite systems: depositional environments, sedimentation rates and accumulation times. Sedimentology 59, 867-898.

Johnson, M., 1991. Sandstone petrography, provenance and plate tectonic setting in Gondwana context of the southeastern Cape-Karoo Basin. South African Journal of Geology 94, 137-154.

Johnson, M.R., van Vuuren, C.J., Visser, J.N.J., Cole, D.J., Wickens, H. deV., Christie, A.D.M., Roberts, D.L., 1997. The foreland Karoo Basin, South Africa. In: Selley, R.C. (Ed.) African Basins—Sedimentary Basins of the World. Elsevier, Amsterdam, pp. 269–317.

Johnson, S.D., Flint, S.S., Hinds, D., Wickens, H.de V., 2001. Anatomy, geometry and sequence stratigraphy of basin floor to slope turbidite systems, Tanqua Karoo, South Africa. Sedimentology 48, 987-1023.

Jones, G.E.D., Hodgson, D.M., Flint, S.S., 2013. Contrast in the process response of stacked clinothems to shelf-slope rollover. Geosphere 9, 299-316.

Jones, G.E.D., Hodgson, D.M., Flint, S.S., 2015. Lateral variability in clinoform trajectory, process regime, and sediment dispersal patterns beyond the shelf-edge rollover in exhumed basin margin-scale clinothems. Basin Research 27, 657-680.

Jopling, A. V., Richardson, E. V., 1966. Backset bedding developed in shooting flow in laboratory experiments: NOTES. Journal of Sedimentary Research 36, 821-825.

Jopling, A.V., Walker, R.G., 1968. Morphology and origin of ripple-drift cross-lamination, with examples from the Pleistocene of Massachusetts. Journal of Sedimentary Research 38, 971-984.

Joseph, P., Babonneau, N., Bourgeois, A., Cotteret, G., Eschard, R., Garin, B., Granjeon, D., Lerat, O., Ravenne, C., Gomes de Souza, O., Guillocheau, F., Quemener, J., 2000. The Annot Sandstone outcrops (French Alps): Architecture description as input for quantification and 3-D reservoir modelling. In: Weimer, P., Slatt, R.M., Coleman, J., Rosen, N.C., Nelson, H., Bouma, A.H., Styzen, M.J., Lawrence, D.T. (Eds.) Deep-Water Reservoirs of the World: Gulf Coast Section SEPM Foundation 20th Annual Research Conference 28, pp. 422-449.

Kane, I.A., Hodgson, D.M., 2011. Sedimentological criteria to differentiate submarine channel levee subenvironments: exhumed examples from the Rosario Fm. (Upper Cretaceous) of Baja California, Mexico, and the Fort Brown Fm. (Permian), Karoo basin, S. Africa. Marine and Petroleum Geology 28, 807-823.

Kane, I.A., Pontén, A.S.M., 2012. Submarine transitional flow deposits in the Palaeogene Gulf of Mexico. Geology 40, 1119-1122.

Kane, I.A., Kneller, B.C., Dykstra, M., Kassem, A., McCaffrey, W.D., 2007. Anatomy of a submarine channel-levee: an example from Upper Cretaceous slope sediments, Rosario Formation, Baja California, Mexico. Marine and Petroleum Geology 24, 540-563.

Kane, I.A., McCaffrey, W.D., Martinsen, O.J., 2009. Allogenic vs. autogenic controls on megaflute formation. Journal of Sedimentary Research 79, 643-651.

Karim, O., Ali, K., 2000. Prediction of flow patterns in local scour holes caused by turbulent water jets. Journal of Hydraulic Research 38, 279-287.

Kenyon, N.H., Millington, J., Droz, L., Ivanov, M.K., 1995. Scour holes in a channel-lobe transition zone on the Rhône Cone. In: Pickering, K.T., Hiscott, R.N., Kenyon, N.H., Ricci-Lucchi, F., Smith, R.D.A (Eds.) Atlas of Deep Water Environments; Architectural Style in Turbidite Systems. Chapman & Hall, London, pp. 212-215.

Keogh, K.J., Berg, F.K., Glitne Petek, 2008. A method for quantifying geological uncertainties in assessing remaining oil targets: a case study from the Glitne Field, North Sea. *In:* Robinson, A., Griffiths, P., Price, S., Hegre, J., Muggeridge, A. (Eds.) The Future of Geological Modelling in Hydrocarbon Development, Geological Society, London, Special Publications 309, pp. 193-203.

Khripounoff, A., Vangriesheim, A., Babonneau, N., Crassous, P., Dennielou, B., Savoye, B., 2003. Direct observation of intense turbidity current activity in the Zaire submarine valley at 4000 m water depth. Marine Geology 194, 151-158.

Kidd, R.B., Lucchi, R.G., Gee, M., Woodside, J.M., 1998. Sedimentary processes in the Stromboli Canyon and Marsili Basin, SE Tyrrhenian Sea: results from side-scan sonar surveys. Geo-Marine Letters 18, 146-154.

Kirschner, R.H., Bouma, A.H., 2000. Characteristics of a distributary channel-levee-overbank system, Tanqua Karoo. In: Bouma, A.H., Stone, J. (Eds.) Fine-Grained Turbidite Systems, AAPG Memoir 80, 337-364.

Klaucke, I., Masson, D.G., Kenyon, N.H., Gardner, J.V., 2004. Sedimentary processes of the lower Monterey Fan channel and channel-mouth lobe. Marine Geology 206, 181-198.

Kleverlaan, K., Cossey, S.P.J., 1993. Permeability barriers within sand-rich submarine fans: outcrop studies of the Tabernas Basin, SE Spain. In: Eschard, R., Doligez, B. (Eds.) Subsurface Reservoir Characterisation from Outcrop Observations: Editions Technip, Paris, pp. 161-164.

Kneller, B.C., 1995. Beyond the turbidite paradigm: physical models for deposition of turbidites and their implications for reservoir prediction. Geological Society of London, Special Publication 94, 31-49.

Kneller, B.C., Branney, M.J., 1995. Sustained high-density turbidity currents and the deposition of thick massive sands. Sedimentology 42, 607-616.

Kneller, B.C., McCaffrey, W.D., 1999. Depositional effects of flow nonuniformity and stratification within turbidity currents approaching a bounding slope: deflection, reflection, and facies variation. Journal of Sedimentary Research 69, 980-991.

Kneller, B.C., McCaffrey, W.D., 2003. The interpretation of vertical sequences in turbidite beds: the influence of longitudinal flow structure. Journal of Sedimentary Research 73, 706-713.

Komar, P.D., 1971. Hydraulic Jumps in turbidity currents. Geological Society of America Bulletin 82, 1477.

Kostic, S., Parker, G., 2006. The response of turbidity currents to a canyon-fan transition: internal hydraulic jumps and depositional signatures. Journal of Hydraulic Research 44, 631-653.

Kuang, Z., Zhong, G., Wang, L., Guo, Y., 2014. Channel-related sediment waves on the eastern slope offshore Dongsha Islanfs, northern South China Sea. Journal of Asian Earth Sciences 79, 540-551.

Kubo, Y., Nakajima, T., 2002. Laboratory experiments and numerical simulation of sediment-wave formation by turbidity currents. Marine Geology 192, 105-121.

Kuenen, P.H., 1963. Turbidites in South Africa. Transcripts of the Geological Society of South Africa 66, 191.

Labourdette, R., 2007. Integrated three-dimensional modelling approach of stacked turbidite channels. AAPG Bulletin 91, 1603-1618.

Labourdette, R., Devilliers, M.C., Bui, T., 2013. History match of a DST using a turbidite elementary channels modelling technique, deep offshore Congo. SPE Reservoir Characterization and Simulation Conference and Exhibition. Society of Petroleum Engineers.

Lang, J., Winsemann, J., 2013. Lateral and vertical facies relationships of bedforms deposited by aggrading supercritical flows: from cyclic steps to humback dunes. Sedimentary Geology 296, 36-54.

Larue, D.K., 2004. Outcrop and waterflood simulation modeling of the 100-foot channel complex, Texas, and the Ainsa II channel complex, Spain: Analogs to multistory and multilateral channelized slope reservoirs. In: Grammer, M., Harris, P.M., Eberli, G.P. (Eds.) Integration of outcrop and modern analogs in reservoir modelling, AAPG Memoir 80, pp. 337-364.

Larue, D. K., Friedmann, F., 2005. The controversy concerning stratigraphic architecture of channelized reservoirs and recovery by waterflooding. Petroleum Geoscience 11, 131-146.

Larue, D.K., Hovadik, J., 2012. Rapid earth modelling for appraisal and development studies of deep-water clastic reservoirs and the concept of 'procycling'. Petroleum Geoscience 18, 201-218.

Lee, S.E., Amy, L.A., Talling, P.J., 2004. The character and origin of thick base-of-slope sandstone units of the Peïra Cava outlier, SE France. In: Joseph, P., Lomas, S.A. (Eds.) Deep-Water Sedimentation in the Alpine Foreland Basin of SE France: New Perspectives on the Grès d'Annot and Related Systems. Geological Society London, Special Publication 221, pp. 331-347.

Lien, T., Walker, R.G., Martinsen, O.J., 2003. Turbidites in the Upper Carboniferous Ross Formation, western Ireland: reconstruction of a channel and spillover system. Sedimentology 50, 113-148.

Link, M.H., Weimer, P., 1991. Seismic facies and sedimentary processes of submarine fans and turbidite systems. Springer New York, pp. 447.

Lonsdale, P., Hollister, C.D., 1979. Near-bottom traverse of Rockall Trough-Hydrographic and geological inferences. Oceanologica Acta 2, 91-105.

López-Gamundi, O.R., Rossello, E.A., 1998. Basin fill evolution and paleotectonic patterns along the Samfrau geosyncline: the Sauce Grande basin-Ventana foldbelt (Argentina) and Karoo basin-Cape foldbelt (South Africa) revisited. Geologische Rundschau 86, 819-834.

Lowe, D.R., 1982. Sediment gravity flows: II Depositional models with special reference to the deposits of high-density turbidity currents. Journal of Sedimentary Research 52, 279-297.

Luthi, S.M., Hodgson, D.M., Geel, C.R., Flint, S.S., Goedbloed, J.W., Drinkwater, N.J., Johannessen, E.P., 2006. Contribution of research borehole data to modelling fine-grained turbidite reservoir analogues, Permian Tanqua–Karoo basin-floor fans (South Africa). Petroleum Geoscience 12, 175-190.

Macdonald, R.G., Alexander, J., Bacon, J.C., Cooker, M.J., 2009. Flow patterns, sedimentation and deposit architecture under a hydraulic jump on a non-eroding bed: defining hydraulic-jump unit bars. Sedimentology 56, 1346-1367.

Macdonald, H.A., Wynn, R.B., Huvenne, V.A., Peakall, J., Masson, D.G., Weaver, P.P., McPhail, S.D., 2011a. New insights into the morphology, fill, and remarkable longevity (>0.2 m.y.) of modern deep-water erosional scours along the northeast Atlantic margin. Geosphere 7, 845-867.

Macdonald, H.A., Peakall, J., Wignall, P.B., Best, J., 2011b. Sedimentation in deep-sea lobe-elements: Implications for the origin of thickening-upward sequences. Journal of the Geological Society of London 168, 319-331.

Mahaffie, M.J., 1994. Reservoir classification for turbidite intervals at the Mars discovery, Mississippi Canyon 807, Gulf of Mexico. In Weimer, P., Bouma, A.H., Perkins, B.F. (Eds.) Submarine Fans and Turbidite Systems: Gulf Coast Society of the Society of Economic Paleontologists and Mineralogists Foundation, 15th Annual Research Conference, pp. 233-244.

Maier, K.L., Fildani, A., Paull, C.K., Graham, S.A., McHargue, T.R., Caress, D.W., McGann, M., 2011. The elusive character of discontinuous deep-water channels: New insights from Lucia Chica channel system, offshore California. Geology 39, 327-330.

Malinverno, A., Ryan, W.B., Auffret, G., Pautot, G., 1988. Sonar images of the path of recent failure events on the continental margin off Nice, France. Geological Society of America Special Papers 229, 59-76.

Marini, M., Milli, S., Ravnås, R., Moscatelli, M., 2015. A comparative study of confined vs. semi-confined turbidite lobes from the Lower Messinian Laga Basin (Central Apennines, Italy): Implications for assessment of reservoir architecture. Marine and Petroleum Geology 63, 142-165.

Masalimova, L.U., Lowe, D.R., Sharman, G.R., King, P.R. Arnot, M.J., 2016. Outcrop characterization of a submarine channel-lobe complex: The Lower Mount Messenger Formation, Taranaki Basin, New Zealand. Marine and Petroleum Geology 71, 360-390.

Mayall, M., Jones, E., Casey, M., 2006. Turbidite channel reservoirs – key elements in facies prediction and effective development. Marine and Petroleum Geology 23, 821-841.

McGilvery, T. A., Cook, D.L., 2003. The influence of local gradients on accommodation space and linked depositional elements across a stepped slope profile, offshore Brunei. In: Roberts, H.H., Rosen, N.C., Fillon, R.H., Anderson, J.B. (Eds.) Shelf margin deltas and linked down slope petroleum systems: Global significance and future exploration potential, Gulf Coast Section SEPM 23rd Annual Research Conference, pp. 387-419.

McHargue, T., Pyrcz, M.J., Sullivan, M.D., Clark, J.D., Fildani, A., Romans, B.W., Covault, J.A., Levy, M., Posamentier, H.W., Drinkwater, N.J., 2011. Architecture of turbidite channel systems on the continental slope: patterns and predictions. Marine and Petroleum Geology 28, 728-743.

McHugh, C.M., Ryan, W.B., 2000. Sedimentary features associated with channel overbank flow: examples from the Monterey Fan. Marine Geology 163, 199-215.

McKay, M.P., Weislogel, A.L., Fildani, A., Brunt, R.L., Hodgson, D.M., Flint, S.S., 2015. U-PB zircon tuff geochronology from the Karoo Basin, South Africa: implications of zircon recycling on stratigraphic age controls. International Geology Review 57, 393-410.

Migeon, S., Savoye, B., Zanella, E., Mulder, T., Faugères, J.C., Weber, O., 2001. Detailed seismic-reflection and sedimentary study of turbidite waves on the Var Sedimentary Ridge (SE France): significance for sediment transport and deposition and for the mechanisms of sediment-wave construction. Marine and Petroleum Geology 18, 179-208.

Migeon, S., Mulder, T., Savoye, B., Sage, F., 2012. Hydrodynamic processes, velocity structure and stratification in natural turbidity currents: results inferred from field data in the Var Turbidite System. Sedimentary Geology 245, 48-62.

Meiburg, E., Kneller, B., 2010. Turbidity currents and their deposits. Annual Review of Fluid Mechanics 42, 135-156.

Morris, S.A., Kenyon, N.H., Limonov, A.F., Alexander, J., 1998. Downstream changes of large-scale bedforms in turbidites around the Valencia channel mouth, north-west Mediterranean implications for palaeoflow reconstruction. Sedimentology 45, 365-377.

Morris, W.R., Normark, W.R., 2000. Sedimentologic and geometric criteria for comparing modern and ancient sandy turbidite elements. In: Weimer, P., Slatt, R.M., Coleman, J., Rosen, N.C., Nelson, H., Bouma, A.H., Styzen, M.J., Lawrence, D.T. (Eds.) Deep Water Reservoirs of the World. GCSSEPM Foundation, Houston, pp. 606-628.

Morris, W.R., Scheihing, M.H., Wickens, H.de V., Bouma, A.H., 2000. Reservoir architecture of deepwater sandstones: examples from the Skoorsteenberg Formation, Tanqua Karoo Sub-basin, South Africa. In: Weimer, P., Slatt, R.M., Coleman, J., Rosen, N.C., Nelson, H., Bouma, A.H., Styzen, M.J., Lawrence, D.T. (Eds.), Deep Water Reservoirs of the World. GCSSEPM Foundation, Houston, pp. 629-666.

Morris, E.A., Hodgson, D.M., Flint, S.S., Brunt, R.L., Butterworth, P.J., Verhaeghe, J. 2014a. Sedimentology, stratigraphic architecture, and depositional context of submarine frontal-lobe complexes. Journal of Sedimentary Research 84, 763-780.

Morris, E.A., Hodgson, D.M., Brunt, R.L., Flint, S.S., 2014b. Origin, evolution and anatomy of silt-prone submarine external levées. Sedimentology 61, 1734-1763.

Moscardelli, L., Wood, L., Mann. P., 2006. Mass-transport complexes and associated processes in the offshore area of Trinidad and Venezuela. American Association of Petroleum Geology Bulletin 90, 1059-1088.

Mulder, T., Alexander, J., 2001. Abrupt change in slope causes variation in the deposit thickness of concentrated particle-driven density currents. Marine Geology 175, 221-235.

Mutti, E., 1977. Distinctive thin-bedded turbidite facies and related depositional environments in the Eocene Hecho Group (South-central Pyrenees, Spain). Sedimentology, 24, 107-131.

Mutti, E., Sonnino, M., 1981. Compensation cycles: a diagnostic feature of sandstone lobes. IAS 2nd European Meeting, Bologna, Abstr., 120-123.

Mutti, E., Normark, W.R., 1987. Comparing examples of modern and ancient turbidite systems: problems and concepts. In: Leggett, J.K., Zuffa, G.G. (Eds.) Marine Clastic Sedimentology: Concepts and Case Studies). Graham & Trotman, Oxford, pp. 1-38.

Mutti, E., Normark, W.R., 1991. An integrated approach to the study of turbidite systems. In: Weimer, P., Link, M.H. (Eds.), Seismic Facies and Sedimentary Processes of Submarine Fans and Turbidite Systems. Springer, New York, pp. 75-106.

Nakajima, T., Satoh, M., Okamura, Y., 1998. Channel-levee complexes, terminal deep-sea fan and sediment wave fields associated with the Toyama Deep-Sea Channel system in the Japan Sea. Marine Geology 147, 25-41.

Nelson, C. H., C. Goldfinger, J. E. Johnson, G. Dunhill, 2000. Variation of modern turbidite systems along the subduction zone margin of Cascadia Basin and implications for turbidite reservoir beds. In: Weimer, P.W., Nelson, C.H. (Eds.) DeepWater Reservoirs of the World: 20th Annual Res. Conf, Gulf Coast Section Society of Economic Paleontologists and Mineralogists, pp. 31.

Normark, W.R., Damuth, J.E., The leg 155 Sedimentology Group, 1997. Sedimentary facies and associated depositional elements of the Amazon Fan. In: Flood, R.D., Piper, D.J.W., Klaus, A., Peterson, L.C. (Eds.) Proceedings of the Ocean Drilling Program, Scientific Results, leg 155: College Station, Texas, pp. 611-651.

Normark, W.R., Dickson, F.H., 1976. Sublacustrine fan morphology in Lake Superior. AAPG Bulletin 60, 1021-1036.

Normark, W.R., Piper, D.J.W., 1991. Initiation Processes and Flow Evolution of Turbidity Currents: Implications for the Depositional Record. In: Osborne, R.H. (Ed.) From Shoreline to Abyss: Contributions in Marine Geology in honor of Francis Parker Shepard, SEPM Special Publication 46, pp. 207-230.

Normark W.R., Hess, G.R., Stow, D.A.V., Bowen, A.J., 1980. Sediment waves on the Monterey Fan levee: a preliminary physical interpretation. Marine Geology 37, 1-18.

Normark, W.R., Piper, D.J., Posamentier, H. Pirmez, C., Migeon, S., 2002. Variability in form and growth of sediment waves on turbidite channel levees. Marine Geology 192, 23-58.

Normark, W.R., Paull, C.K., Caress, D.W., Ussler, W., Sliter, R., 2009. Fine-scale relief related to late Holocene channel shifting within the floor of the upper Redondo Fan, offshore Southern California. Sedimentology 56, 1690-1704.

Oliveira, C.M., Hodgson, D.M., Flint, S.S., 2009. Aseismic controls on in situ soft-sediment deformation processes and products in submarine slope deposits of the Karoo Basin, South Africa. Sedimentology 56, 1201-1225

Ortiz-Karpf, A., Hodgson, D.M., McCaffrey, W.D., 2015. The role of mass-transport complexes in controlling channel avulsion and the subsequent sediment dispersal patterns on an active margin: The Magdalena Fan, offshore Colombia. Marine and Petroleum Geology 64, 58-75.

Palanques, A., Kenyon, N.H., Alonso, B., Limonov, A., 1995. Erosional and depositional patterns in the Valencia mouth: An example of a modern channel-lobe transition zone channel. Marine Geophysical Research 17, 503-517.

Parkash, B., 1970. Downcurrent changes in sedimentary structures in Ordovician turbidite greywackes. Journal of Sedimentary Research 40, 572-590.

Parkash, B., Middleton, G.V., 1970. Downcurrent textural changes in Ordovician turbidite greywackes. Sedimentology 14, 259-293.

Parker, G., 1982. Conditions for the ignition of catastrophically erosive turbidity currents. Marine Geology 46, 307-327.

Parsons, D.R., Peakall, J., Aksu, A.E., Flood, R.D., Hiscott, R. N., Beşiktepe, Ş., Mouland, D., 2010. Gravity-driven flow in a submarine channel bend: direct field evidence of helical flow reversal. Geology 38, 1063-1066.

Paull, C.K., Caress, D.W., Ussler, W., Lundsten, E. Meiner-Johnson, M., 2011. High-resolution bathymetry of the axial channels within Monterey and Soquel submarine anyons, offshore central California. Geosphere 7, 1077-1101.

Paull, C.K., McGann, M., Sumner, E.J., Barnes, P.M., Lundsten, E.M., Anderson, K., Gwiazda, R., Edwards, B., Caress, D.W., 2014. Sub-decadal turbidite frequency during the early Holocene: Eel Fan, offshore northern California. Geology 42, 885-858.

Peakall, J., McCaffrey, B., Kneller, B., 2000. A process model for the evolution, morphology, and architecture of sinuous submarine channels. Journal of Sedimentary Research 70, 434-448.

Peakall, J., Kane, I.A., Masson, D.G., Keevil, G., McCaffrey, W., Corney, R., 2012. Global (latitudinal) variation in submarine channel sinuosity. Geology 40, 11-14.

Peakall, J., Wells, M.G., Cossu, R., Kane, I. A., Masson, D. G., Keevil, G.M., McCaffrey, W., Corney, R., 2013. Global (latitudinal) variation in submarine channel sinuosity: reply. Geology 41, e288.

Pemberton, E.A., Hubbard, S.M., Fildani, A., Romans, B., Stright, L. 2016. The stratigraphic expression of decreasing confinement along a deep-water sediment routing system: Outcrop example from southern Chile. Geosphere, GES01233-1.

Pickering, K.T., 1981. Two types of outer fan lobe sequence, from the late Precambrian Kongsfjord Formation submarine fan Finnmark North Norway. Journal of Sedimentary Research 51, 1277-1286.

Pickering, K.T., Hilton, V.C., 1998. Turbidite systems of southeast France. Vallis Press, London, 229 pp.

Piper, D.J.W., Normark, W.R., 1983. Turbidite depositional patterns and flow characteristics, Navy Submarine Fan, California Borderland. Sedimentology 30, 681-694.

Piper, D.J., Shor, A.N., Farre, J.A., O'Connell, S., Jacobi, R., 1985. Sediment slides and turbidity currents on the Laurentian Fan: Sidescan sonar investigations near the epicentre of the 1929 Grand Banks earthquake. Geology 13, 538-541.

Piper, D.J.W., Sayoye, B., 1993. Processes of late Quartenary turbidity current flow and deposition on the Var deep-sea fan, north-west Mediterranean Sea. Sedimentology 40, 557-582.

Piper, D.J., Kontopoulos, N., 1994. Bed forms in submarine channels: comparison of ancient examples from Greece with studies of Recent turbidite systems. Journal of Sedimentary Research 64, 247-252.

Piper, D.J., Shor, A.N., Farre, J.A., O'Connell, S., Jacobi, R., 1985. Sediment slides and turbidity currents on the Laurentian Fan: Sidescan sonar investigations near the epicentre of the 1929 Grand Banks earthquake. Geology 13, 538-541.

Pirmez, C., Beaubouef, R.T., Friedmann, S.J., Mohrig, D.C., 2000. Equilibrium profile and baselevel in submarine channels: examples from Late Pleistocene systems and implications for the architecture of deepwater reservoirs. In: Weimer, P., Slatt, R.M., Coleman, J., Rosen, N.C., Nelson, H., Bouma, A.H., Styzen, M.J., Lawrence, D.T. (Eds.) Deep water reservoirs of the world, GCSSEPM Foundation, Houston, pp. 782-805.

Ponce, J.J., Carmona, N., 2011. Coarse-grained sediment waves in hyperpycnal clinoform systems, Miocene of the Austral foreland basin, Argentina. Geology 39, 763-766.

Posamentier, H.W., 2003. Depositional elements associated with a basin floor channel-levee system: case study from the Gulf of Mexico. Marine and Petroleum Geology 20, 677-690.

Posamentier, H.W., Kolla, V., 2003. Seismic geomorphology and stratigraphy of depositional elements in deep-water settings. Journal of Sedimentary Research 73, 367-388.

Posamentier, H.W., Erskine, R.D., Mitchum, R.M., Jr., 1991. Submarine fan deposition in a sequence stratigraphic framework. In: Weimer, P., Link, M.H. (Eds.) Seismic Facies and

Sedimentary Processes of Submarine Fans and Turbidite Systems, New York, Springer-Verlag, pp. 127-136.

Postma, G., Cartigny, M.J., 2014. Supercritical and subcritical turbidity currents and their deposits – A synthesis. Geology 42, 987-990.

Postma, G., Cartigny, M., Kleverlaan, K., 2009. Structurless, coarse-tail graded Bouma Ta formed by internal hydraulic jump of the turbidity current? Sedimentary Geology 219, 1-6.

Postma, G., Kleverlaan, K., Cartigny, M.J.B., 2014. Recognition of cyclic steps in sandy and gravelly turbidite sequences and consequences for the Bouma facies. Sedimentology 61, 2268-2290.

Postma, G., Hoyal, D.C., Abreu, V., Cartigny, M.J., Demko, T., Fedele, J.J., Kleverlaan, K., Pederson, K.H., 2016. Morphodynamics of supercritical turbidity currents in the channel-lobe transition zone. In: Lamarche, G, Mountjoy, J., Bull, S., Hubble, T., Krastel, S., Lane, E., Micallef, A., Moscardelli, L., Mueller, C., Pecher, I., Woelz, S.(Eds.) Submarine Mass Movements and their Consequences, Advances in Natural and Technological Hazards Research 41, Springer International Publishing, pp. 469-478.

Praeg, D.B., Schafer, C.T., 1989. Seabed features of the Labrador slope and rise near 55° N revealed by SEAMARC I sidescan sonar imagery. Atlantic Geoscience Centre, Bedford Institute of Oceanography.

Prather, B.E., 2003. Controls on reservoir distribution, architecture and stratigraphic trapping in slope settings. Marine and Petroleum Geology 20, 529-545.

Prather, B.E., O'Byrne, C., Pirmez, C. Sylvester, Z., 2016. Sediment partitioning, continental slopes and base-of-slope systems. Basin Research, DOI: 10.1111/bre.12190.

Prélat, A., 2010. Evolution, architecture and hierarchy of distributary deepwater deposits: a high resolution outcrop investigation of submarine lobe deposits from the Permian Karoo Basin, South Africa. Unpublished PhD Thesis, University of Liverpool, 317pp.

Prélat, A., Hodgson, D.M., 2013. The full range of turbidite bed thickness patterns in submarine lobes: controls and implications. Journal of the Geological Society 170, 209-214.

Prélat, A., Hodgson, D.M., Flint, S.S., 2009. Evolution, architecture and hierarchy of distributary deep-water deposits: a high-resolution outcrop investigation from the Permian Karoo Basin, South Africa. Sedimentology 56, 2132-2154.

Prélat, A., Covault, J.A., Hodgson, D.M., Fildani, A., Flint, S.S., 2010. Intrinsic controls on the range of volumes, morphologies, and dimensions of submarine lobes. Sedimentary Geology 232, 66-76.

Pringle, J.K., Clark, J.D., Westerman, A.R., Gardiner, A.R., 2003. The use of GPR to image three-dimensional (3-D) turbidite channel architecture in the Carboniferous Ross Formation. County Clare , western Ireland. In: Bristow, C.S., Jol, H. (Eds.) GPR in Sediments. Geological Society of London, Special Publication 211, pp. 315-326.

Pringle, J.K., Howell, J.A., Hodgetts, D., Westerman, A.R., Hodgson, D.M., 2006. Virtual outcrop models of petroleum reservoir analogues: a review of the current state-of-the-art. First Break, 24, 33-42.

Pringle, J., Brunt, R.L., Hodgson, D.M., Flint, S.S., 2010. Capturing stratigraphic and sedimentological complexity from submarine channel complex outcrops to digital 3D models, Karoo Basin, South Africa. Petroleum Geoscience 16, 307-330.

Pyles, D.R., Tomasso, M., Jennette, D.C., 2012. Flow processes and sedimentation associated with erosion and filling of sinuous submarine channels. Geology 40, 143-146.

Pyles, D.R., Strachan, L.J., Jennette, D.C., 2014. Lateral juxtapositions of channel and lobe elements in distributive submarine fans: Three-dimensional outcrop study of the Ross Sandstone and geometric model. Geosphere 10, 1104-1122.

Pyrcz, M.J., Deutsch, C.V., 2014. Geostatistical reservoir modelling, Oxford University Press, 448 pp.

Pyrcz, M.J., Catuneanu O., Deutsch, C.V. 2005. Stochastic surface-based modeling of turbidite lobes. AAPG Bulletin, 89, 177-191.

Raudkivi, A.J., 1998. Loose Boundary Hydraulics. A.A. Balkema, Rotterdam, The Netherlands, 260 pp.

Reading, H.G., Richards, M., 1994. Turbidite systems in deep-water basin margins classified by grain size and feeder system. AAPG Bulletin 78, 792-822.

Ricci-Lucchi, F., 1975. Depositional cycles in two turbidite formations of Northern Apennines (Italy). Journal of Sedimentary Petrology 45, 3-43.

Richards, M., Bowman, M., 1998. Submarine fans and related depositional systems II: variability in reservoir architecture and wireline log character. Marine and Petroleum Geology 15, 821-839.

Richards, M., Bowman, M., Reading, H., 1998. Submarine-fan systems I: characterization and stratigraphic prediction. Marine and Petroleum Geology 15, 689-717.

Ringrose, P., Bentley, M., 2015. Reservoir Model Design. Springer, 249 pp.

Rotzien, J.R., Lowe, D.R., King, P.R., Browne, G.H., 2014. Stratigraphic architecture and evolution of a deep-water slope channel-levee and overbank apron: The Upper Miocene Upper Mount Messenger Formation, Taranaki Basin. Marine and Petroleum Geology 52, 22-41.

Russell, H.A.J., Arnott, R.W.C., 2003. Hydraulic-jump and hyperconcentrated-flow deposits of a glacigenic subaqueous fan: Oak Ridges Moraine, southern Ontario, Canada. Journal of Sedimentary Research 73, 887-905.

Saikia, K., Khan, W., Ramakrishnan, S., 2015. Challenges in deepwater reservoir characterization: From well log interpretation and well testing to 3D geocellular modelling. SPE Annual Technical Conference and Exhibition, Society of Petroleum Engineers, SPE 175071.

Saller, A., Werner, K., Sugiaman, F., Fransiskus, C.A., May, R., Glenn, D., Craig, B., 2008. Characteristics of Pleistocene deep-water fan lobes and their application to an upper Miocene reservoir model, offshore East Kalimantan, Indonesia. AAPG Bulletin 92, 919-949.

Sawyer, D.E., Flemings, P.B., Dugan, B., Germaine, J.T., 2009. Retrogressive failures recorded in mass transport deposits in the Ursa Basin, Northern Gulf of Mexico. Journal of Geophysical Research: Solid Earth 114, 1978-2012.

Scaglioni, P., Ruvo, L., Cozzi, M., 2006. Implicit net-to-gross in the petrophysical characterization of thin-layered reservoirs. Petroleum Geoscience 12, 325-333.

Schminke, H.U., Fisher, R.V., Waters, A.C., 1973. Antidune and chute and pool structures in the base surge deposits of the Laacher See area, Germany. Sedimentology, 553-574.

Schwarz, E., Arnott, R.W.C., 2007. Anatomy and evolution of a slope channel-complex set (Neoproterozoic Isaac Formation, Windermere Supergroup, southern Canadian Cordillera): implications for reservoir characterizations. Journal of Sedimentary Research 77, 89-109.

Scott, E.D., Bouma, A.H., Wickens, H.deV., 2000. Influence of tectonica on submarine fan deposition, Tanqua and Laingsburg subbasins, South Africa. In: Bouma, A.H., Stone, C.G. (Eds.) Fine-Grained Turbidite Systems. SEPM Special Publication 68, p. 47-56.

Shanmugam, G., Moiola, R.J., 1991. Types of Submarine Fan Lobes: Models and Implications (1). AAPG Bulletin 75, 156-179.

Shanmugam, G., Bloch, R.B., Mitchell, S.M., Beamish, G.W., Hodgkinson, R.J., Damuth, J.E., Straume, T., Syvertsen, S.E., Shields, K.E., 1995. Basin-floor fans in the North Sea: sequence stratigraphic models vs. sedimentary facies. AAPG Bulletin 79, 477-511.

Shaw, J., Puig, P., Han, G., 2013. Megaflutes in a continental shelf setting, Placentia Bay, Newfoundland. Geomorphology 189, 12-25.

Sixsmith, P.J., 2000. Stratigraphic development of a Permian turbidite system on a deforming basin floor: Laingsburg Formation. Karoo Basin, South Africa. Unpublished Ph.D. thesis. University of Liverpool, 229pp.

Sixsmith, P., Flint, S.S., Wickens, H. de V., Johnson, S., 2004. Anatomy and stratigraphic development of a basin floor turbidite system in the Laingsburg Formation, main Karoo Basin, South Africa. Journal of Sedimentary Research 74, 239-254.

Sohn, Y.K., 1997. On traction-carpet sedimentation. Journal of Sedimentary Research 67, 502-509.

Southard, J.B., 1991. Experimental determination of bed-form stability. Annual Review of Earth and Planetary Sciences 19, 423-455.

Southard, J.B., Boguchwal, L.A., 1990. Bed configurations in steady unidirectional water flows. Part 2. Synthesis of flume data. Journal of Sedimentary Research 60, 658-679.

Sprague, A.R.G., Garfield, T.R., Goulding, F.J., Beaubouef, R.T., Sullivan, M.D., Rossen, C., Campion, K.M., Sickafoose, D.K., Abreu, V., Schellpeper, M.E., Jensen, G.N., Jennette, D.C., Pirmez, C., Dixon, B.T., Ying, D., Ardill, J., Mohrig, D.C., Porter, M.L., Farrell, M.E., Mellere, D., 2005. Integrated slope channel depositional models: the key to successful prediction of reservoir presence and quality in offshore west Africa. CIPM, cuarto E-Exitep. pp. 1-13.

Spychala, Y.T., Hodgson, D.M., Flint, S.S., Mountney, N.P., 2015. Constraining the sedimentology and stratigraphy of submarine intraslope lobe deposits using exhumed examples from the Karoo Basin, South Africa. Sedimentary Geology 322, 67-81.

Stephen, K.D., Clark, J.D., Gardiner, A.R., 2001. Outcrop-based stochastic modelling of turbidite amalgamation and its effects on hydrocarbon recovery. Petroleum Geology 7, 163-172.

Stevenson, C.J., Jackson, C.A-L., Hodgson, D.M., Hubbard, S.M., Eggenhuisen, J.T., 2015. Deep-Water Sediment Bypass, Journal of Sedimentary Research 85, 1058-1081.

Stoker, S.J., Gray, J.C., Haile, P., Andrews, I.J., Cameron, T.D.J., 2006. The importance of stratigraphic plays in the undiscovered resources of the UK Continental Shelf. In: Allen, M.R., Goffey, G.E., Morgan, R.K., Walker, I.M. (Eds.) The Deliberate Search for the Stratigraphic for the Stratigraphic Trap. Geological Society of London, Special Publication 254, pp. 153-168.

Stow, D.A., Johansson, M., 2000. Deep-water massive sands: nature, origin and hydrocarbon implications. Marine and Petroleum Geology 17, 145-174.

Straub, K.M., Pyles, D.R., 2012. Quantifying the hierarchical organization of compensation in submarine fans using surface statistics. Journal of Sedimentary Research 82, 889-898.

Strebelle, S., Payrazyan, K., Caers, J., 2003. Modeling of a deepwater turbidite reservoir conditional to seismic data using principal component analysis and multiple-point geostatistics. SPE Journal 8, 227-235.

Strong, N., Paola, C., 2008. Valleys that never were: time surfaces versus stratigraphic surfaces. Journal of Sedimentary Research 78, 579-593.

Sullivan, M., Jensen, G., Goulding, F., Jennette, D., Foreman, L., Stern, D., 2000. Architectural analysis of deep-water outcrops: Implications for exploration and

development of the Diana sub-basin, western Gulf of Mexico. In: Weimer, P., Slatt, R.M., Coleman, J., Rosen, N.C., Nelson, H., Bouma, A.H., Styzen, M.J., Lawrence, D.T. (Eds.) Deep Water Reservoirs of the World, GCSSEPM Foundation, Houston, pp. 1010-1032.

Sullivan, M.D., Foreman, J.L., Jennette, D.C., Stern, D., Jensen, G.N., Goulding, F.J., 2004. An integrated approach to characterization and modeling of deep-water reservoirs, Diana field, western Gulf of Mexico. In: Grammer, G.M., Harris, P.M., Eberli, G.P. (Eds.) Integration of outcrop and modern analogs in reservoir modelling. AAPG Memoir 80, pp. 215-234.

Sumner, E.J., Amy, L.A., Talling, P.J., 2008. Deposit structure and processes of sand deposition from decelerating sediment suspensions. Journal of Sedimentary Research 78, 529-547.

Sumner, E.J., Talling, P.J., Amy, L.A., Wynn, R.B., Stevenson, C.J., Frenz, M., 2012. Facies architecture of individual basin-plain turbidites: Comparison with existing models and implications for flow processes. Sedimentology 59, 1850-1887.

Sumner, E.J., Peakall, J., Parsons, D., Wynn, R., Darby, S., Dorrell, R., McPhail, S., Perrett, J., Webb, A., White, D., 2013. First direct measurements of hydraulic jumps in an active submarine density current. Geophysical Research Letters 40, 5904-5908.

Sumner, E.J., Peakall, J., Dorrell, R.M., Parsons, D.R., Darby, S.E., Wynn, R.B., McPhail, S.D., Perrett, J., Webb, A., White, D., 2014. Driven around the bend: Spatial evolution and controls on the orientation of helical bend flow in a natural submarine gravity current. Journal of Geophysical Research: Oceans 119, 898-913.

Sylvester, Z., Pirmez, C., Cantelli, A., 2011. A model of submarine channel-levee evolution based on channel trajectories: Implications for stratigraphic architecture. Marine and Petroleum Geology 28 716-727.

Symons, W.O., Sumner, E.J., Talling, P.J., Cartigny, M.J., Clare, M.A., 2016. Large-scale sediment waves and scours on the modern seafloor and their implications for the prevalence of supercritical flows. Marine Geology 371, 130-148.

Talling, P.J., Wynn, R.B., Masson, D.G., Frenz, M., Cronin, B.T., Schiebel, R., Akhmetzhanov, A.M., Dallmeier-Tiessen, S., Benetti, S., Weaver, P.P.E., Georgiopoulou, A., Zühlsdorff, C., 2007. Onset of submarine debris flow deposition far from original giant landslide. Nature 450, 541-544.

Talling, P.J., Masson, D.G., Sumner, E.J., Malgesini, G., 2012. Subaqueous sediment density flows: Depositional processes and deposit types. Sedimentology 59, 1937-2003.

Talling, P.J., Paull, C.K., Piper, D.J.W., 2013. How are subaqueous sediment density flows triggered, what is their internal structure and how does it evolve? Direct observations from monitoring of active flows. Earth-Science Reviews 125, 244-287.

Tankard, A.J., Jackson, M.P.A., Eriksson, K.A., Hobday, D.K., Hunter, D.R., Minter, W.E.L., 1982. Crustal evolution of South Africa: 3.8 Billion years of Earth history. Springer-Verlag, 523 pp.

Tankard, A., Welsink, H., Aukes, P., Newton, R., Stettler, E., 2009. Tectonic evolution of the Cape and Karoo basins of South Africa. Marine and Petroleum Geology 26, 1379-1412.

Terlaky, V., Rocheleau, J., Arnott, R.W.C., 2016. Stratal composition and stratigraphic organization of stratal elements in an ancient deep-marine basin-floor succession, Neoproterozoic Windermere Supergroup, British Columbia, Canada. Sedimentology 63, 136-175.

Theron, A.C., 1967. The sedimentology of the Koup Subgroup near Laingsburg. Unpublished M.Sc thesis, University of Stellenbosch, 22 pp.

Unrug, R., 1997. Rodinia to Gondwana: the geodynamic map of Gondwana supercontinent assembly. GSA today 7, 1-6.

Urlaub, M., Talling, P. J., & Masson, D. G., 2013. Timing and frequency of large submarine landslides: implications for understanding triggers and future geohazard. Quaternary Science Reviews 72, 63-82.

Van der Mark, C.F., Blom, A., Hulscher, S.J.M.H., 2008. Quantification of variability in bedform geometry. Journal of Geophysical Research: Earth Surface 113, F03020, doi:10.1029/ 2007JF000940.

Van der Merwe, W.C., Hodgson, D.M., Flint S.S., 2009. Widespread syn-sedimentary deformation of a muddy deep-water basin-floor: the Vischkuil Formation (Permian), Karoo Basin, South Africa. Basin Research 21, 389-406.

Van der Merwe, W.C., Flint, S.S., Hodgson, D.M., 2010. Sequence stratigraphy of an argillaceous, deepwater basin-plain succesion: Vischkuil Formation (Permian), Karoo Basin, South Africa. Marine and Petroleum Geology 27, 321-333.

Van der Merwe, W.C., Hodgson, D.M., Flint, S.S., 2011. Origin and terminal architecture of a submarine slide: a case study from the Permian Vischkuil Formation, Karoo Basin, South Africa. Sedimentology 58, 2012-2038.

Van der Merwe, W.C., Hodgson, D.M., Brunt, R.L., Flint, S.S., 2014. Depositional architecture of sand-attached and sand-detached channel-lobe transition zones on an exhumed stepped slope mapped over a 2500 km^2 area. Geosphere 10, 1076-1093.

Van der Werff, W., Johnson, S. 2003. High resolution stratigraphic analysis of a turbidite system, Tanqua Karoo Basin, South Africa. Marine and Petroleum Geology 20, 45-69.

Van Lente, B., 2004. Chemostratigraphic Trends and Provenance of the Permian Tanqua and Laingsburg Depocentres, southwestern Karoo Basin, South Africa. Unpubl. Ph.D Thesis, University of Stellenbosch. 439 pp.

Veevers, J., Cole, D., Cowan, E. 1994. Southern Africa: Karoo basin and Cape fold belt. In: Veevers, J.J., Powell, C.Mc.A. (Eds.) Permian-Triassic Pangean basins along the Panthalassan margin of Gondwanaland. Geological Society of America Memoir 184, pp. 223-279.

Vicente-Bravo, J.V., Robles, S., 1995. Large-scale mesotopographic bedforms from the Albian Black Flysch, northern Spain: characterization, setting and comparison with recent analogues. In: Pickering, K.T., Hiscott, R.N., Kenyon, N.H., Ricci-Lucchi, F., Smith, R.D.A. (Eds.) Atlas of Deep Water Environments; Architectural Style in Turbidite Systems. Chapman & Hall, London, pp. 282-286.

Visser, J.N.J., 1989. The Permo-Carboniferous Dwyka Formation of southern Africa: deposition by a predominantly subpolar marine ice sheet. Palaeogeography, Palaeoclimatology, Palaeoecology 70, 377-391.

Visser, J.N.J., 1993. Sea-level changes in a back-arc-foreland transition: the late Carboniferous-Permian Karoo Basin of South Africa. Sedimentary Geology 83, 115-131.

Visser, J.N., 1997. Deglaciation sequences in the Permo-Carboniferous Karoo and Kalahari basins of southern Africa: a tool in the analysis of cyclic glaciomarine basin fills. Sedimentology 44, 507-521.

Visser, J.N.J., Young, G.M., 1990. Major element geochemistry and paleoclimatology of the Permo-Carboniferous glacigene Dwyka Formation and postglacial mudrocks in souther Africa. Palaeogeography, Palaeoclimatology, Palaeoecology 81, 49-57.

Visser, J.N.J., Praekelt, H.E., 1996. Subduction, mega-shear systems and Late Palaeozoic basin development in the African segment of Gondwana. Geologische Rundschau 85, 632-646.

Pysklywec, R.N., Mirovica, J.X., 1999. The role of subduction-induced subsidence in the evolution of the Karoo Basin. The Journal of Geology 107, 155-164.

Walker, R.G., 1978. Deep-water sandstone facies and ancient submarine fans: models for exploration for stratigraphic traps. AAPG Bulletin 62, 932-966.

Wei, T., Peakall, J., Parsons, D.R., Chen, Z., Zhao, B., Best, J., 2013. Three-dimensional gravity-current flow within a subaqueous bend: Spatial evolution and force balance variations. Sedimentology 60, 1668-1680.

Wickens, H.de V., 1994. Basin floor fan building turbidites of the southwestern Karoo Basin, Permian Ecca Group, South Africa. Unpublished Ph.D. Thesis, University of Port Elizabeth. 233 pp.

Wickens, H.de V., Bouma, A.H., 2000. The Tanqua fan complex, Karoo Basin, South Africa-outcrop analog for fine-grained, deepwater deposits. In: Bouma, A.H., Stone, C.G. (Eds.) Fine-grained Turbidite Systems. AAPG Memoir 72, pp. 153-164.

Wild, R., Flint, S.S., Hodgson, D.M., 2005. Architecture and stratigraphic evolution of multiple, vertically-stacked slope channel compexes, Tanqua depocentre, Karoo Basin, South Africa. In: Hodgson, D.M., Flint, S.S. (Eds.) Submarine Slope Systems: Processes and Products, Geological Society, London, Special Publication 244, pp. 89-111.

Wild, R., Flint, S.S., Hodgson, D.M., 2009. Stratigraphic evolution of the uppser slope and shelf edge in the Karoo Basin, South Africa. Basin Research 21, 502-527.

Williams, G.J.J., Mansfield, M., McDonald, D.G., Bush, M.D., 2004. Top-down reservoir modelling. SPE Annual Technical Conference and Exhibition, Society of Petroleum Engineers, SPE 89974.

Winn, R.D., Dott, R.H., 1977. Large-scale traction-produced structures in deep-water fan-channel conglomerates in southern Chile. Geology 5, 41-44.

Winn, R.D., Dott, R.H., 1979. Deep-water fan-channel conglomerates of Late Cretaceous age, southern Chile. Sedimentology 26, 203-228.

Wynn, R.B., Stow, D.A., 2002. Classification and characterisation of deep-water sediment waves. Marine Geology 192, 7-22.

Wynn, R.B., Kenyon, N.H., Masson, D.G., Stow, D.A., Weaver, P.P., 2002a. Characterization and recognition of deep-water channel-lobe transition zones. AAPG Bulletin 86, 1441-1462.

Wynn, R.B., Piper, D.J.W., Gee, M.J.R., 2002b. Generation and migration of coarse-grained sediment waves in turbidity current channels and channel-lobe transition zones. Marine Geology 192, 59-78.

Wynn, R.B., Cronin, B.T., Peakall, J., 2007. Sinuous deep-water channels: Genesis, geometry and architecture. Marine and Petroleum Geology 24, 341-387.

Xu, J.P., Noble, M.A., Rosenfeld, L.K., 2004. In-situ measurements of velocity structure within turbidity currents. Geophysical Research Letters 31, doi:10.1029/2004GL019718.

Young, R.A., Slatt, R.M., Staggs, J.G., 2003. Application of ground penetrating radar imaging to deepwater (turbidite) outcrops. Marine and Petroleum Geology 20, 809-821.

Zhang, X.,Pyrcz, M.J., Deutsch, C.V., 2009. Stochastic surface modeling of deepwater depositional systems for improved reservoir models. Journal of Petroleum Science and Engineering 68, 118-134.

Zou, F., Slatt, R., Bastidas, R., Ramirez, B., 2012. Integrated outcrop reservoir characterization, modelling, and simulation of the Jackfork Group at the Baumgartner Quarry area. AAPG Bulletin 96, 1429-1448.

Appendix A
LOBE 2 core details

Within Appendix A all details on the sedimentary cores studied for this thesis and the LOBE 2 project are presented.

A.1 LOBE 2 core locations

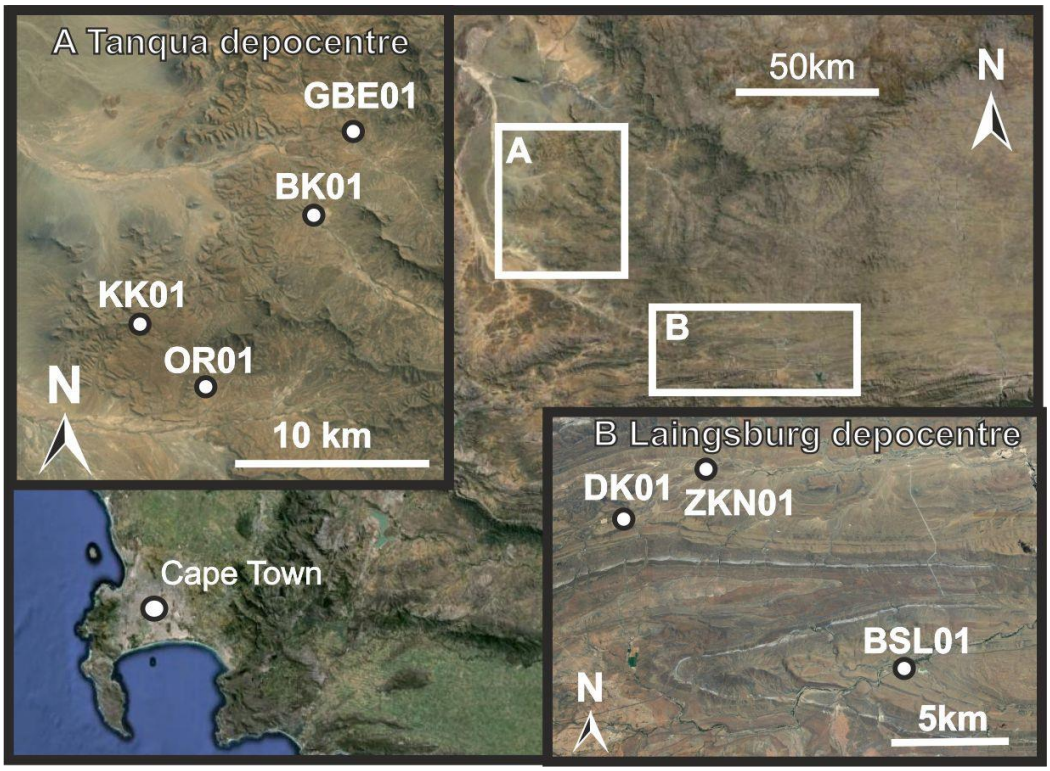

Core	UTM	
OR01	405628	6368089
BK01	412230	6379945
KK01	402474	6372476
GBE01	415248	6386042
DK01	460983	6331775
ZKN01	464561	6333936
BSL01	472843	6325459

A.2 LOBE 2 core descriptions

Legend

Cl = Clay
MSi = Muddy Siltstone
FSi = Fine Siltstone
CSi = Coarse Siltstone
VFS = Very Fine Sandstone
LFS = Lower Fine Sandstone
UFS = Upper Fine Sandstone
MS = Medium Sandstone

Thin-bedded: 0-0.1m
Medium-bedded: 0.1-0.5m
Thick-bedded: >0.5m

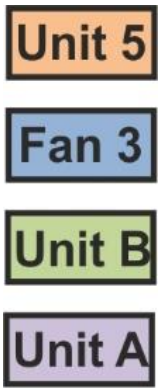

A.2.1 BK01 – Unit 5

Core interval:	46.50-0.00 m
Total thickness:	46.5 0m
Box:	BK01 1-10

Description

The boundary between Fan 4 and Unit 5 is marked by two claystones .The top of the upper claystone is used to define the stratigraphic base of Unit 5, although the sedimentary facies at the top of Fan 4 and the base of Unit 5 are very similar.

0-13 m: The basal 13 m of Unit 5 shows little variability and comprises an interbedded thin-bedded FSi and normal-graded thin to medium-bedded (up to 50 cm) VFS package. The sandstone beds show both planar parallel- and ripple cross-lamination. Some ripple cross-laminated beds are climbing. Sandstone bed thickness slightly increases upwards, while bioturbation becomes less prone.

13-25 m: The following 8 m interbedded package is characterised by medium-bedded LFS beds with climbing-ripple lamination with stoss-side preservation. A number of these beds show initial inverse, followed by normal grading. Bioturbation is low to absent in the basal part of Unit 5. A number of erosion surfaces are identified within this thin-bedded interval.

25-46.5 m: The first thick LFS beds start to appear alternating with packages (0.5-4 m) of thin-bedded sandstones and siltstones. Thick-bedded sandstones (>1 m) are mostly structureless but show bands of mudstone chips and climbing-ripple lamination or convolute laminations at bed tops. Bed bases are sharp, and can be erosional and occasionally contain mudstone clast materials. Multiple erosion surfaces are also present within the thin to medium-bedded sandstones.

A.2.2 BK01 – Fan 3

Core interval:	152.20-121.44 m
Total thickness:	30.76 m
Box:	BK01 27-33

Description

0-5.7 m: The basal 6m shows a thickening upwards package with 2m of thin-bedded FSi, overlain by interbedded thin to medium-bedded LFS/VFS and FSi. Multiple medium-bedded sandstone beds show sharp erosive structureless bases and mustone chip-rich banded tops.

5.7-30.8 m: The main stratigraphy of Fan 3 shows an alteration between a total of four thick-bedded LFS intervals (2-6 m) and four packages of medium to thin-bedded VFS and FSi (1-2 m). The thick-bedded sandstones are dominantly structureless with mustone chip-rich tops. Bed amalgamation is common. The thin-bed packages show numerous erosional surfaces and are sandstone-prone. Ripple- and planar-lamination are common and biotubation levels are medium to low. Some medium-bedded LFS contain a substantial amount of rip-up mudstone clasts at the base and smaller mudstone chip fragments at the top of the bed. The top of Fan 3 shows an abrupt finning/thinning-upwards sequence from thin-bedded VFS to FSi.

A.2.3 KK01 – Fan 3

Core interval:	166,39-65.24 m
Total thickness:	101.15 m (incl. partial duplication) – 59.65 m (without duplication)
Box:	KK01 15-37

NOTE: A large thrust fault is present within the top of Fan 3, duplicating a substantial part (41.5 m) of the stratigraphy.

Description

0-5.5 m: The basal 5 m shows a thickening-upwards package of thin to medium-bedded VFS-LFS and FSi. Sandstone beds show ripple-lamination, including climbing. The interval has a medium level of bioturbation.

5.5-27.4 m: This is followed by a >20 m interval of dominantly thick-bedded structureless LFS. Two 1 m thick intervals of more thin-bedded VFS are present at the lower part. The structureless sandstones show numerous amalgamation surfaces and banded tops in the upper section.

27.4–38.5 m: A thick package of thin- to medium-bedded VFS-LFS with occasional thin-bedded FSi. Ripple-lamination is common within the sandstone beds, including climbing. Some of the sandstone beds in the base contain mudstone chips concentrated in bands chips.

38.5–46.0 m: Thick-bedded dominantly structureless LFS, similar to the 5.5-27.4 m package. The sandstone beds can be rich in mudstone chips and occasionally contain mudstone rip-up clasts. Bed bases are sharp and abrupt grain size breaks indicate amalgamation surfaces.

46.0–65.2 m: An overall thinning upwards succession of medium to thin-bedded structured VFS and thin-bedded FSi. Numerous erosion surfaces are present within the base of this package. Sandstones show a combination of ripple, planar and convolute lamination. Planar lamination becomes more common within the thin-bedded top of Fan 3.

FAULT: The fault-zone is characterised by heavily fractured and distorted sediments including skewed and folded siltstone beds and completely fractured lower fine sandstones. Quartz veins can be observed all over. The occurrence of distortion is rather abrupt in the base, but the number of fractures fades out more gently towards the top. The total damage zone is 8.4 m thick.

A 2.4 GBE01 – Unit 5

Core interval:	80.31 – 0.99 m
Total thickness:	79.32 m
Box:	GBE01 01-18

NOTE: A large fault zone and possibly thrust is present within the middle of the Unit 5 stratigraphy. There is however no direct evidence of duplication.

Log has not been drawn

Description

0-26.4 m: The base shows an overall thickening upwards succession of interbedded thin-bedded siltstones and pass to towards medium-bedded structured and normal-graded VFS-LFS sandstones. Sandstones show planar, ripple and convolute laminations. Climbing ripple lamination is common. A number of erosion surfaces are present within the top of the package.

26.4-35.1 m: Thick structureless amalgamated UFS with the occasional mudstone chip or clast.

45.23- 47.1 m: Fault zone showing folded and tectonically deformed sandstones with numerous quartz veins. At the top a breccia is present.

47.1m-21.08 m: Thick-bedded mostly structureless LFS with the occasional medium-bedded structured VDS. Bed amalgamation is common. Tops show planar or climbing ripple lamination.

21.08-0.99 m: Overall sandstone-prone thickening upwards package from interbedded structured thin-bedded and medium-bedded VFS to structureless LFS at the top. Sandstones are dominantly planar laminated, but also show ripple lamination. Some thin planar-laminated FSi beds are present among the sandstones.

A 2.5 GBE01 – Fan 3

Core interval: 143.64-134.52 m
Total thickness: 9.12 m
Box: GBE01 31-32

Description

143.6-140.8 m: The basal 1.8 m is comprised of a weakly bioturbated thin-bedded FSi interval.

140.8-136.8 m: A 4 m thick sandstone-prone thickening-upwards succession. Bases of sandstone beds in the first 1.5 m are dark, possibly due to a high silt or mud component. Internal structures within the sandstones are purely planar-laminated and no ripple-lamination has been observed. The top 2 m shows medium-bedded structureless LFS with argillaceous (siltstone and mudstone) clast-rich tops. Several beds have a planar-laminated and normal-graded division at the top of the argillaceous division.

136.8-135.0m: The basal 20 cm is siltstone-prone (FSi) with multiple erosion surfaces and a 8 cm thick clast-rich debrite. The remaining 1.1 m shows a thinning-upwards package of medium to thin-bedded VFS with structureless bases and banded/planar-laminated/ripple-laminated tops. Overall, it shows an low level of bioturbation.

135.0-134.5m: The top 50cm of Fan 3 is defined by a fine to muddy thin-bedded FSi interval with a moderate level of bioturbation.

A 2.6 OR01 - Unit 5

Core interval: 50,28-0,70 m
Total thickness: 49.58 m (top of Unit 5 has not been reached)
Box: OR01 01-11

Description

0-13. 6m: The boundary between Fan 4 and Unit 5 is not well defined. The top of the last true >10 cm thick claystone has been defined as the base of Unit 5, which shows an overall

coarsening- and thickening-upwards succession with an interbedding of thin-bedded MSi-FSi and normal-graded VFS towards more medium-bedded VFS. Sandstone beds show both planar and ripple-lamination. Multiple erosion surfaces are present within a thin-bedded interval towards the top. A minor amount of sandstone beds are mudstone chip-rich and show banding.

13.6-23.11 m: Alternation between thick mostly structured VFS sandstones and interbedded intervals of thin-bedded normal-graded VFS and thin-bedded FSi. Sandstones show a combination of planar, convolute and ripple lamination, including climbing. Various erosion surfaces are present in some of the thin-bedded intervals.

23.11-39.2 m: One >15 m thick structureless FS without clear amalgamation surfaces. The base shows a 20cm thick soft sediment deformed package of muddy materials, which does not seem to be structurally related. Various mudstone chip stringers are randomly dispersed within the sandstone.

39.2-49.6 m: Sandstone-prone package of thin to medium-bedded structured VFS-LFS with the occasional thin-bedded FSi. The package contains a high number of erosion surfaces within the thin-bedded packages, especially at the top. Sandstones show both planar and ripple lamination, but are dominated by climbing ripple lamination.

A 2.7 OR01 – Fan 3

Core interval:	212.93 – 151.45 m
Total thickness:	61.48 m
Box:	OR01 33-47

Description

213-210.6 m: The base of Fan 3 is marked by a 2.4 m thin-bedded FSi interval with a moderate level of bioturbation. The top contains a number of thin ripple-laminated sandstone beds with erosive bases.

210.6-205.5 m: Thick to medium-bedded LFS are interbedded with thin-bedded VFS. The thick-bedded structureless sandstone beds have sharp bases and show large numbers of mudstone chip and clast materials, predominantly in bed bases and tops. No clear amalgamation surfaces are present. The thin-bedded sandstones are generally planar-laminated and erosional bases are not uncommon.

205.5–187.2 m: Thick-bedded amalgamated structureless LFS-UFS. Bed tops contain mudstone chip-rich bands and bed bases are occasionally dewatered.

187.2- 164.0 m: Alteration between thick-bedded structureless LFS and interbedded intervals of medium-bedded structured VFS and thin-bedded FSi. Thick-bedded sandstones

show banded tops and sharp bases, occasionally with rip-up mudstone clasts. Medium-bedded sandstones are dominantly ripple or convolute laminated.

164.0-151.5 m: Thick-bedded LFS with limited bed amalgamation. Bed tops show both mudstone-chip banding as ripple-lamination. The top shows a rapid thinning upwards sequence to medium-bedded VFS and thin-bedded FSi with a moderate to high level of bioturbation.

A 2.8 DK01 – Unit B1

Core interval: 91.60 m-86.52 m
Total thickness: 5.08 m

Box: DK01 18-17

Description

Unit B1 consists of an interbedded package of laminated thin-bedded FSi and thin to medium-bedded VFS. The top of the package is more siltstone prone than the base. Several erosive surfaces are present among the interval. VFS beds are structured and normally graded showing an assemblage of climbing ripple-lamination, planar-lamination and wavy laminations. Except for in the base, there is hardly any bioturbation present within this interval

B1 → B2 Clay

Core interval: 86.52-86.25 m

Total thickness: 0.26 m

Box: DK01 17

Description

The claystone interval between subunit B1 and B2 is exceptionally thin. It shows no evidence of bioturbation or any other structure.

A 2.9 DK01 – Unit B2

Core interval: 86.25- 0.00m

Total Thickness: 86.25m

Box: DK01 17-01

Description

86.25- 81.75 m: Slightly thickening/coarsening upwards package of thin-bedded Fsi and thin to medium-bedded VFS. Several erosive surfaces are present within this package.

Sandstone beds are structured and occasionally show mudstone clasts at the base of the bed. Structures include climbing ripple, planar and wavy lamination. Thin sandstone beds are mostly planar-laminated. Some sandstone beds at the base of this package contain muddy bands with dewatering flame structures.

81.75-66.75 m: Thinning upwards package of thick to medium-bedded LFS and VFS. Occasionally interbedded with thin intervals of thin-bedded FSi. The thickes LFS have dominant structureless bases with mudclast materials and mudclast chip bands at the top of the bed. Medium-bedded sandstones show a combination of ripple, wavy and planar laminations. Erosional bases within the sandstones are abundant.

66.75m-23.50 m: Thick package of interbedded medium to thin-bedded structured VFS and thin-bedded FSi. Locally erosional surfaces are abundant at sandstone bed bases. Structures include ripple (including stoss-side preserved climbing), wavy and planar lamination. Thin sandstone beds show dominantly planar lamination.

23.50-0.00 m: Package of interbedded thin-bedded VFS and thin-bedded FSi. Siltstone beds are often planar laminated. Sandstone beds show dominantly ripple-lamination, but can also show wavy and planar lamination. Thicker sandstone beds often include climbing ripple-lamination. Bioturbation is almost absent.

A.3 LOBE 2 descriptive core logs

BK01- Unit 5

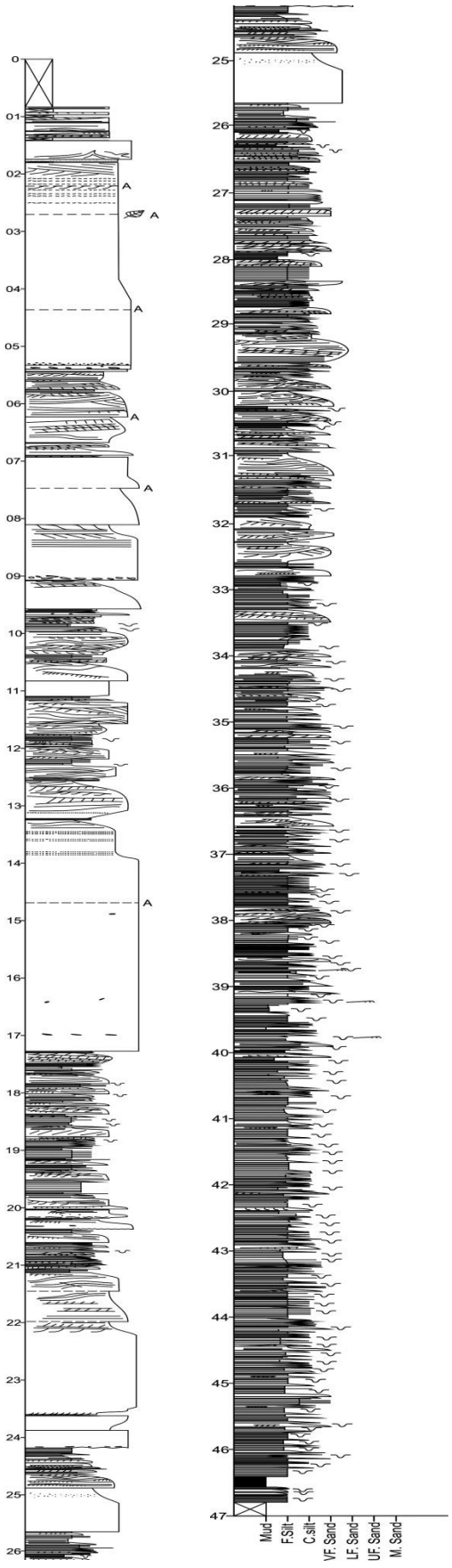

BK01 – Fan 3

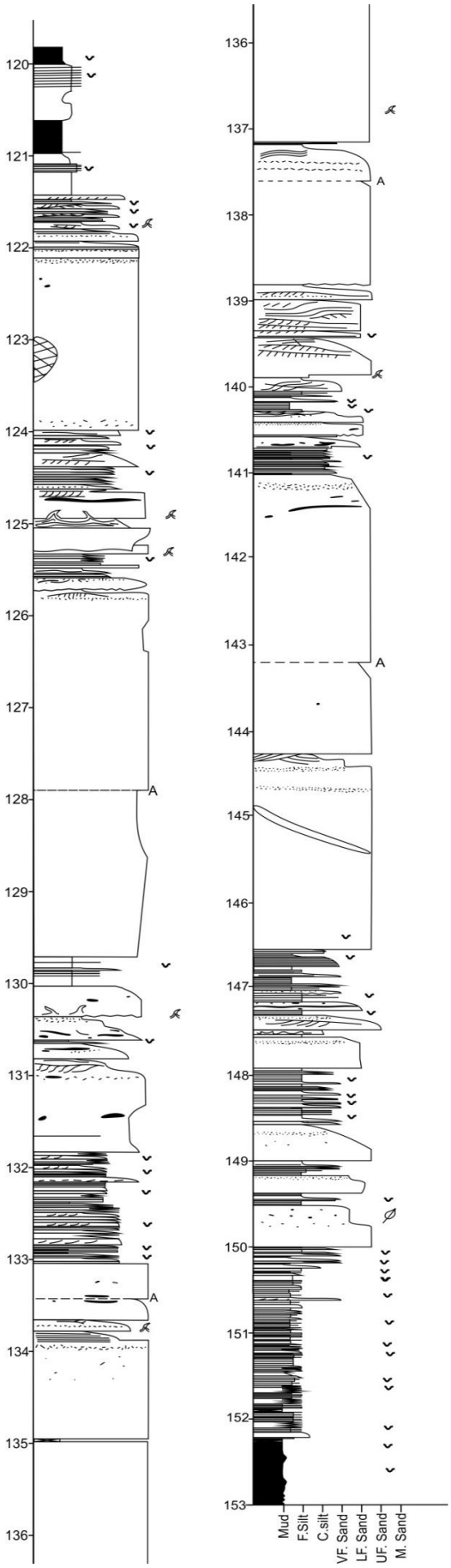
120
121
122
123
124
125
126
127
128
129
130
131
132
133
134
135
136
A
136
137
138
139
140
141
142
143
144
145
146
147
148
149
150
151
152
153
A
Mud
F.Silt
C.silt
VF. Sand
LF. Sand
UF. Sand
M. Sand

KK01 – Fan 3

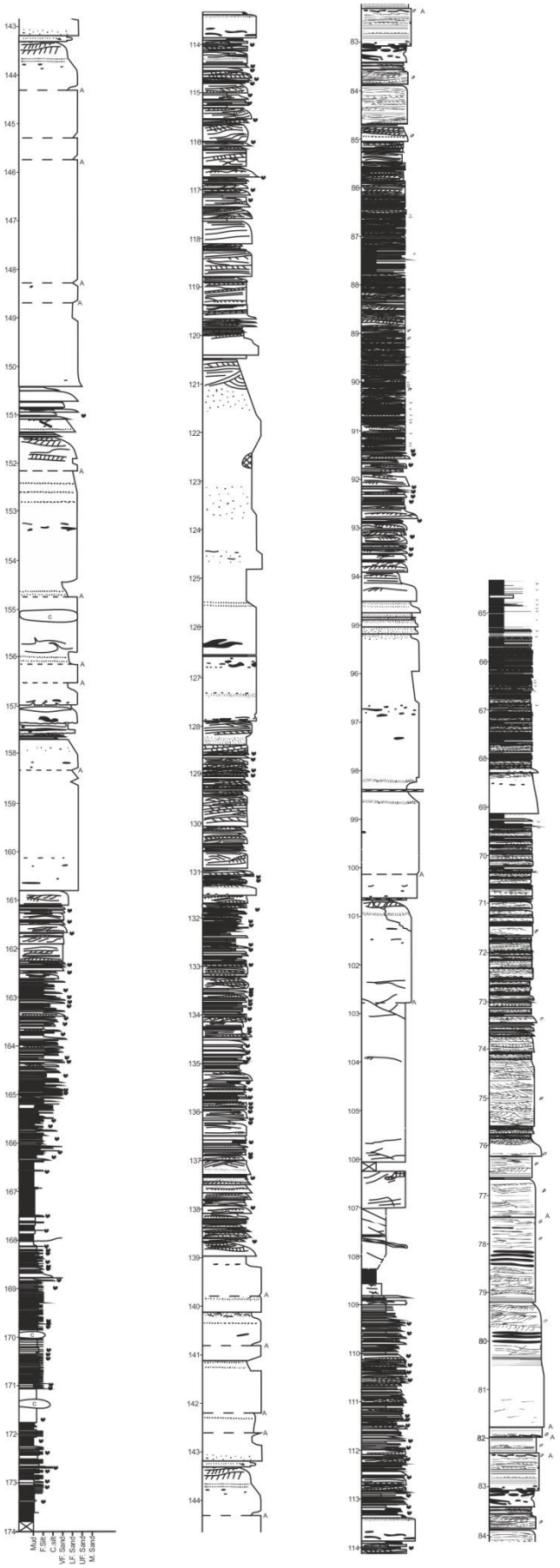

GBE01 – Fan 3

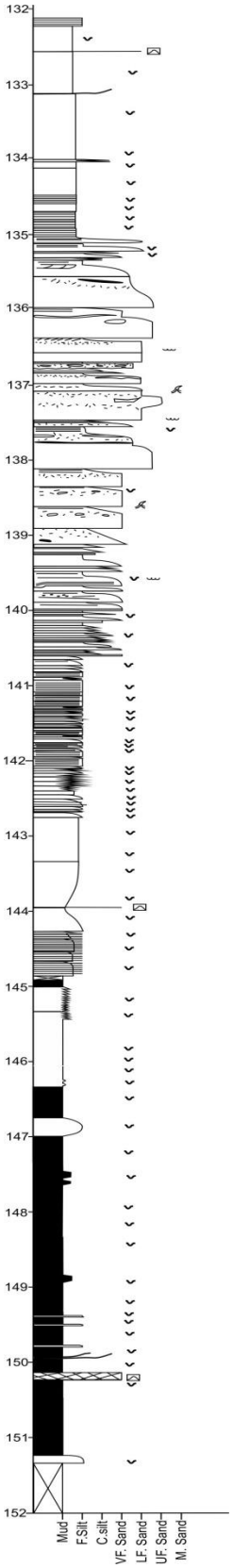
132
133
134
135
136
137
138
139
140
141
142
143
144
145
146
147
148
149
150
151
152
Mud
F.Silt
C.silt
VF. Sand
LF. Sand
UF. Sand
M. Sand

OR01 – Unit 5

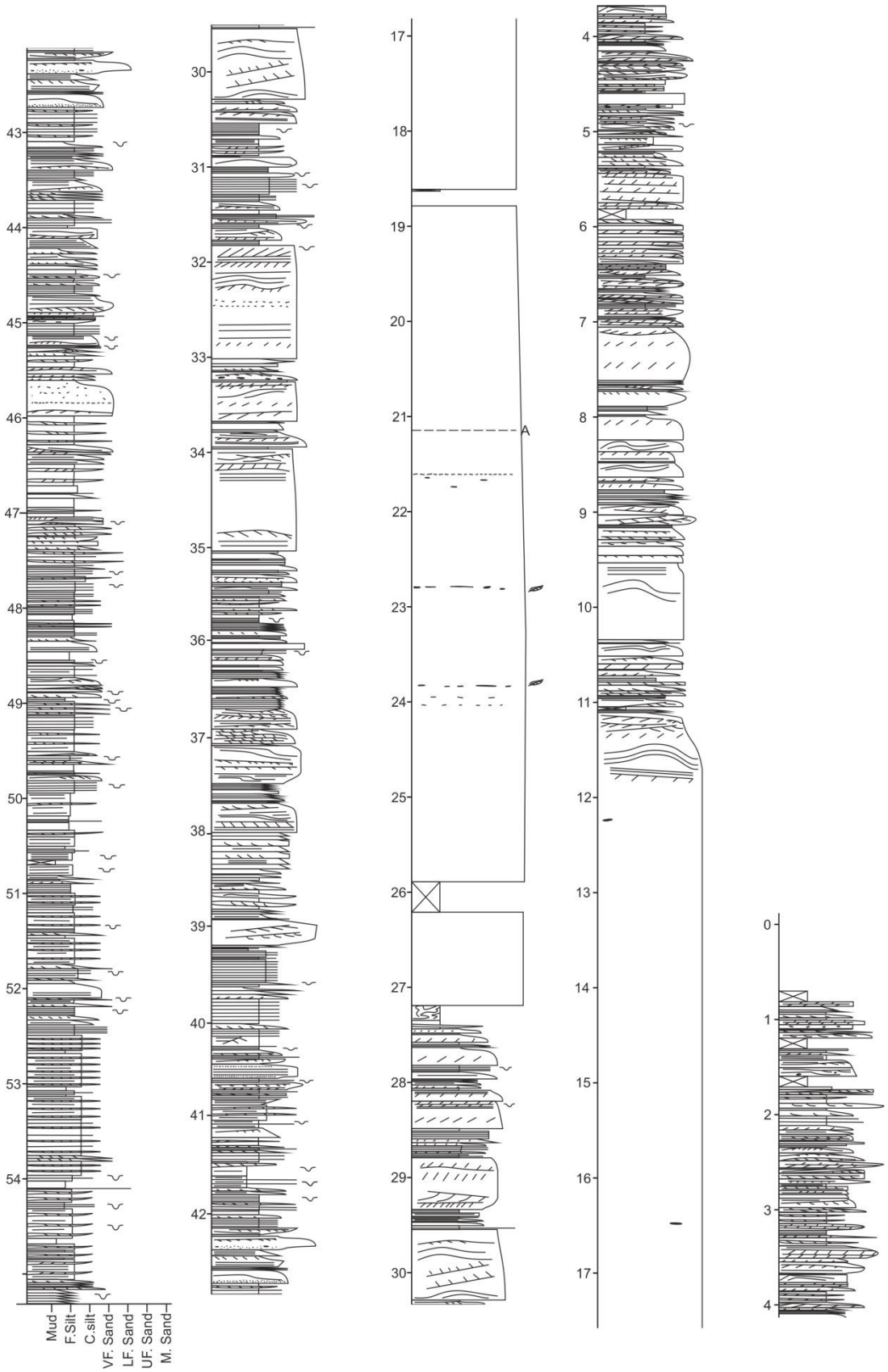
43
44
45
46
47
48
49
50
51
52
53
54
30
31
32
33
34
35
36
37
38
39
40
41
42
17
18
19
20
21
22
23
24
25
26
27
28
29
30
A
4
5
6
7
8
9
10
11
12
13
14
15
16
17
0
1
2
3
4
Mud
F.Silt
C.silt
VF. Sand
LF. Sand
UF. Sand
M. Sand

OR01 – Fan 3

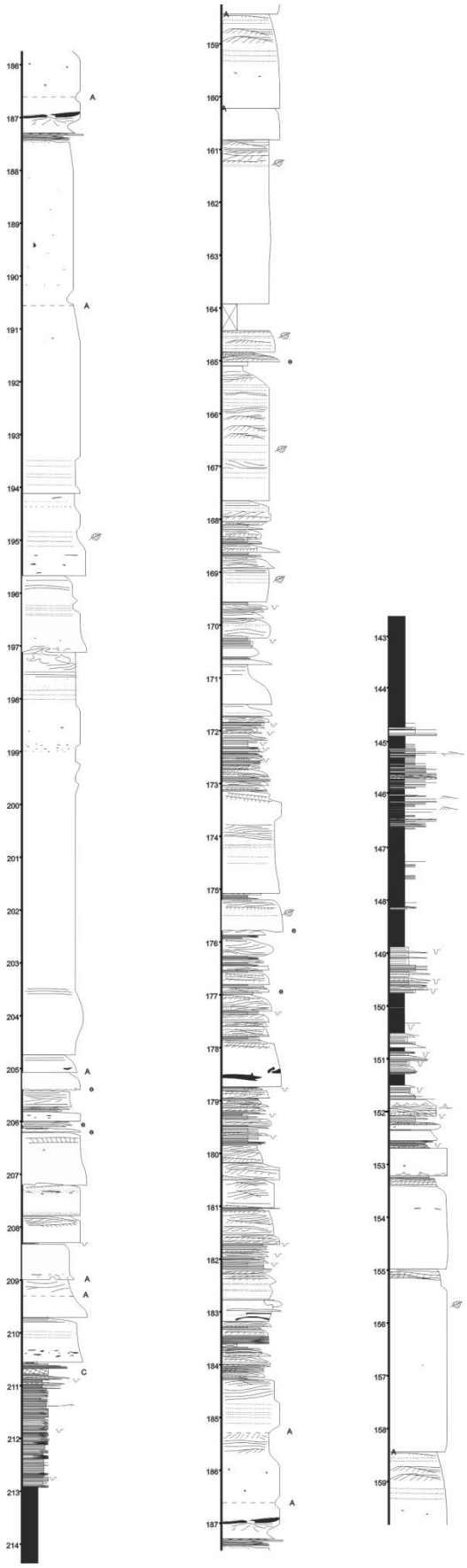

DK01 – Unit B

Appendix B
Outcrop data details

Within Appendix B, all details on sedimentary log data which could not be presented within any of the thesis chapters, is presented.

B.1 Outcrop log locations

Chapter 4

System	Area			UTM Zone
Fan 3	Kleine Rietfontein			34 H
Panel log name	UTM Base		UTM Top	
K1	397003	6369068	397067	6369076
K2	397010	6369707	-	-
K3	396946	6369739	397002	6369728
K4	396935	6369791	396974	6369817
K5	396963	6369839	396954	6369832
K6	396830	6369952	396961	6369899
K7	396958	6370156	397145	6370104
K8-K9	397217	6370202	397197	6370269
K10	397160	6370499	397339	6370410
K11	397434	6371072	397517	6371027
K12	397539	6371251	397574	6371247
K12	-	-	397625	6371295
K13	396788	6371481	396715	6371540
K14	397796	6369904	397518	6370083
K15	398127	6370001	397958	6370045
K16	398462	6369936	398497	6369942
K17	397885	6369852	397922	6369867
K18	397868	6369788	397839	6369777
K19	397189	6369631	397170	6369694
K20	398384	6369369	398403	6369393
K21	397021	6368618	397047	6368590
K21	397010	6368657	397028	6368689
K22	397420	6368815	-	-

System	Area			UTM Zone
Unit A5	Wilgerhout River			34 H
Log Name	UTM Base		UTM Top	
W1	485982	6327777	-	-
W2	485987	6327780	-	-
W3-W4-W5	486033	6327807	-	-
W6	486060	6327815	-	-
W7	486089	6327899	486061	6327775
W8-W9	486082	6327825	-	-
W10	486109	6327805	-	-
W11	486130	6327831	-	-
W12	486168	6327837	486158	6327817
W13	486194	6327894	486230	6327814
W14	486229	6327853	486232	6327835
W15	486257	6327819	486256	6327920
W16	486330	6327877	-	-
W17	486368	6327953	486363	6327881

Chapter 5

System	Area			UTM Zone
Unit B	Doornkloof			34 H
Log Name	UTM Base		UTM Top	
01	460500	6331182	-	-
02	460920	6331379	-	-
03	460934	6331384	-	-
04	460983	6331396	-	-
05	461005	6331402	-	-
06	461058	6331404	-	-
07	461082	6331435	-	-
08	461312	6331435	461309	6331513
09	461330	6331499	-	-
10	461355	6331501	-	-
11	461379	6331506	-	-
12	461407	6331508	-	-
13	461433	6331512	-	-
14	461458	6331514	-	-
15	461482	6331514	-	-
16	461503	6331518	-	-
17	461531	6331519	-	-
18	461550	6331524	-	-
19	461567	6331527	-	-
20	461624	6331485	461594	6331552
21	461627	6331536	-	-
22	461683	6331502	461669	6331676
23	461681	6331554	-	-
24	461713	6331527	461808	6331735
25	461791	6331625	461792	6331640

26	461836	6331622	461866	6331653
27	461847	6331625	-	-
28	461860	6331625	-	-
29	461869	6331627	-	-
30	461878	6331627	-	-
31	461886	6331629	-	-
32	461894	6331629	-	-
33	461904	6331630	-	-
34	461912	6331630	-	-
35	461923	6331638	461926	6331658
36	461962	6331628	-	-
37	461953	6331623	-	-
38	462002	6331630	461991	6331659
39	462081	6331631	462029	6331661
40	462047	6331636	-	-
41	462080	6331630	462028	6331661
42	462502	6331582	462548	6331753

Chapter 6

System	**Area**		**UTM Zone**	
Unit 5	**Blaukop**		**34H**	
Panel Log name	**UTM Base**		**UTM Top**	
01	412073	6378737	412072	6378754
02	412378	6379118	-	-
03	412529	6379118	412542	6379105
04	412505	6379188	412527	6379149
05	412664	6379212	412671	6379200
06	412785	6379168	412773	6379154
07	412711	6379251	412743	6379230
08	412626	6379348	-	-
09	412583	6379358	-	-
10	412532	6379392	-	-
11	412487	6379424	-	-
12	412472	6379437	-	-
13	412334	6379620	-	-
14	412260	6379656	-	-
15	412234	6379668	-	-
16	412175	6379702	-	-
17	411880	6379870	411855	6379888
18	411931	6379968	-	-
19	411978	6380071	411962	6380087
20	412168	6380112	412199	6380093
21	412319	6380194	412319	6380174
22	412273	6380230	412300	6380186
23	412369	6380430	412394	6380416
24	412378	6380514	412402	6380442
25	412404	6380607	412415	6380614
26	412416	6380656	412435	6380622

System	Area			UTM Zone
Fan 3	Ongeluks River			34 H
Log Name	UTM Base		UTM Top	
OR01	403898	6365901	-	-
OR02	403968	6365922	403946	6365943
OR03	403991	6365929	-	-
OR04	404122	6365968	-	-
OR05	404175	6365976	-	-
OR06	404216	6365976	-	-

System	Area			UTM Zone
Fan 3	De Syfer			34 H
Log Name	UTM Base		UTM Top	
Sy1	400654	6367407	400689	6367428
Sy2	400597	6367677	400636	6367656
Sy03	399547	6367597	399568	6367600
Sy04	399593	6367578	-	-
Sy05	399612	6367567	-	-
Sy06	399641	6367548	-	-
Sy07	399682	6367522	-	-
Sy08	399707	6367504	-	-

System	Area			UTM Zone
Fan 3	Kleine Riet Fontein			34 H
Log Name	UTM Base		UTM Top	
KRF01	396958	6370156	397145	6370104

B.2 Palaeoflow data

Chapter 4

Kleine Riet Fontein – Fan 3

	K1	
Base	Middle	Top
342	55	88
	355	34
	28	0
	0	52
	88	90
	308	340
		70
		88
		82
		60
		42
		92

	K7	
Base	Middle	Top
29	212	75
59	160	148
355	155	150
34	134	146
17	168	143
22	142	83
354	108	140
118	168	85
102	161	85
98	142	96
133	108	112
80	168	40
154	161	44
138	144	6
92	114	36
48	146	60
45	140	48
114	122	26
158	90	22
42	115	34
164	103	60
46	50	98
34	204	106
82	190	10
78	98	22
38	63	31
37	154	54
78	68	17
56	144	53
82	190	62
38	166	28
37	135	
62	137	
74	136	
92	118	
153	42	
202	38	
78	60	

	K8	
Base	Middle	Top
12	62	30
38	90	8
54	5	31
74	25	40
32	68	20
24	343	22
345	338	58
18	26	
24	358	
310		
356		
355		
78		
31		
345		
11		
65		
20		
17		
40		
33		
45		
34		
18		
15		
35		
36		
18		
27		

	62	50
	42	120
	78	40
	74	56
	93	134
	136	68
	186	161
	129	161
	98	98
	60	62
	76	112
	32	120
	114	98
	88	152
	78	100
	38	70
	115	54
	100	74
	112	60
	85	118
	100	78
	94	55
	49	18
	74	30
	104	60
	95	54
	170	94
		92
		80
		60
		24
		88
		74
		94
		54
		106
		173
		60
		54

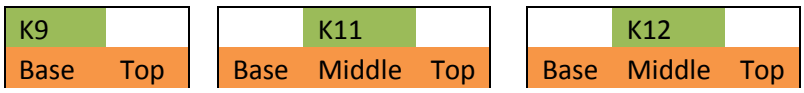

58	157
355	156
50	185
60	154
18	136
344	135
74	10
	10
	22
	9
	354
	22
	342
	16
	244
	0
	10
	13
	55
	18
	25
	359
	348
	46

12	62	30
38	90	8
54	5	31
74	25	40
32	68	20
26	343	22
345	338	58
18	26	308
24	358	340
310	78	350
356	50	290
355	352	302
78	50	334
31		
345		
11		
65		
20		
17		
40		
33		
45		
34		
18		
15		
35		
36		
18		
27		
94		
332		
40		
352		
58		
78		
56		
310		
125		
130		
110		
152		
42		
60		
5		
204		
149		
50		

342	338	349
353	335	5
341	30	3
338	350	30
348	340	8
30	0	10
358	355	340
2	320	325
40	338	305
253	352	335
354	338	348
0	348	355
42	358	346
21	338	8
288	335	332
328	35	0
32	20	2
17	350	345
33		355
28		300
12		302
15		355
330		309
34		333
4		308
345		328
44		340
348		348
		8
		315
		332
		358
		335

	K13	
Base	Middle	Top
325	348	290
305	298	325
342	26	328
280	4	334
330	340	320
326	14	270
4	15	349
325	345	308
282	345	262
14	332	306
345	342	292
4	0	345
330	358	325
326	345	274
342	3	290
342	302	325
14	326	355
		325

	K14	
Base	Middle	Top
68	50	314
348	350	318
38	358	348
80	34	343
40	350	20
354	6	300
14	338	335
340	355	270
292	14	352
300	32	342
260	352	4
258	14	36
298	0	16
264	26	346
316	22	346
270	352	0
340	322	32
333	30	18
354	0	8
328	8	0
5	358	9
35	354	8
2	28	12
340		
76		
350		
348		
32		
28		
38		
352		

	K15	
Base	Middle	Top
56	306	270
88	338	236
72	350	236
40	336	350
82	340	330
32	0	298
48	4	310
78	0	0
52	354	
58	350	
52	10	
32	8	
40	48	
50	0	
10		
350		
354		
332		
6		
28		
38		
326		
340		
26		
34		
358		
348		
12		
0		
4		
346		
330		
16		
6		
350		
350		
325		
338		
0		
350		
350		
310		

		340
		338
		340
		10

K16	
Middle	Top
18	100
22	32
68	36
0	126
42	34
54	58
22	100

K17
Base
62
42
90
95
16
18
86
356
18
340
350
0
354
334

	K19	
Base	Middle	Top
24	280	2
342	0	350
28	312	5
2	8	298
4	10	334
332	350	322
314	358	342
358	342	
334	34	
14	308	
328	352	
352	338	
	2	
	318	
	0	
	320	
	334	
	300	
	0	
	328	
	335	
	345	
	20	
	0	
	320	
	316	
	344	
	340	
	336	
	328	

K20	
Middle	Top
100	358
10	354
350	0
18	296
348	284
352	326
46	298
350	315
16	338
354	

Unit A5	Scour-fill	Underlying heterolics
	95	94
	73	76
	103	107
	75	92
	101	73
	89	83
	70	89
	94	85
	107	
	71	
	79	
	89	
	94	
	86	
	95	
	94	
	92	
	99	
	89	
	101	
	95	
	96	

Chapter 5

Doornkloof – Unit B

	Unit B1				Unit B2		
Log #	2	04-07	15	22-24	20	22	24
	108	82	134	65	88	342	108
	110	88	122	116	310	308	65
	65	78	90	114	286	270	348
		60	80	125		315	358
		90	135	70		315	73
		85	85	55		270	60
		110	68	60		318	58
		98	108	85		335	25
		118	110	120		286	54
				70			31
				84			80
				110			65
				104			38
							68
							35
							95
							60
							5
							42
							38

Old Railway – Unit B

Unit B2	WEST		EAST		
	120	124	144	138	134
	190	116	110	119	104
	180	145	132	72	145
	142	103	113	114	112
	128	138	130	109	104
	145	139	144	100	96
	126	120	118	112	138
	119	108	107	128	122
	138	107	99	130	126
	110	137	118	140	136
	108	111	110	125	100
	123	122	95	114	118
	140	106	124	119	
	142	92	111	106	
	128	150	112	135	
	122		126	142	
	108		103	115	
	102		117	122	

Chapter 6

Blaukop – Unit 5

Log #	22	21	20	18	11	7	26	3	2	9	14	15	24	25	16	17
LOBE1	30	78			344?										20	
	44	34													26	
	36	26													82	
	48	42													40	
LOBE 2															24	
LOBE 3		66														
		32														
		330														
		350														
LOBE 4					332											
					14											
					275											
					340											
					346											
LOBE 5		38				46	316			350				30	5	

		38 64 40				74 344	315 20 350 350 0 12 10 0 346 358							310 338 278 68 318 342 80 322 344 52	20 18 350	
LOBE 6															15 0 25	
LOBE 7								8 10	332					0 18 32 28 8 30		
LOBE 8															74 58 55 40 340 50	
LOBE 9			32 310 330 30 28 330 0 28									280 310	348 300 297 294			
LOBE 10											14 0 270 0 340 20 354 298 38		355 0 274 315 314 320 355 325 342 340 298			40 20 38 40 54 52 32

													10			
LOBE 11				110 42								330				350 340 340

B.3 Original outcrop logs

Legend

Structures

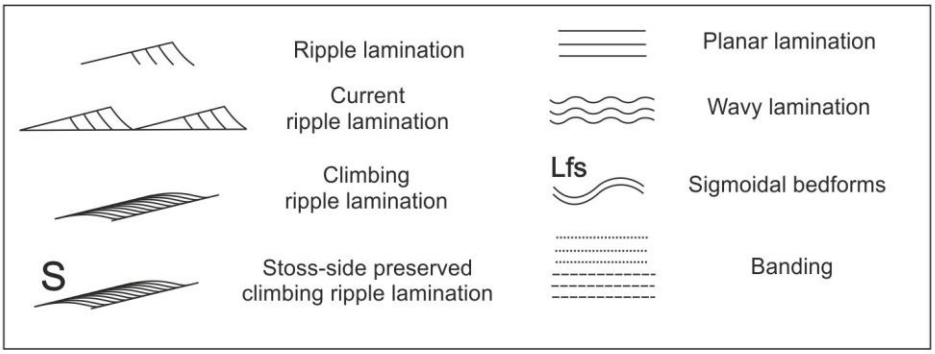

Other

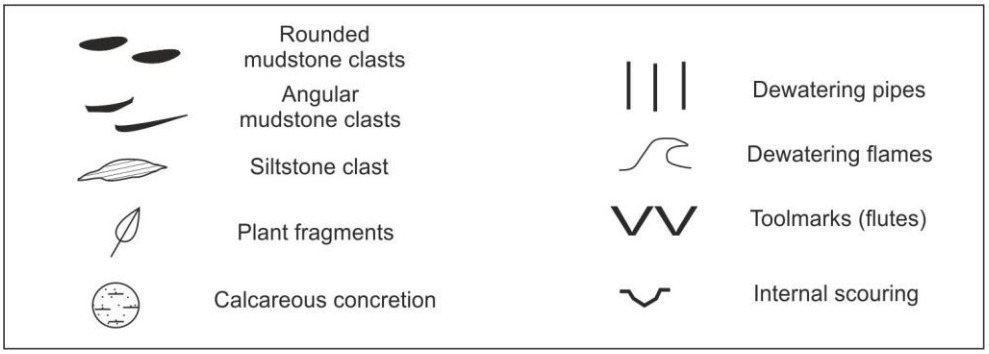

Surfaces

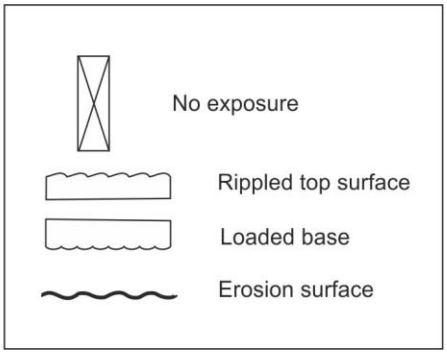

Chapter 4

Kleine Riet Fontein – Fan 3

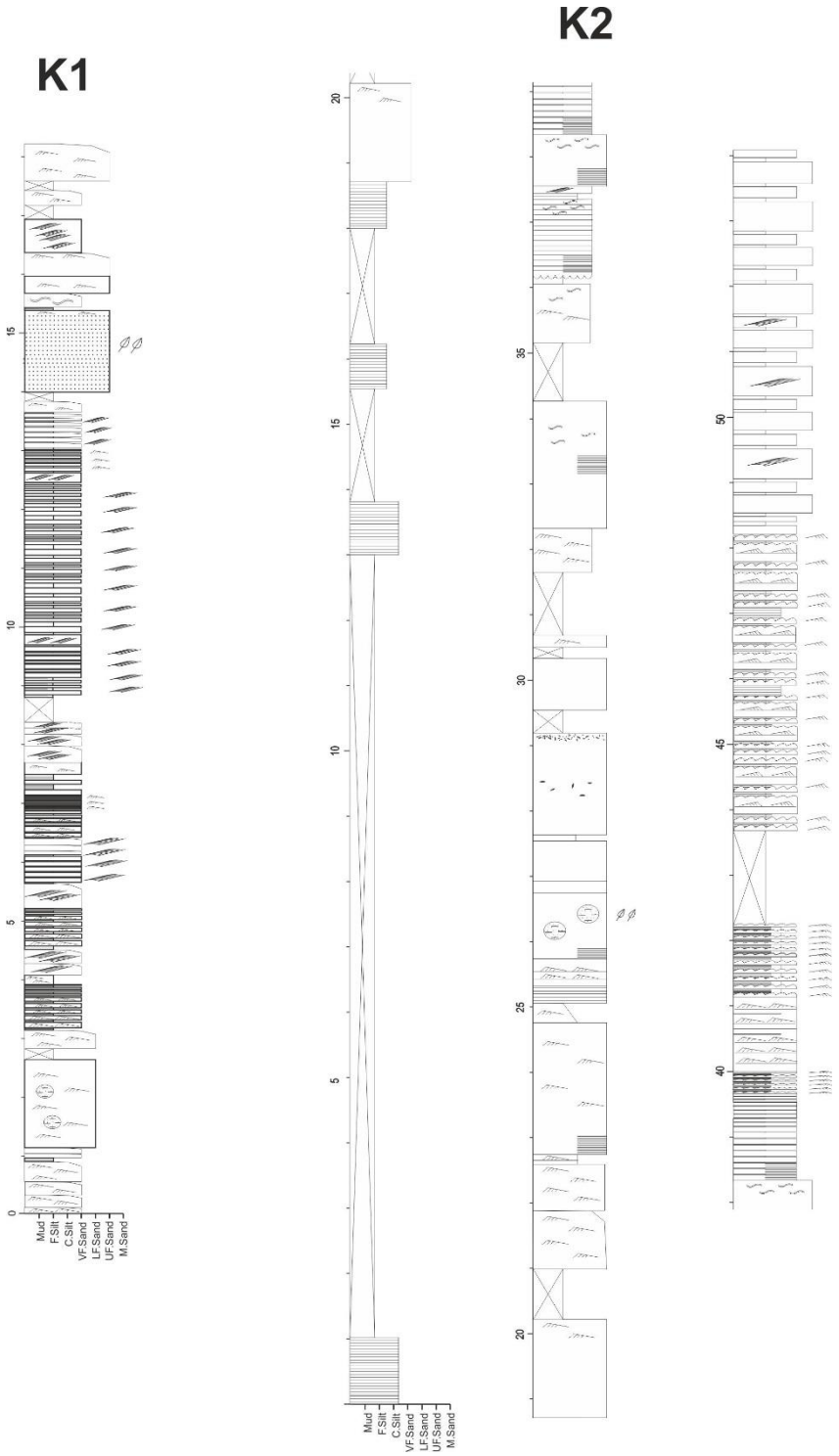

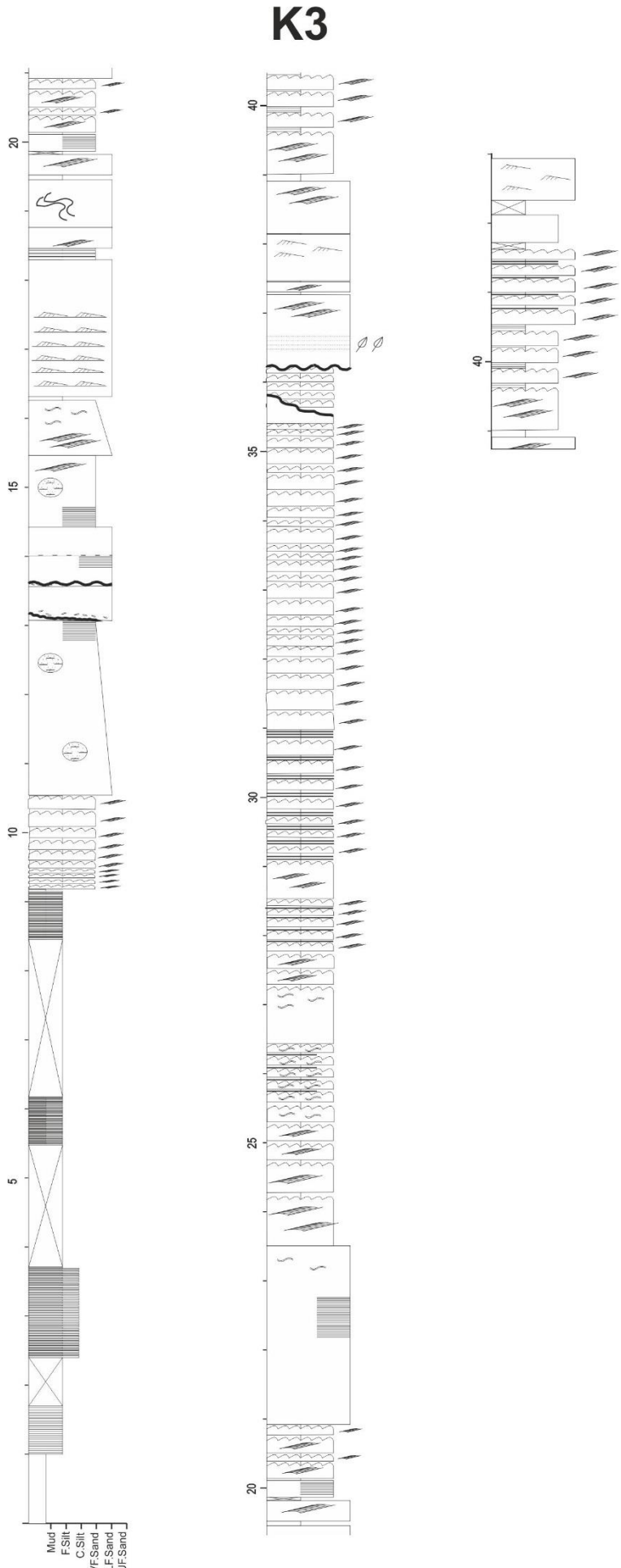
K3
Mud
F.Silt
C.Silt
VF.Sand
LF.Sand
UF.Sand

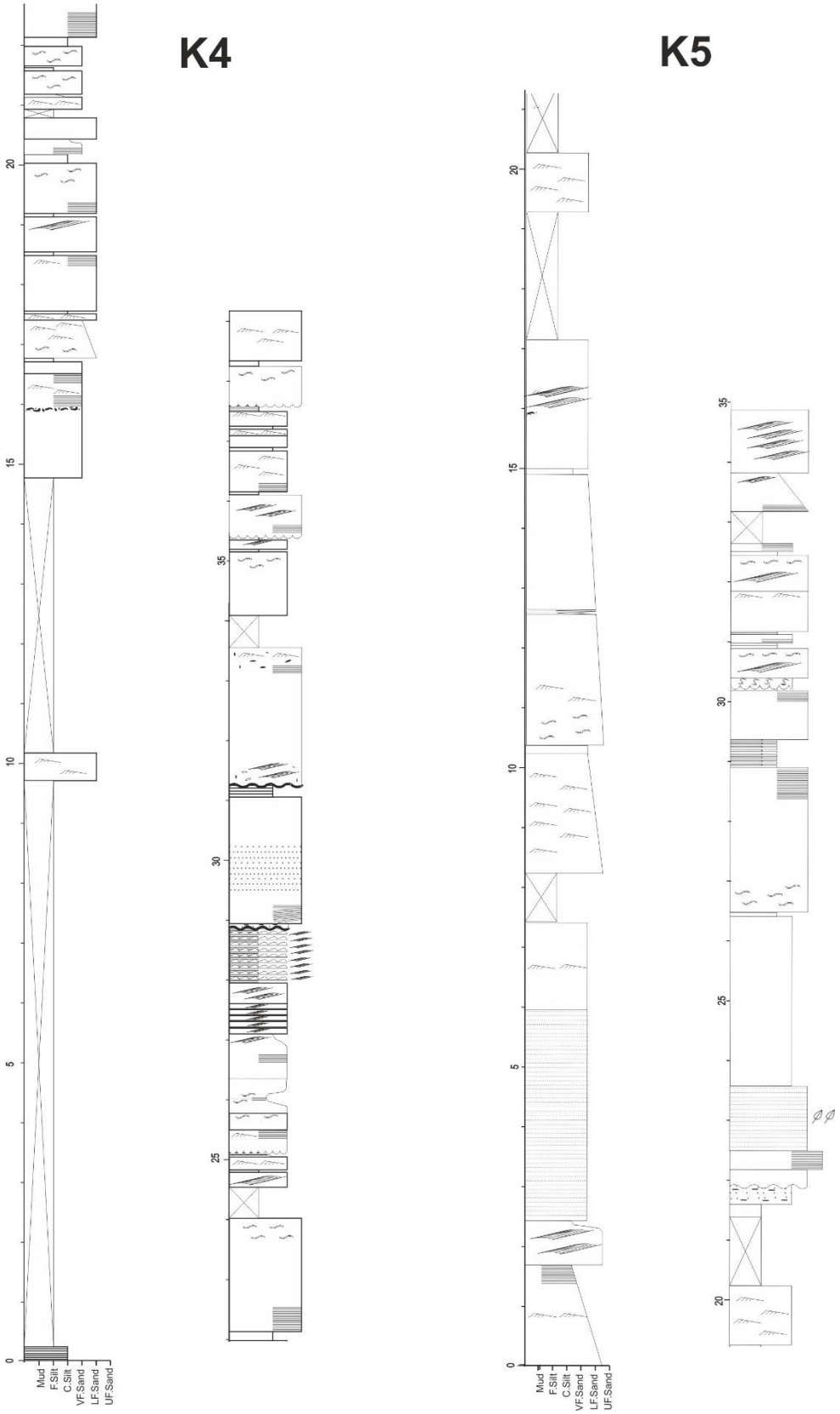
K4
K5
0
5
10
15
20
25
30
35
Mud
F.Silt
C.Silt
VF.Sand
LF.Sand
UF.Sand

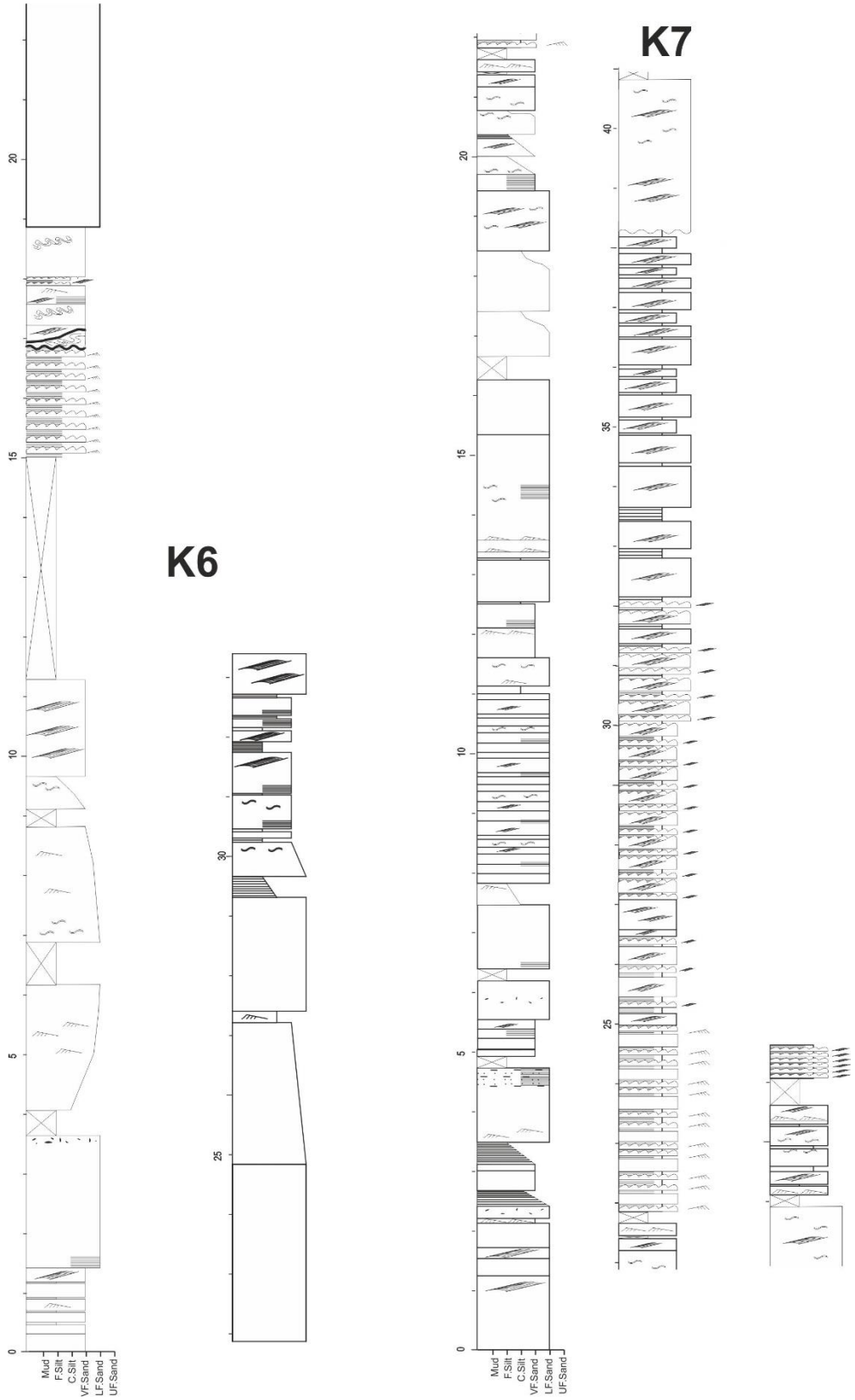
K6
K7
0
5
10
15
20
25
30
35
40
Mud
F.Silt
C.Silt
VF.Sand
LF.Sand
UF.Sand

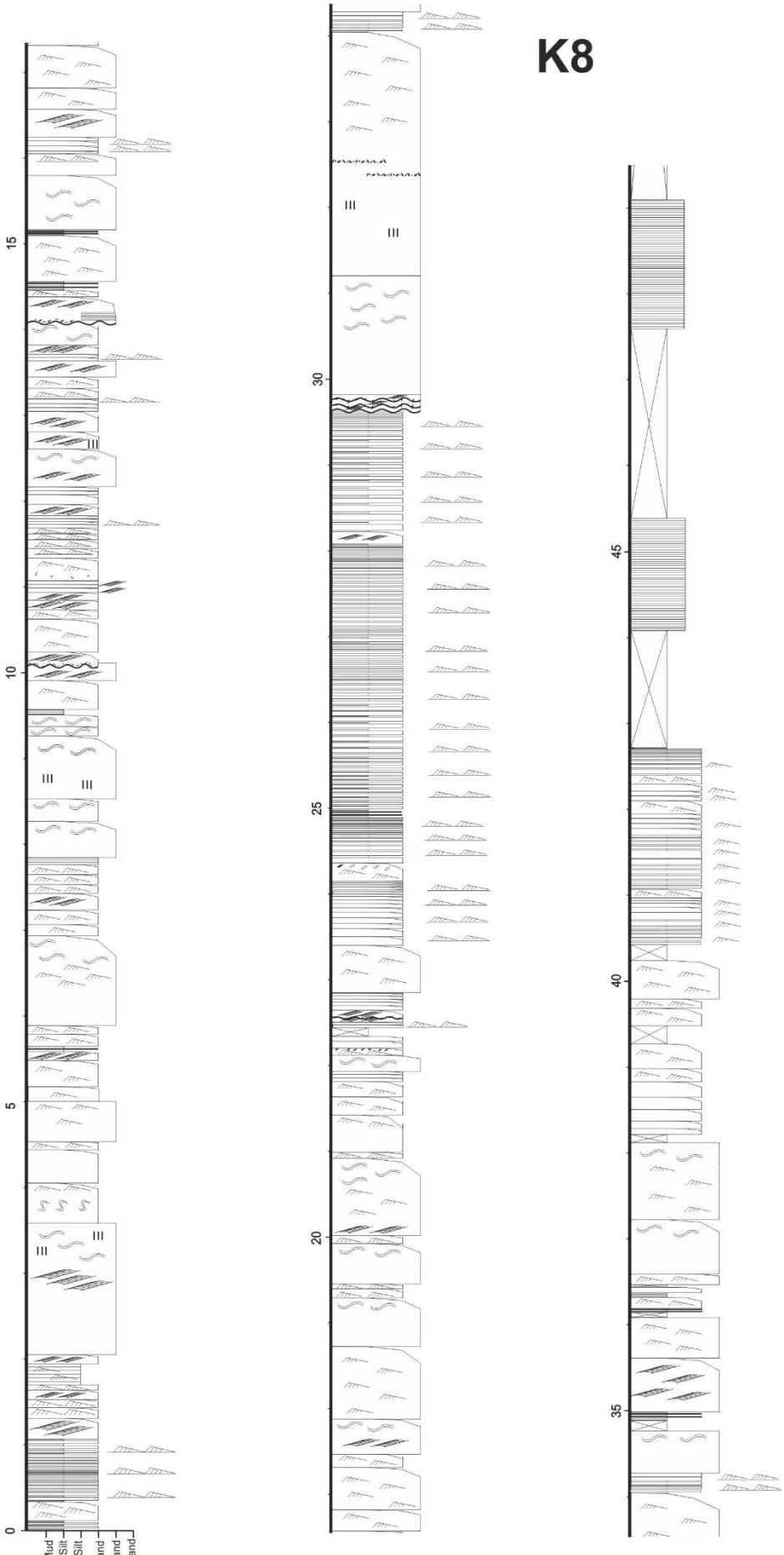
K8
0
5
10
15
20
25
30
35
40
45
Mud
F.Silt
C.Silt
VF.Sand
LF.Sand
UF.Sand

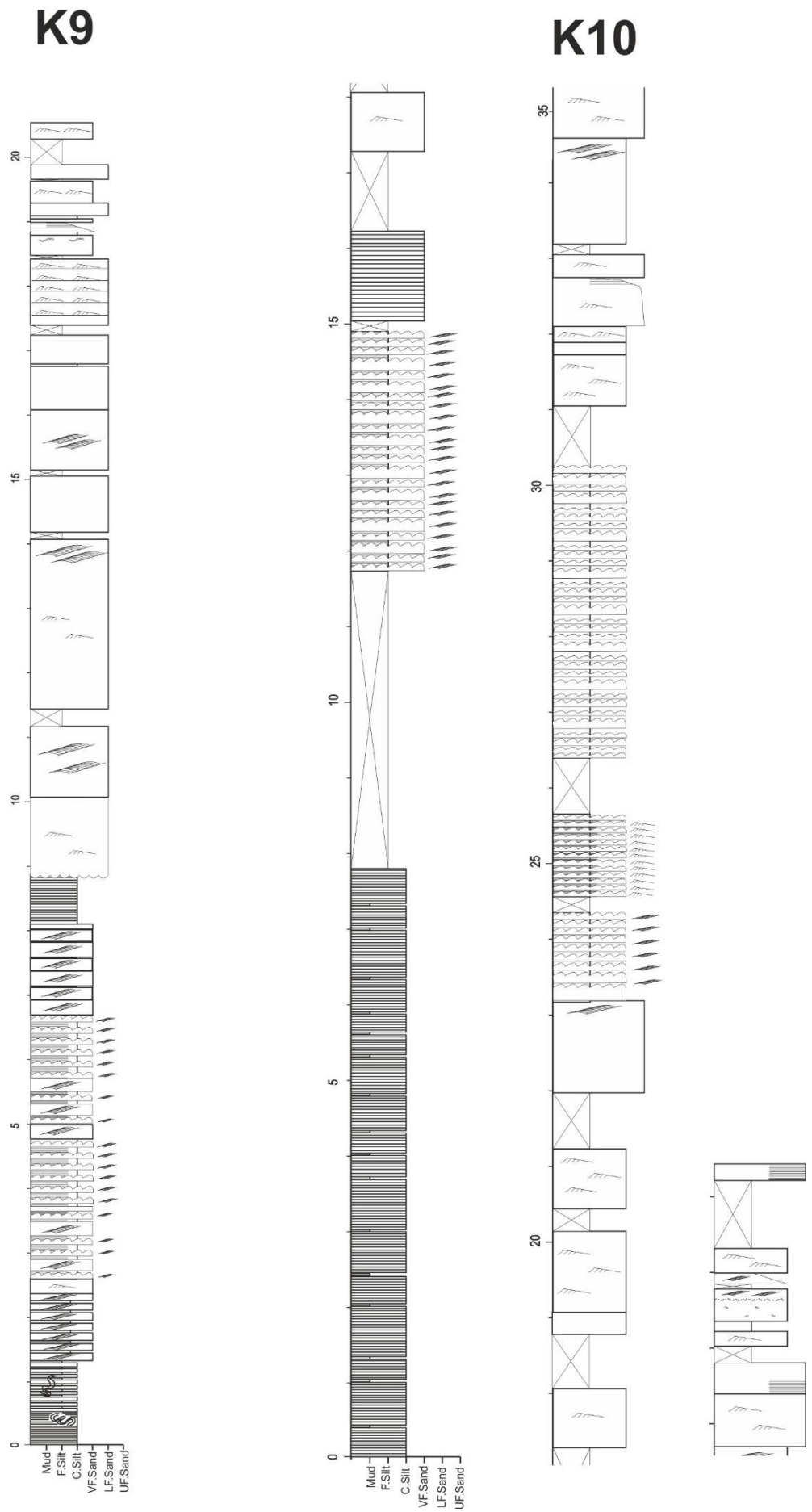
K9
K10
0
5
10
15
20
25
30
35
Mud
F.Silt
C.Silt
VF.Sand
LF.Sand
UF.Sand

K17

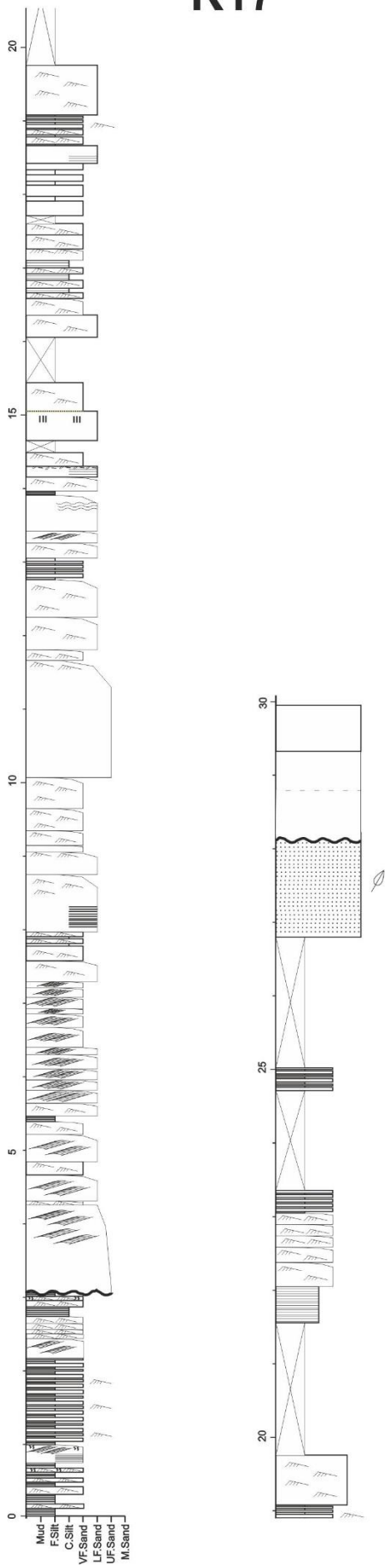
20
15
10
5
0
Mud
F.Silt
C.Silt
VF.Sand
LF.Sand
UF.Sand
M.Sand
30
25
20

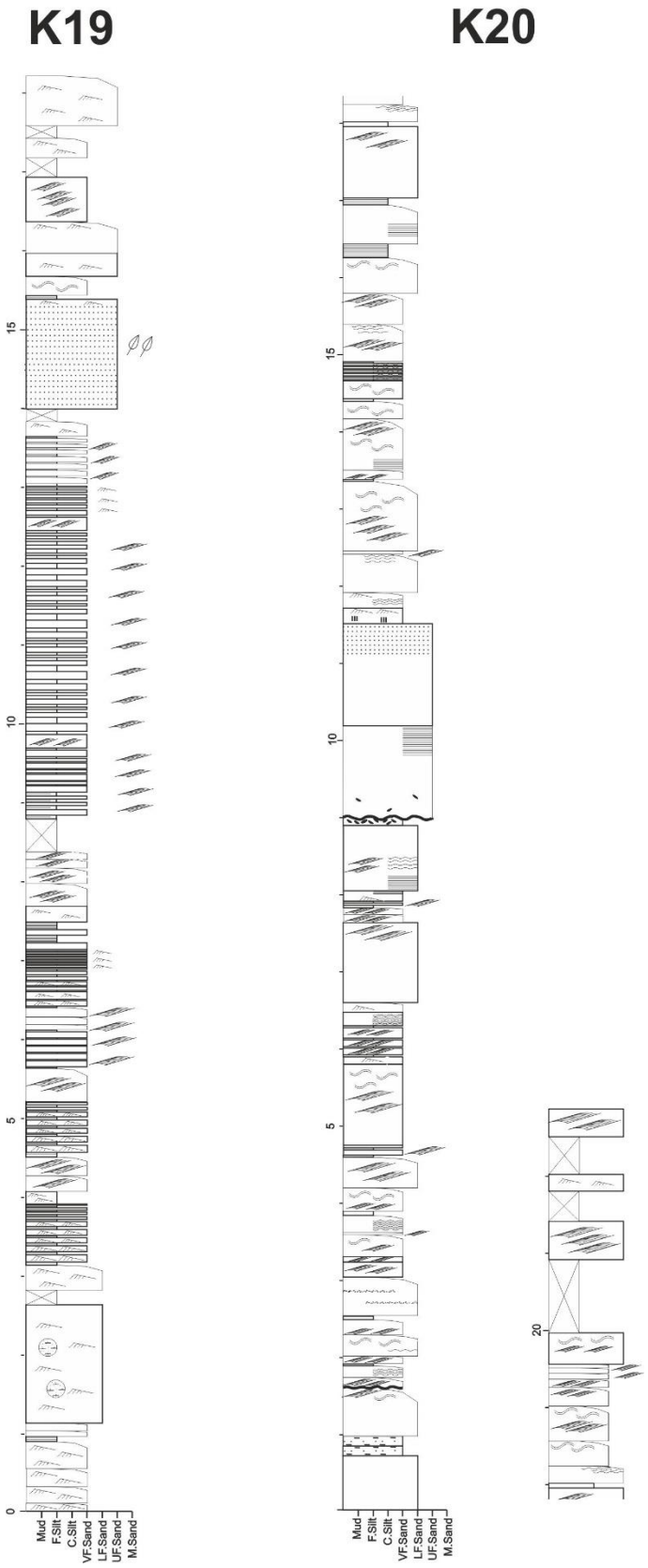
K19
K20
0
5
10
15
20
Mud
F.Silt
C.Silt
VF.Sand
LF.Sand
UF.Sand
M.Sand

Wilgerhout – Unit 5

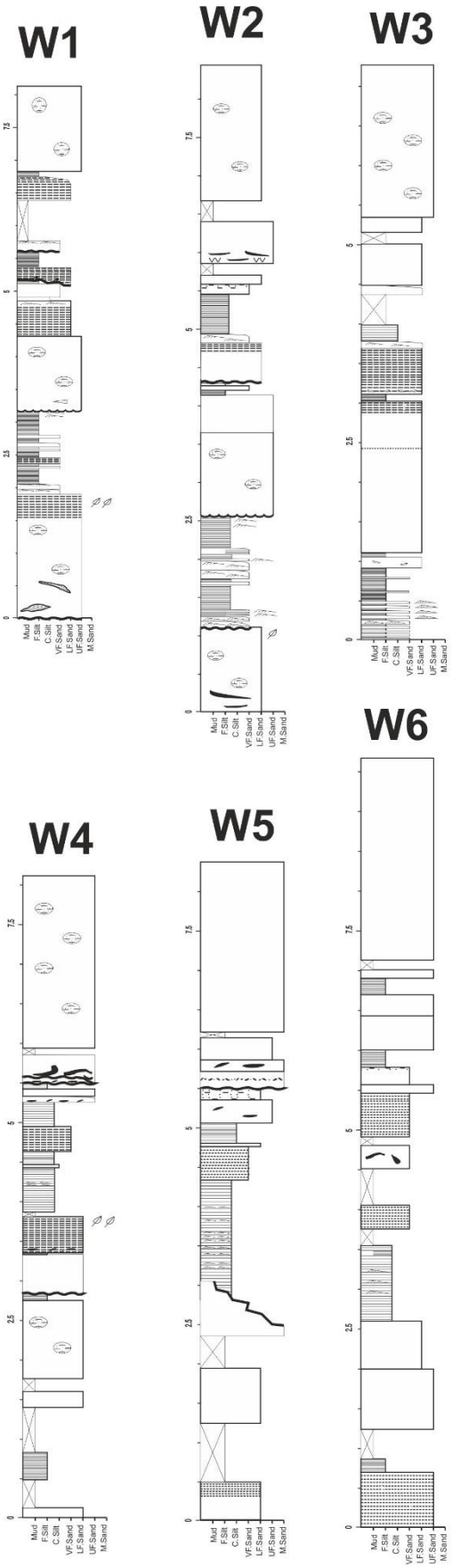


W7
W8
W9
Mud
F.Silt
C.Silt
VF.Sand
LF.Sand
UF.Sand
M.Sand


W10
W11
W12
Mud
F.Silt
C.Silt
VF.Sand
LF.Sand
UF.Sand
M.Sand


W13
W14
W15
0
10
20
30
Mud
F.Silt
C.Silt
VF.Sand
LF.Sand
UF.Sand
M.Sand

W16

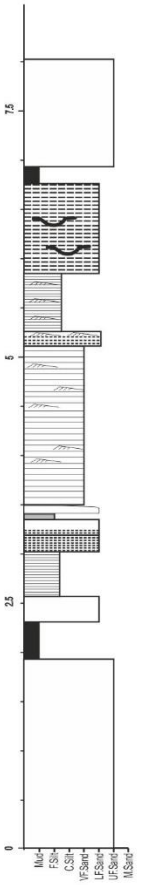
7.5
5
2.5
0
Mud
FSlt
CSlt
VFSand
LFSand
UFSand
MSand

W17

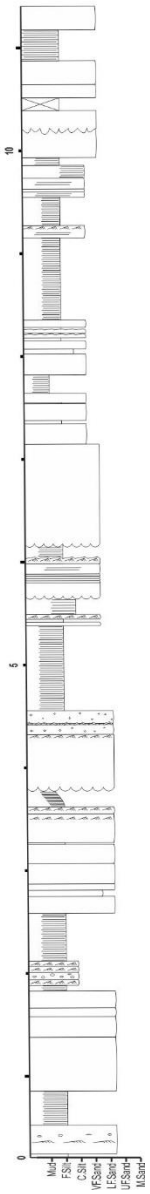
10
5
0
Mud
FSlt
CSlt
VFSand
LFSand
UFSand
MSand

Chapter 5

Unit B – Doornkloof

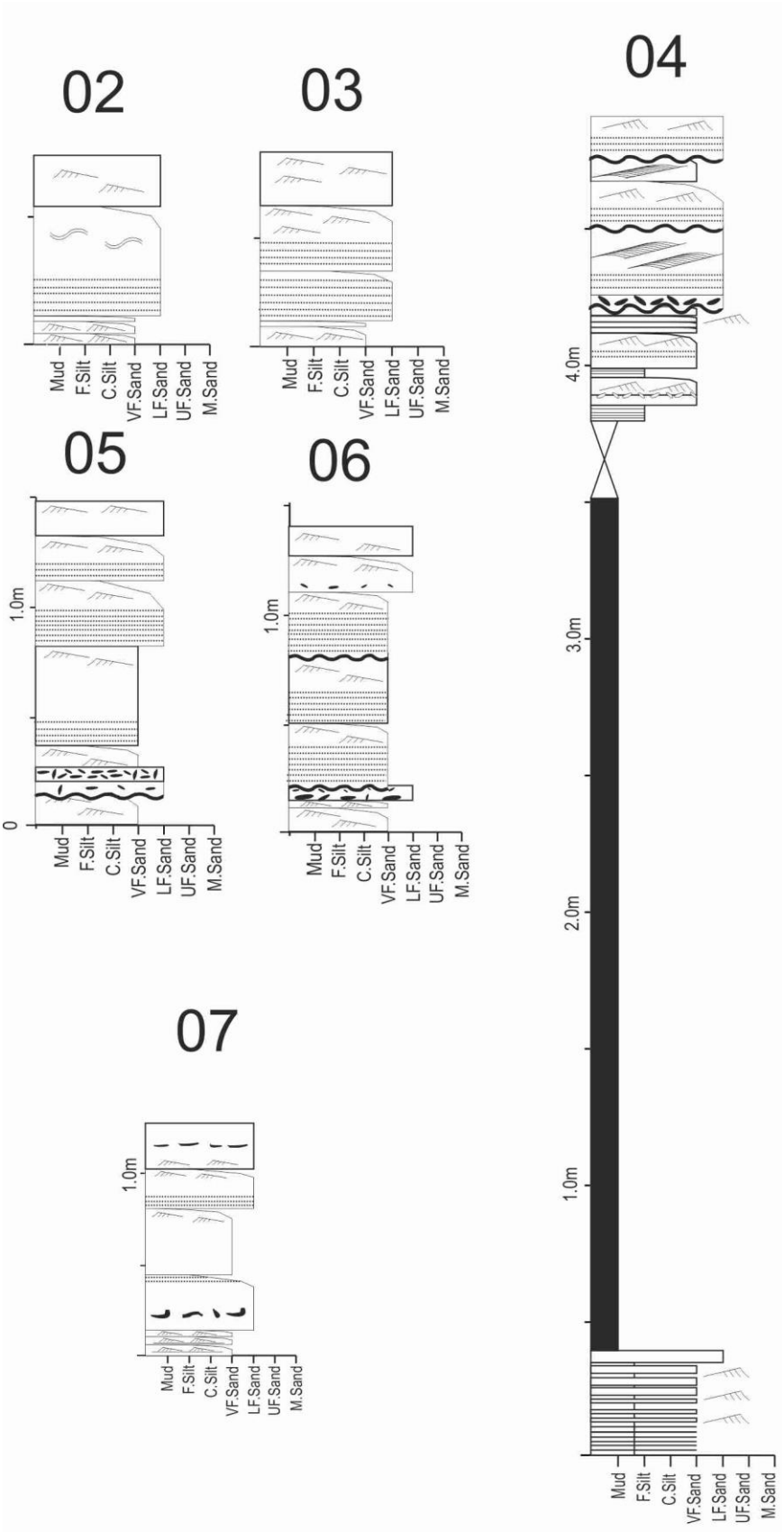

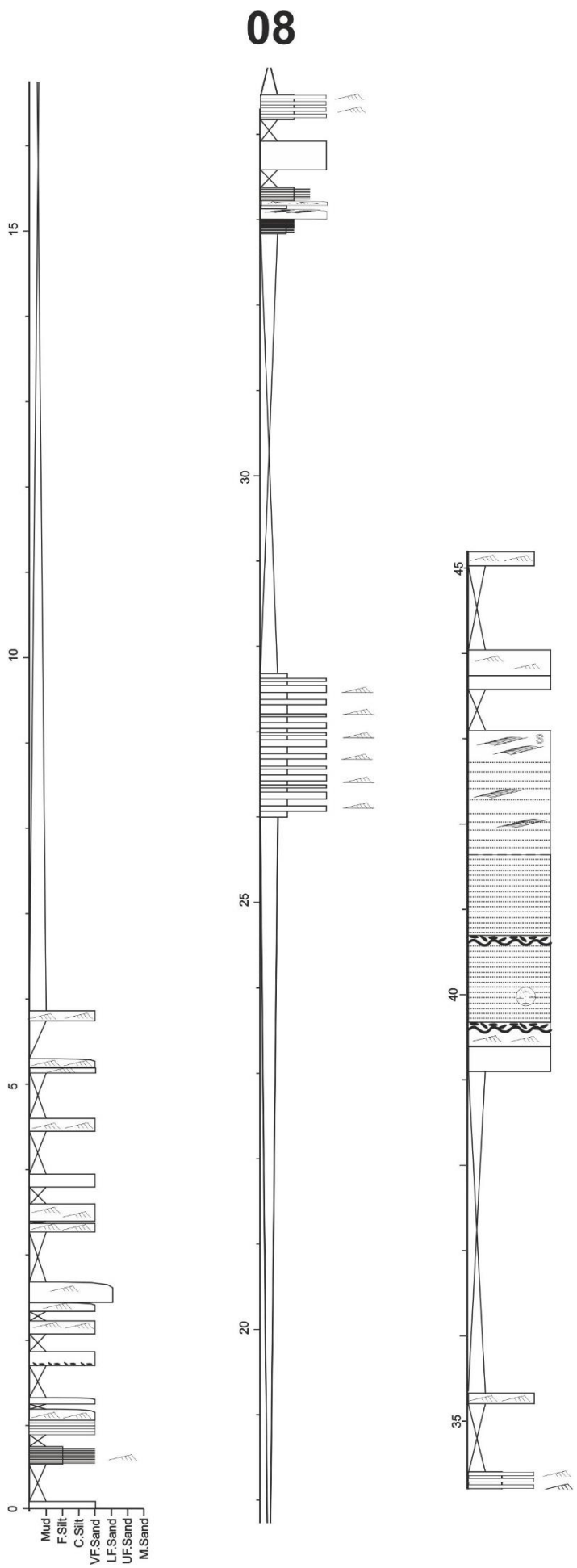
08
0
5
10
15
20
25
30
35
40
45
Mud
F.Silt
C.Silt
VF.Sand
LF.Sand
UF.Sand
M.Sand

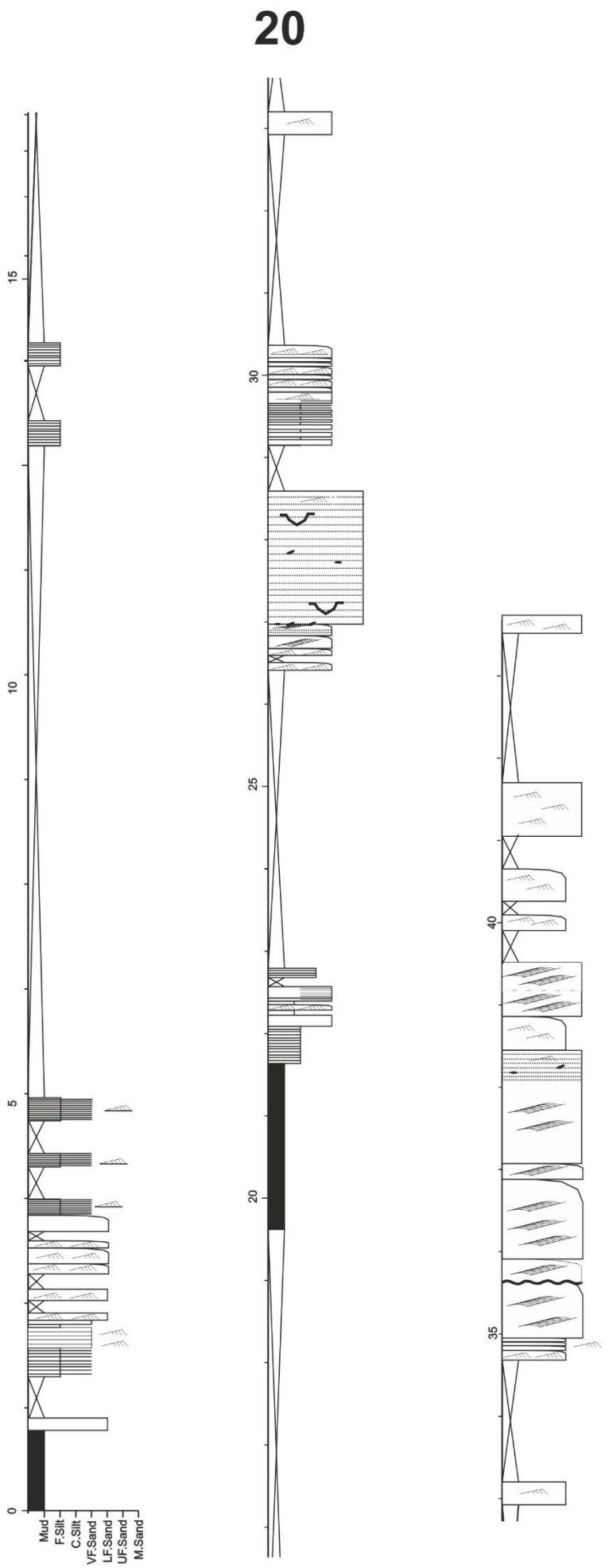
20
0
5
10
15
20
25
30
35
40
Mud
F.Silt
C.Silt
VF.Sand
LF.Sand
UF.Sand
M.Sand

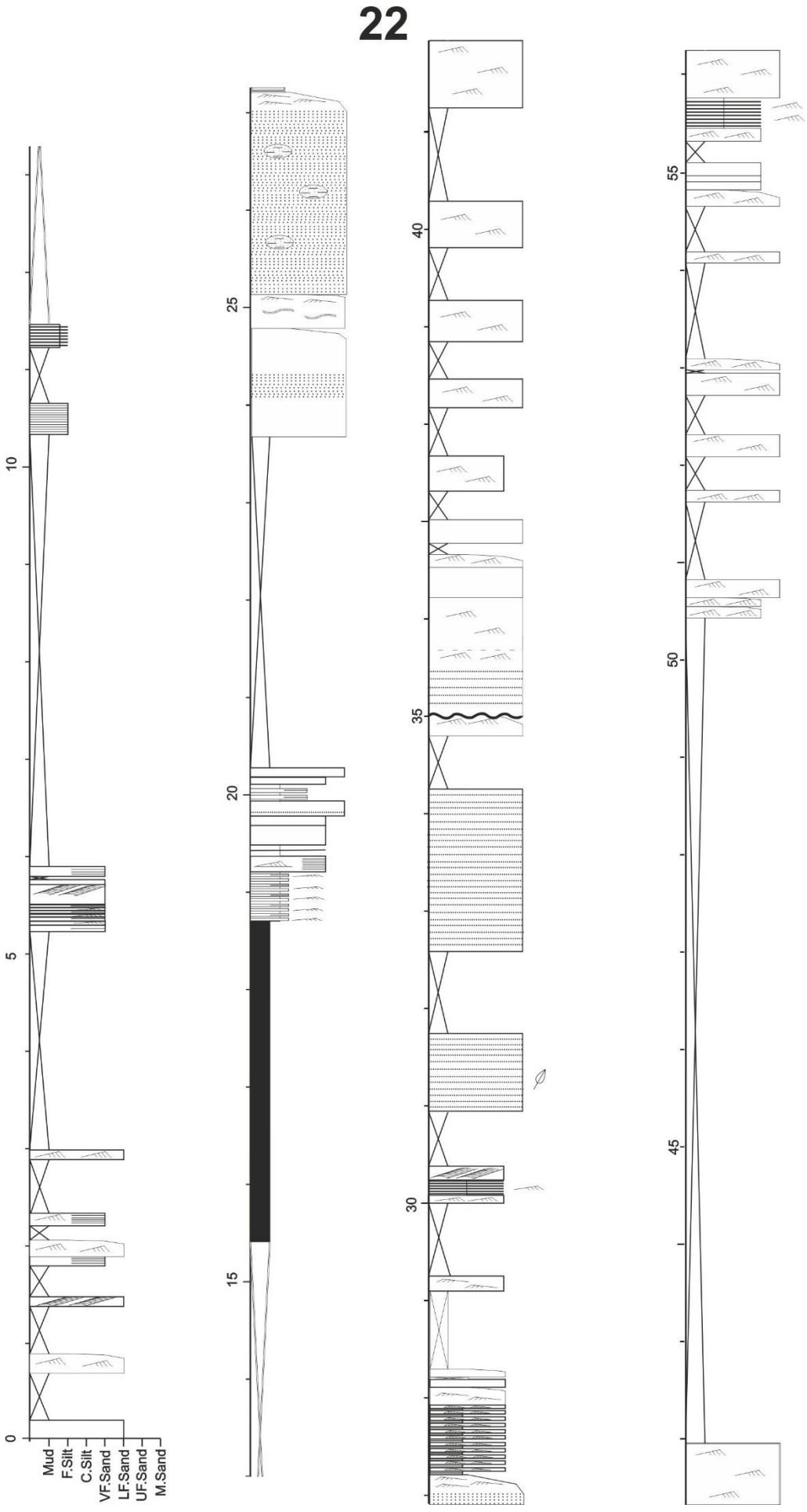
22
0
5
10
15
20
25
30
35
40
45
50
55
Mud
F.Silt
C.Silt
VF.Sand
LF.Sand
UF.Sand
M.Sand


24
Mud
F.Silt
C.Silt
VF.Sand
LF.Sand
UF.Sand
M.Sand
0
5
10
15
20
25
30
35
40
45
50
55
60
65
70
75

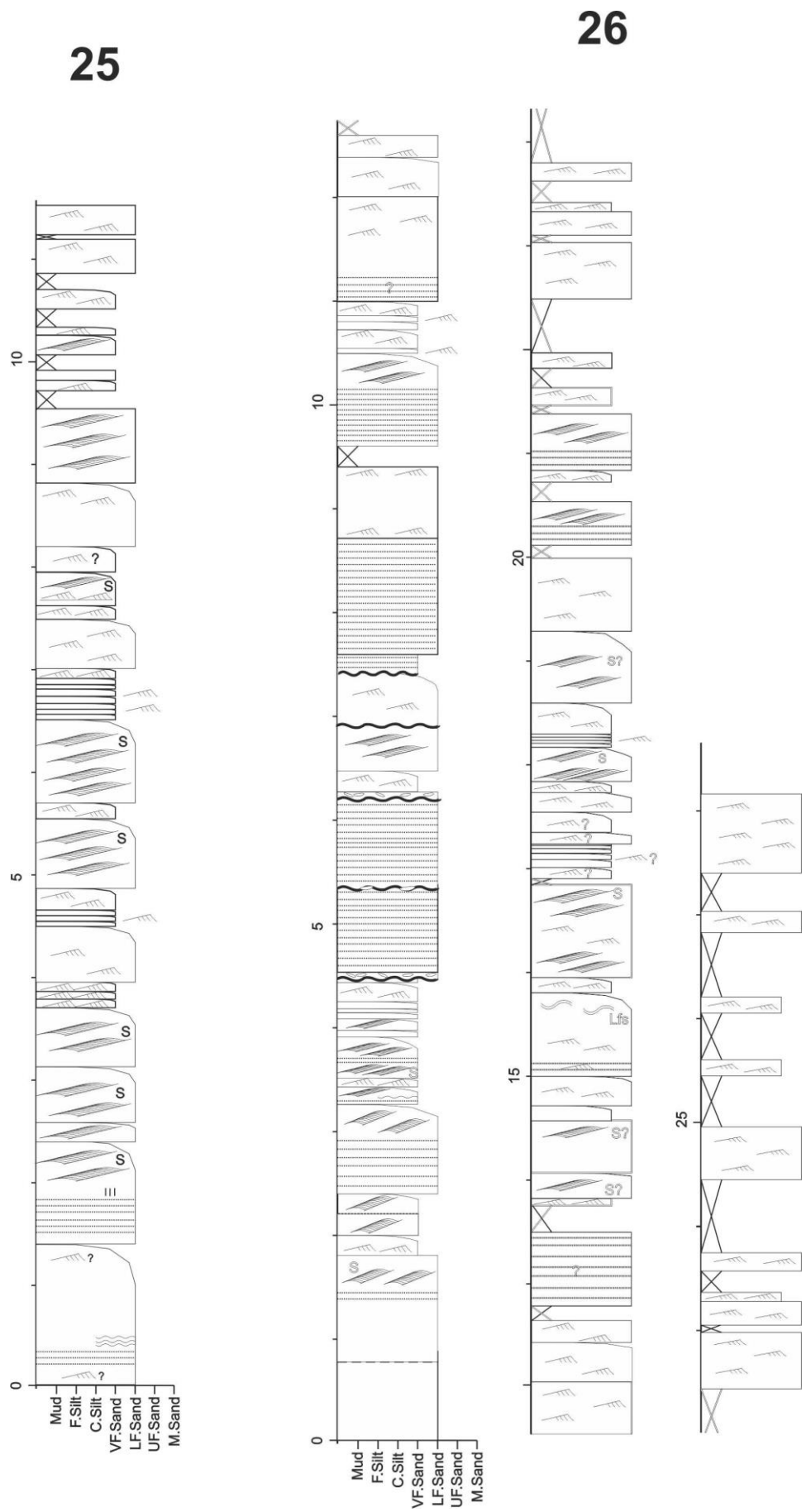
25
26
0
5
10
15
20
25
Mud
F.Silt
C.Silt
VF.Sand
LF.Sand
UF.Sand
M.Sand
S
S?
?
Lfs

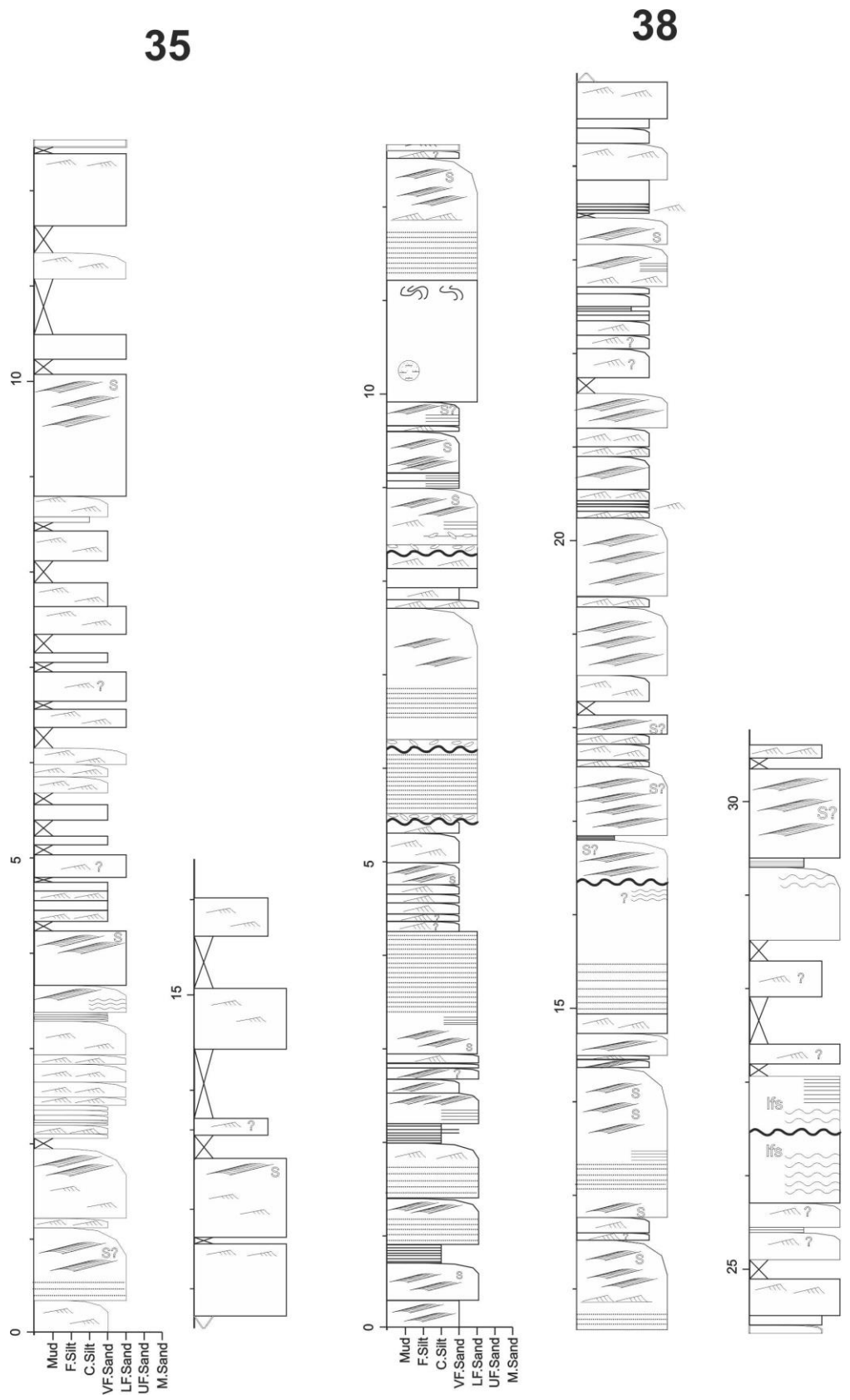
35
38
0
5
10
15
20
25
30
Mud
F.Silt
C.Silt
VF.Sand
LF.Sand
UF.Sand
M.Sand
S
S?
?
lfs

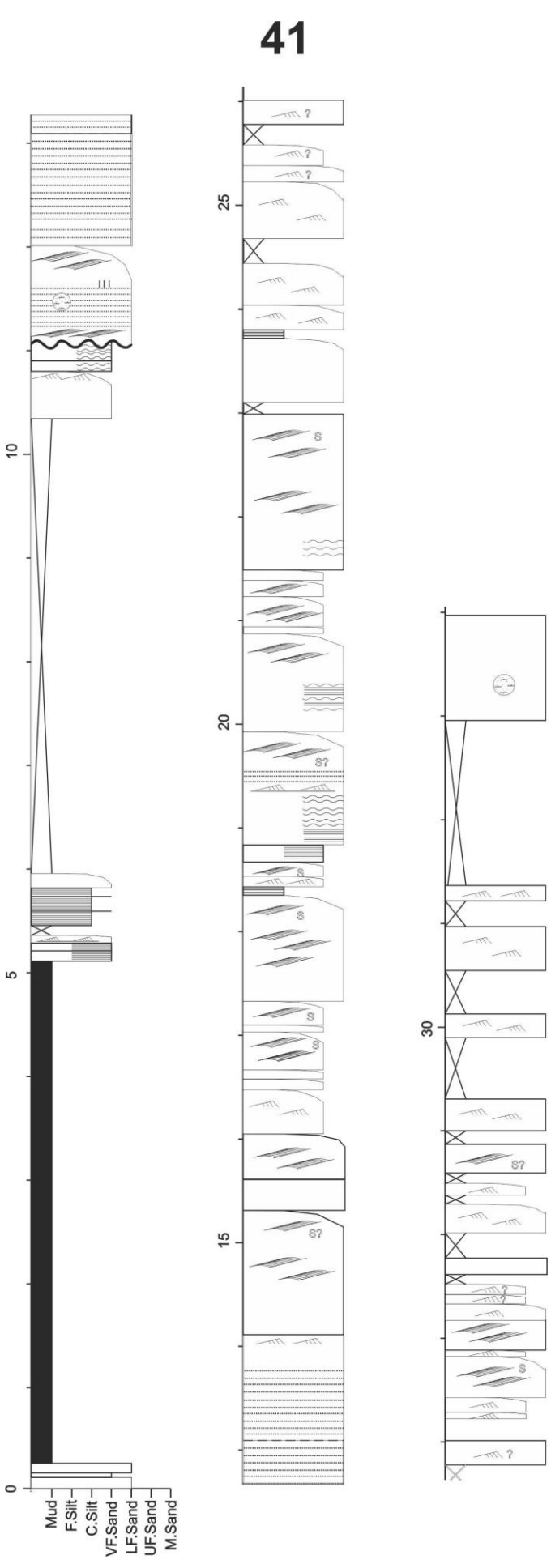
41
0
5
10
15
20
25
30
Mud
F.Silt
C.Silt
VF.Sand
LF.Sand
UF.Sand
M.Sand

42

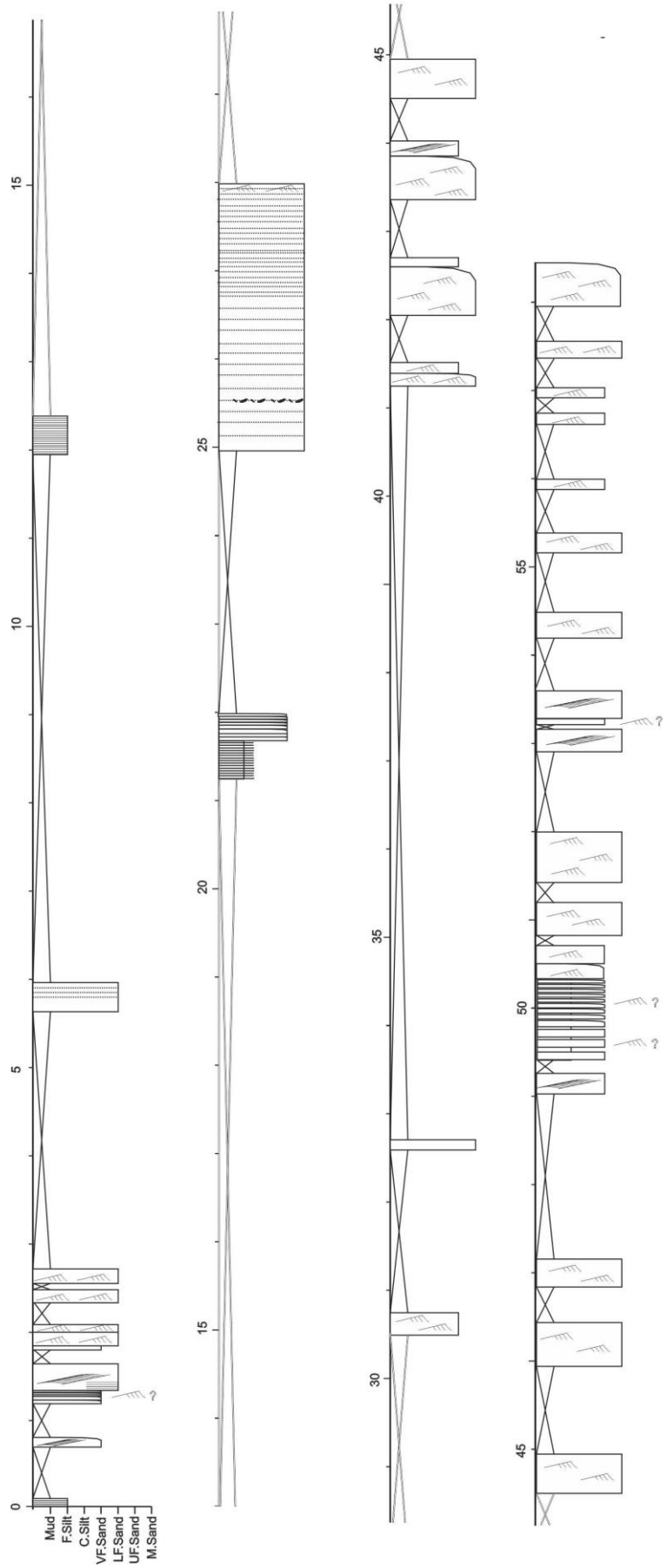
0
5
10
15
15
20
25
30
35
40
45
45
50
55
?
?
?
?
Mud
F.Silt
C.Silt
VF.Sand
LF.Sand
UF.Sand
M.Sand

Chapter 6

Unit 5 – Blaukop

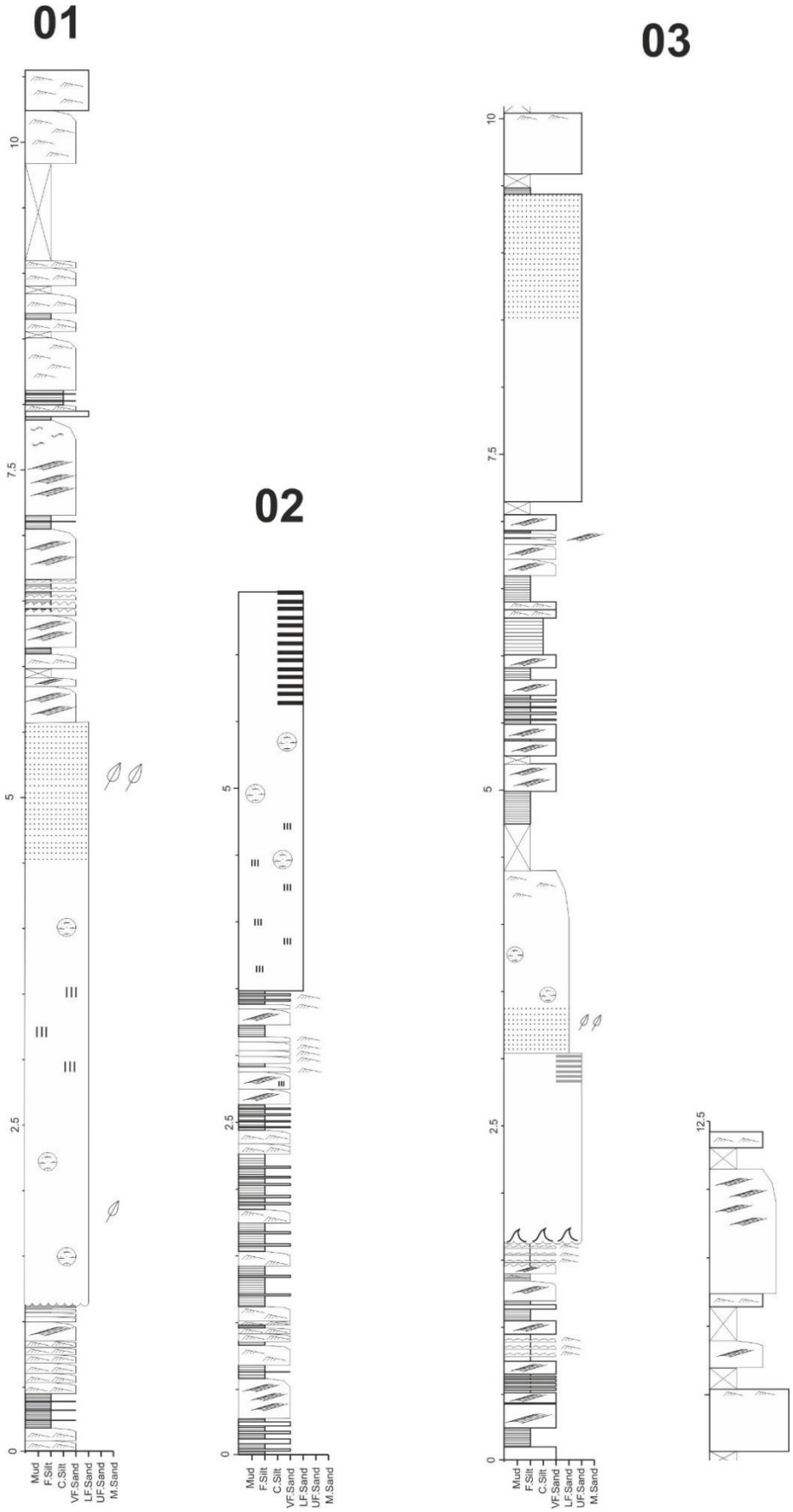

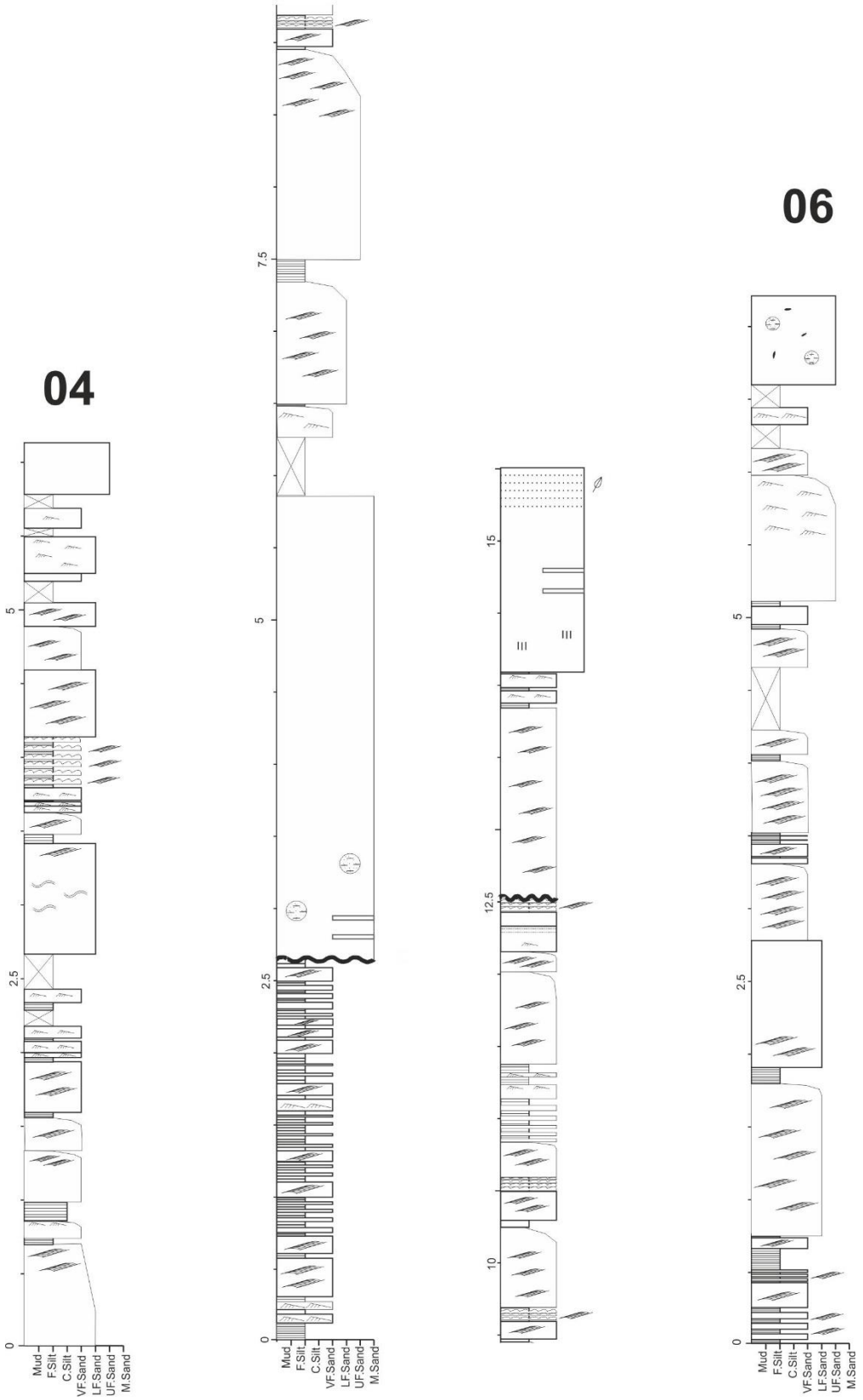
04
05
06
0
2.5
5
7.5
10
12.5
15
Mud
F.Silt
C.Silt
VF.Sand
LF.Sand
UF.Sand
M.Sand

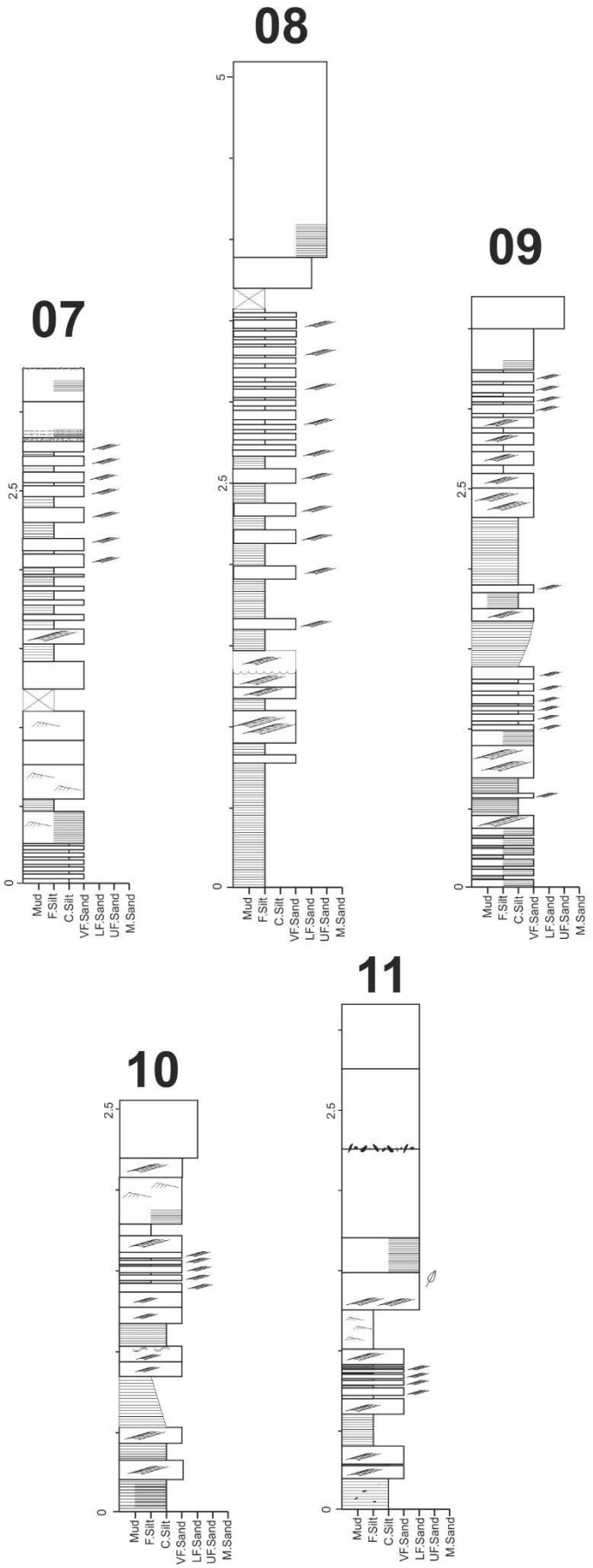
08
09
07
11
10
5
2.5
0
Mud
F.Silt
C.Silt
VF.Sand
LF.Sand
UF.Sand
M.Sand


12
13
14
15
2.5
5
7.5
0
Mud
F.Silt
C.Silt
VF.Sand
LF.Sand
UF.Sand
M.Sand

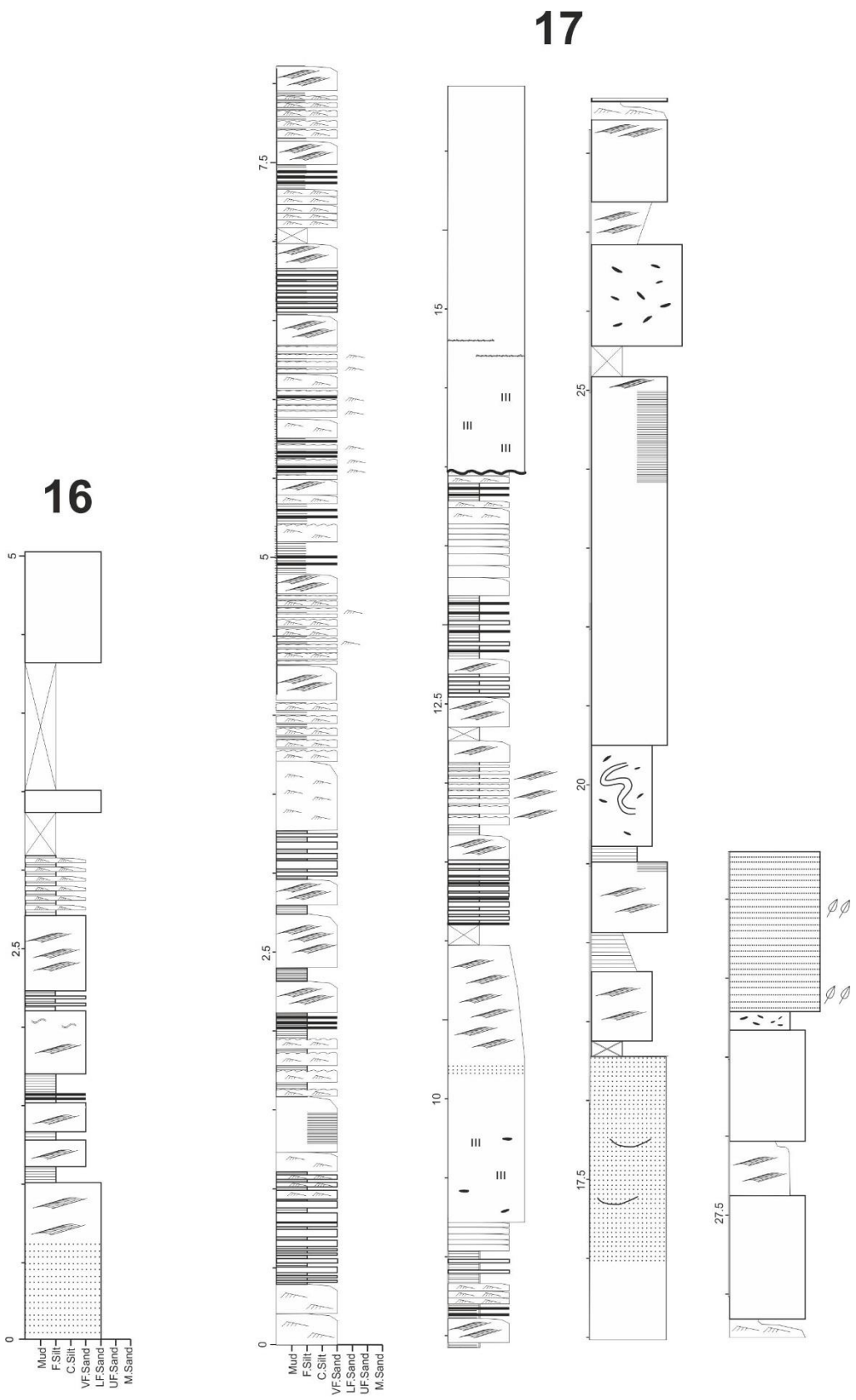
16
17
0
2.5
5
7.5
10
12.5
15
17.5
20
25
27.5
Mud
F.Silt
C.Silt
VF.Sand
LF.Sand
UF.Sand
M.Sand

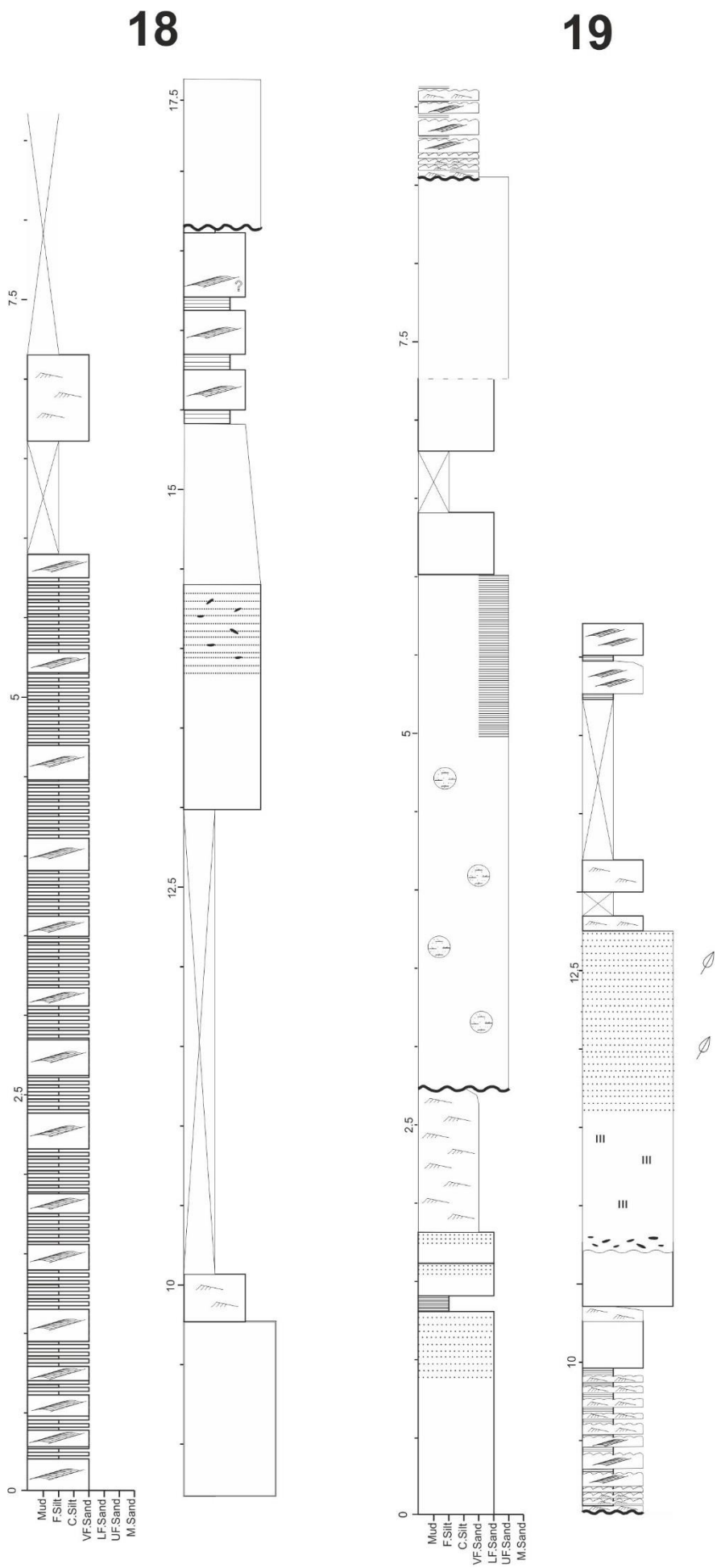
18
19
0
2.5
5
7.5
10
12.5
15
17.5
Mud
F.Silt
C.Silt
VF.Sand
LF.Sand
UF.Sand
M.Sand

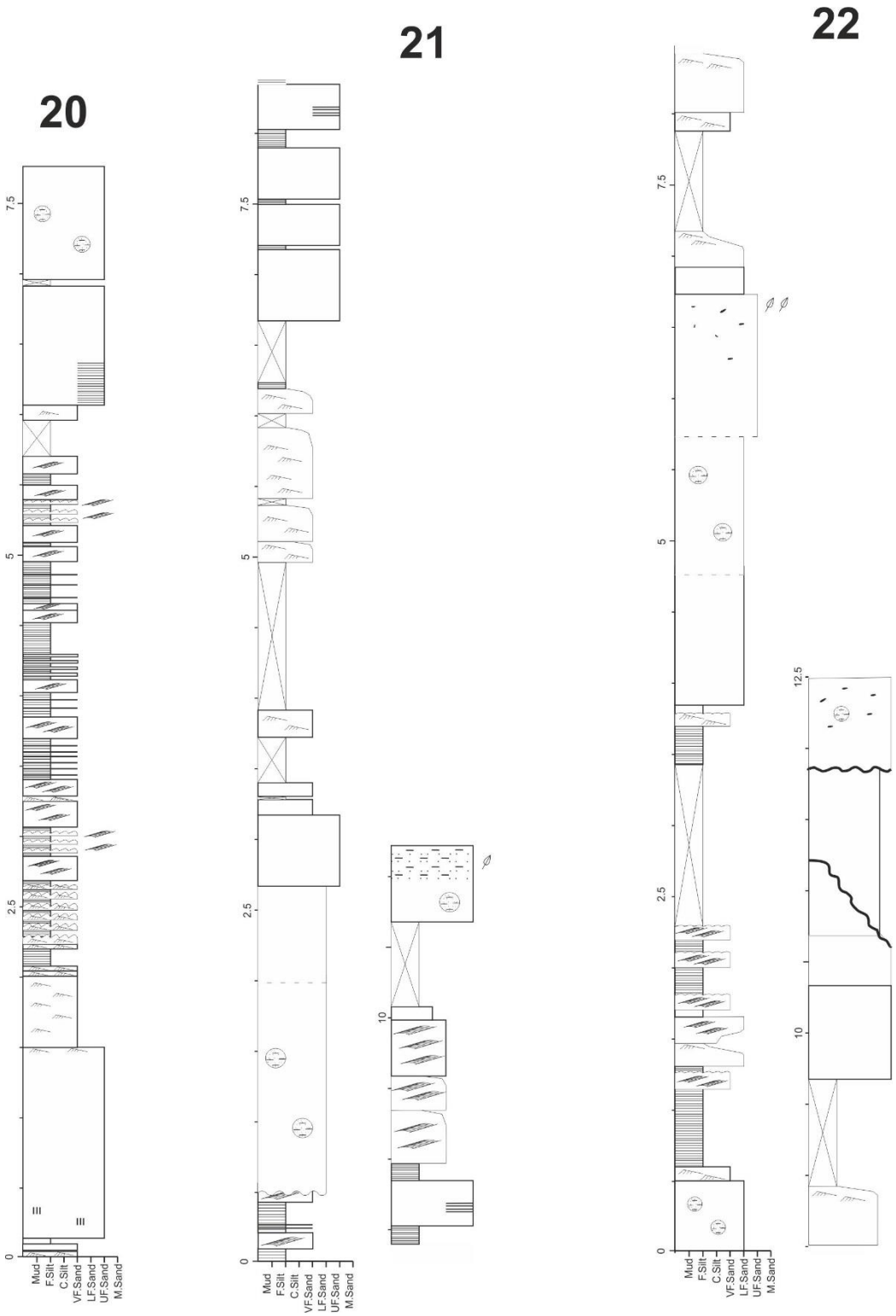
20
21
22
0
2.5
5
7.5
10
12.5
Mud
F.Silt
C.Silt
VF.Sand
LF.Sand
UF.Sand
M.Sand

23

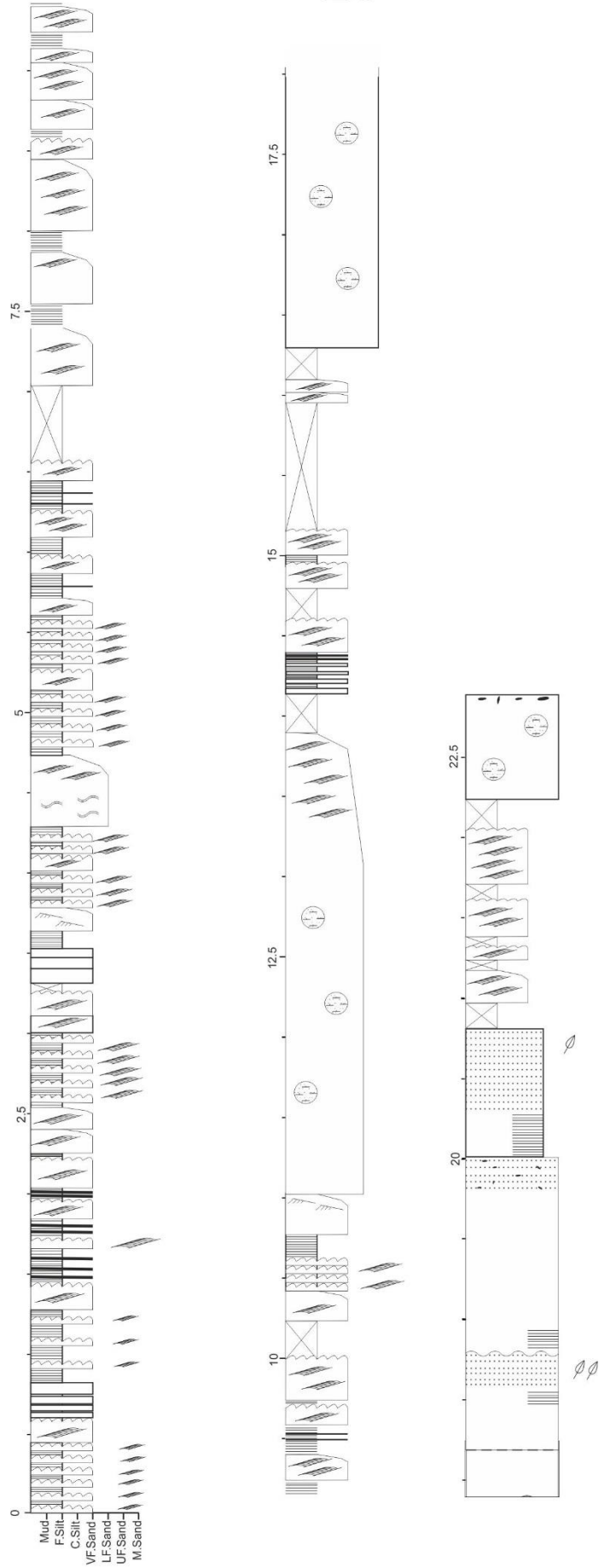
0
2.5
5
7.5
10
12.5
15
17.5
20
22.5
Mud
F.Silt
C.Silt
VF.Sand
LF.Sand
UF.Sand
M.Sand

24


0
2.5
5
7.5
10
12.5
15
17.5
20
22.5
25
27.5
Mud
F.Silt
C.Silt
VF.Sand
LF.Sand
UF.Sand
M.Sand

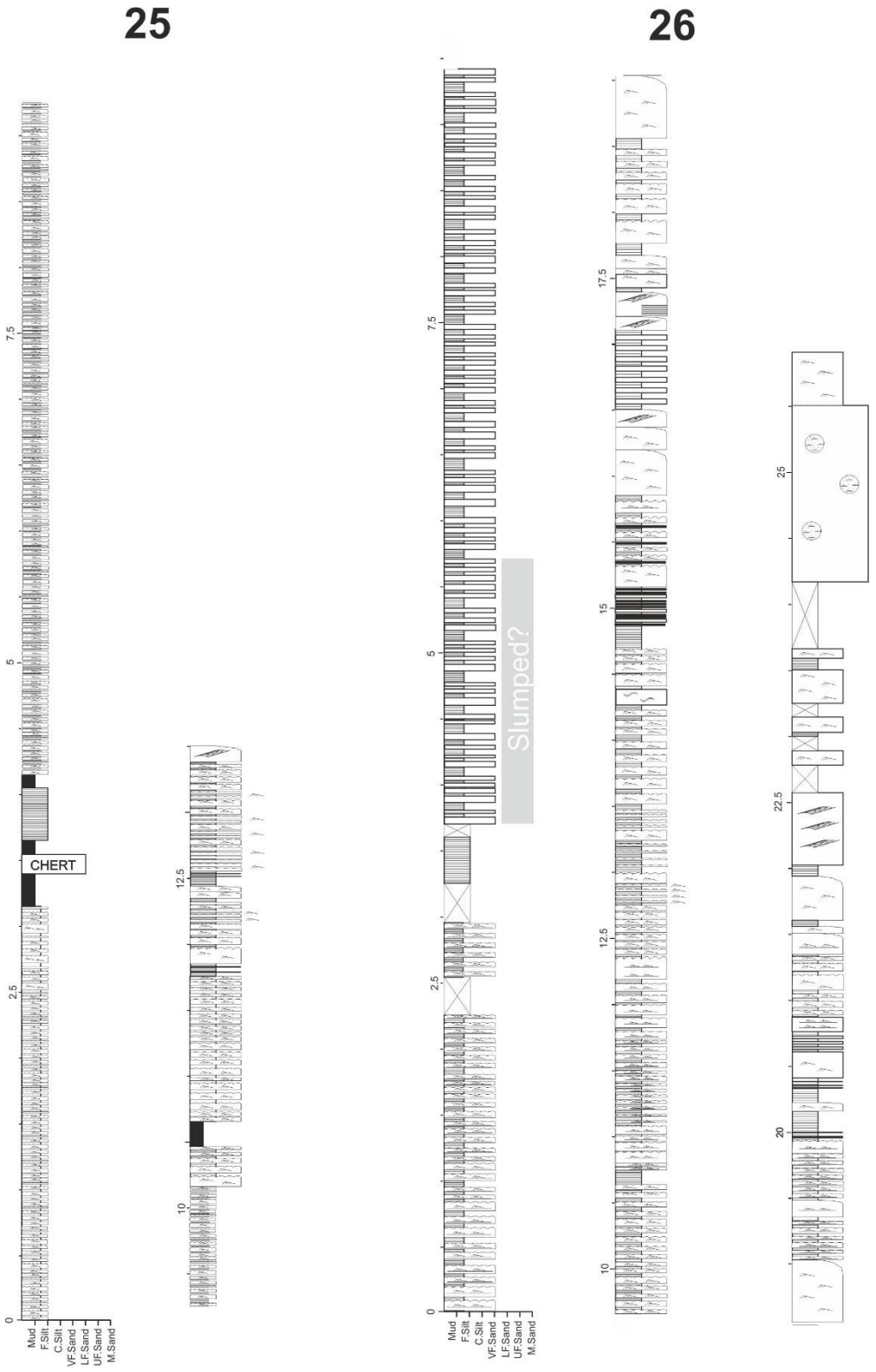
25
26
CHERT
Slumped?
Mud
F.Silt
C.Silt
VF.Sand
LF.Sand
UF.Sand
M.Sand